Università degli Studi di Ferrara

DOTTORATO DI RICERCA IN "SCIENZE CHIMICHE"

CICLO XXXIII

COORDINATORE Prof. Cavazzini Alberto

_____

Studio della distribuzione di mercurio in matrici ambientali

_____

Settore Scientifico Disciplinare CHIM/01-CHIM/12

Dottorando

Dott. Vardè Massimiliano

_____
(firma)

Relatore

Prof.ssa Pasti Luisa

_____
(firma)

Relatore

Prof. Cavazzini Alberto

_____
(firma)

Anni 2017/2020

pagina lasciata intenzionalmente bianca

Indice

Ringraziamenti

Questo lavoro di dottorato è il risultato del sostegno e dello sforzo di numerose persone a cui sono estremamente grato.

Innanzitutto, mi è doveroso ringraziare i relatori, la prof.ssa Luisa Pasti, e il prof. Alberto Cavazzini.

Ringrazio i due valutatori, le proff. Chiara Cavaliere del Dipartimento di Chimica dell'Università degli Studi di Roma Sapienza, e Sara Bogialli del Dipartimento di Scienze Chimiche dell'Università degli Studi di Padova per i loro utili suggerimenti.

In ordine cronologico, rispetto ai lavori fatti nel triennio 2017-2020, desidero sinceramente fare i miei ringraziamenti a:

- Franco Cofone, (CNR-Nanotec), per l'assistenza tecnica agli strumenti e, al mio "modus operandi";

- Alessandro Servidio e Annalisa Rosselli, (ex CNR-IIA), per la loro compagnia dentro e fuori il laboratorio;

- Mario Di Traglia del Dipartimento di Sanità Pubblica dell'Università degli Studi di Roma Sapienza, per le sue competenze statistiche e per la sua pazienza nei miei confronti;

- Carmine Apollaro e Giovanni Vespasiano, del Dipartimento di Biologia, Ecologia e Scienze della Terra dell'Università degli Studi della Calabria, per aver arricchito con la geochimica e la simpatia moltissime delle mie giornate lavorative;

- Antonio Procopio, del Dipartimento di Scienze della Salute dell'Università degli Studi Magna Graecia di Catanzaro, per aver creduto e sostenuto il lavoro del Hg nelle acque minerali;

-Warren R.L. Cairns, (CNR-ISP), perché una telefonata di auguri di Buon Natale può portare a lavorare a 1100 Km di distanza da casa;

- Andrea Spolaor, (CNR-ISP), per avermi coinvolto nei suoi studi e nelle attività polari fin dal mio arrivo alla sede del CNR-IDPA di Venezia-Mestre;

- Maria Villoslada Hidalgo e Raffaello Tedesco, dell'Università degli Studi Ca' Foscari di Venezia, per il supporto giornaliero al buon umore;

-Carlo Barbante, e tutti i numerosi colleghi del CNR-ISP e del DAIS-Ca' Foscari di Venezia-Mestre;

- Paolo Cristofanelli, Davide Putero, Francescopiero Calzolari, Maurizio Busetto, Luca Naitza, e Paolo Bonasoni, del CNR-ISAC di Bologna;

- Francesca Becherini, (CNR-ISP), per avermi dimostrato costanza e tenacia per il lavoro di Col Margherita;

È stato un privilegio lavorare con tutti voi, e nel prossimo futuro, spero di poterlo continuare a fare con lo stesso spirito di gruppo che ha caratterizzato i primi lavori insieme.

Questi 3 anni di lavoro e la tesi di dottorato li desidero dedicare a mio papà (ad maiora semper!) e al mio grande amico Gianluca Zamparelli.

pagina lasciata intenzionalmente bianca

Abstract

The objective of this PhD thesis is the study of mercury and the assessment of its behavior in the different environmental matrices investigated.
The doctoral thesis consists of:

- a first introductory part, where the main characteristics of mercury and its environmental importance are described.
- a second part, where the abstracts of the published papers (in indexed journals) or in the submission phase are presented.

The extended works, attached in the appendix, were carried out during the three-year period of the doctoral school, from November 2017 to November 2020.

- The first work, (in the submission phase), aims to understand the behavior of Hg in ambient air at a high-altitude station in the Eastern Alps, through the Hg analysis on a monthly, seasonal, and daily basis variations. Ancillary variables (ozone and meteorological parameters) were used for the study of atmospheric Hg, and the analysis of the back-trajectories of the air masses and the planetary boundary layer (PBL) with the aim of identifying potential emission sources.

- The second publication shows the investigation of total mercury concentrations in Italian bottled waters, using a very sensitive analytical method, and the possible relationships between mercury, the chemical-physical parameters of the water and the lithology of the aquifer. Furthermore, the determination of Hg levels on a large number of samples can allow us to estimate the intake of mercury from natural mineral waters for different groups of the population.

- The overall objective of the third study is the comparison of the inorganic content of water intended for human consumption (drinking water) and natural mineral waters (bottled water) collected in a region of Southern Italy (Calabria). This comparison was made using compositional data analysis (CoDA) and a new graphical-numerical approach. Among the 29 selected parameters, the Hg content was also examined. The comparison of total mercury concentrations between bottled waters and tap waters highlighted differences in the Hg levels of the two typologies of water attributable to the different origins and their management.

- The fourth publication aims to understand the behavior of Hg in the snow on the Antarctic plateau through the analysis of data relating to three surface snow sampling campaigns during three austral summers. The study demonstrates how weather conditions can affect mercury deposition processes and its relative abundance in the surface layers of snow.

Parole chiave

Mercurio; Atmosfera; Acque potabili; Acque minerali; Neve superficiale.

Keywords

Mercury; Atmosphere; Drinking waters; Natural mineral waters; Surface snow.

pagina lasciata intenzionalmente bianca

Capitolo 1

1.1 Introduzione

Il mercurio è un elemento chimico (simbolo Hg, numero atomico 80, peso atomico 200.59 u) naturalmente presente nell'ambiente. Nella tavola periodica fa parte dei metalli di transizione del gruppo II B (con zinco e cadmio). Il Hg è inodore, liquido a temperatura ambiente e ha colorazione argento vivo, caratteristica dalla quale deriva il suo simbolo (prende origine dal greco hydrárgyros, composto da ὕδωρ = acqua e ἄργυρος = argento, da cui deriva il nome latino Hydrargyrum). Presenta densità 13.534 g/cm^3 a 25 °C, punto di fusione a -38.7 °C, punto di ebollizione a 356.7 °C e una tensione di vapore di 0.002 mm Hg a 25 °C. Volatile quando sottoposto al riscaldamento, ha la capacità di formare amalgama con l'oro (NRC, 2000). Metallo conosciuto dall'uomo fin dall'antichità, citato nei testi dell'antica Grecia e dell'antica Roma e ritrovato in reperti archeologici in Egitto, Cina e India dove per secoli è stato impiegato per effetti terapeutici e come disinfettante (Caley, 1928; Mukhi et al., 2017; Farrar and Williams, 1977).

La sua abbondanza nella crosta terrestre è pari a 80 μg/kg e una concentrazione media negli oceani di 0.3 ng/L (∼1.5 pM) (Gonzalez-Raymat et al., 2017). Nei minerali è raro trovare il Hg come metallo nativo. Infatti, è principalmente presente come solfuro di mercurio (HgS, cinabro, di colore rosso), minerale di formazione idrotermale, e in tracce, nella livingstonite ($HgSb_4S_8$) e nella corderoite ($Hg_3S_2Cl_2$). Nelle aree ad attività vulcanica denominate cinture mercurifere, sono situati i giacimenti di mercurio più abbondanti. Almadén (Spagna), Idrija (Slovenia) e il monte Amiata (Italia), sono tra i più grandi depositi di mercurio al mondo. Dismesse da pochi decenni, le numerose miniere in queste aree sono state sfruttate per oltre 2000 anni (Navarro, 2008; Gosar et al. 1997).

A livello industriale il Hg è impiegato in apparecchiature elettriche ed elettroniche: interruttori, termostati, sensori e relays sono i principali prodotti che contengono mercurio (Randall, 1995). La commercializzazione di termometri, manometri e barometri contenenti mercurio è stata vietata in Italia a decorrere da aprile del 2009 (D.M. 30/07/2008) per il recepimento della Direttiva 2007/51/CE, anticipando l'azione dell'UNEP (Programma delle Nazioni Unite per l'ambiente). L'UNEP attraverso la Convenzione di Minamata, nel 2013 ha proposto agli stati di tutto il mondo un accordo internazionale con l'obiettivo di ridurre le emissioni e le contaminazioni da Hg (e i suoi composti) prodotte dalle attività antropiche, attraverso il controllo del ciclo di vita di questo elemento, dalla sua estrazione mineraria fino alla gestione dei rifiuti. Il trattato entrato in vigore nel 2017, ad oggi è stato sottoscritto da

128 paesi e ratificato da 125. I paesi aderenti si impegnano a rispettare un programma vincolante per la gestione dell'inquinamento da mercurio su scala globale, con l'obiettivo di proteggere l'ambiente e la salute della popolazione (https://www.mercuryconvention.org/).

1.2 Il mercurio

Il mercurio è un inquinante ubiquitario, persistente e tossico per l'ambiente e il biota. Le sorgenti di Hg sono riconducibili alle attività umane (combustione di prodotti petroliferi, produzione di acciaio, impianti di cloro-alcali, produzione di cemento, inceneritori industriali, di rifiuti urbani, e sanitari, processi di trattamento delle acque reflue, miniere artigianali e su piccola scala di oro e di mercurio), e a processi naturali (Driscoll et al., 2013).

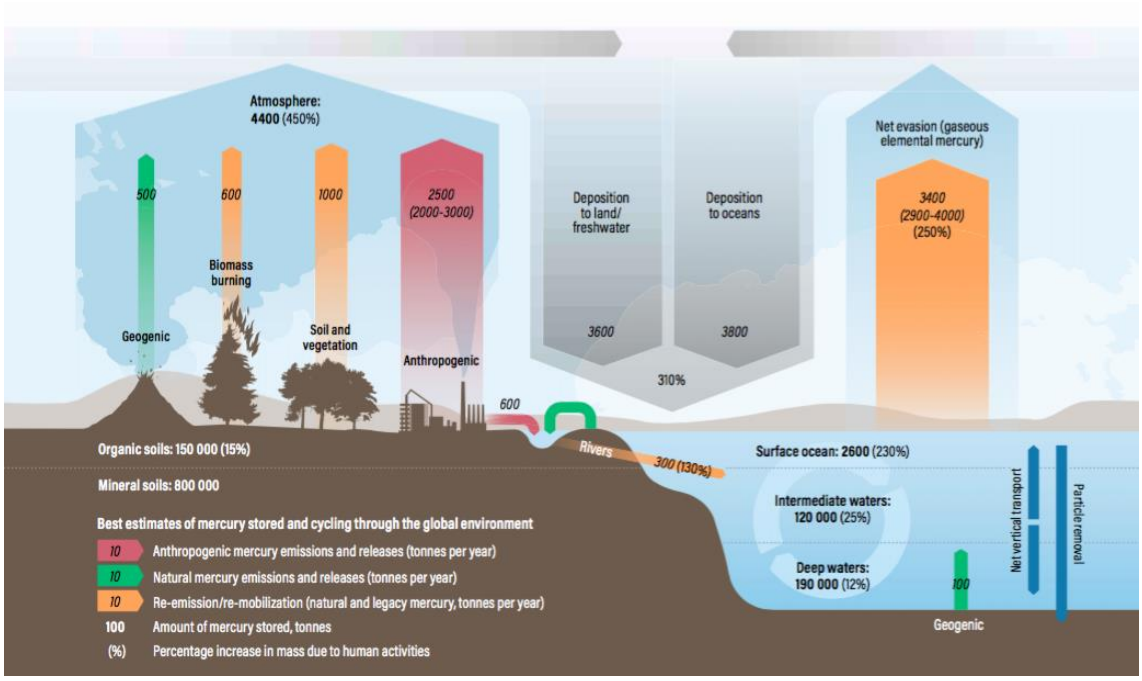

Figura 1. Il bilancio globale del mercurio con l'impatto delle attività umane sul ciclo del mercurio e l'aumento del mercurio accumulato nel suolo e negli oceani (UNEP, 2019).

Le emissioni da fonti naturali come le emissioni vulcaniche, gli incendi boschivi, le sorgenti geotermiche, processi erosivi di rocce e del suolo sono state calcolate tra 76-300 Mg/anno. In generale, le ultime stime sul budget globale di Hg affermano che, dopo il picco di emissioni globali registrato nel 1970, e la significativa diminuzione nel periodo 1980-2000, il leggero incremento osservato dal 2010 al 2015 ha raggiunto attualmente un livello stabile di emissioni totali in atmosfera pari a circa 2000 Mg/anno (Streets et al., 2019). Nel 2018

l'UNEP ha confermato che le emissioni di Hg da fonti antropogeniche ammontano a circa 2200 Mg/anno su scala globale (UNEP, 2019) e che sul budget totale annuale in atmosfera il contributo maggiore è dato delle attività dell'uomo (Fig. 1).

La principale via di trasporto del Hg su larga scala è l'atmosfera. Nella dispersione del Hg in aria si possono distinguere le emissioni primarie, che hanno origine sia antropica che naturale. Generate da sorgenti sulla superficie terrestre il Hg ricade sia al suolo che sui grandi bacini di acqua dolce e oceani attraverso fenomeni di deposizione secca e umida. Il Hg^0 depositato sulla superficie può successivamente essere ossidato a Hg^{2+}, reimmesso in atmosfera come mercurio elementare, viene considerato come Hg proveniente da emissioni secondarie (Driscoll et al., 2013). Una volta rilasciato nell'ambiente il Hg viene quindi trasportato, distribuito nei vari comparti ambientali aria, acqua e suolo, subendo accumulo nelle falde acquifere, nei sedimenti lacustri e oceanici. Il Hg è presente naturalmente in tre stati di ossidazione (Hg^0, Hg^+, Hg^{2+}), ma l'instabilità del legame Hg-Hg determina la prevalenza del mercurio elementare e del Hg^{2+} che contribuiscono al totale di mercurio presente nell'ambiente. Nei composti di Hg^+ (mercurosi) il Hg si presenta come ione dimero Hg_2^{2+}, caratterizzato da legame covalente metallo-metallo tra due atomi.

Il mercurio si combina con elementi come cloro, ossigeno, e zolfo per formare composti inorganici, e con il carbonio per formare composti organici, di cui il più noto è il metilmercurio (CH_3Hg^+). Le forme del Hg rilevanti dal punto di vista tossicologico sono i sali inorganici di Hg (es. $HgCl_2$ solubilità in acqua 69 g/L a 20°C), i composti organici del Hg (liposolubili) e il Hg metallico (solubilità in acqua 5.6×10^{-5} g/L a 25°C) (Langford et al., 1999). Le trasformazioni chimiche di ossidazione e riduzione che subiscono le diverse forme del Hg ne regolano la mobilità e l'accumulo negli ecosistemi terrestri, d'acqua dolce e marini (Bigham et al., 1964). Infatti, le diverse forme chimiche mostrando proprietà chimiche e fisiche peculiari, presentano differenti vie di esposizione ed effetti tossicologici (Davis et al., 1997). Negli ecosistemi acquatici, le trasformazioni di metilazione e demetilazione ricoprono particolare importanza poiché determinano il bioaccumulo e la tossicità del CH_3Hg^+ (Bishop et al., 2020). Il CH_3Hg^+, composto neurotossico, oltre al bioaccumulo negli organismi, subisce successiva biomagnificazione lungo la catena trofica, per impattare sulla salute dell'uomo (Driscoll et al., 2013). L'assunzione di CH_3Hg^+ per l'essere umano avviene principalmente attraverso l'alimentazione, con il consumo di pesce, in particolare predatori di grossa taglia, crostacei e molluschi (UNEP, 2019). Per tale motivo, l'Autorità Europea per la Sicurezza Alimentare (EFSA, 2015) ha suggerito il numero massimo di porzioni di pesce/crostacei/molluschi da assumere alla settimana in relazione al gruppo di popolazione (es. bambino, donne in gravidanza) e il Comitato di Esperti congiunto

FAO/WHO sugli Additivi Alimentari (JECFA) ha fissato a 1.3 µg/kg bw la dose settimanale tollerabile provvisoria (PTWI) per il metilmercurio e a 4 µg/kg bw per il mercurio inorganico (EFSA, 2012). La differenza di PTWI tra metilmercurio e mercurio inorganico è dovuta alla differente tossicità sull'uomo e al diverso contenuto di metilmercurio rispetto al mercurio totale, che nelle specie ittiche rappresenta 80-100% nei pesci e 50-80% in crostacei e molluschi. Nel cibo diverso dal pesce si presume che tutto il Hg presente sia sotto forma di mercurio inorganico. L'esposizione al mercurio per l'uomo, diversa dalla dieta, è stata valutata, per esempio, per il rilascio di mercurio inorganico dalle amalgame dentali, dopo rottura di dispositivi contenenti Hg (es. termometri a mercurio) (Goh and Ng, 1988; Faria and de Freitas, 1992; Kanerva et al., 1993; EFSA, 2012; Richter et al., 1982), e per contatto con composti chimici in attività di laboratorio (Kanerva et al., 1994). In ambito professionale, studi sugli effetti di esposizione a vapori e polveri contenenti mercurio hanno riguardato i lavoratori di impianti cloro-soda (Piikivi and Tolonen, 1989), aziende produttrici di leghe di zinco-mercurio (Roels et al., 1985), e l'industria della lavorazione del vetro (Danziger and Possick, 1973; IARC, 1993).

Le elevate concentrazioni di mercurio generate dai disastri ambientali (es. Minamata - Giappone 1958, Bassora - Iraq 1970) e la consapevolezza del rischio per la salute umana derivante all'esposizione al CH_3Hg^+ dovuto al crescente rilascio di Hg da fonti antropiche sono i principali motivi di interesse scientifico e politico sul Hg.

Per la fine del 2020, la Convenzione di Minamata (UNEP) aveva fissato il divieto alle attività di nuove miniere, l'eliminazione progressiva di quelle attive, e l'attuazione di ulteriori misure di controllo per la riduzione delle emissioni in atmosfera. L'obiettivo della Convenzione di Minamata è di evitare altri disastri ambientali, come avvenuto nel passato, promuovere l'uso di energia pulita per realizzare uno sviluppo sostenibile, raggiungere un benessere maggiormente diffuso, e rafforzare la protezione degli ecosistemi e degli esseri viventi (The Lancet, 2017).

1.3 Ciclo biogeochimico

Il mercurio e alcuni suoi composti (inorganici e organici) sono contraddistinti da peculiari proprietà chimico-fisiche come tensione di vapore relativamente alta, differente solubilità in acqua e nei lipidi, che in aggiunta alla resistenza nei processi di degradazione fotochimica, chimica, e/o biologica, rendono elevato il loro grado di mobilità. L'insieme di queste caratteristiche conferiscono al Hg la capacità di diffondersi su scala globale e raggiungere i diversi comparti ambientali (atmosfera, idrosfera e litosfera), in una articolata interazione nell'ambiente definito ciclo biogeochimico del Hg (Schroeder et al., 1989) (Fig. 2).

1.4 Mercurio in atmosfera

L'atmosfera è la principale via per il trasporto di Hg e riveste un ruolo importante nel ciclo biogeochimico globale del mercurio. Oltre a fungere da serbatoio, l'atmosfera ha rilevanza nei meccanismi di trasporto e nelle reazioni chimiche e fotochimiche che coinvolgono il mercurio.

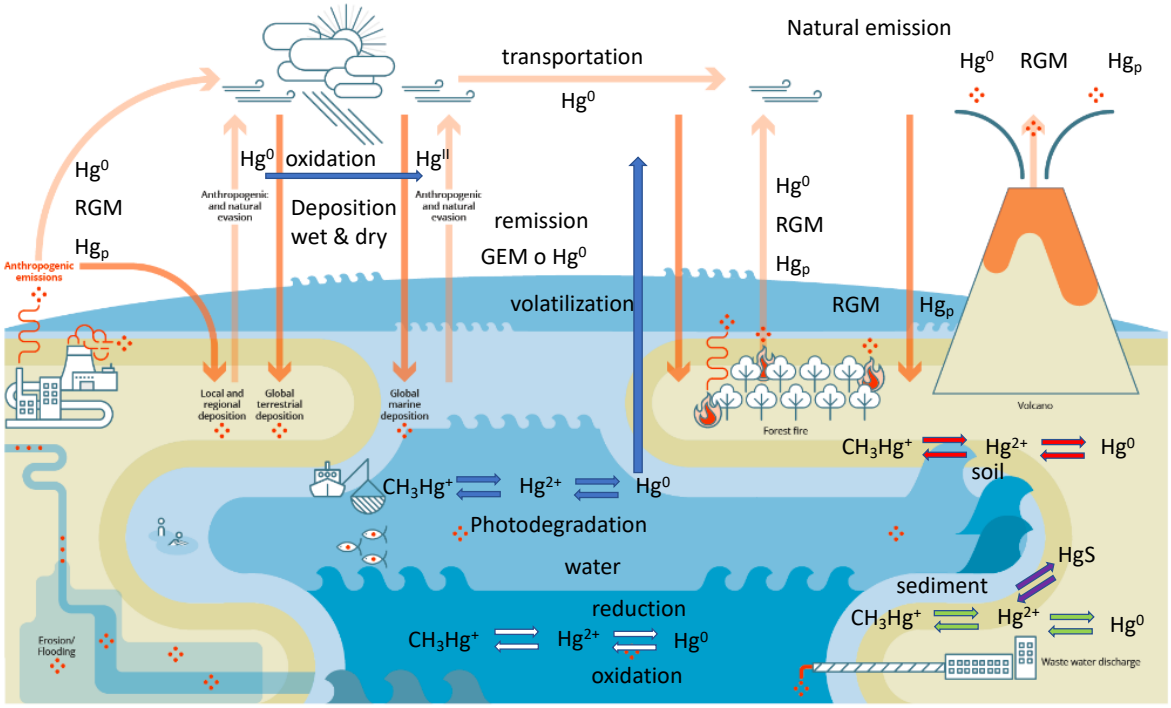

Figura 2. Schema delle sorgenti e degli ecosistemi coinvolti nel ciclo biogeochimico del mercurio (modificato da: The global mercury cycle: European Environment Agency, 2020). (Note: GEM= gaseous elemental mercury; RGM=Reactive gaseous mercury; Hg_p= Particle bound mercury)

La maggior parte del mercurio viene emesso in atmosfera da sorgenti antropogeniche e naturali, e raggiunge la superficie terrestre attraverso le precipitazioni atmosferiche.

In generale, le emissioni di Hg sono costituite da mercurio elementare, e da mercurio inorganico (Hg^{2+}) in fase gassosa e particellare. La frazione più abbondante in atmosfera si presenta come Hg^0 che rappresenta tipicamente una quantità >95% rispetto al totale. Una volta emesso in atmosfera, essendo relativamente inerte può rimanere per lungo tempo (0.5-1 anno), ed essere trasportato a lunghe distanze su scala globale. La costituzione di reti di monitoraggio a livello nazionale come il Canadian Atmospheric Mercury Network (CAMNet) (Temme et al., 2007), l'American Atmospheric Mercury Network (AMNet) (Lan et al., 2012), Asia Pacific Mercury Monitoring Network (APMMN) (Sheu et al., 2019), e internazionale come il Global Mercury Observation System (GMOS) (Sprovieri et al., 2016; 2017) (Fig. 3), oltre al monitoraggio su scala locale che ha permesso di investigare i livelli di concentrazioni di Hg in atmosfera in siti industriali, urbani, rurali e in zone remote comprese le aree polari (Sprovieri et al., 2010).

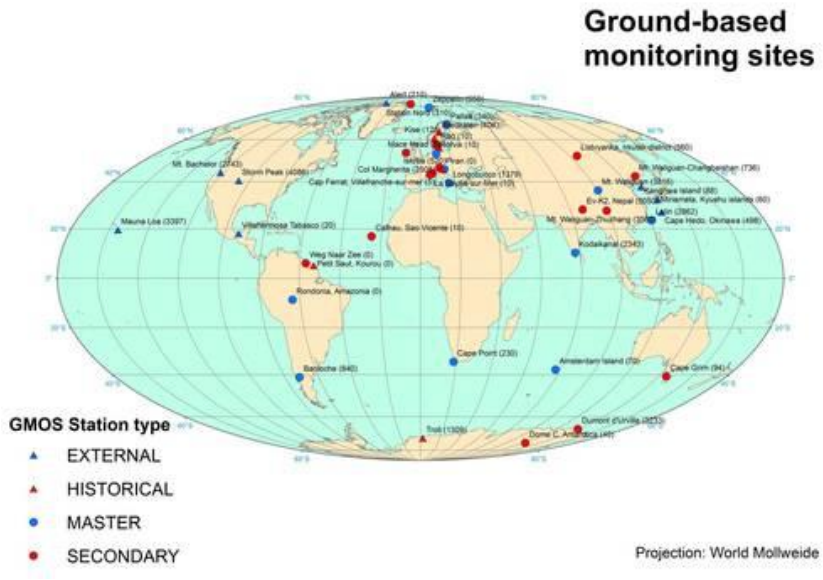

Figura 3. Localizzazione delle stazioni di monitoraggio del progetto GMOS.

In generale, le concentrazioni medie annue di mercurio in atmosfera nei siti di background nell'emisfero nord risultano superiori (1.5-1.7 ng/m^3) rispetto a quelle delle zone tropicali (~1.5 ng/m^3), dell'emisfero sud (1.0-1.3 ng/m^3) e delle aree polari rispettivamente in Antartide (~1.0 ng/m^3) e in Artico (~1.5 ng/m^3), che al momento registrano un numero inferiore di record di misure e di osservatori permanenti (Angot 2016; Sprovieri et al., 2016; 2017). Tuttavia, le specie presenti come Hg^{2+} sia in fase gassosa che adsorbita al particolato atmosferico possono essere velocemente rimosse dall'atmosfera (giorni o settimane), perché

più reattive e solubili, e depositarsi in aree molto più prossime alla sorgente di emissione. Sulla superficie terrestre il Hg^0 entra in contatto sia con gli ecosistemi terrestri venendo assorbito per esempio da piante e suolo con i quali avviene uno scambio dinamico, sia con le superfici di acque dolci (laghi e fiumi) e oceani dove i composti di Hg^{2+} vengono portati dalle precipitazioni atmosferiche (es. pioggia e neve) (Lyman et al., 2020).

1.5 Mercurio in ambiente acquatico

La presenza e il comportamento del mercurio in ambiente acquatico differiscono da quanto osservato in atmosfera, e altre differenze si riscontrano tra i sistemi di acqua dolce e quelli marini. L'importanza dello studio del Hg nei sistemi acquatici assume rilevanza data dal pericolo derivato dalla potenziale presenza e/o formazione di CH_3Hg^+ nelle acque, nei sedimenti e nei pesci, oltre al rischio per la salute umana dovuta all'assunzione del pesce contaminato.

In ambiente acquatico il Hg si può presentare nei suoi tre stati di ossidazione (Hg^0, Hg^+, Hg^{2+}). Le forme chimiche sono; il mercurio elementare; i composti inorganici; composti organici, come il CH_3Hg^+ e il dimetilmercurio $(CH_3)_2Hg$.

In forma fisica si presenta come mercurio disciolto, particellato, associato alle frazioni colloidali.

Il CH_3Hg^+ nei sedimenti acquatici viene prodotto per metilazione a partire da una frazione di Hg^{2+} tramite batteri, i quali trovano le ottimali condizioni tra composizione e struttura dei sedimenti, condizioni redox e presenza di carbonio organico e zolfo (Selin et al., 2009).

Fonti di contaminazione naturali dell'ambiente acquatico sono le deposizioni atmosferiche (secche e umide) e i fenomeni erosivi di suoli contaminati, mentre lo sversamento di acque reflue domestiche, le attività agricole e industriali sono le principali fonti di aree antropizzate (Wang et al., 2004).

Negli oceani, la concentrazione media di Hg nella maggior parte delle specie è inferiore a 0.5 mg/kg mentre quelle più elevate (0.2-5 mg/kg) sono state trovate nei pesci predatori, come tonno e pesce spada (Biddinger e Gloss, 1984; WHO, 1989). Le differenze dei livelli di Hg nelle varie specie ittiche, evidenziate da numerosi studi, sono riconducibili ad una serie di fattori come il tipo di specie, la taglia, il periodo di pesca e la posizione geografica. Concentrazioni massime ammissibili a 0.5 mg/kg per pesci, crostacei e molluschi, e a 1.0 mg/kg per pesci di grossa taglia, sono state fissate nelle normative della maggior parte dei

paesi e delle organizzazioni internazionali (es. EFSA, 2018; FAO/WHO, 2011; Guerrin et al., 1990; Kimáková et al., 2018; Wagemann et al., 1998).

Condizioni di pH, redox e il livello di concentrazione di composti organici ed inorganici del Hg^{2+} influenzano la distribuzione delle diverse forme chimiche del Hg nelle acque marine. In generale, la quantità di Hg disciolto, legato alle sostanze umiche, è inferiore nelle acque di mare rispetto alle acque dolci per la competizione dello ione cloruro, così come risulta inferiore la metilazione del Hg per i contributi della salinità e della presenza di complessi contenenti gli ioni solfuro e cloruro. Negli ultimi decenni sono state effettuate numerose campagne oceanografiche con lo scopo di misurare il profilo di concentrazione del Hg nelle acque superficiali e profonde. Le concentrazioni relative al Mar Mediterraneo risultano essere a livelli medi superiori (3.4 pM) rispetto a quanto determinato nelle acque dell'Oceano Atlantico (1-2 pM), dell'Oceano Pacifico e nel Mar del Giappone (~1.0 pM). L'incremento dei livelli di Hg disciolto e di CH_3Hg^+ riscontrati in funzione della profondità negli oceani suggeriscono l'influenza di fattori come: (1) forte attività tettonica sottomarina (2) processo di metilazione microbiologicamente mediata nelle acque più profonde; (3) degradazione fotochimica e/o attività microbica in superficie (Pirrone and Mason, 2010).

Nelle acque destinate al consumo umano, potabili e/o minerali naturali, i livelli di Hg rientrano mediamente nell'intervallo di concentrazione da circa 0.2 ng/L a 0.5 µg/L. Tuttavia, attualmente sono pochi gli studi, su base regionale e nazionale, che forniscono informazioni sul Hg e altri metalli pesanti per valutare i livelli di concentrazione e le potenziali sorgenti (Cicchella, et al., 2010; de Wuilloud et al., 2002; Dinelli et al., 2012; Mann, et al., 2003; Vardè et al., 2015a; 2015b; 2017; 2019a; 2019b; 2019c; 2019d). La comparazione tra i livelli di Hg tra acque potabili e minerali può fornire indicazioni sull'eventuale apporto di Hg dai bacini di approvvigionamento dell'acqua da fiumi, laghi, e acque sotterranee, dai processi di potabilizzazione e dai fenomeni corrosivi di solidi contenenti Hg presenti nelle tubazioni della rete di distribuzione. Le concentrazioni di Hg nelle acque minerali possono invece dipendere dall'interazione acqua-roccia all'interno delle falde acquifere (Vardè et al., 2015b; 2017; 2019a; 2019b; 2019c; 2019d). Per le acque destinate al consumo umano (acque potabili) la normativa internazionale e nazionale di settore fissa il limite di Hg a livelli di pochi µg/L (es. 2.0 µg/L, US-EPA, 2018; 1.0 µg/L, Direttiva EU 1998/83/EC; D.Lgs. 31/2001). In Italia, per le acque minerali è stabilito a 1.0 µg/L il limite di concentrazione massima per il mercurio totale (D.M. 29/12/2003).

1.6 Mercurio nel suolo

Il mercurio, come altri metalli pesanti, è un elemento naturale distribuito nella crosta terrestre. La sua presenza è legata al tipo di minerale che caratterizza il suolo, oltre agli eventuali apporti provenienti dalle attività antropiche (es. scarichi industriali) o da sorgenti naturali (es. emissioni vulcaniche).

Nei suoli caratterizzati da argille, graniti, e feldspati la concentrazione di Hg è generalmente inferiore a 0.01 mg/kg, mentre nei suoli e nei sedimenti non mercuriferi di aree di background le concentrazioni possono arrivare a 0.2 mg/kg. L'aumento delle concentrazioni di Hg in queste aree viene imputato all'apporto delle precipitazioni atmosferiche. Rispetto alle rocce, i suoli mostrano una variazione maggiore nella concentrazione di Hg per l'influenza di fattori chimici e/o ambientali. Il minerale di mercurio più diffuso è il cinabro (HgS, rosso), caratterizzato da cristalli di forma α-esagonale, mentre il meta-cinabro (HgS, nero), si presenta con forma cristallina β-cubica. A partire dal minerale, il mercurio viene ottenuto dopo condensazione del Hg vaporizzato durante l'arrostimento del cinabro con temperature che raggiungono i 500°C.

I suoli in prossimità di miniere di oro e di altri metalli possono contenere livelli di Hg da 0.05 mg/kg fino a 2 mg/kg (Beckers e Rinklebe, 2017). Le misure di Hg effettuate nelle vicinanze di depositi di mercurio hanno mostrato livelli fino 100 mg/kg (Adriano, 2001). Il contenuto di mercurio nei suoli ha le concentrazioni maggiori presso i siti di miniere di Hg. Nell'area della miniera di Idrija (Slovenia) i livelli di Hg determinati variano da 3 mg/kg nelle zone adiacenti alle miniere, fino a 37000 mg/kg all'interno del sito di estrazione (Gosar et al., 2006; Tersic et al., 2011).

Complessivamente, fattori come le caratteristiche tettoniche e mineralogiche dell'area, la composizione del suolo (presenza di sostanza organica e di microflora, di agenti complessanti organici e inorganici, di ossidi/idrossidi pedogenetici), il potenziale redox (E_h), la forma chimica di Hg (principalmente Hg^{2+}) e il pH, determinano la speciazione, l'assorbimento, il grado di biodisponibilità, il destino e la mobilità del Hg nei suoli e il potenziale livello di contaminazione (Davis et al., 1997).

La contaminazione del Hg da scarichi di un impianto cloro-soda ha determinato per decenni nel suolo la presenza del Hg in forma idrosolubile, e la sua persistenza è risultata dipendente sia dalla forma chimica (complessi di Hg^{2+}) che dalle caratteristiche fisiche e chimiche del suolo stesso. Suoli irrigati con acque contaminate da scarichi di un impianto di produzione di acetaldeide hanno fatto registrare livelli di Hg fino a oltre 300 mg/kg (Matsuyama et al., 2004). In generale, i suoli non contaminati dovrebbero presentare una concentrazione media

non superiore a 0.1 mg/Kg. Tuttavia, in alcuni paesi, questo livello medio di Hg è risultato superiore (Beckers e Rinklebe, 2017). In particolare, la formazione di CH_3Hg^+ nei suoli, nei sedimenti salmastri e di acqua dolce, avviene in condizioni anaerobiche per azione di batteri solfato-riducenti, come sottoprodotto del loro metabolismo (Compeau and Bartha, 1985; Gilmour et al., 1992; King et al., 2000).

Inoltre, il CH_3Hg^+ essendo un catione si combina facilmente con gli ioni presenti negli acidi umici e fulvici del suolo come il cloruro (Cl^-), l'idrossido (OH^-), e il nitrato (NO_3^-) (Skyllberg et al., 2006). Oltre alla metilazione biotica di Hg promossa dai batteri, sono state osservate condizioni abiotiche per la formazione di CH_3Hg^+, evidenziate nei terreni agricoli trattati con nitrato di mercurio (Beckert et al., 1974; Hintelmann, 2010; Rogers, 1977). In superficie, nei suoli di background, le proprietà fisiche del suolo, i parametri meteorologici e le concentrazioni di Hg nell'aria governano sia le emissioni che l'adsorbimento di Hg proveniente dalle deposizioni atmosferiche. Lo scambio di Hg suolo-aria può essere influenzato da una serie di fattori, come la produzione di Hg^0 per riduzione di Hg^{2+}, la diffusione/trasporto di Hg^0 all'interno del suolo, in superficie, e allo strato limite suolo-aria. Alcune osservazioni hanno dimostrato come l'emissione di Hg^0 dal suolo viene attivata dalla radiazione solare mentre la sua deposizione avviene principalmente durante la notte. L'umidità del suolo, la temperatura e la presenza di ossidanti atmosferici risultano importanti fattori nel controllo delle emissioni da suoli a basso contenuto di mercurio (Gustin et al., 2006; Xin and Gustin, 2007).

1.7 Mercurio nel biota

Il più grave disastro legato all'inquinamento da Hg avvenne nel distretto di Minamata in Giappone tra gli anni 1953-1960. Con 1000 morti e circa due milioni di casi di avvelenamento, vennero accertate alterazioni congenite e danni neurologici riconducibili all'assunzione di pesce contaminato da CH_3Hg^+. Alte concentrazioni di CH_3Hg^+ misurate nei pesci e nei molluschi (da 5 a 40 μg/g) furono causate dallo sversamento delle acque reflue di un'industria chimica (Chisso Co. Ltd.) all'interno della baia di Minamata, nel mare di Shiranui (D'Itri and D'Itri, 1978; Harada 1995; Villanueva and Botello, 1998).

L'azienda Chisso Corp., dal 1932 e fino al 1968, aveva utilizzato il Hg inorganico come catalizzatore per la produzione di acetaldeide e cloruro di vinile, sottoprodotti intermedi per la realizzazione di materie plastiche. Effetti cronici sull'uomo con esposizione a basse

concentrazioni sono stati riconosciuti a carico dell'apparato digerente, dei polmoni e dei reni, del sistema immunitario, oltre a danni al feto con successivi effetti sulle abilità motorie e visive, sulla capacità di ragionamento e della memoria (Ekino et al., 2007; Ratcliffe et al., 1996).

Tra il 1971 e il 1972 a Bassora, in Iraq, si registrano oltre 400 morti e circa 6000 persone avvelenate, a causa dell'impiego di un fungicida a base di etilmercurio nelle coltivazione di cereali (Bakir et al., 1973; Ratcliffe et al., 1996).

Una contaminazione da Hg con concentrazioni fino a 0.5 mg/Kg nei pesci del lago Saint Clair fu rilevata in Canada tra il 1970 e il 1971. A causa del rilascio di Hg da parte di un'industria chimica (impianto cloro-soda) nelle acque del lago le autorità imposero il divieto di pesca nel lago e nel fiume Saint Clair (Mahan, 2000).

Gli incidenti ambientali occorsi nel recente passato sono la testimonianza di come un uso e gestione errati di elementi e/o sostanze chimiche tossiche possa arrecare danni inestimabili all'ambiente e all'uomo. Le conoscenze scientifiche maturate nel corso degli ultimi decenni hanno sensibilizzato notevolmente sia l'opinione pubblica che i policy makers.

1.8 Tossicità del mercurio

Le differenti forme chimiche, di natura inorganica e organica, con cui si presenta il mercurio, hanno la capacità di legarsi ai gruppi contenenti zolfo e selenio, provocano l'alterazione della struttura terziaria e quaternaria delle proteine, compromettendo la funzione cellulare. In questo modo il Hg ha la potenziale capacità di alterare le funzioni di varie strutture cellulari e di molti organi. I vapori di mercurio elementare (Hg^0) hanno come organo bersaglio il sistema nervoso centrale. Effetti negativi sono stati evidenziati anche al sistema nervoso periferico, al sistema immunitario, alla funzionalità endocrina, renale e muscolare, oltre ad alcuni tipi di dermatite (Berlin, 2003; Bernhoft, 2012).

L'esposizione acuta al mercurio elementare provoca stati di aumentata eccitabilità e tremori. Altri sintomi riconosciuti sono la perdita di memoria, insonnia, depressione, affaticamento e nei casi più gravi delirio e allucinazioni (Baldi et al., 1953; Garnier et al., 1981). Questi sintomi neurologici sono comunemente persistenti anche se possono regredire con l'interruzione dell'esposizione. Elevate concentrazioni di sali inorganici di Hg^{2+} (es. $HgCl_2$) provocano danni ai reni e al tratto gastro intestinale accompagnati da dolori addominali,

vomito e diarrea. In alcuni casi si può arrivare al decesso a causa di sopravvenuta peritonite o shock setticemico (Barnes et al., 1980).

L'esposizione professionale cronica a Hg^0 raramente ha causato avvelenamento. I danni sono principalmente a carico del sistema immunitario e dei reni. Altre reazioni di ipersensibilità hanno provocato asma e dermatite.

Il CH_3Hg^+ può interferire con le funzioni cellulari o subcellulari, con la trascrizione del DNA e con la sintesi proteica, anche durante la fase di sviluppo del cervello. Altre evidenze accertate sono la rottura di elementi subcellulari nel sistema nervoso centrale e in altri organi, la generazione di radicali liberi, la distruzione dei neurotrasmettitori, e danni al sistema nervoso periferico. La capacità del metilmercurio di reagire con i gruppi sulfidrilici in tutto il corpo può dare origine a sindrome da stanchezza cronica (Bernhoft 2012).

1.9 Materiali e metodi

Nei paragrafi che seguono verranno descritti i principali metodi strumentali per la determinazione del Hg in aria ambiente e in matrici acquose, ovvero le matrici ambientali prese in esame nei casi studio della tesi.

1.9.1 Determinazione del Hg in atmosfera

Le specie di mercurio determinate in aria ambiente sono classificate nelle tre forme: mercurio elementare, mercurio inorganico e mercurio organico. Il mercurio metallico a causa della sua elevata volatilità vaporizza velocemente dal suo stato liquido. Il mercurio inorganico rappresenta la forma salina inorganica, classificata come reattiva o ossidata, i cui composti più conosciuti sono $HgCl_2$, $HgBr_2$, $Hg(OH)$, $HgOBr$, $Hg(NO_3)_2$, $HgSO_4$ e HgO. In atmosfera, la frazione di mercurio che si trova adsorbita al materiale particellare rappresenta una quantità circa <1%. Pertanto, dal punto di vista "operazionale" si possono distinguere tre classi: il mercurio gassoso elementare (GEM o Hg^0), il mercurio reattivo (ossidato) gassoso (RGM, GOM o $Hg^{2+}_{(g)}$) e il mercurio reattivo (ossidato) nel materiale particellare totale o nella frazione PM2.5 (TPM, PBM o $Hg_{(p)}$). La frazione di mercurio nei composti organici in fase gassosa, rappresenta una piccola frazione (<3%) sul totale del mercurio gassoso in atmosfera, prevalentemente CH_3Hg^+ e $(CH_3)_2Hg$. Questa frazione organica non è comunemente misurata, per le bassissime concentrazioni in aria ambiente e le difficoltà tecniche di determinazione (Pandey et al., 2011). La forma prevalente in atmosfera è il GEM (>95%), mentre la restante percentuale di mercurio reattivo è distribuita tra la fase gassosa e quella particellare.

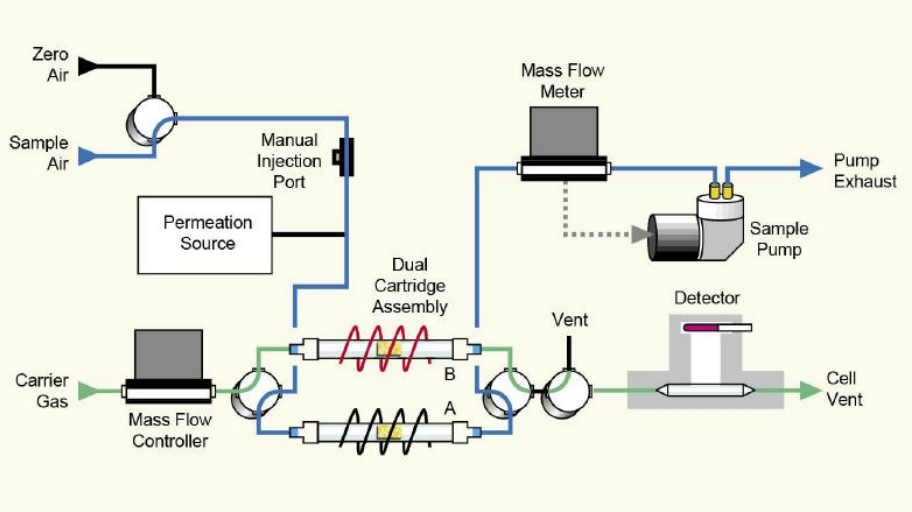

Figura 4. Schema dell'analizzatore di mercurio (Tekran 2537)

Numerosi studi sul mercurio in atmosfera hanno utilizzato per la determinazione di mercurio gassoso totale (TGM=GEM+RGM) o GEM, un analizzatore automatico che si basa sulla preconcentrazione del Hg campionato su 2 trappole di oro, successivo desorbimento termico, seguito dalla determinazione in spettrometria di fluorescenza atomica a vapori freddi (CV-AFS) (es. Tekran 2537) (Fig. 4) (Lyman et al., 2020; Pandey et al., 2011). Altra strumentazione automatica sfrutta il sistema preconcentrazione/desorbimento su trappola di oro con un sistema di rivelazione basato su assorbimento atomico a vapori freddi (CV-AAS) (es. Mercury Vapor Monitor VM-3000, Mercury Instrument, Envea; Gardis-7) o assorbimento atomico con effetto Zeeman (Mercury Monitor RA-915AM, Lumex). La determinazione del mercurio gassoso può essere eseguita anche con metodi manuali, effettuando il campionamento su trappole di oro e successivamente utilizzando strumentazione da laboratorio per il desorbimento e la quantificazione del Hg tramite CV-AFS o CV-AAS (Pandey et al., 2011; Lyman et al., 2020). Alcuni studi, impiegando la strumentazione menzionata, hanno calcolato l'incertezza della misura del Hg atmosferico espresso come TGM o GEM, per definire la forma di Hg gassoso più corretta presente in atmosfera (Gustin et al., 2015; Lyman et al., 2020). Nella pratica, a monte degli analizzatori di mercurio sono stati applicati dei sistemi di pirolizzazione del campione per la determinazione complessiva di GEM, RGM e PBM. Diversamente, è stato adottato l'impiego di filtri o cicloni per la rimozione del PBM, i quali però possono dare luogo alla eliminazione indesiderata di RGM o alla formazione secondaria di RGM dal PBM (Lyman et al., 2020). La determinazione delle tre forme "speciate" del mercurio atmosferico viene effettuata con una strumentazione che integra all'analizzatore di GEM, moduli aggiuntivi. Nel complesso, il sistema di campionamento e analisi per la speciazione del mercurio è basato su 4 unità gestite in maniera sincronizzata per mezzo di un controller (Tekran 2537/1130/1135) (Fig. 5). L'aria ambiente viene campionata attraverso la linea riscaldata alla temperatura di 50 °C per mezzo del modulo pompa e dalla pompa dell'analizzatore. L'aria campione passa (i) all'ingresso attraverso un ciclone con il quale avviene la selezione del particolato atmosferico (diametro aerodinamico <2.5μm); (ii) successivamente l'aria campionata arriva all'interno del denuder anulare ricoperto con un soluzione satura di KCl, nel quale viene adsorbito il mercurio reattivo (RGM); (iii) una volta avvenuto il desorbimento termico l'aria campione raggiunge una sezione tubolare di quarzo nella quale è alloggiato un filtro di quarzo sul quale viene raccolto il particolato fine (PM2.5). Simultaneamente, una parte del campione di aria raggiunge l'analizzatore dove viene effettuata la misura di GEM. Il sistema di speciazione in condizione ordinarie è programmato

per il campionamento di RGM e PBM generalmente ogni due ore, mentre l'analizzatore Tekran 2537 esegue la misura del mercurio elementare con cadenza temporale di cinque minuti, in modo da avere in totale 24 cicli di analisi relativi alla misura del mercurio elementare gassoso. Metodi alternativi per la raccolta del PBM hanno sfruttato campionatori ad alto volume (es. flusso >300 L/min) su filtri in quarzo pre-trattati termicamente. La determinazione del Hg sul particolato viene eseguita successivamente impiegando metodi standardizzati e strumentazione da laboratorio idonea all'analisi di Hg a basse concentrazioni (ICP-MS, CV-AAS, CV-AFS).

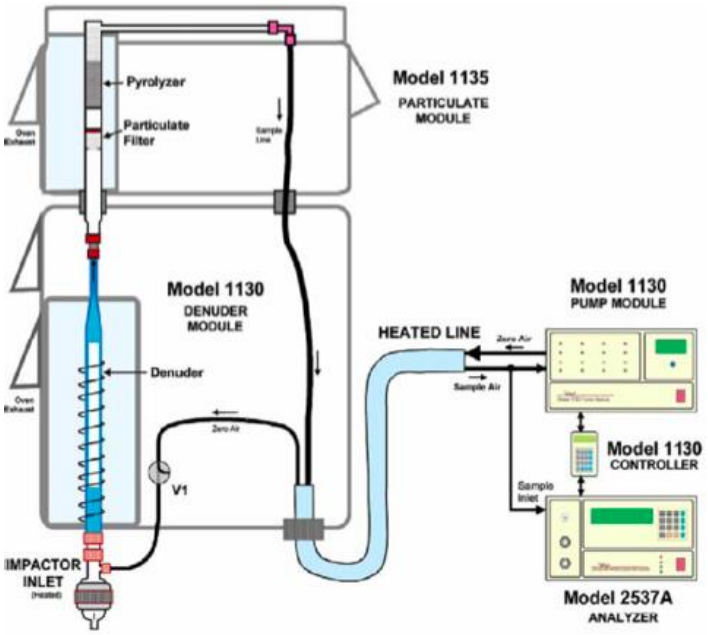

Figura 5. Schema del sistema integrato di speciazione del mercurio (Tekran)

Per entrambi i sistemi di campionamento e determinazione del Hg (automatico e manuale su filtro), ad oggi non esiste una modalità standardizzata di calibrazione per le specie reattive. Questo gap operativo comporta incertezza sulle determinazioni di PBM e RGM, considerando che RGM può aderire al filtro e/o al materiale particellare. In aggiunta il PBM può subire reazione di riduzione e quindi volatilizzare come GEM (Gustin et al., 2015).

1.9.2 Normativa in aria ambiente: assenza di valore limite

La determinazione del mercurio in atmosfera deve essere eseguita rispettando la conformità al metodo di riferimento del Comitato Europeo di Standardizzazione (CEN) attualmente basato sull'impiego della spettrometria di fluorescenza atomica (AFS) o della spettrometria

di assorbimento atomico (AAS), così come riportato nella Direttiva 2004/107/EC. Metodi standard nazionali e internazionali (es. ISO, Organizzazione Internazionale per la Standardizzazione), o altri metodi se dimostrati equivalenti, possono in alternativa essere applicati. Il Comitato Tecnico CEN/TC 264 "Qualità dell'aria ambiente" ha elaborato nel 2010 i metodi standard per la determinazione del mercurio gassoso totale (EN 15852:2010) e del mercurio totale nelle deposizioni atmosferiche (EN 15853:2010). Attualmente non sono stati fissati valori limite di concentrazione per il mercurio in aria ambiente e nelle precipitazioni atmosferiche a livello europeo o nazionale. Le più recenti Direttive Europee (2004/107/EC; 2008/50/CE) e il Decreto Legislativo italiano (D.Lgs. 155/2010) raccomandano misure indicative di Hg (gassoso, reattivo e particolato), classificato come inquinante pericoloso per l'uomo e l'ambiente, suggerendo punti di campionamento di fondo ogni 100000 km^2. In dettaglio, il decreto ministeriale (D.M. 29/11/2012), in attuazione del Decreto Legislativo n.155/2010, procede all'individuazione delle stazioni speciali di misurazione della qualità dell'aria e prevede la misura della concentrazione di Hg (gassoso totale, mercurio reattivo e particolato) su una stazione e la misura di Hg totale nelle deposizioni su 5 stazioni (D.M. 29/11/2012).

Per l'Europa, la Direttiva 2008/50/CE (recepita in Italia nel D.Lgs. 155/2010) fissa i criteri relativi alle caratteristiche delle stazioni di monitoraggio. Secondo i criteri di macro scala, le stazioni vengono classificate, sulla base della loro localizzazione, in: urbane, suburbane, rurali e di fondo rurale. Per meglio comprendere i meccanismi di formazione e trasporto degli inquinanti gassosi e del particolato atmosferico, è stato istituito con Decreto Ministeriale (D.M. 5/05/2015) un miglioramento della rete delle stazioni di monitoraggio presente nei regolamenti precedenti, fornendo i metodi di riferimento per il campionamento e l'analisi, e prevedendo l'installazione di stazioni supplementari per misurazioni aggiuntive (mercurio gassoso totale in aria ambiente e mercurio totale nelle deposizioni atmosferiche). La Direttiva (UE) 2015/1480 recepita con Decreto Ministeriale (D.M. 26/01/2017) ha modificato alcune parti relative ai metodi di riferimento, alla validazione dei dati e all'ubicazione dei punti di prelievo per la valutazione della qualità dell'aria ambiente riportate negli allegati delle Direttive 2004/107/CE e 2008/50/CE. Linee guida europee per una migliore qualità dell'aria ambiente relative al mercurio sono considerate essenziali per poter effettuare il controllo delle emissioni di mercurio atmosferico e per riuscire nella riduzione dell'impatto del mercurio sulla salute umana e sul biota (Pirrone 2001). Per il monitoraggio del mercurio e i suoi composti, espressi come mercurio totale, da fonti stazionarie, è stato fissato il valore limite giornaliero a 50 $\mu g/m^3$ (D.Lgs. 133/2005, Allegato 1). La determinazione del Hg totale alle emissioni deve avvenire mediante un sistema di

misura automatizzato seguendo il metodo di riferimento (EN 14884: 2005). Tuttavia, in Italia non sono state ancora stabilite linee guida per la qualità dell'aria ambiente per il Hg, e soltanto un valore limite per il Hg e i suoi composti bivalenti inorganici aerodispersi è stato fissato a 20 ng/m^3 su 8 ore, esclusivamente per l'esposizione professionale nei luoghi di lavoro (D.M. 6/08/2012). L'agenzia statunitense per le sostanze tossiche e il registro delle malattie (Agency for Toxic Substances and Disease Registry, ATSDR) e la Environmental Protection Agency (US-EPA) hanno suggerito rispettivamente i seguenti valori guida, entrambi basati sulla concentrazione media annuale: (i) 0.2 µg/m^3 come livello di rischio minimo (MRL) per sostanze pericolose (ATSDR, 2020); (ii) 0.3 µg/m^3 come concentrazione di riferimento per l'esposizione cronica per inalazione (RfC) al mercurio elementare (US-EPA) (IRIS, 1988). L'Organizzazione mondiale della Sanità (World Health Organization, WHO) ha stabilito a 1.0 µg/m^3 il livello più basso per i vapori di mercurio inorganico con effetti avversi osservati (LOAEL) (WHO, 2012).

1.9.3 Determinazione del Hg in matrici acquose

La misura e il controllo del Hg nei corpi idrici è cruciale per valutare gli effetti negativi del Hg sulla qualità dell'acqua e sugli organismi viventi, e più in generale per la protezione dell'ambiente e della salute pubblica. In acqua, la forma ossidata di mercurio (Hg^{2+}) è la più abbondante. La determinazione del Hg risulta fondamentale poiché la sua presenza può portare alla conversione nelle forme organiche più tossiche (CH_3Hg^+, $(CH_3)_2Hg$) e bioaccumulabili. In acqua, la concentrazione di mercurio si trova generalmente nell'intervallo di pochi ppt-ppb. Nelle acque superficiali e nelle acque sotterranee il livello medio di Hg è inferiore a 0.5 µg/L, nelle deposizioni atmosferiche tra 5-100 ng/L, e nelle acque potabili la concentrazione media è circa 25 ng/L, anche se sono stati accertati negli USA casi di superamento del limite di 2.0 µg/L (US-EPA, 2018), così come riscontrato nell'isola di Izu Oshima Island (Giappone), con concentrazioni di Hg fino a 5.5 µg/L nelle acque sotterranee (WHO, 2005).

I metodi strumentali più diffusi per la determinazione/speciazione del mercurio in acqua sono l'assorbimento atomico a vapori freddi (CV-AAS) e la spettrometria di massa con sorgente di ionizzazione al plasma accoppiato induttivamente (ICP-MS). Negli ultimi anni, l'impiego di questi strumenti, con metodi analitici ottimizzati e a reagenti di elevata purezza, hanno permesso di raggiungere limiti di quantificazione fino a sub-ppt (Cairns et al., 2008; de Wuilloud et al., 2002; Minnich et al., 2008; Passariello et al., 1996). Altri strumenti comunemente utilizzati includono la spettrometria di emissione atomica al plasma accoppiato induttivamente (ICP-AES) o di emissione ottica (ICP-OES), la spettrometria di assorbimento atomico elettrotermico (ET-AAS) (Arpadjan et al., 1997), e la gascromatografia-spettrometria di massa con desorbimento termico (TD-GC-MS) (Ito et al., 2009). Altre tecniche analitiche utilizzate per la determinazione del mercurio in acqua (e in altre matrici ambientali), sono il sistema a iniezione di flusso per la rilevazione di Hg (FIMS), e il sistema di analisi a iniezione di flusso accoppiato alla spettrometria a fluorescenza atomica (FIA-AFS). Diverse procedure di pretrattamento, pre-concentrazione e rilevamento sono state applicate per l'analisi di speciazione del mercurio in acque naturali (Leopold et al., 2010). L'ICP-MS con la tecnica della diluizione isotopica (ID) e generazione di vapori freddi ha dimostrato elevata sensibilità e selettività. Tuttavia, il costo della strumentazione ID-ICP-MS e degli standard isotopici può essere ancora proibitivo per molti laboratori di controllo e di ricerca (Mann et al., 2003). La spettrometria di fluorescenza atomica a vapori freddi (CV-AFS) è una tecnica meno costosa, e negli ultimi anni ha trovato ampio impiego per l'elevata sensibilità e il basso consumo di campione, oltre a risentire di basse interferenze (Knox et al., 1995; Zi et al., 2009).

1.9.3.1 Determinazione del Hg tramite CV-AFS e metodo US-EPA 1631

I campioni di acqua da analizzare, all'arrivo in laboratorio vengono registrati, inseriti in un sacchetto di plastica e conservati in ambiente pulito e buio a temperatura ambiente (~20°C), per evitare contaminazioni indesiderate (Rahmanian et al., 2015). Il campione di acqua (50 mL) viene trasferito in una provetta in polipropilene (PP), preventivamente lavata con una soluzione di acido cloridrico diluito, e immediatamente aggiunto HCl (UpA, ultrapuro) alla concentrazione finale dello 0.5% (v/v) allo scopo di minimizzare la volatilizzazione di Hg.

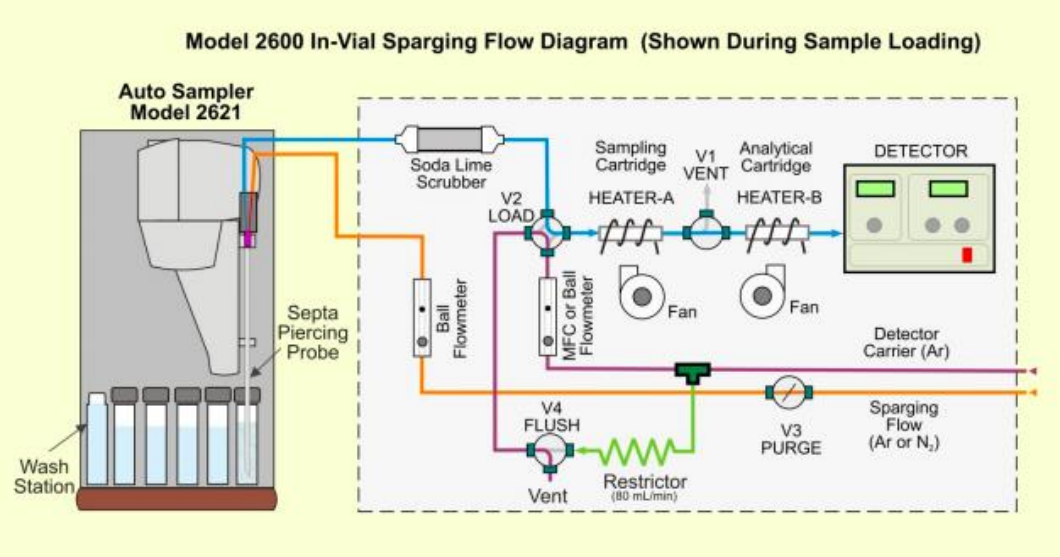

Figura 6. Schema semplificato di uno spettrometro di fluorescenza a vapori freddi

Addizionando bromocloruro (BrCl) alla concentrazione finale dello 0.5% (v/v), tutte le forme del Hg vengono ossidate a Hg^{2+}. Per omogeneizzare il campione e consentire la digestione a temperatura ambiente, ciascuna provetta in PP viene sigillata e agitata, e controllata la persistenza del colore giallo della soluzione per garantire l'eccesso di BrCl. Un'ora prima dell'analisi, viene aggiunta idrossilammina cloridrato ($NH_2OH•HCl$) (soluzione allo 0.2% v/v), per ridurre qualsiasi eccesso di BrCl. Il mercurio bivalente (Hg^{2+}) viene così ridotto a mercurio elementare (Hg^0) utilizzando stagno cloruro diidrato ($SnCl_2•2H_2O$). Successivamente, il Hg^0 viene pre-concentrato su una doppia trappola in oro, dove viene amalgamato in due fasi, prima su una trappola campione e poi su trappola analitica (Gill and Fitzgerald, 1987). Il mercurio elementare viene desorbito termicamente dalle trappole d'oro e trasportato nella cella della CV-AFS. In Fig. 6 è riportato lo schema

semplificato dello spettrometro a fluorescenza atomica a vapori freddi (CV-AFS) della Tekran serie 2600 che sfrutta il metodo US-EPA 1631 versione E (US-EPA, 2002) per la determinazione del Hg in ultratracce in matrici acquose.

1.10 Studio del mercurio in Italia

Le Agenzie Regionali per la Protezione Ambientale (ARPA) coordinate dall'Istituto per la Protezione e la Ricerca Ambientale (ISPRA) hanno effettuato negli ultimi anni misure di mercurio su scala locale in aree di particolare interesse ambientale, come quelle in prossimità di una centrale geotermica (Bagnoli and Gartner, 2017), di una centrale termica a carbone, di un inceneritore e in un'area rurale utilizzando analizzatori automatici e sistemi di monitoraggio in continuo delle emissioni per il Hg (Fontana et al., 2018).

Altre misurazioni di mercurio atmosferico sono state effettuate in zone suburbane/rurali da gruppi di ricerca di università e agenzie di ricerca (Munthe et al., 2001; Sprovieri et al., 2016; Vardè et al., 2014; 2019e; 2019f) in ambiente marino e costiero (Bagnato et al., 2013; Barago et al., 2020; Castagna et al., 2018; Fantozzi et al., 2013), in aree vulcaniche/geotermiche e minerarie (Bagnato et al., 2009; Barghigiani et al., 1990; Cabassi et al., al., 2017; Dedeurwaerder et al., 1982; Ferrara et al., 1994; Ferrara et al., 1998; Ferrara et al., 2000).

L'esecuzione congiunta di misure di mercurio in aria ambiente e nelle deposizioni atmosferiche, e l'organizzazione di attività di ricerca condivise tra i paesi dell'Unione Europea era stata suggerita, con l'obiettivo di realizzare una rete europea di stazioni di monitoraggio per indagini integrate sul mercurio (Pirrone and Wichmann-Fiebig 2003).

Il network europeo non è stato ad oggi realizzato, né tantomeno una rete di osservazione volontaria per la misura delle specie di mercurio in atmosfera.

Tuttavia, attraverso il finanziamento del settimo programma quadro della Comunità Europea (FP7) è stato realizzato il primo sistema di osservazione globale sul mercurio (GMOS) con il compito di sostenere la Convenzione di Minamata. La rete di monitoraggio del mercurio atmosferico è costituita da oltre 35 osservatori collocati sia nell'emisfero settentrionale che meridionale. Le misure di Hg raccolte nel periodo 2010-2015 sono state integrate da attività di monitoraggio effettuate durante campagne oceanografiche e da studi nell'alta troposfera tramite aeroplani (Sprovieri et al., 2016).

In Italia, l'accordo tra il Ministero dell'Ambiente, Tutela del Territorio e del Mare (MATTM), Enti di ricerca (CNR ed ENEA) e l'Istituto Superiore di Sanità (ISS), ha permesso di istituire l'accordo "Reti Speciali" con la finalità di costituire una rete di stazioni di monitoraggio ai sensi del D.Lgs. 155/2010 per la misura di diversi inquinanti atmosferici (es. IPA, As, Cd, Ni, Hg, ozono e suoi precursori, concentrazione di massa di PM2.5 e caratterizzazione chimica). Sono stati selezionati siti di background e rurali, dislocati da nord a sud dell'Italia, per contribuire al miglioramento della conoscenza dei fenomeni di formazione e trasporto dei contaminanti atmosferici, potenziare efficacemente le strategie di riduzione delle

emissioni e migliorare la qualità dell'aria per la protezione dell'ambiente e della salute della popolazione.

Capitolo 2

In questo capitolo sono presentate le sintesi dei lavori pubblicati e/o pronti per la fase di sottomissione su rivista indicizzata. I lavori per esteso, inseriti nell'appendice, sono successivi al Capitolo 2 e seguono l'ordine riportato di seguito.

2.1 Caso studio 1: Mercurio in atmosfera in un sito di alta quota nelle Alpi italiane

Pubblicazione 1/A (in fase di sottomissione)

Nell'ambito del progetto Integrated Global Observing Systems for Persistent Pollutants (iGOSP, http://www.igosp.eu/) e precedentemente del Global Mercury Observation System (GMOS, http://www.gmos.eu/) per lo studio del mercurio atmosferico su scala mondiale, l'Osservatorio di Col Margherita (MRG), insieme all'osservatorio di Monte Curcio in Sila, rappresenta una delle 2 stazioni remote di alta quota in Italia. L'altitudine e la distanza dalle principali fonti antropiche e naturali di inquinanti atmosferici fanno di MRG un sito ideale per il monitoraggio del mercurio e per lo studio del suo ciclo nelle Alpi orientali. In questo caso studio, è stato preso in considerazione un dataset continuo di concentrazioni di mercurio gassoso totale (TGM), ozono e i principali parametri meteorologici, relativo all'osservatorio di Col Margherita, per indagare la variabilità del TGM a livello stagionale, mensile e diurno e per esplorare la relazione con i parametri ambientali considerati. Le misurazioni di TGM sono state effettuate da marzo 2018 a maggio 2019. La concentrazione media su base annuale di TGM è risultata superiore alle precedenti misure registrate durante GMOS. La variazione stagionale del TGM è stata caratterizzata da valori elevati nella primavera-estate 2018 e valori più bassi in inverno. Nelle diverse stagioni si è inoltre osservato un profilo giornaliero simile per il TGM, con concentrazioni inferiori durante il giorno e più elevate nella tarda serata/notte. Strumenti di valutazione spaziale, cambiamenti temporali delle concentrazioni di TGM, analisi delle retro-traiettorie e dello strato limite del pianeta (PBL) hanno suggerito che i livelli di TGM risultano influenzati dalla meteorologia locale, dal trasporto regionale e a lungo raggio delle masse d'aria. In inverno, i livelli di TGM inferiori sono stati associati a: (i) alta velocità del vento, (ii) basso livello della quota del PBL e (iii) masse d'aria "più pulite" provenienti dal settore dell'Europa occidentale. In primavera ed estate, l'altezza del PBL oltre il sito di MRG può aver contribuito al trasporto di mercurio gassoso da aree più inquinate, come confermato dall'analisi delle retro-traiettorie delle masse d'aria che hanno transitato dall'Europa nord-orientale e continentale. Durante la stagione di copertura nevosa,

è stata eseguita una indagine sugli eventi di picco del TGM. È stata inoltre esaminata la potenziale influenza dei processi di riemissione del mercurio reattivo precedentemente depositato sulla superficie del manto nevoso.

2.2 Caso studio 2: Comparazione dei livelli di mercurio nelle acque potabili e nelle acque minerali naturali in Calabria

Pubblicazione 2/A

In questo studio è stato effettuato il confronto del contenuto inorganico delle acque destinato al consumo umano (potabili) e delle acque minerali naturali (in bottiglia) campionate in Calabria. Tale comparazione è stata realizzata utilizzando l'analisi compositiva dei dati (CoDA, Compositional Data Analysis) e un nuovo approccio grafico-numerico. Trentuno campioni di acque potabili, da differenti province del territorio calabrese, e ventuno campioni di acque minerali naturali, di varie marche prodotte in Calabria, sono stati raccolti. In totale, sono stati analizzati 29 parametri tra i principali componenti inorganici e in traccia. La determinazione del mercurio totale è stata eseguita in un laboratorio "pulito" dedicato mediante la spettrometria di fluorescenza atomica a vapori freddi. L'analisi compositiva dei dati è stata impiegata per identificare le principali relazioni tra i parametri chimico-fisici, evidenziando le differenze tra le acque potabili e le acque minerali in bottiglia. Tuttavia, il Hg non è stato incluso nell'analisi CoDA in quanto determinato con un metodo analitico differente, una diversa strategia/tipologia di campionamento e un livello di concentrazioni risultato di un ordine di grandezza inferiore rispetto agli altri parametri.

In generale, alcuni elementi (Al, Mn, Fe, Zn, and Pb) sono risultati particolarmente arricchiti nelle acque del rubinetto; la causa è probabilmente riconducibile a processi di corrosione all'interno delle tubazioni metalliche della rete di distribuzione dell'acqua potabile. Altri elementi (Li, Ca, Cr, Ni e Cd), sembrano essere per lo più derivati da fonti naturali che influenzano la variabilità complessiva delle acque minerali.

In dettaglio, i livelli medi di Hg sono risultati superiori nelle acque potabili rispetto alle acque minerali, così come le acque in bottiglia frizzanti hanno mostrato concentrazioni medie di Hg superiori rispetto alle acque naturali.

Nel complesso, Cr, Cu, Hg e Pb sono risultati principalmente arricchiti nelle acque minerali frizzanti in bottiglia. In particolare, per il Hg questa caratteristica può essere imputata alla qualità della CO_2 addizionata, o dovuta al rilascio dal sistema di stoccaggio. Gli indici compositivi innovativi utilizzati non hanno evidenziato grandi differenze rispetto alle concentrazioni massime consentite (MAC) nelle due tipologie di acqua. Per la salute del consumatore è indifferente bere acqua potabile o in bottiglia. I risultati rappresentano una base fondamentale per sviluppare adeguati piani di monitoraggio al fine di verificare il mantenimento degli standard di qualità dell'acqua destinata al consumo umano.

2.3 Caso studio 3: Mercurio nelle acque minerali naturali italiane

Pubblicazione 3/A

In questo lavoro è stata effettuata la determinazione delle concentrazioni di mercurio totale nelle acque minerali naturali in bottiglia con l'obiettivo di quantificare il Hg a livelli di ultratracce e comprendere le eventuali relazioni tra la concentrazione di Hg, gli altri parametri ancillari, e le caratteristiche del luogo di provenienza. Il totale di 244 acque italiane campionate rappresentano 164 differenti marchi. In aggiunta, per confronto, sono stati raccolti 11 campioni di acque in bottiglia di altri paesi europei. Le acque italiane provengono da 136 sorgenti dislocate in 18 regioni italiane. I campioni di acque in bottiglia sono stati analizzati impiegando la spettrometria di fluorescenza atomica a vapori freddi, e le concentrazioni di Hg sono state rilevate nell'intervallo da sub-nanogrammi a pochi nanogrammi per litro. Le differenze nelle concentrazioni di Hg sono risultate correlate alle caratteristiche ambientali delle sorgenti, e/o all'influenza di attività umane. Le concentrazioni più elevate si sono riscontrate nei campioni provenienti da regioni caratterizzate dalla presenza di aree minerarie e/o da attività termale/vulcanica. Inoltre, i dati analitici ottenuti hanno permesso di stimare l'assunzione di mercurio dal consumo di acque minerali da parte della popolazione, suddivisa in tre gruppi (adulti, bambini e neonati). L'assunzione giornaliera media di mercurio è risultata notevolmente inferiore, non solo al valore tollerabile provvisorio fissato dalla legislazione europea e italiana, ma anche al valore stimato come dose provvisoria settimanale tollerabile raccomandato dal JECFA, il Comitato di esperti congiunto FAO/WHO sugli additivi alimentari.

2.4 Caso studio 4: Studio dei fattori che controllano la presenza di mercurio nella neve superficiale e lo scambio di Hg tra neve e atmosfera nel plateau Antartico

Pubblicazione 4/A

In questo studio, per la comprensione dell'influenza dei principali parametri ambientali coinvolti nel ciclo del mercurio nella neve superficiale, sono stati elaborati i dati di misure di tre differenti campagne effettuate durante le estati australi sul plateau Antartico.

La strategia di campionamento della neve superficiale è stata modificata progressivamente per ricreare le migliori condizioni operative e ottenere risultati affidabili per la valutazione dei fattori che controllano la presenza di mercurio nel manto nevoso e il loro contributo all'abbondanza del Hg in atmosfera.

La diminuzione della concentrazione di mercurio nella neve e il suo probabile rilascio in atmosfera hanno fornito un effetto diretto sui livelli di mercurio atmosferico. L'aumento del mercurio atmosferico rilevato risulta in ritardo di alcune ore, e questo shift può dipendere dalla struttura verticale e dalla velocità di miscelazione dell'atmosfera (oltre che dalle condizioni meteorologiche). Questi risultati confermano l'ipotesi di influenza reciproca tra il mercurio presente nella neve e in atmosfera.

Sebbene soltanto alcune prove sono emerse dai risultati ottenuti, non risulta comunque netta la distinzione dei processi predominanti e sono necessarie ulteriori indagini, su una scala temporale più lunga, per identificare sia il ruolo dell'intrusione di masse d'aria sia quello dei processi di trasporto a medio e lungo raggio sui livelli di mercurio atmosferico nel plateau Antartico.

Conclusioni

Questa tesi di dottorato, strutturata su 4 distinti lavori, ha l'obiettivo di fornire informazioni riguardanti i livelli di concentrazione e il comportamento di Hg in differenti matrici ambientali: (i) in atmosfera, (ii) nelle acque potabili, (iii) nelle acque minerali naturali e (iv) nella neve superficiale. I complessi meccanismi del ciclo biogeochimico del mercurio spingono i ricercatori all'impiego di un approccio multidisciplinare e di strategie di indagini innovative. Di seguito sono riassunti i principali spunti conclusivi del lavoro di dottorato, presenti nelle pubblicazioni allegate.

- Lo studio delle concentrazioni del mercurio in aria ambiente in un sito Alpino di alta quota suggerisce l'importanza del monitoraggio a lungo termine di questo elemento tossico. Per migliorare la conoscenza della dinamica dei processi in cui è coinvolto il Hg risulta essenziale utilizzare le informazioni derivanti dalla misura di altri parametri ambientali e meteorologici. Inoltre, risulta indispensabile determinare il Hg in tutte le altre matrici che giocano un ruolo di scambio con l'atmosfera (es. neve).

- L'impiego della spettroscopia di fluorescenza atomica a vapori freddi ha permesso di quantificare il Hg a livelli di ultratracce nelle acque potabili e minerali, caratterizzazione che in Italia non era ancora stata realizzata. Oltre ad assicurare per il Hg i bassi livelli di concentrazione e il rispetto ai valori limite di legge, i due casi studio hanno consentito di valutare le differenze tra acque potabili e acque minerali naturali, e tra acque minerali e frizzanti, e di attribuire le potenziali cause della presenza di Hg nelle varie tipologie di campioni esaminati. La conoscenza delle concentrazioni di Hg nei numerosi campioni di acqua ha inoltre permesso di stimare l'assunzione di Hg da parte della popolazione.

- L'analisi di un ampio dataset ottenuto da tre campagne di misura condotte in Antartide ha fornito un quadro dei principali parametri ambientali coinvolti nel ciclo geochimico del mercurio nella neve superficiale del Plateau Antartico. La strategia di campionamento è stata modificata da una campagna alla successiva affinché le migliori condizioni operative scelte potessero produrre risultati affidabili e migliorare la comprensione dei fattori che controllano la presenza di mercurio nella neve superficiale e il potenziale contributo al Hg atmosferico. Sebbene alcune indicazioni siano emerse dai risultati ottenuti, non è risultato semplice discernere i processi predominanti. Sono necessari

ulteriori studi su scala temporale più lunga per poter identificare il ruolo dell'intrusione delle masse d'aria e dei processi di trasporto, a medio e lungo raggio, sui livelli di mercurio atmosferico nel plateau Antartico.

Prospettive future degli studi sul Hg in campo ambientale

- Il monitoraggio del mercurio a lungo termine in stazioni di alta quota, attualmente ancora in numero ridotto rispetto a quelli condotti in altre località, è cruciale per la comprensione dei trend di concentrazione in aree montane remote. La gestione degli osservatori in siti montani risulta ad oggi estremamente dispendiosa per i costi da sostenere, e richiede enormi sforzi anche in termini di personale qualificato e di tempo-uomo. In aggiunta, la determinazione del mercurio gassoso reattivo in forma ossidata (RGM) e del mercurio nella fase particellare (Hg_p) viene ritenuta importante per lo studio del comportamento in atmosfera e nelle altre matrici ambientali, così come l'implementazione di strumenti per la misura di parametri ancillari chimici (oltre a O_3, Br e altri potenziali ossidanti) e fisici (componenti della radiazione solare) per lo studio dei processi fotochimici e ossido-riduttivi che coinvolgono il Hg (Gustin et al., 2021; Zhang et al., 2019).

- Un ottimale monitoraggio del Hg a lungo termine necessita inoltre dell'impiego di piattaforme innovative, con l'utilizzo di nuovi dispositivi (es. campionatori passivi, PAS e sensori) da affiancare e testare in termini di QA/QC nelle condizioni tipiche delle aree montane remote (minore pressione atmosferica, altezza PBL e libera troposfera, condizioni metereologiche dinamiche), oltre a sviluppare/implementare tools modellistici per una migliore rappresentazione della dinamica dei processi chimico-fisici del Hg (Huang et al., 2014; Mao et al., 2016; Mazzolai et al., 2004; McLagan et al., 2018).

- I risultati ottenuti studiando il Hg nella neve superficiale in Antartide suggeriscono di approfondire la ricerca del comportamento del Hg tra la superficie del manto nevoso e l'atmosfera. Queste ricerche, ad alta risoluzione temporale, dovrebbero essere condotte, con continuità e su differenti stagioni, nelle aree remote caratterizzate dall'abbondante presenza di neve, per meglio comprendere la dinamica dei processi del Hg, in termini di reattività e riemissione-riciclo tra atmosfera-neve, e poter valutare il potenziale impatto della presenza del Hg nell'ambiente (es. Artico e siti montani) (Spolaor et al., 2018; Spolaor et al., 2019).

- La presenza di Hg nelle acque potabili è un problema attuale in relazione allo stato di salute dell'ambiente e della popolazione potenzialmente esposta. Una adeguata strategia di campionamento spazio-temporale affiancata da rigorose procedure analitico-strumentali devono continuamente essere applicate per studiare e comprendere le cause della presenza di contaminanti tossici come il Hg. Le determinazioni di Hg nelle acque potabili e minerali

naturali, effettuate con strumentazione dedicata per il Hg, hanno dimostrato la capacità di misurare questo metallo tossico a concentrazioni di ultratracce e di poter valutare le sorgenti e/o altre condizioni causa di potenziale contaminazione con l'applicazione di approcci multidisciplinari (Apollaro et al., 2019; ARPAV, 2019, Università degli Studi di Ferrara, 2019, Vardè et al., 2019a).

Bibliografia

Adriano, D.C., (2001). *Trace elements in terrestrial environments*. New York: Springer-Verlag, 1-796, https://doi.org/10.1007/978-0-387-21510-5.

Angot, H., Dastoor, A., De Simone, F., Gårdfeldt, K., Gencarelli, C. N., Hedgecock, I. M., Langer, S., Magand, O., Mastromonaco, M. N., Nordstrøm, C., Pfaffhuber, K. A., Pirrone, N., Ryjkov, A., Selin, N. E., Skov, H., Song, S., Sprovieri, F., Steffen, A., Toyota, K., Travnikov, O., Yang, X., and Dommergue, A., (2016). *Chemical cycling and deposition of atmospheric mercury in polar regions: review of recent measurements and comparison with models*, Atmos. Chem. Phys., 16, 10735–10763, https://doi.org/10.5194/acp-16-10735-2016.

Apollaro, C., Buccianti, A., Vespasiano, G., Vardè, M., Fuoco, I., Barca, D., Bloise, A., Miriello, D., Cofone, C., Servidio, A., De Rosa, R., (2019). *Comparative geochemical study between the tap waters and the bottled mineral waters in Calabria (Southern Italy) by compositional data analysis (CoDA) developments*, Appl. Geochem., 107, 19-33, https://doi.org/10.1016/j.apgeochem.2019.05.011.

Arpadjan, S., Vuchkova, L., Kostadinova, E., (1997). *Sorption of arsenic, bismuth, mercury, antimony, selenium and tin on dithiocarbamate loaded polyurethane foam as a preconcentration method for their determination in water samples by simultaneous inductively coupled plasma atomic emission spectrometry and electrothermal atomic absorption spectrometry*, Analyst, 122, 243-246, https://doi.org/10.1039/A606917G.

ARPAV, (2020). *Monitoraggio delle acque sotterranee in alcuni comuni della provincia di Treviso per il controllo dell'inquinamento da mercurio (Hg), dati ottobre 2019*. Servizio Osservatorio Acque Interne, Mercurio, https://www.arpa.veneto.it/temi-ambientali/acqua/file-e-allegati/documenti/acque-interne/acque-sotterranee/mercurio201910.pdf.

ATSDR, (2020). *Inorganic Mercury - Minimal Risk Levels (MRLs) for Hazardous Substances*, Agency for Toxic Substances and Disease Registry, MRL List – October 2020, https://www.atsdr.cdc.gov/mrls/mrllist.asp.

Bagnato, E., Parello, F., Valenza, M., Caliro, S., (2009). *Mercury content and speciation in the Phlegrean Fields volcanic complex: Evidence from hydrothermal system and fumaroles*, J. Volcanol. Geotherm. Res., 187 (3-4), 250-260, https://doi.org/10.1016/j.jvolgeores.2009.09.010.

Bagnato, E., Sprovieri, M., Barra, M., Bitetto, M., Bonsignore, M., Calabrese, S., Di Stefano, V., Oliveri, E., Parello, F., Mazzola, S., (2013). *The sea-air exchange of mercury (Hg) in the marine boundary layer of the Augusta basin (southern Italy): Concentrations and evasion flux,* Chemosphere, 93(9), 2024-2032, https://doi.org/10.1016/j.chemosphere.2013.07.025.

Barago, N., Floreani, F., Acquavita, A., Covelli, S., Higueras, P., (2020). *Spatial and Temporal Trends of Gaseous Elemental Mercury over a Highly Impacted Coastal Environment (Northern Adriatic, Italy)*, Atmosphere 11(9), 935, https://doi.org/10.3390/atmos11090935.

Bagnoli, A., and Gartner, I., (2018). *Monitoraggio delle aree geotermiche toscane: Concentrazioni di H_2S e Hg nelle aree geotermiche toscane. Monitoraggi ARPAT e validazione dati Enel (Area Vasta Sud. Report anno 2017)*. Arpa Toscana 2018, Prot. n° 0046235, 1-41, (Technical Report).

Baldi, G.E., Vigliani, E., Zurlo, N., (1953). *Il mercurialismo cronico nei cappellifici*, Med. Lav., 44, 161-198.

Barghigiani, C., Bargagli, R., Siegel, B.Z., Siegel, S.M., (1990). *A comparative study of mercury distribution on the aeolian volcanoes, vulcano and Stromboli*, Water Air Soil Pollut., 53, 179-188, https://doi.org/10.1007/BF00155002.

Barnes, J.L., McDowell, E.M., McNeil, J.S., Flamenbaum, W., & Trump, B.F., (1980). *Studies on the pathophysiology of acute renal failure*, Virchows Archiv B Cell Pathol 32, 201–232, https://doi.org/10.1007/BF02889029.

Beckers, F., & Rinklebe, J., (2017). *Cycling of mercury in the environment: Sources, fate, and human health implications: A review*, Critical Reviews in Environmental Science and Technology, 47(9), 693-794, https://doi.org/10.1080/10643389.2017.1326277.

Beckert, W.F., Moghissi, A.A., Au, F.H.F., Bretthauer, E.W., and McFarlane, J.C., (1974). *Formation of methylmercury in a terrestrial environment*, Nature 249, 674–675, https://doi.org/10.1038/249674a0.

Berlin, M., (2003). *Dental Materials and Health*. Lidmark A, (ed.) Stockholm, Statens Offentliga Utredningar, 17–57.

Bernhoft, R.A., (2012). *Mercury Toxicity and Treatment: A Review of the Literature*, Int. J. Environ. Res. Public Health, 460508, 10, https://doi.org/10.1155/2012/460508.

Biddinger, G.R., Gloss, S.P., (1984). *The Importance of Trophic Transfer in the Bioaccumulation of Chemical Contaminants in Aquatic Ecosystems*, Resid. Rev. 91, 103-145, https://doi.org/10.1007/978-1-4612-5258-0_4.

Bigham, G.N., Henry, B., Bessinger, B., (1964). *1-Mercury*, Environ. Forensics, Academic Press, 1-17, https://doi.org/10.1016/B978-012507751-4/50023-9.

Bishop, K., Shanley, J.B., Riscassi, A., de Wit, H.A., Eklöf, K., Meng, B., Mitchell, C., Osterwalder, S., Schuster, P.F., Webster, J., (2020). *Recent advances in understanding and measurement of mercury in the environment: terrestrial Hg cycling*, Sci. Total Environ., 721, 137647, https://doi.org/10.1016/j.scitotenv.2020.137647.

Cabassi, J., Tassi, F., Venturi, S., Calabrese, S., Capecchiacci, F., D'Alessandro, W., Vaselli, O., (2017). *A new approach for the measurement of gaseous elemental mercury (GEM) and H_2S in air from anthropogenic*

and natural sources: Examples from Mt. Amiata (Siena, Central Italy) and Solfatara Crater (Campi Flegrei, Southern Italy), J. Geochem. Explor., 175, 48-58, https://doi.org/10.1016/j.gexplo.2016.12.017.

Cairns, W.R.L., Ranaldo, M., Hennebelle, R., Turetta, C., Capodaglio, G., Ferrari, C.F., Dommergue, A., Cescon, P., Barbante, C., (2008). *Speciation analysis of mercury in seawater from the lagoon of Venice by on-line pre-concentration HPLC-ICP-MS*, Anal. Chim. Acta, 622, 62-69, https://doi.org/10.1016/j.aca.2008.05.048.

Caley, E. R., (1928). *Mercury and its compounds in ancient times*, J. Chem. Educ., 5(4), 419-424, https://doi.org/10.1021/ed005p419.

Castagna, J., Bencardino, M., D'Amore, F., Esposito, G., Pirrone, N., Sprovieri, F., (2018). *Atmospheric mercury species measurements across the Western Mediterranean region: Behaviour and variability during a 2015 research cruise campaign*, Atmos. Environ., 173, 108-126, https://doi.org/10.1016/j.atmosenv.2017.10.045.

Cicchella, D., Albanese, S., De Vivo, B., Dinelli, E., Giaccio, L., Lima, A., Valera, P., (2010). *Trace elements and ions in Italian bottled mineral waters: Identification of anomalous values and human health related effects*, J. Geochemical Explor., 107, 336-349, https://doi.org/10.1016/j.gexplo.2010.04.004.

Compeau, G.C., and Bartha, R., (1984). *Methylation and demethylation of mercury under controlled redox, pH and salinity conditions*, Appl. Environ. Microb., 48, 1203–1207.

D.Lgs. 31/2001, Decreto Legislativo 2 febbraio 2001, n. 31 Attuazione della direttiva 98/83/CE relativa alla qualità' delle acque destinate al consumo umano. (GU Serie Generale n.52 del 03-03-2001 - Suppl. Ordinario n. 41).

D.Lgs. 133/2005, Decreto Legislativo 11 maggio 2005, n. 133 Attuazione della direttiva 2000/76/CE, in materia di incenerimento dei rifiuti. (GU Serie Generale n.163 del 15-07-2005 - Suppl. Ordinario n. 122), Allegato 1, Norme tecniche e valori limite di emissione per gli impianti di incenerimento di rifiuti, valori di emissione in atmosfera.

D.Lgs. 155/2010, Decreto Legislativo 13 agosto 2010, n. 155 Attuazione della direttiva 2008/50/CE relativa alla qualità' dell'aria ambiente e per un'aria più pulita in Europa. (10G0177) (GU Serie Generale n.216 del 15-09-2010 - Suppl. Ordinario n. 217).

D.M. 29/12/2003, Decreto 29 dicembre 2003, Attuazione della direttiva n. 2003/40/CE della Commissione nella parte relativa ai criteri di valutazione delle caratteristiche delle acque minerali naturali di cui al decreto ministeriale 12 novembre 1992, n. 542, e successive modificazioni, nonché' alle condizioni di utilizzazione dei trattamenti delle acque minerali naturali e delle acque di sorgente. (GU Serie Generale n.302 del 31-12-2003).

D.M. 30/07/2008, Decreto 30 luglio 2008, Recepimento della direttiva 2007/51/CE, che modifica la direttiva 76/769/CEE per quanto riguarda le restrizioni alla commercializzazione di alcune apparecchiature di misura contenenti mercurio. (GU Serie Generale n.245 del 18-10-2008).

D.M. 6/08/2012, Decreto 6 agosto 2012, Recepimento della direttiva 2009/161/UE della Commissione del 17 dicembre 2009 che definisce il Terzo elenco di valori indicativi di esposizione professionale in attuazione della direttiva 98/24/CE del Consiglio e che modifica la direttiva 2009/39/CE della Commissione. (12A09782) (GU Serie Generale n.218 del 18-09-2012). Allegato XXXVIII, valori limite di esposizione professionale, mercurio e composti inorganici divalenti del mercurio compresi ossido mercurico e cloruro di mercurio (misurati come mercurio).

D.M. 29/11/2012, Decreto 29 novembre 2012 Individuazione delle stazioni speciali di misurazione della qualità dell'aria previste dall'articolo 6, comma 1, e dall'articolo 8, commi 6 e 7 del decreto legislativo 13 agosto 2010, n. 155. (12A13349) (GU Serie Generale n.299 del 24-12-2012).

D.M. 5/05/2015, Decreto 5 maggio 2015, Metodi di valutazione delle stazioni di misurazione della qualità dell'aria di cui all'articolo 6 del decreto legislativo 13 agosto 2010, n. 155. (15A04273) (GU Serie Generale n.128 del 05-06-2015).

D.M. 26/01/2017, Decreto 26 gennaio 2017, Attuazione della direttiva (UE) 2015/1480 del 28 agosto 2015, che modifica taluni allegati delle direttive 2004/107/CE e 2008/50/CE nelle parti relative ai metodi di riferimento, alla convalida dei dati e all'ubicazione dei punti di campionamento per la valutazione della qualità' dell'aria ambiente. (17A00999) (GU Serie Generale n.33 del 09-02-2017).

D'ltri, P.A., D'ltri, F.M., (1978). *Mercury contamination: A human tragedy*, Environmental Management 2, 3–16, https://doi.org/10.1007/BF01866442.

Danziger, S.J., and Possick, P.A., (1973). *Metallic mercury exposure in scientific glassware manufacturing plants*, J. Occup. Med., 15(1):15-20.

Davis, A., Bloom, N.S., Que Hee, S.S., (1997). *The environmental geochemistry and bioaccessibility of mercury in soils and sediments: a review*, Risk Anal., 17, 557-569, https://doi.org/10.1111/j.1539-6924.1997.tb00897.x.

Dedeurwaerder, H., Decadt, G., & Baeyens, W., (1982). *Estimations of mercury fluxes emitted by Mount Etna Volcano*. Bull Volcanol, 45, 191–196, https://doi.org/10.1007/BF02597729.

de Wuilloud, J.C.A., Wuilloud, R.G., Silva, M.F., Olsina, R.A., Martinez, L.D., (2002). *Sensitive determination of mercury in tap water by cloud point extraction pre-concentration and flow injection-cold vapor-inductively coupled plasma optical emission spectrometry*, Spectrochim. Acta B: Atomic Spectroscopy, 57(2), 365-374, https://doi.org/10.1016/S0584-8547(01)00393-7.

Dinelli, E., Lima, A., Albanese, S., Birke, M., Cicchella, D., Giaccio, L., Valera, P., De Vivo, B., (2012). *Comparative study between bottled mineral and tap water in Italy*, J. Geochemical Explor., 112, 368-389, https://doi.org/10.1016/j.gexplo.2011.11.002.

Direttiva 98/83/CE del Consiglio del 3 novembre 1998 concernente la qualità delle acque destinate al consumo umano. Official Journal of the European Union (1998) L 330, 1-28, 5.12.1998.

Direttiva 2004/107/CE del Parlamento europeo e del Consiglio, del 15 dicembre 2004, concernente l'arsenico, il cadmio, il mercurio, il nickel e gli idrocarburi policiclici aromatici nell'aria ambiente. Official Journal of the European Union (2004) L 23, 3-16, 26.1.2005.

Direttiva 2007/51/CE del Parlamento europeo e del Consiglio del 25 settembre 2007, che modifica la direttiva 76/769/CEE del Consiglio per quanto riguarda le restrizioni alla commercializzazione di alcune apparecchiature di misura contenenti mercurio (Testo rilevante ai fini del SEE), Official Journal of the European Union (2007) L 257, 13–15, 3.10.2007.

Direttiva 2008/50/CE del Parlamento europeo e del Consiglio, del 21 maggio 2008, relativa alla qualità dell'aria ambiente e per un'aria più pulita in Europa. Official Journal of the European Union (2008) L 152, 1-44, 11.06.2008

Direttiva (UE) 2015/1480 della Commissione, del 28 agosto 2015, che modifica vari allegati delle direttive 2004/107/CE e 2008/50/CE del Parlamento europeo e del Consiglio recanti le disposizioni relative ai metodi di riferimento, alla convalida dei dati e all'ubicazione dei punti di campionamento per la valutazione della qualità dell'aria ambiente. Official Journal of the European Union (2015) L 226, 4-11, 29.8.2015.

Driscoll, C.T., Mason, R.P., Chan, H.M., Jacob, D.J., Pirrone, N., (2013). *Mercury as a global pollutant: sources, pathways, and effects*, Environ. Sci. Technol., 47, 4967-4983, https://doi.org/10.1021/es305071v.

EFSA, (2012). Panel on Contaminants in the Food Chain (CONTAM), *Scientific Opinion on the risk for public health related to the presence of mercury and methylmercury in food*. EFSA Journal 10(12), 2985, 1-241, https://doi.org/10.2903/j.efsa.2012.2985.

EFSA, (2015). Scientific Committee, *Statement on the benefits of fish/seafood consumption compared to the risks of methylmercury in fish/seafood*. EFSA Journal, 13(1), 3982, 1-36, https://doi.org/10.2903/j.efsa.2015.3982.

EFSA, (2018). European Food Safety Authority, *Scientific Opinion on the risk for public health related to the presence of mercury and methylmercury in food*, EFSA Journal,10(12), 2985, https://doi.org/10.2903/j.efsa.2012.2985.

EN 14884:2005, (2005). Air quality-Stationary source emissions-Determination of total mercury: automated measuring systems.

EN 15852:2010, (2010). Ambient Air Quality-Standard Method for The Determination of Total Gaseous Mercury, Comité Européen de Normalisation.

EN 15853:2010, (2010). Ambient air quality-Standard method for the determination of mercury deposition, Comité Européen de Normalisation.

Ekino, S., Susa, M., Ninomiya, T., Imamura, K., Kitamura, T., (2007). *Minamata disease revisited: an update on the acute and chronic manifestations of methyl mercury poisoning*, J. Neurol. Sci., 262, 131-144, https://doi.org/10.1016/j.jns.2007.06.036.

FAO/WHO, (2011). Report of the Joint FAO/WHO Expert Consultation on the Risks and Benefits of Fish Consumption. Rome, Food and Agriculture Organization of the United Nations; Geneva, World Health Organization, 50, Food and Agriculture Organization/World Health Organization.

Fantozzi, L., Manca, G., Ammoscato, I., Pirrone, N., Sprovieri, F., (2013). *The cycling and sea-air exchange of mercury in the waters of the Eastern Mediterranean during the 2010 MED-OCEANOR cruise campaign*, Sci. Total Environ., 448, 151-162, https://doi.org/10.1016/j.scitotenv.2012.09.062.

Faria A., de Freitas C., (1992). *Systemic contact dermatitis due to mercury*, Contact Dermatitis, 27: 110–111, https://doi.org/10.1111/j.1600-0536.1992.tb05219.x.

Farrar, W.V., Williams, A.R., (1977). *A History of Mercury*. In: McAuliffe C.A. (eds) The Chemistry of Mercury. Aspects of Inorganic Chemistry. Palgrave Macmillan, London, https://doi.org/10.1007/978-1-349-02489-6_1.

Ferrara, R., Maserti, B.E., De Liso, A., Cioni, R., Raco, B., Taddeucci, G. Edner, H., Ragnarson, P., Svanberg, S., Wallinder, E., (1994). *Atmospheric mercury emission at Solfatara volcano (Pozzuoli, Phlegraean Fields-Italy)*, Chemosphere, 29(7), 1421-1428, https://doi.org/10.1016/0045-6535(94)90275-5.

Ferrara, R., Mazzolai, B., Edner, H., Svanberg, S., Wallinder, E., (1998). *Atmospheric mercury sources in the Mt. Amiata area, Italy*, Sci. Total Environ., 213(1-3), 13-23, https://doi.org/10.1016/S0048-9697(98)00067-9.

Ferrara, R., Mazzolai, B., Lanzillotta, E., Nucaro, E., Pirrone, N., (2000), *Volcanoes as emission sources of atmospheric mercury in the Mediterranean basin*, Sci. Total Environ., 259(1-3), 115-121, https://doi.org/10.1016/S0048-9697(00)00558-1.

Fontana, M., Possamai, S., Spagnolo, P., Cappa, C., Bussi, C., Lollobrigida, F., Sacco, M., Milizia, L., Milingo, M., (2018). *Rapporto di sintesi sui dati prodotti dalla stazione di monitoraggio della qualità dell'aria ubicata nel Comune di Beinasco-Giardino Pubblico Aldo Mei, di proprietà di TRM S.p.A.*, Anno 2017, Prot. n° 27947 Rapporto Tecnico, 1-64, http://www.cittametropolitana.torino.it/cms/ambiente/qualita-aria/dati-qualita-aria/relazioni-annuali.

Garnier, R., Fuster, J., Conso, F., Dautzenberg, B., Sors, C., & Fournier, E., (1981). *Acute mercury vapor poisoning*, Toxicol Europ Res, 3(2), 77-86.

Gill, G.A., Fitzgerald, W.F., (1987). *Picomolar mercury measurements in seawater and other materials using stannous chloride reduction and two-stage gold amalgamation with gas phase detection*, Mar. Chem., 20, 227-243, https://doi.org/10.1016/0304-4203(87)90074-0.

Gilmour, C.C., Podar, M., Bullock, A.L., Graham, A.M., Brown, S.D., Somenahally, A.C., Johs, A., Hurt, R.A.Jr., Bailey, K.L., and Elias, D.A., (2013). *Mercury methylation by novel microorganisms from new environments*, Environ. Sci. Technol., 47, 11810–11820, https://doi.org/10.1021/es403075t.

Goh, C.L., Ng, S.K., (1988). *Occupational allergic contact dermatitis from metallic mercury*, Contact Dermatitis, 19: 232–233, https://doi.org/10.1016/S0733-8635(18)30156-6.

Gonzalez-Raymat, H., Liu, G., Liriano, C., Li, Y., Yin, Y., Shi, J., Jiang, G., Cai, Y., (2017). *Elemental mercury: Its unique properties affect its behavior and fate in the environment*, Environ. Pollut., 229, 69-86, https://doi.org/10.1016/j.envpol.2017.04.101.

Gosar, M., Pirc, S., Bidovec, M., (1997). *Mercury in the Idrijca River sediments as a reflection of mining and smelting activities of the Idrija mercury mine*, J. Geochem. Explor., 58, 125-131, https://doi.org/10.1016/S0375-67429600064-7.

Guerrin, F., Burgat-Sacaze, V., and de Saqui-Sannes, P., (1990). *Levels of heavy metals and organochlorine pesticides of cyprinid fish reared four years in a wastewater treatment pond*, Bull. Environ. Contamination Toxicol., 44, 461- 467, https://doi.org/10.1007/BF01701230.

Gustin, M.S., Engle, M., Ericksen, J., Lyman, S., Stamenkovic, J., Xin, M., (2006). *Mercury exchange between the atmosphere and low mercury containing substrates*, Appl. Geochem, 21, 1913-1923, https://doi.org/10.1016/j.apgeochem.2006.08.007.

Gustin, M. S., Amos, H. M., Huang, J., Miller, M. B., and Heidecorn, K., (2015). *Measuring and modeling mercury in the atmosphere: a critical review*, Atmos. Chem. Phys., 15, 5697–5713, https://doi.org/10.5194/acp-15-5697-2015.

Gustin, M.S., Dunham-Cheatham, S.M., Huang, J., Lindberg, S., Lyman, S.N., (2021). *Development of an Understanding of Reactive Mercury in Ambient Air: A Review*, Atmosphere, 12, 73, https://doi.org/10.3390/atmos12010073.

Harada, M., (1995). *Minamata disease: methylmercury poisoning in Japan caused by environmental pollution*, Crit. Rev. Toxicol., 25, 1-24, https://doi.org/10.3109/10408449509089885.

Hintelmann, H., (2010). *Organomercurials. Their formation and pathways in the environment*, In Sigel, A., Sigel, H., and Sigel, R. K. O. (eds.) Metal Ions in Life Sciences: Volume 7, Chapter 11, Organometallics in Environment and Toxicology, Cambridge: Royal Society of Chemistry, https://doi.org/10.1039/9781849730822-00365.

Huang, J., Lyman, S. N., Hartman, J. S. and Gustin, M. S., (2014). *A review of passive sampling systems for ambient air mercury measurements*, Environ. Sci. Process. Impacts, 16(3), 374–392, https://doi.org/10.1039/c3em00501a.

IARC, (1993), *Beryllium, cadmium, mercury and exposures in the glass manufacturing industry*. IARC monographs on the evaluation of carcinogenic risks to humans, Vol 58, International Agency for Research on Cancer, Lyon, 239–347. ISBN 92 832 1258 4.

IRIS, (1988). Chemical assessment summary and US Environmental Protection Agency, National Center for Environmental Assessment: *Mercury, Elemental, Integrated Risk Information System*, https://cfpub.epa.gov/ncea/iris/iris_documents/documents/subst/ 0370_summary.pdf.

Ito, R., Kawaguchi, M., Sakui, N., Okanouchi, N., Saito, K., Seto, Y., Nakazawa, H., (2009). *Stir bar sorptive extraction with in situ derivatization and thermal desorption-gas chromatography-mass spectrometry for trace analysis of methylmercury and mercury (II) in water sample*, Talanta, 77, 1295-1298, https://doi.org/10.1016/j.talanta.2008.09.001.

Kanerva, L., Komulainen, M., Estlander, T., Jolanki, R., (1993). *Occupational allergic contact dermatitis from mercury*, Contact Dermatitis, 28: 26–28, https://doi.org/10.1111/j.1600-0536.1993.tb03319.x

Kanerva, L., Tarvainen, K., Estlander, T., Jolanki, R., (1994). *Occupational allergic contact dermatitis caused by mercury and benzoyl peroxide*, Eur J Dermatol, 4: 359–361, https://doi.org/10.1016/S0733-8635(18)30156-6.

Kimáková, T., Kuzmová, L., Nevolná, Z., Bencko, V., (2018). *Fish and fish products as risk factors of mercury exposure*, Ann Agric Environ Med., 25(3), 488-493, https://doi.org/10.26444/aaem/84934.

King, J.K., Kostka, J.E., Frischer, M.E., and Saunders, F.M., (2000). *Sulfate-reducing bacteria methylate mercury at variable rates in pure culture and in marine sediments*, Appl.Environ. Microb., 66(6), 2430-2437, https://doi.org/10.1128/AEM.66.6.2430-2437.2000.

Knox, R., Kammin, W.R., Thomson, D., (1995). *Atomic Fluorescence Determination of Mercury in Freshwater Ecosystems*, J. Automat. Chem., 17, 65-71, https://doi.org/10.1155/S1463924695000113.

Lan, X., Talbot, R., Castro, M., Perry, K., and Luke, W., (2012). *Seasonal and diurnal variations of atmospheric mercury across the US determined from AMNet monitoring data*, Atmos. Chem. Phys., 12, 10569–10582, https://doi.org/10.5194/acp-12-10569-2012.

Langford, N., Ferner, R., (1999). *Toxicity of mercury*. J Hum Hypertens, 13, 651–656, https://doi.org/10.1038/sj.jhh.1000896.

Leopold, K., Foulkes, M., Worsfold, P.J., (2009). *Gold-Coated Silica as a Preconcentration Phase for the Determination of Total Dissolved Mercury in Natural Waters Using Atomic Fluorescence Spectrometry*, Solutions, 34, 3421-3428, https://doi.org/10.1039/B820701A.

Lyman, S.N., Cheng, I., Gratz, L.E., Weiss-Penzias, P., Zhang, L., (2020). *An updated review of atmospheric mercury*, Sci. Total Environ., 707, 135575, https://doi.org/10.1016/j.scitotenv.2019.135575.

Manahan, S.E., (2000). *Chimica dell'ambiente*, Editore: Piccin, Padova, (Zoccolillo, L., cur.), Ed. italiana sulla 6. ed. americana, XVI, 1-894.

Mann, J.L., Long, S.E., Kelly, W.R., (2003). *Direct determination of mercury at picomole L^{-1} levels in bottled water by isotope dilution cold-vapor generation inductively coupled plasma mass spectrometry*, J. Anal. At. Spectrom., 18, 1293-1296, https://doi.org/10.1039/b306640a.

Mao, H., Cheng, I., Zhang, L., (2016). *Current understanding of the driving mechanisms for spatiotemporal variations of atmospheric speciated mercury: a review*, Atmos. Chem. Phys., 16, 12897-12924, https://doi.org/10.5194/acp-16-12897-2016.

Matsuyama, A., Qu, L.Y., Yasutake, A., Yamaguchi, M., Aramaki, R., Xiaojie, L., Pin, J., Li, L., Mei, L., Yumin, A., Yasuda, Y., (2004). *Distribution of methylmercury in an area polluted by mercury containing wastewater from an organic chemical factory in China*, Bull. Environ. Contam. Toxicol., 73, 846-852, https://doi.org/10.1007/s00128-004-0504-z.

Mazzolai, B., Mattoli, V., Raffa, V., Tripoli, G., Accoto, D., Menciassi, A., Dario, P., (2004). *A microfabricated physical sensor for atmospheric mercury monitoring*, Sens. Actuators A Phys., 113, 282-287, https://doi.org/10.1016/j.sna.2004.01.012.

McLagan, D. S., Mitchell, C. P. J., Steffen, A., Hung, H., Shin, C., Stupple, G. W., Olson, M. L., Luke, W. T., Kelley, P., Howard, D., Edwards, G. C., Nelson, P. F., Xiao, H., Sheu, G.-R., Dreyer, A., Huang, H., Abdul Hussain, B., Lei, Y. D., Tavshunsky, I., and Wania, F., (2018). *Global evaluation and calibration of a passive air sampler for gaseous mercury*, Atmos. Chem. Phys., 18, 5905–5919, https://doi.org/10.5194/acp-18-5905-2018.

Minnich, M.G., Miller, D.C., Parsons, P.J., (2008). *Determination of As, Cd, Pb, and Hg in urine using inductively coupled plasma mass spectrometry with the direct injection high efficiency nebulizer*, Spectrochim. Acta Part B At. Spectrosc., 63, 389-395, https://doi.org/10.1016/j.sab.2007.11.033.

Mukhi, P., Mohapatra, S.S., Bhattacharjee, M., Ray, K.K., Muraleedharan, T.S., Arun, A., Sathyavathi, R., Juluri, R.R., Satyam, P.V., Panda, A.K., Biswas, A., Nayak, S., Bojja, S., Pratihar, S., Roy, S., (2017). *Mercury based drug in ancient India: The red sulfide of mercury in nanoscale,* J. Ayurveda Integr. Med., 8(2), 93-98, https://doi.org/10.1016/j.jaim.2017.01.009.

Munthe, J., Wängberg, I., Pirrone, N., Iverfeldt, Å., Ferrara, R., Ebinghaus, R., Feng, X., Gårdfeldt, K., Keeler, G., Lanzillotta, E., Lindberg, S.E., Lu, J., Mamane, Y., Prestbo, E., Schmolke, S., Schroeder, W.H., Sommar, J., Sprovieri, F., Stevens, R.K., Stratton, W., Tuncel, G., Urba, A., (2001). *Intercomparison of methods for sampling and analysis of atmospheric mercury species*, Atmos. Environ., 35, 3007-3017, https://doi:10.1016/S1352-2310(01)00104-2.

Navarro, A., (2008). *Review of characteristics of mercury speciation and mobility from areas of mercury mining in semi-arid environments*, Rev Environ Sci Biotechnol., 7, 287–306, https://doi.org/10.1007/s11157-008-9139-6.

NRC, (2000). *Toxicological Effects of Methylmercury. Chemistry, Exposure, Toxicokinetics, and Toxicodynamics*, Chapter 2, 31-71, Washington DC, The National Academies Press, National Research Council. https://doi.org/10.17226/9899.

Pandey, S.K., Kim, K.-H., Brown, R.J., (2011). *Measurement techniques for mercury species in ambient air*, Trends Anal. Chem., 30, 899-917, https://doi.org/10.1016/j.trac.2011.01.017.

Passariello, B., Barbaro, M., Quaresima, S., Casciello, A., Marabini, A., (1996). *Determination of mercury by Inductively Coupled Plasma-Mass Spectrometry*, Microchem. J., 54, 348-354, https://doi.org/10.1006/mchj.1996.0110.

Piikivi, L., Tolonen, U., (1989). *EEG findings in chlor-alkali workers subjected to low long term exposure to mercury vapour*. Br J Ind Med 46: 370–375, https://www.jstor.org/stable/27726801.

Pirrone, N., (2001). *Mercury research in Europe: towards the preparation of the EU air quality directive*, Atmospheric Environment, 35(17), 2979-2986, https://doi.org/10.1016/S1352-2310(01)00101-7.

Pirrone, N., Wichmann-Fiebig, M., (2003). *Some recommendations on mercury measurements and research activities in the European Union*, Atmospheric Environment, 37(1), 3-8, https://doi.org/10.1016/S1352-2310(03)00234-6.

Pirrone, N., Mason, R.P., (Eds.), (2009). *Hg Fate and Transport in the Global Atmosphere, Measurements and Models*, Springer, Geneva, 1-602, https://doi.org/10.1007/978-0-387-93958-2.

Rahmanian, N., Ali, S.H.B., Homayoonfard, M., Ali, N.J., Rehan, M., Sadef, Y., Nizami, A.S., (2015). *Analysis of physicochemical parameters to evaluate the drinking water quality in the state of perak, Malaysia*, J. Chem., 2015, https://doi.org/10.1155/2015/716125.

Randall, P.M., (1995). *Mercury reduction in products and processes: a review of the electrical and electronic industries*,
Environ Prog, 14, 232-239, https://doi.org/10.1002/ep.670140411.

Ratcliffe, H.E., Swanson, G.M., & Fischer, L.J., (1996). *Human Exposure to Mercury: A Critical Assessment of the Evidence of Adverse Health Effects*, J. Toxicol. Environ. Health, 49(3), 221-270, https://doi.org/10.1080/00984108.1996.11667600.

Richter, E.D., Peled, N., Luria, M., (1982). *Mercury exposure and effects at a thermometer factory*. Scan J Health Environ Health; 1: 161–6, https://www.jstor.org/stable/40964508.

Roels, H., Gennart, J.P., Lauwerys, R., Buchet, J.P., Malchaire, J., Bernard, A., (1985). *Surveillance of workers exposed to mercury vapour: validation of a previously proposed biological threshold limit value for mercury concentration in urine*, Am J Ind Med, 7: 45–71, https://doi.org/10.1002/ajim.4700070106.

Rogers, R.D., (1977). *Abiological methylation of mercury in soil*, J. Environ. Qual., 6, 463–467, https://doi.org/10.2134/jeq1977.00472425000600040029x.

Schroeder, W.H., Munthe, J. & Lindqvist, O., (1989). *Cycling of mercury between water, air, and soil compartments of the environment*, Water Air Soil Pollut, 48, 337–347, https://doi.org/10.1007/BF00283335.

Selin, N.E., (2009). *Global biogeochemical cycling of mercury: a review*, Annu. Rev. Environ. Resour., 34, 43-63, https://doi.org/10.1146/annurev.environ.051308.084314.

Sheu, G.-R., Gay, D.A., Schmeltz, D., Olson, M., Chang, S.-C., Lin, D.-W., Nguyen, L.S.P., (2019). *A New Monitoring Effort for Asia: The Asia Pacific Mercury Monitoring Network (APMMN)*, Atmosphere, 10(9), 481, https://doi.org/10.3390/atmos10090481.

Skyllberg, U., Bloom, P.R., Qian, J., Lin, C.M., Bleam, W.F., (2006). *Complexation of mercury (II) in soil organic matter: EXAFS evidence for linear two-coordination with reduced sulfur groups*, Environ. Sci. Technol., 40, 4174-4180, https://doi.org/10.1021/es0600577.

Spolaor, A., Angot, H., Roman, M., Dommergue, A., Scarchilli, C., Vardè, M., Del Guasta, M., Pedeli, X., Varin, C., Sprovieri, F., Magand, O., Legrand, M., Barbante, C., and Cairns, W.R.L., (2018). *Feedback mechanisms between snow and atmospheric mercury: Results and observations from field campaigns on the Antarctic plateau*, Chemosphere, 197, 306–317, https://doi.org/10.1016/j.chemosphere.2017.12.180.

Spolaor, A., Barbaro, E., Cappelletti, D., Turetta, C., Mazzola, M., Giardi, F., Björkman, M. P., Lucchetta, F., Dallo, F., Pfaffhuber, K. A., Angot, H., Dommergue, A., Maturilli, M., Saiz-Lopez, A., Barbante, C., and Cairns, W.R.L., (2019). *Diurnal cycle of iodine, bromine, and mercury concentrations in Svalbard surface snow*, Atmos. Chem. Phys., 19, 13325–13339, https://doi.org/10.5194/acp-19-13325-2019.

Sprovieri, F., Pirrone, N., Ebinghaus, R., Kock, H., and Dommergue, A., (2010). *A review of worldwide atmospheric mercury measurements*, Atmos. Chem. Phys., 10, 8245–8265, https://doi.org/10.5194/acp-10-8245-2010.

Sprovieri, F., Pirrone, N., Bencardino, M., D'Amore, F., Carbone, F., Cinnirella, S., Mannarino, V., Landis, M., Ebinghaus, R., Weigelt, A., Brunke, E.-G., Labuschagne, C., Martin, L., Munthe, J., Wängberg, I., Artaxo, P., Morais, F., Barbosa, H.D.M. J., Brito, J., Cairns, W., Barbante, C., Diéguez, M.D.C., Garcia, P.E., Dommergue, A., Angot, H., Magand, O., Skov, H., Horvat, M., Kotnik, J., Read, K.A., Neves, L. M., Gawlik, B.M., Sena, F., Mashyanov, N., Obolkin, V., Wip, D., Feng, X. B., Zhang, H., Fu, X., Ramachandran, R., Cossa, D., Knoery, J., Marusczak, N., Nerentorp, M., Norstrom, C., (2016). *Atmospheric mercury concentrations observed at ground-based monitoring sites globally distributed in the framework of the GMOS network*, Atmos. Chem. Phys., 16, 11915–11935, https://doi.org/10.5194/acp-16-11915-2016.

Sprovieri, F., Pirrone, N., Bencardino, M., D'Amore, F., Angot, H., Barbante, C., Brunke, E.-G., Arcega-Cabrera, F., Cairns, W., Comero, S., Diéguez, M. D. C., Dommergue, A., Ebinghaus, R., Feng, X. B., Fu, X., Garcia, P. E., Gawlik, B. M., Hageström, U., Hansson, K., Horvat, M., Kotnik, J., Labuschagne, C., Magand, O., Martin, L., Mashyanov, N., Mkololo, T., Munthe, J., Obolkin, V., Ramirez Islas, M., Sena, F., Somerset, V., Spandow, P., Vardè, M., Walters, C., Wängberg, I., Weigelt, A., Yang, X., and Zhang, H., (2017). *Five-year records of mercury wet deposition flux at GMOS sites in the Northern and Southern hemispheres*, Atmos. Chem. Phys., 17, 2689–2708, https://doi.org/10.5194/acp-17-2689-2017.

Streets, D.G., Horowitz, H.M., Lu, Z., Levin, L., Thackray, C.P., Sunderland, E.M., (2019). *Global and Regional Trends in Mercury Emissions and Concentrations, 2010–2015*, Atmos. Environ, 201, 417-427, https://doi.org/10.1016/j.atmosenv.2018.12.031.

Temme, C., Blanchard, P., Steffen, A., Banic, C., Beauchamp, S., Poissant, L., Tordon, R., Wiens, B., (2007). *Trend, seasonal and multivariate analysis study of total gaseous mercury data from the Canadian atmospheric mercury measurement network (CAMNet)*, Atmos. Environ., 41(26), 5423-5441, https://doi.org/10.1016/j.atmosenv.2007.02.021.

Teršič, T., Gosar, M., Biester, H., (2011). *Distribution and speciation of mercury in soil in the area of an ancient mercury ore roasting site, Frbejžene trate (Idrija area, Slovenia)*, J. Geochem. Explor., 110, 136–145, https://doi.org/10.1016/j.gexplo.2011.05.002.

The Lancet, (2017). *Minamata Convention on mercury: a contemporary reminder*, Editorial, The Lancet 390, (10097), 822, https://doi.org/10.1016/S0140-6736(17)32287-0.

UNEP, (2019). *Global Mercury Assessment 2018: Sources, Emissions, Releases and Environmental Transport*, United Nations Environment Programme Chemical and Health Branch, Geneva, Switzerland, United Nations Environment Programme, https://www.unenvironment.org/resources/publication/global-mercury-assessment-2018.

Università degli Studi di Ferrara, (2019). *Caratterizzazione del sistema multi – acquifero della Pianura Padana*. Accordo di collaborazione tecnico-scientifica ai sensi dell'art. 15 L. N. 241/1990 D.D.G. ARPAV n. 256 del 26 ottobre 2017. Rapporto Dicembre 2018, Prof. Guido Sciavicco e Prof.ssa Carmela Vaccaro, 07 febbraio 2019, Dipartimento di Fisica e Scienze della Terra, Dipartimento di Matematica.

US-EPA, (2002). Method 1631, revision E: *mercury in water by oxidation, purge and trap, and cold vapor atomic fluorescence spectrometry*, United States Environmental Protection Agency.

US-EPA, (2018). *Ground Water and Drinking Water, National Primary Drinking Water Regulations*, Edition of the Drinking, Water Standards and Health Advisories Tables, United States Environmental Protection Agency.

Vardè, M., Servidio, A., Cofone, F., Rosselli, A., Sprovieri, F., (2014). *First measurements of Total Mercury (THg) in wet deposition at a high altitude site in Southern Italy (1379m a.s.l.)*, In Atti: XXV Congresso Nazionale della Società Chimica Italiana, Arcavacata di Rende, 7-12 settembre 2014, p. 76.

Vardè, M., Cofone, F., Servidio, A., Rosselli, A., Mannarino, V., Di Traglia, M., (2015a). *Determination of Ultra-Trace Total Mercury in Bottled Waters Produced in Calabria (Southern Italy)*, In Atti: XV Congresso Nazionale di Chimica dell'Ambiente e dei Beni Culturali della Società Chimica Italiana, Divisione di Chimica dell'Ambiente e dei Beni Culturali Bergamo (BG), 14-18 giugno 2015, pp. 176-177.

Vardè, M., Rosselli, A., Servidio, A., Cofone, F., Mannarino, V., Di Traglia, M. (2015b). *Mercury at Picomole L^{-1} (pM) Level in Drinking Water by Cold Vapor Atomic Fluorescence Spectrometry (CV-AFS) along four Provinces in Southern Italy (Calabria)*, In Atti: XV Congresso Nazionale di Chimica dell'Ambiente e dei Beni Culturali della Società Chimica Italiana, Divisione di Chimica dell'Ambiente e dei Beni Culturali Bergamo (BG), 14-18 giugno 2015, pp. 178-179.

Vardè, M., Cofone, F., Rosselli, A., Servidio, A., Di Traglia, M., Dallo, F., Vespasiano, G., Apollaro, C., (2017). *Quanto mercurio nelle acque minerali naturali della Campania?,* In Atti: XXVI Congresso Nazionale della Società Chimica Italiana (SCI) Paestum (SA), 10-14 settembre 2017, p. 42.

Vardè, M., Servidio, A., Vespasiano, G., Pasti, L., Cavazzini, A., Di Traglia, M., Rosselli, A., Cofone, F., Apollaro, C., Cairns, W.R.L., Scalabrin, E., De Rosa, R., Procopio, A., (2019a). *Ultra-trace determination of total mercury in Italian bottled waters*, Chemosphere, 219, 896-913, https://doi.org/10.1016/j.chemosphere.2018.12.020.

Vardè, M., Cairns, W.R.L., Servidio, A., Vespasiano, G., Cofone, F., Rosselli, A., Di Traglia, M., Apollaro, C., Pasti, L., Cavazzini, A., and Procopio, A., (2019b). *Mercury in Italian bottled water: ultra-trace determination and evaluation of intake using a health risk assessment approach*, In Atti: ICMGP 2019, 14th International Conference on Mercury as a Global Pollutant, September 7-13, 2019. Cracovia, Polonia, 7-13 settembre 2019.

Vardè, M., Servidio, A., Vespasiano, G., Pasti, L., Cavazzini, A., Di Traglia, M., Rosselli, A., Cofone, F., Apollaro, C., Cairns, W.R.L., Scalabrin, E., De Rosa, R., A. Procopio, A., (2019c). *Determinazione di ultra-tracce di mercurio totale nelle acque minerali naturali italiane*, In Atti: 7^ Incontri Mediterranei – Inquinamento indoor e outdoor: valutazione dei rischi, figure e competenze, AIDII (Associazione Italiana degli Igienisti Industriali), Lamezia Terme (CZ), 3-4 ottobre 2019.

Vardè, M., Servidio, A., Cofone, F., Vespasiano, G., Rosselli, A., Pasti, L., Cavazzini, A., Apollaro, C., (2019d). *Comparison of ultra-low levels of total mercury in tap waters and bottled mineral waters in a region of southern Italy (Calabria)*, In Atti: XIX Giornata della Chimica dell'Emilia Romagna, SCI, UniMoRe, Modena, Italy, 6 dicembre 2019.

Vardè, M., Cofone, F., Servidio, A., Rosselli, A., Di Traglia, M., Pasti, L., Cavazzini, A., Cesari, D., Scoto, F., Cairns, W.R.L., Barbante, C., (2019e). *Wet deposition of total mercury at a suburban site in Southern Italy (Calabria): concentrations, fluxes and assessment of source areas*, In Atti: ICMGP 2019, 14th International Conference on Mercury as a Global Pollutant, Cracovia, Polonia, 7-13 settembre 2019.

Vardè, M., Cofone, F., Servidio, A., Rosselli, A., Di Traglia, M., Manna, G., Pasti, L., Cavazzini, A., Cesari, D., Scoto, F., Cairns, W.R.L., Barbante, C., (2019f). *Mercurio nelle precipitazioni atmosferiche in un sito suburbano in Calabria: determinazione delle concentrazioni, dei flussi di deposizione e valutazione delle potenziali sorgenti*, In Atti: 7^ Incontri Mediterranei – Inquinamento indoor e outdoor: valutazione dei rischi, figure e competenze, (Associazione Italiana degli Igienisti Industriali), Lamezia Terme (CZ), 3-4 ottobre 2019.

Villanueva, F.S., and Botello, A.V., (1998). *Metal pollution in coastal areas of Mexico*, Rev. Environ. Contam. Toxicol., 157, 53-94, 1998, https://doi.org/10.1007/978-1-4612-0625-5_3.

Wagemann, R., Trebacz, E., Boila, G., and Lockhart, W.L., (1998). *Methyl mercury and total mercury in tissues of arctic marine mammals*, Sci. Total Environ., 218, 19-31, https://doi.org/10.1016/S0048-9697(98)00192-2.

Wang, Q., Kim, D., Dionysiou, D.D., Sorial, G.A., Timberlake, D., (2004). *Sources and remediation for mercury contamination in aquatic systems—a literature review*, Environmental Pollution, 131, 2, 323-336, https://doi.org/10.1016/j.envpol.2004.01.010.

WHO, (1989). *Environmental Health Criteria, Mercury-environmental aspects*, 84, 115, World Health Organization.

WHO, (2005). *Mercury in Drinking-water*, World Heal. Organ, Geneva, 1-8, World Health Organization.

WHO, (2000). *Air quality guidelines (AQGs) for Europe*-Second edition, WHO Regional Publications, European Series, No. 91, World Health Organization.

Xin, X., and Gustin, M.S., (2007). *Gaseous elemental mercury exchange with low mercury containing soils: Investigation of controlling factors*, Appl. Geochem., 22, 1451-1466, https://doi.org/10.1016/j.apgeochem.2007.02.006.

Zhang, L., Zhou, P., Cao, S., and Zhao, Y., (2019). *Atmospheric mercury deposition over the land surfaces and the associated uncertainties in observations and simulations: a critical review*, Atmos. Chem. Phys., 19, 15587–15608, https://doi.org/10.5194/acp-19-15587-2019.

Zi, H.-J., Wu-Er, G., Su-Ping, H., Xian-Juan, J., Ling-Zhong, W., (2009). *Determination of trace inorganic mercury in mineral water by flow injection on-line sorption preconcentration-cold vapor atomic fluorescence spectrometry*, Fenxi Huaxue/Chinese J. Anal. Chem., 37, 1029-1032, https://doi.org/10.1016/S1872-2040(08)60116-4.

Appendice

Elenco dei lavori nella tesi di dottorato

1/A
Caso studio 1 (in fase di sottomissione)

M. Vardè, Carlo Barbante, Elena Barbaro, Francesca Becherini, Maurizio Busetto, Paolo Bonasoni, Francescopiero Calzolari, Paolo Cristofanelli, Federico Dallo, Fabrizio De Blasi, Jacopo Gabrieli, Andrea Gambaro, Davide Putero, Andrea Spolaor, and Warren R.L. Cairn, Characterization of atmospheric total gaseous mercury at a remote high-elevation site (Col Margherita observatory, 2543 m a.s.l.) in the Italian Alps

2/A
Caso studio 2 (accettato 17 maggio 2019)

C. Apollaro, A. Buccianti, G. Vespasiano, **M. Vardè**, I. Fuoco, D. Barca, A. Bloise, D. Miriello, F. Cofone, A. Servidio, R. De Rosa (2019).
Comparative geochemical study between the tap waters and the bottled mineral waters in Calabria (Southern Italy) by compositional data analysis (CoDA) developments.
Appl. Geochem., 107, 19-33. https://doi.org/10.1016/j.apgeochem.2019.05.011

3/A
Caso studio 3 (accettato 2 dicembre 2018)

M. Vardè, A. Servidio, G. Vespasiano, L. Pasti, A. Cavazzini, M. Di Traglia, A. Rosselli, F. Cofone, C. Apollaro, W.R.L. Cairns, E. Scalabrin, R. De Rosa and A. Procopio (2019).
Ultra-trace determination of total mercury in Italian bottled waters.
Chemosphere, 219, 896-913. https://doi.org/10.1016/j.chemosphere.2018.12.020

4/A
Caso studio 4 (accettato 28 dicembre 2017)

A. Spolaor, H. Angot, M. Roman, A. Dommergue, C. Scarchilli, **M. Vardè**, M. Del Guasta, X. Pedeli, C. Varin, F. Sprovieri, O. Magand, M. Legrand, C. Barbante, W.R.L. Cairns (2018).
Feedback mechanisms between snow and atmospheric mercury: Results and observations from field campaigns on the Antarctic plateau.
Chemosphere, 197, 306-317. https://doi.org/10.1016/j.chemosphere.2017.12.180

Elenco di altre pubblicazioni non inerenti al tema della tesi di dottorato

Attività di ricerca collegata all'Osservatorio di Col Margherita

5/A
E. Barbaro, E. Morabito, E. Gregoris, M. Feltracco, J. Gabrieli, **M. Vardè**, W.R.L. Cairns, F. Dallo, F. De Blasi, R. Zangrando, C. Barbante, A. Gambaro, (2020).
Col Margherita Observatory: A background site in the Eastern Italian Alps for investigating the chemical composition of atmospheric aerosols,
Atmos. Environ., 221, 15 January 2020, 117071, https://doi.org/10.1016/j.atmosenv.2019.117071
(accettato 22 ottobre 2019)

6/A
L. Naitza, P. Cristofanelli, A. Marinoni, F. Calzolari, F. Roccato, M. Busetto, D. Sferlazzo, E. Aruffo, P. Di Carlo, M. Bencardino, F. D'Amore, F. Sprovieri, N. Pirrone, F. Dallo, J. Gabrieli, **M. Vardè**, G. Resci, C. Barbante, P. Bonasoni, D. Putero, (2020).
Increasing the maturity of measurements of essential climate variables (ECVs) at Italian atmospheric WMO/GAW observatories by implementing automated data elaboration chains, Comput. Geosci., 2020, April 2020, 104432, https://doi.org/10.1016/j.cageo.2020.104432
(accettato 31 gennaio 2020)

Attività di ricerca collegate alla contaminazione ambientale in altri comparti

7/A
R. Tedesco, M.d.C. Villoslada Hidalgo, **M. Vardè**, N.M. Kehrwald, C. Barbante, G. Cozzi, (2021). *Trace and rare earth elements determination in milk whey from the Veneto region, Italy*,
Food Control, 121, 107595, https://doi.org/10.1016/j.foodcont.2020.107595
(accettato 29 agosto 2020)

Attività di ricerca collegate alle aree polari

8/A
M. Feltracco, E. Barbaro, A. Spolaor, M. Vecchiato, A. Callegaro, F. Burgay, **M. Vardè**, N. Maffezzoli, F. Dallo, F. Scoto, R. Zangrando, C. Barbante, A. Gambaro, (2021).
Year-round measurements of size-segregated low molecular weight organic acids in Arctic aerosol,
Sci. Total Environ., 763, 1 April 2021, 142954, https://doi.org/10.1016/j.scitotenv.2020.142954
(accettato 9 ottobre 2020)

Characterization of atmospheric total gaseous mercury at a remote high-elevation site (Col Margherita observatory, 2543 m a.s.l.) in the Italian Alps

Massimiliano Vardè[1,2,3], Carlo Barbante[1,3], Elena Barbaro[1,3], Francesca Becherini[1,3], Maurizio Busetto[4], Paolo Bonasoni[4], Francescopiero Calzolari[4], Paolo Cristofanelli[4], Federico Dallo[1,3], Fabrizio De Blasi[1,3], Jacopo Gabrieli[1,3], Andrea Gambaro[3,1], Davide Putero[5], Andrea Spolaor[1,3], and Warren R.L. Cairns[1,3]

[1]Institute of Polar Sciences, National Research Council of Italy (CNR-ISP), Venice-Mestre, 30172, Italy
[2]Department of Chemical and Pharmaceutical Sciences, University of Ferrara (DipSCF-UniFE), Ferrara, 44121, Italy
[3]Department of Environmental Sciences, Informatics and Statistics, Ca' Foscari University of Venice (DAIS-UniVE), Venice-Mestre, 30172, Italy
[4]Institute of Atmospheric Sciences and Climate, National Research Council of Italy (CNR-ISAC), Bologna, 40129, Italy
[5]Institute of Atmospheric Sciences and Climate, National Research Council of Italy (CNR-ISAC), Torino, 10133, Italy

Correspondence to: Massimiliano Vardè (massimiliano.varde@cnr.it) and Warren R.L. Cairns (warrenraymondlee.cairns@cnr..it)

Keywords

Atmospheric mercury; Ozone; High-altitude station; Meteorological condition; Air masses trajectories; Planet boundary layer; South Eastern Dolomites; Italy.

Abstract

The Col Margherita observatory (MRG) is the highest altitude background station located in the Eastern Italian Alps settled in the framework of the Global Mercury Observation System (GMOS) project for the study of atmospheric mercury. Its elevation and the distance from major anthropogenic and natural sources make it the ideal site for the monitoring of baseline mercury levels and the investigation of its cycle. In this work, a continuous dataset of total gaseous mercury (TGM), ozone and meteorological variables was studied in detail to investigate TGM variability at seasonal, monthly and diurnal level and to explore its relation with environmental parameters. TGM measurements were carried out from March 2018 to May 2019. The annual mean TGM concentration was higher than the previously reported year-round mercury measurements during GMOS. At MRG, the seasonal variation of TGM was characterized by high values in spring-summer 2018 and lower values in winter. A similar diel pattern of TGM over different seasons was obtained, with low concentrations in the daytime and higher in the late evening-night. Spatial patterns and temporal changes in TGM, back-trajectories and planet boundary layer (PBL) analysis showed that TGM levels were influenced by local meteorology, regional and long-range transport of air masses. Low levels of TGM in winter were associated to high wind speed, low PBL height and cleaner air masses from the west sector, whilst higher PBL height in spring and summer may contribute to the transport of gaseous mercury from polluted areas, as confirmed by back-trajectories analysis of air masses passing from Northeast and continental Europe. During the snow cover season, the investigation of TGM peak events also demonstrated the potential influence of reemission processes of previously reactive mercury deposited onto snow surfaces.

1 Introduction

High-elevation monitoring sites are crucial for studying environmental pollution and the impact of climate change on mountain glaciers and on the ecosystems of remote and pristine mountainous areas (Beniston et al., 1997). In particular, the presence and variability of Hg and O_3, two widely recognized harmful pollutants for both humans and ecosystems, have been widely investigated over the last few decades in remote mountain sites and polar regions (Berg et al., 2013; Cole and Steffen 2010; Ebinghaus et al., 2002; Faïn et al., 2009; Fu et al., 2010, 2016; Kang et al., 2019; Lu and Schroeder 2004; Sprovieri et al., 2016; Steffen et al., 2015; Yin et al., 2017, 2018). Long-term monitoring of atmospheric Mercury

(Hg) at high mountain sites is one of the keys to understanding the global cycling and fate of Hg, by decoupling global trends from local sources at the Earth's surface, since most anthropogenic Hg emissions occur at lower altitudes (Sprovieri et al., 2016). Most atmospheric mercury observations are of either gaseous elemental mercury (GEM) or total gaseous mercury (TGM). These are effectively operationally defined fractions depending on the instrumentation used. GEM which is mercury in its gaseous elemental state Hg^0 makes up over 95% of the TGM in the atmosphere whilst the remainder is a mixture of reactive gaseous mercury (RGM) and particulate bound mercury. The global atmospheric residence time of GEM is thought to be in the order of 0.5-2 years, whilst the latter two remain for days or weeks limiting their transport to a local or regional scale. However, a more recent study by Horowitz et al. (2017) suggests that under certain conditions, the atmospheric lifetime of GEM can be much shorter. Hg observations at high altitude sites also help to reduce the gap between field measurements and model simulations, especially if combined with Hg studies over oceans (Mao et al., 2016) and aircraft-based measurements (Ebinghaus et al., 2007; Slemr et al., 2009; 2016). Regional and global networks of in-situ monitoring stations have been developed for the study of Hg (Canadian Atmospheric Mercury Network-CAMNet, American Atmospheric Mercury Network-AMNET, Global Mercury Observation System-GMOS, Asia Pacific Mercury Monitoring Network-APMMN), aimed at establishing long-term air quality and meteorological datasets (Blanchard et al., 2002; Gay et al., 2013; Kaiser et al., 2007; Kellerhals et al., 2003; Temme et al., 2007; Tørseth et al., 2012; Schultz et al., 2015; Sheu et al., 2019; Sprovieri et al., 2016). Limited accessibility to remote areas and logistical complexities results in elevated maintenance and management costs for mountain sites, with the consequence of a lack of long-term data from alpine/mountain sites for analytes such as Hg (Mao et al., 2016) and persistent organic pollutants (POPs) (Loewen et al., 2005). A coordinated Global Mercury Observation System (GMOS) was established during a five-year project (2010-2015) funded by the European Commission with the aim of providing a global dataset of Hg background concentrations in ambient air and wet deposition, in the lower/upper troposphere and lower stratosphere, as well as in the marine environment (Sprovieri et al., 2016; 2017). It also aimed to provide reference levels for monitoring progress in implementation of the Minamata Convention (https://www.mercuryconvention.org/). The text of the Minamata convention was approved in 2013 and entered into force on August 16th, 2017. The GMOS project coordinated Hg data collection and quality-control using a real-time web-based QA/QC system. The system called GMOS-Data Quality Management (G-DQM), plugged into a cyberinfrastructure and deployed as a service, has been finalised to provide a high-quality dataset for Hg in air and

precipitation. A Spatial Data Infrastructure was finally developed assuring a timely up to date sharing of information on Hg (D'Amore et al., 2015). The same kind of effort should be made to establish a common procedure and instrumental method for the monitoring of other environmental parameters, i.e. for non-continuous measurements, in order to share robust and reliable datasets, thus avoiding and/or reducing uncertainties and increasing measurement traceability. Col Margherita (MRG) observatory was part of the 40 ground-based stations of the GMOS project and is now involved in the Integrated Global Observing Systems for Persistent Pollutants (iGOSP) project, Strand 3 of Era-Planet Horizon 2020 Program funded by the EU. The MRG observatory has also been recently included in the WMO Global Atmosphere Watch (GAW) Programme as a regional Station. In Europe, major contributors to atmospheric Hg emissions are anthropogenic sources with 239.3 Mg y^{-1} (Pacyna et al., 2006). Emissions of Hg from primary natural sources and re-emission processes (mainly Hg emissions from surface waters and volcanoes) were estimated as between 110 to 177 Mg y^{-1} for the Mediterranean region and Continental Europe (referring to the EMEP domain), respectively (Pacyna et al., 2006; Pirrone et al., 2001; Travnikov and Iluyin, 2005). Italian atmospheric emissions of Hg from major industrial/man-made sources, published in the National Emission Inventory Report, showed a reduction trend between 1990 and 2017 from 15.2 to 9.2 Mg y^{-1} in accordance with what was previously reported in the scenarios for atmospheric Hg emissions in Europe (Pacyna et al., 2006). This slight decrease was obtained using the best available technologies, introducing control and abatement systems for several activities such as coal and oil combustion, processes in inorganic chemical industries (i.e. chlorine production), iron and steel, coal industry, non-ferrous metal and non-metallic mineral sector, waste incineration, cement production, and geothermal production. For instance, part of the reduction in Hg emissions was due to the conversion of chlor-alkali production plants from the Hg cells to the membrane technology (Taurino et al., 2019) and through the use of abatement systems for Hg and hydrogen sulphide (H_2S) in geothermal power plants (Parisi et al., 2019). Moreover, in Italy there are also several natural sources from north to south such as the mining districts of Mt. Amiata (Breder et al., 1984; Cabassi et al., 2017; Ferrara et al., 1998; Vaselli et al., 2013), active volcanoes (e.g. Etna, Stromboli and Vulcano) (Bagnato et al., 2007; Ferrara et al., 1990; 2000) and geothermal areas (e.g. Campi Flegrei) (Bagnato et al., 2009; 2014; Bagnoli and Gartner, 2018; Cabassi et al. 2017; Ferrara et al., 1994) that were not considered in the above-mentioned report. Even if the estimated budget from these sources represents a small fraction of the annual global volcanic output, it may account (i.e. Mt. Etna volcano) for about 5% of Hg emitted in the Mediterranean basin from anthropogenic activities (Bagnato et al., 2007;

Ferrara et al., 1990; 2000). Since Hg emission data are still incomplete, more effort should be undertaken to consolidate Hg emission assessments. Support for this can come from Hg measurements in the atmosphere, as well as other environmental media, to improve our knowledge of the impact of Hg on contaminated and remote/rural sites. In this context, and by considering the lack of long-term measurements of Hg in Italy, with the availability of only a few datasets at remote and/or rural sites (Sprovieri et al., 2016), it is particularly necessary to present and analyse the results of atmospheric monitoring of TGM at MRG from March 2018 to May 2019. To explain the variability of TGM, other data recorded at MRG are considered and analysed: near-surface ozone (O_3), snow depth and meteorological parameters (e.g., temperature, humidity, atmospheric pressure, wind direction and speed). Long-term measurements of O_3 at high altitude stations have been previously carried out in Italy (Bonasoni et al., 1993; Bonasoni et al., 2000; Cristofanelli et al., 2013a; Cristofanelli et al., 2013b; Cristofanelli et al., 2018; Vecchi and Valli, 1998) as well as in alpine locations of other European countries (see Okamoto and Tanimoto, 2016; Schultz et al., 2017; Cooper et al., 2020 and reference therein). Tropospheric O_3 is recognised as a powerful greenhouse gas (UNEP and WMO, 2011), it influences the oxidation capacity of the troposphere and it affects the health of the human population, as well as the integrity of ecosystem and crop yields (Lefohn et al., 2018; Fleming et al., 2018 and reference therein). It also damages vegetation such as forests and agricultural crops, and the services they provide, in particular food production and carbon sequestration (Stocker et al., 2013). Levels of tropospheric O_3 at regional scales are strongly affected by anthropogenic emissions of precursor species: CO, NO_2, CH_4 and NM-VOCs (UNEP and WMO, 2011). Stratosphere Troposphere Exchange (STE) and lightning production are the main natural tropospheric O_3 sources, so the intrusion of stratospheric air-masses can affect O_3 variability at mountain sites (e.g. Gaudel et al., 2018). O_3 also acts as a powerful oxidizing agent and is able to determine the overall oxidative capacity of the troposphere, affecting the fate of other atmospheric compounds including TGM (Schultz et al., 2015). Even if they are representative of the lower tropospheric layers and are often affected by PBL air-masses (Cooper et al., 2020), continuous observations of O_3 at high altitude sites can still provide valuable information in support of regional strategies for the control of tropospheric O_3, as well as contributing to the validation of models of global and regional air quality or climate. Moreover, for measurements performed at high altitude sites, analysis of the O_3 temporal variability can help in attributing the origin of air masses in conjunction with other atmospheric tracers and transport models (e.g. Cristofanelli et al., 2016). The main objective of this study is to investigate (i) seasonal and diurnal variations of TGM; (ii) the relationship between TGM

and other variables (ozone and the main meteorological parameters); (iii) analysis of back-trajectories and the atmospheric planetary boundary layer (PBL); and (iv) identification of potential sources in terms of local, regional and/or long-range transport.

2 Measurements and methods

2.1 Site description

The Col Margherita atmospheric observatory (GAW ID: MRG, 46.36683° N, 11.79192° E, 2543 m a.s.l.) is located in the mountainous area of the Belluno Dolomites (UNESCO World Heritage site), between the Veneto and Trentino-Alto Adige regions, in Northeast Italy. It is included in the ski area of the San Pellegrino pass, in the municipality of Falcade. MRG is about 15 km far from Falcade (Belluno) and Moena (Trento) (Fig. 1). These two towns, with a total of 4500 inhabitants, means that this area has a population density of less than 35 inhabitants/km^2 which can change significantly in the summer and winter due to tourism.

(a)

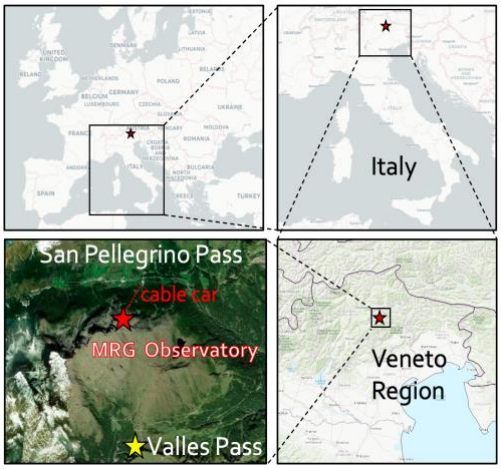

(b)

Figure 1. Geographical location (a) and picture (b) of the Col Margherita Observatory in the South-eastern Alps, Italy.

MRG observatory was established in October 2012 as a GMOS secondary site for background monitoring of TGM in air and mercury in precipitation (Sprovieri et al., 2016; 2017). Operationally, TGM is defined as the sum of the gaseous elemental mercury (GEM) and reactive/oxidized gaseous mercury (RGM or GOM) species (Lin et al., 2019; Munthe et

al., 2001; Prete et al., 2018; Wängberg et al., 2007). The MRG site is ideal for the study of synoptic atmospheric currents thanks to its elevation and morphological characteristics. In fact, it is located on the southern side of the Alps, between the emission sources of the Po Valley basin, one of the most populated regions with high air pollution levels in Southern Europe (Bigi and Ghermandi, 2016; Diémoz et al., 2019), and the industrial areas of Northeastern Europe, comprising Austria, East Germany, the Czech Republic and southeast Poland (Kaiser et al., 2007). There are no known significant local mercury sources such as cement plants, incinerators, industrial activity, or mining activities near the summit or in the surrounding areas. The nearest commercial and industrial areas are about 60 km from the site, where the main urban districts of the Adige Valley (north-east) and Belluno area (south-west) are located. At a distance of about 20 km from MRG there is the mining district of Valle Imperina (pyrite) and in the surrounding area there are other mines (Vallalta and Transacqua), where mining activities closed permanently in the 1960s. In particular, Vallalta was well known for the extraction of cinnabar and native Hg (Wahsha et al., 2014). The atmospheric composition at Col Margherita is related to the transport of air masses on a regional scale, according to the updated Köppen-Geiger classification map (Kottek et al.2006), the climate at MRG can be included in the "Polar" class, but it shows continental features, due to the large temperature ranges. In fact, it is characterized by temperate summers and cold winters. During the analyzed period, the hourly mean temperatures range between -18°C (Dec-Feb) to 18°C (Jul-Aug) with abundant rainfall in summer and snow in the winter. In winter, westerly winds are prevalent, with speed up to 34 m s^{-1}, in other seasons the ESE direction becomes more relevant, but is associated with a lower wind speed. Snow deposition usually starts in November/December and can occur until April/May with continuous snow cover on the ground for the entire period that disappears usually by late May. In winter, wind speeds are high enough that freshly fallen snow does not always remain in place for a long time, but can accumulate in drifts even against the station. Measurements of TGM were performed at MRG from October 2012 to July 2015 within the GMOS project (Sprovieri et al., 2016), where the site is quoted with the code CMA and a mean TGM concentration of 1.7 ± 0.2 ng m^{-3} was reported. The monitoring re-started again in March 2018 within the EU ERA-PLANET iGOSP project (2017-2020). A near-surface O_3 instrument was installed in June 2017 and measurements are ongoing.

2.2 Sampling methods and analysis

2.2.1 Atmospheric mercury measurements

TGM was measured using a Tekran model 2537B instrument (Tekran Instruments Corp., Toronto, Ontario, Canada) following the GMOS project protocols (GMOS SOP, 2011). The continuous Hg analyzer was installed in the autumn of 2012, with the sample inlet probe on top of the shelter, 4 m above the ground. A cylindrical frame in Teflon was mounted to protect the inlet from rain and snow. Due to the high elevation of the site and the consequently reduced atmospheric pressure, an open-phase filter holder with 47 mm Teflon filters (pore size 0.5 μm) was used instead of the 0.2 μm filter recommended in the GMOS SOP to remove particulate matter. This was mounted on the outside opening of the heated fluorocarbon sampling line to avoid atmospheric particulate matter accumulating in the sample line where it could absorb Hg and modify the results. Another 0.2 μm filter mounted on the instrument before the sample in port, prevented particulate matter from reaching the gold preconcentration cartridges. The cabin, where the analyzer was housed, is heated in the winter and ventilated with outside air in the summer. The median temperature inside the MRG observatory was 17.8 °C. TGM measurements were performed by the Hg analyzer using dual gold Hg traps in sequence, with thermal desorption of the Hg and its detection atomic fluorescence spectrometry at 253.7 nm (Munthe et al., 2001; Tekran, 2012). Ultra-high purity (grade 5.0) argon (Società Italiana Acetilene e Derivati, SIAD, Italy) was used as carrier gas. A sampling flow rate of 0.5 L min^{-1} (at standard temperature and pressure) and a 10-minute sampling interval were selected, to ensure a stable sampling volume and to avoid straining the sampling pump due to the low atmospheric pressure (MRG is at an altitude higher than that recommended by Tekran specifications (Tekran, 2012)). Automated calibration of 2537B analyzer, using the internal permeation source, has been set every 72 hours and manual injections and/or standard additions of known amounts of Hg have been performed twice per year using the Tekran Model 2505 external calibration unit, during yearly maintenance cycles and on site, respectively. All GMOS technical recommendations regarding TGM/GEM measurements were followed by site operators during periodic visits at the MRG. Results for TGM were reported as the average mass of TGM per volume of air at 273.15 K and 101.325 kPa (0°C and 1 atm), measured over a specified time interval (10 min). TGM concentrations are reported as nanogram per cubic meter (ng m^{-3}). The time reference system for the dataset is UTC, the same as used in all GMOS reports and publications. The Hg dataset of MRG has been stored in the Data Storage Layer of the Cyber

Infrastructure created for GMOS to provide all users with a common QA/QC procedure and the data management through the Spatial Data Infrastructure (SDI) using the GMOS-Data Quality Management (G-DQM) system, with an automated process for data set treatment.

2.2.2 Near-surface ozone measurements

The O_3 analyzer was installed at MRG on 17th June 2017 and measurements are still ongoing. Surface O_3 measurements are carried out using a Thermo 49c UV-absorption photometric analyzer (Thermo Environmental Instruments Inc., USA), following the EC reference method (EN 14625:2012). The limit of detection (LOD) was 1 ± 1 ppbv (Thermo Environmental Instruments Inc., 2000). The metrological traceability of O_3 measurements to the WMO reference scale is assured by comparison to a laboratory calibrator (Thermo Tei 49i-PS, Thermo Scientific Inc., USA) at the Institute of Atmospheric Science and Climate - National Research Council of Italy (CNR-ISAC) which, in turn, is routinely certified against the Standard Reference Photometer SRP#15 maintained at the WMO/GAW "World Calibration Centre for surface O_3, CO_2, CH_4 and CO" (WCC-Empa Standard Reference Photometer SRP#15). Comparison against the CNR-ISAC laboratory standard is performed roughly every 2 years or after the occurrence of major instrumental failures. These comparison exercises allow us to estimate that the total combined instrumental uncertainty of the O_3 analyzer is less than 1.5 ppb within the range 1-100 ppb, according to the uncertainty methodology calculation provided by Klausen et al. (2003). This temporal frequency is not optimal (a calibration every 2-3 months is recommended by WMO 2013), but this represents the best compromise between the metrological requirements and the difficulty in accessing the measurement site. Zero and span checks were executed on a daily basis. The zero air was generated using an activated charcoal cartridge, while an internal UV source was used to generate a span level of approximately 100 ppb. These checks regularly test the calibration and can identify possible instrumental problems. The execution of quality control/quality check (QA/QC) actions (including the inspection of daily data products, the analysis of instrumental internal parameters or data outliers) are supported by the use of a system based on a suite of automatic processing routines which also produce data files following the WMO/GAW common data model (Naitza et al., 2020). Public access to the MRG O_3 data products is available at https://nextdata.bo.isac.cnr.it.

2.2.3 Meteorological parameters

Meteorological sensors are installed on a compact aluminum tower at 3 m above the ground (ATW3, Campbell Scientific), 10 m away from the observatory. The parameters measured and the sensors used were: air temperature (T) and relative humidity (RH) (CS215 - Campbell Scientific); air pressure (P) (PTB110 barometer – Vaisala); snow depth (SD) (Sonic Ranging Sensor SR50A - Campbell Scientific); wind direction (WD) and wind speed (WS) (Wind monitor-hd alpine model 05108-45 – Young). Sampling time was 5 minutes, but hourly averages were used for data analysis. Data of global solar radiation (SR) (t055 TPIR - SIAP+MICROS) and cumulative precipitation (R) (FAK015AA - MTX s.r.l.) have been taken from the Weather Station located at Passo Valles (2032 m asl) 3 Km away from MRG.

2.2.4 Backward trajectory analysis and boundary layer height

To determine the synoptic origin of the air masses reaching the measurement site, 120-h 3D back-trajectories were calculated every 6 hours (00, 06, 12, and 18 UTC) with the LAGRANTO model (Sprenger and Wernli, 2015; Wernli and Davies, 1997). The model calculations were based on the ERA5 reanalysis dataset of the European Centre for Medium-Range Weather Forecasts (ECMWF, see Hersbach et al., 2020). For each set, 7 back-trajectories were computed, with starting points shifted by ± 1° in latitude/longitude and in a vertical range of ± 50 hPa with respect to the station location, to partially compensate for the absence of subgrid scale processes in LAGRANTO. The temporal resolution for the back-trajectories is one point every hour. To identify the main flows of the synoptic-scale occurring at the measurement site, a cluster analysis was applied to the LAGRANTO back-trajectories (see, e.g., Dorling et al., 1992). The standard Euclidean distance between each pair of trajectories was chosen as the method to compute the different clusters. Only the trajectories with endpoints of 750 hPa were selected, as being more representative of the exact location of the station (results including trajectories at 700 and 800 hPa showed similar patterns). The planetary boundary layer (PBL) height for MRG was estimated by using the ERA5 reanalysis dataset (Hersbach et al., 2020). ERA5 provides data with a spatial resolution of 0.25° x 0.25°, and with a temporal resolution of one hour. The calculations for estimating the PBL height are based on the bulk Richardson number (a measure of atmospheric conditions). It is well known that derived PBL heights can suffer from

uncertainties in mountainous regions; nevertheless, the closest ERA5 PBL height value to MRG was used, in the absence of any other direct or indirect available measurement.

3 Results and discussion

3.1 Temporal trends of TGM

3.1.1 Annual and seasonal patterns of TGM

TGM measurements were carried out with continuous data coverage from March 2018 to May 2019 with the exception of the autumn 2018, when the Hg analyzer was not operational. Overall, measurements at MRG in the period 2018 - 2019 had some programmed interruptions due to routine equipment maintenance, but there are other gaps, particularly in the summer-autumn rainy season, due to unstable power supply issues caused by thunderstorms, which are a frequent occurrence in the Dolomites in summer. Despite these missing measurements, a total of n. 29050 data points were collected every 10-mins (Fig. 2a). From March 2018 to May 2019, mean concentration of TGM was 3 ± 1 ng m^{-3} , which is higher than the previous long-term averaged value (1.7 ± 0.3 ng m^{-3}) calculated from measurements performed between December 2013 to July 2015 (Sprovieri et al., 2016; Table ESM1).

(a)

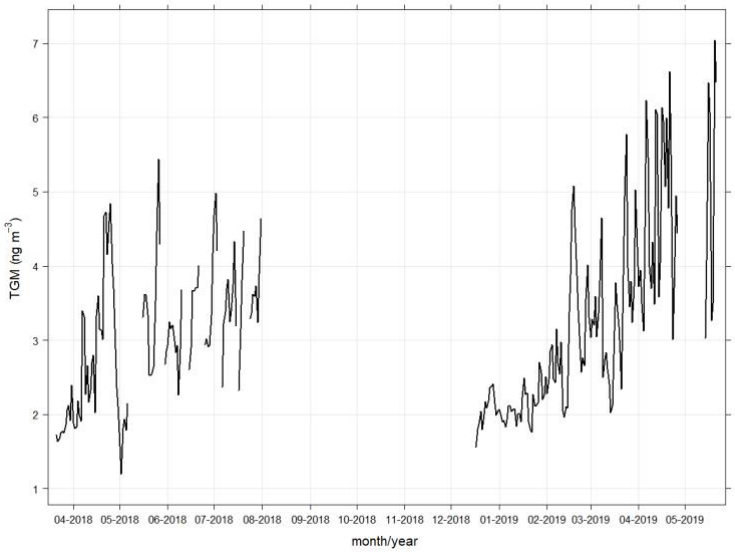

360

(b)

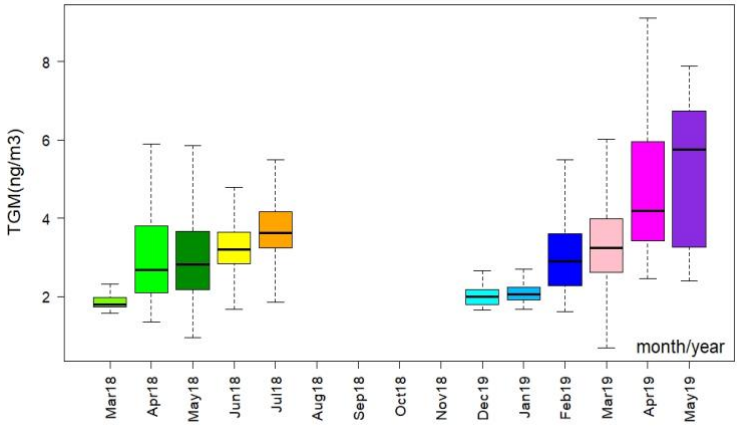

(c)

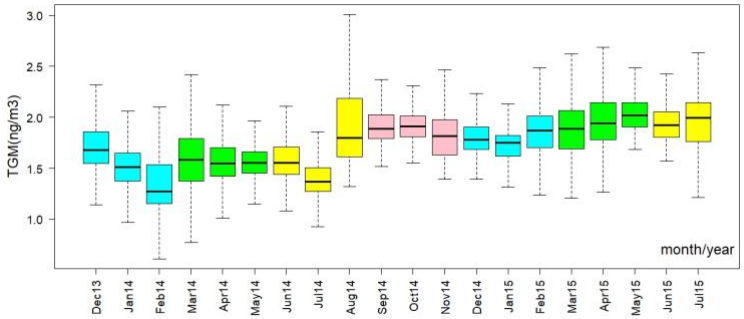

(d)

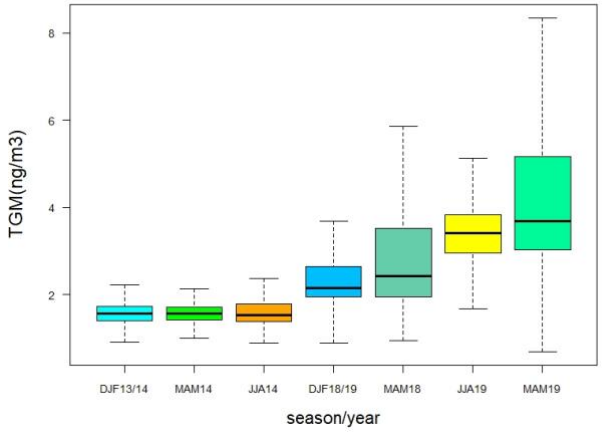

361
362

Figure 2. Temporal trend of daily total gaseous mercury (TGM) concentration (ng m^{-3}) in the atmosphere at MRG 2. a) from March 2018 to May 2019; 2 b) monthly (2018 - 2019) box and whisker plots of TGM concentrations; 2 c) monthly box and whisker plots of TGM from December 3013 to June 2015; 2 d) The seasonal TGM means for 2013 - 2014 and 2018 - 2019 (seasons available for comparison). Seasons are defined as 3-month periods: winter (DJF: December, January, February), spring (MAM: March, April, May), summer (JJA: June, July, August) and fall (SON: September, October, November).

This value, regardless of years, is the highest amongst all the TGM values measured in other mountainous, continental and coastal sites at remote and rural locations in Europe (Denzler et al., 2017; Kentisbeer et al., 2015; Kock et al., 2005; Lee et al., 1998; Slemr and Scheel, 1998; Wängberg et al., 2016), with few exceptions related to short field campaigns in various sites (Halle/Leipzig/Bitterfeld and Langenbrügge) at low altitudes in the Northwestern and Central Europe (Ebinghaus et al., 1995). In addition, only a few measurements carried out at elevated remote and rural sites in China showed TGM concentrations higher than at MRG (Fu et al 2008; Fu et al. 2009; Chen et al. 2013; Chen et al., 2016; Yu et al. 2015; Wan et al. 2009). The mean concentrations of atmospheric gaseous mercury (TGM and GEM) observed in elevated or mountainous sites all over the world are reported in Table ESM1, data from Sprovieri et al. 2016. The median value of TGM in the 2018 - 2019 period was 2.91 ng m^{-3}, 1.22 ng m^{-3} higher than the 2014 median value at MRG (Sprovieri et al., 2016) and 1.61 ng m^{-3} higher than the 2011 - 2012 median value recorded in the Swiss Alps (at Jungfraujoch, 3580 m) (Denzler et al., 2017). This variance is not explained by instrumental variations, because as well as manual calibration checks every 6 months, the instrument recalibrates against an internal permeation source that releases a constant amount of mercury every 72 hours. Additionally, the lamp brilliance and detector gain are adjusted automatically, and manually if need be, especially after lamp changes to keep the instrumental response constant and avoid risk of high results not being registered by going off scale. The mean instrumental response factor for 2013-2015 was $5.09x10^6 \pm 7.02x10^5$ whilst in 2018-2019 it was $6.22x10^6 \pm 1.03x10^6$ which does not explain the large difference in concentrations. A higher response with the same Hg release from the Perm source would result in lower registered concentrations. Higher concentrations would only occur if the perm source was releasing less mercury compared to the set permeation rate which is factory calibrated before delivery, our biannual calibration checks would seem to preclude this possibility. For 2018-2019, monthly average TGM concentrations ranged from a minimum of 1.89 ng m^{-3} (in March and December 2018) to a maximum of 5.19 ng m^{-3} (May 2019) (Table 1). A clear increasing tendency was registered in 2018 from March to July, while a larger increase was

observed in 2019 from January to May (Table 1 and Fig. 2a, 2b). Figure 2c shows the monthly means during the previous, longer TGM measurement period from December 2013 to July 2015. In this dataset, the lowest monthly TGM mean value was registered in February 2014, and the highest in May 2015. So, at MRG, the annual TGM cycle is characterised by an increasing tendency from winter to spring/summer.

Table 1. Main statistical parameters of monthly and seasonal concentrations TGM (in ng m^{-3}) during the measurement period at Col Margherita Observatory. (DJF=winter, MAM=spring, JJA=summer)

Year	2018								2019						
Month	Mar	Apr	May		Jun	Jul	Aug		Dec	Jan	Feb		Mar	Apr	May	
Season				MAM				JJA				DJF				MAM
Min	1.57	1.35	0.94	0.94	1.67	1.75		1.67	0.61	1.67	1.49	0.71	0.69	2.45	2.40	0.69
1st Q	1.72	2.09	2.17	1.94	2.83	3.25		2.96	1.79	1.90	2.27	1.94	2.40	3.41	3.28	3.03
Median	1.79	2.67	2.81	2.42	3.19	3.62		3.40	2.00	2.05	2.90	2.15	3.24	4.18	5.75	3.68
3rd Q	1.98	3.80	3.66	3.51	3.64	4.17		3.83	2.18	2.21	3.58	2.64	3.53	5.93	6.76	5.16
Max	3.81	5.89	6.62	6.62	5.32	6.03		6.03	3.15	3.10	6.20	6.20	6.65	9.12	7.90	9.12
Mean	1.89	2.99	3.00	2.79	3.21	3.69		3.45	1.89	2.11	3.06	2.41	3.03	4.69	5.17	4.13
St.dev.	0.29	1.04	1.12	1.06	0.62	0.76		0.74	0.49	0.29	0.95	0.81	0.84	1.52	1.70	1.54

Looking at the inter-annual variability, the difference between the 2019 and 2018 mean TGM concentrations in March, April and May was 1.52 ng m^{-3}, 1.70 ng m^{-3} and 2.17 ng m^{-3} respectively. April and May of both years were characterized by the largest variability, as clearly indicated by the high standard deviation values (Table 1). Slemr et al. (1996) and Slemr and Scheel (1998) reported that high standard deviation of monthly mean TGM values at the Wank mountain site in Southern Germany were related to the arrival of polluted air masses in these months. Moreover, Slemr et al. (2011) underlined the approximate synchronicity in the seasonal variation of Hg between the northern and southern hemispheres, concluding that a decrease in the trend of Hg emissions between 1996 and 2009 was due to an unchanged distribution of its sources. Looking at 2018, when at least 3 out of 4 seasons are available, TGM concentrations at MRG show a pronounced seasonality (Fig. 2d), with the highest concentration in summer (3.45 ± 0.74 ng m^{-3}) and the lowest in winter 2018 - 2019 (2.41 ± 0.81 ng m^{-3}) (Table 1). Unfortunately, autumn 2018 is missing, therefore the whole yearly trend cannot be completed. Moreover, a remarkable increase in mean TGM was registered when comparing spring 2018 with spring 2019, with an increase from. 2.79 ± 1.06 ng m^{-3} to 4.13 ± 1.54 ng m^{-3} (Table 1). During the GMOS monitoring period, the seasonal variation of TGM in 2014 increased in the following order: winter 2013 - 2014 (1.54 ± 0.37 ng m^{-3}), spring (1.58 ± 0.26 ng m^{-3}), summer (1.65 ± 0.42 ng m^{-3}) and autumn (1.91 ± 0.19 ng m^{-3}). This trend was confirmed the following year, with the mean

TGM concentration in winter 2014 - 2015 resulting lower (1.83 ± 0.32 ng m^{-3}) than spring (1.93 ± 0.26 ng m^{-3}) and summer (1.95 ± 0.26 ng m^{-3}) (Fig. 2d). The seasonal trend in TGM level has already been discussed in several papers. Maxima in summer and minima in winter have been observed in some remote locations in both northern and southern hemispheres. Including high-elevation sites (Karthik et al., 2017; Yin et al., 2018) and baseline monitoring stations (Slemr et al., 2008). Summer peaks in atmospheric Hg level were also observed in the Arctic (Fisher et al., 2012; Schroeder et al., 1998; Steffen et al. 2015) and minima in springtime, with so-called atmospheric Hg depletion events occuring (AMDEs), sometimes concurrently with ozone depletion events (ODEs) (Angot et al., 2016; Dommergue et al., 2010; Lindberg et al., 2001; Skov et al., 2004). An enhanced convective activity in the warm season was associated with maxima in the concentration of atmospheric Hg in the upper troposphere during measurements of CARIBIC (Civil Aircraft for Regular Investigation of the Atmosphere Based on an Instrumented Container) flights performed onboard a passenger aircraft over Europe. Seasonal minima in TGM concentrations were observed between December-April (Slemr et al., 2009). This seasonality is similar to that observed for O_3: during 2018, O_3 showed a clear seasonal variability with the lowest monthly mean values in December (35.5 nmol mol^{-1}) and the highest in July (49.6 nmol mol^{-1}) (Fig. 3). This seasonal cycle nicely fits with the typical seasonal variability affecting near-surface O_3 at other high-altitude sites in the alpine region, also characterised by a winter minimum and a broad spring-summer maximum (Cristofanelli et al., 2015). The summer peak is usually related to the increase in the photochemical production of O_3 in the lower troposphere, coupled with a more efficient vertical transport of polluted air masses rich in reactive photochemical precursors (e.g CO, NOx, VOCs) and the influence of transport processes (Crutzen, 1970; Kaiser et al., 2007; Reiter et al., 1990). A clear enhancement in photochemical and oxidative atmospheric processes at MRG in the summer season was documented in the study conducted by Barbaro et al. (2020), confirming a production of dicarboxylic acids and two photo-oxidation products of α-pinene activated by some oxidants, such as hydroxyl radical (OH) radicals and ozone, both considered in modeling simulation studies of Hg as key oxidation pathways in the free troposphere (Travnikov et al., 2017).

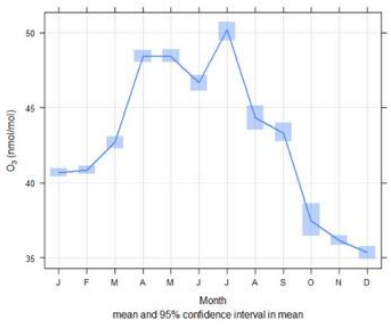

Figure 3. Average monthly variations of O_3 at MRG: the continuous line represents the monthly average values and the vertical bars the 95% confidence interval.

As our TGM dataset does not satisfy one-way ANOVA assumptions, a non-parametric test (i.e. the Kruskal-Wallis KW test) was applied to the hourly data to calculate 95% confidence limits: it confirmed the robustness of differences among all the available seasons (p-value < 0.001). Then, as KW test indicates that a difference does exist between seasons, but not between which ones specifically, several post-hoc tests (Dunn, Conover, Nemenyi, pairwise comparison) were performed and a difference was found between all seasons (p-value < 0.001) (Table ESM2). The frequency distributions of hourly averaged TGM concentrations are shown in Fig. ESM1 for the whole measurement period. A log-normal distribution profile was obtained for the whole period, with concentration values between 0.69 and 9.12 ng m^{-3}, the range from 2.0 to 3.0 ng m^{-3} being the most frequent. In a seasonal view of the data, the range 2.0 - 3.0 ng m^{-3} was the most frequent also in spring 2018 and winter 2018 - 2019, accounting for approximately 35% and 18%, respectively. The range from 3.0 to 4.0 ng m^{-3} instead was prevalent in summer 2018 and spring 2019, with a frequency higher than 50% and 35%, respectively (Fig. ESM1). Differences in the seasonal frequency distribution have been observed in other sites as characteristics of TGM behaviour (Slemr and Scheel, 1998; Wan et al., 2009). In contrast with TGM levels at MRG, other authors (Sheu et al., 2010) documented higher GEM levels in winter/autumn than in summer at a high-elevation station in Taiwan and winter/spring enhancement of Hg concentrations in several locations (Kim et al., 2005). This seasonal pattern found its explanation in several mechanisms such as low planetary boundary layer height, low oxidation rate and enhancement of anthropogenic Hg emissions during winter, as well as meteorological differences between cold and warm seasons. Seasonal variation of wind speed and direction had an impact on atmospheric Hg levels, as reported by Fu et al. (2010) and Karthik et al. (2017). This dependency was attributed to the simultaneous contribution of regional sources and long-range transport (Fu

et al., 2010). High concentrations were related to other atmospheric pollutants behaviour (e.g. CO) and to the wind direction, and attributed to the transport from the emission sources to the monitoring site (Diao et al. 2017). As discussed by Kentisbeer et al. (2014), when the influence from anthropogenic sources resulted scarce or none, as in case of remote sites, far from industrial or urban Hg emission, high Hg concentrations were investigated using air mass back trajectories analysis. To understand if any additional factor may have contributed to the trend of TGM from winter to spring 2019 compared to spring-summer 2018, further investigations are needed. In particular, the determination of total Hg in both bulk deposition and surface snow samples collected on a monthly basis will be performed, and in snow pits realized in spring 2019. A factor to be considered is that Hg stored in forest vegetation and soil is released during biomass burning in smoke and/or ash, and thus emitted in both gaseous and particulate species (Gustin et al., 2008; Witt et al., 2009). Biomass burning input at MRG has been recently documented through the quantification of organic tracers (anhydrosugars and phenolic compounds) onto PM10 samples found in the spring/summer campaign (Barbaro et al., 2020). Therefore, Hg chemical analyses in both bulk deposition and surface snow samples might provide important information on the effects of a forest fire occurred in a large area (650-900 ha) of the Agordina valley 10 Km away from MRG site at the end of October 2018 in terms of Hg liberated into the atmosphere that could have precipitated to the earth's surface via dry and wet deposition process (Arpav 2018; Witt et al., 2009).

3.1.2 Daily patterns and weekly trend of TGM

Diel variations of TGM in different seasons exhibit a similar pattern, decreasing from the late evening to the daily minimum, generally reached in the first part of the day, and then increasing until the maximum in the second part (Fig. 4a). The hours of the extreme values are different according to the season, and they are gradually anticipated of several hours passing from summer (min at 12:00 and max at 22:00 UTC) to winter (min at 7:00 and max at 2:00. UTC). Moreover, the TGM hourly average concentrations follow the scale: winter < spring < summer. The amplitude of TGM daily variation changes seasonally too, and it was larger in summer (0.70 ng m^{-3}) than in winter (0.19 ng m^{-3}). Previous studies at low altitude sites (e.g. Stamenkovic et al., 2007), showed higher TGM concentrations during night-time due to the increase in PBL stability that trapped atmospheric Hg, later emitted from different sources. This cannot be the case for MRG which is located at a mountain top, however the nighttime air masses may contain residual layers reminiscent of the daytime upward transport of air-masses from the regional boundary layer (e.g. Weiss-Penzias et al.,

2006). Summer maxima were also observed by other authors (Kellerhals et al., 2003; Stamenkovic et al., 2007). Spring 2019 is an exception, as TGM daily variation displayed a trimodal trend (Fig. ESM2). Moreover, the features in seasonal and daily cycles indicate that further data are necessary before drawing final conclusions for TGM at MRG over time (Kentisbeer et al., 2015).

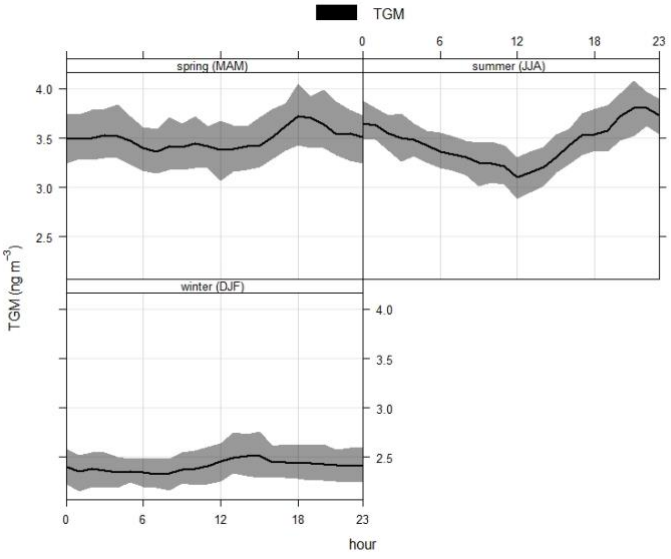

Figure 4. Time variation of average hourly TGM concentrations in the different seasons in 2018 at MRG. The 95% confidence level is shown by vertical bars.

Regarding the meteorological parameters, wind speed, solar radiation and temperature show an opposite diel trend with respect to TGM (Fig. ESM3), with the exception of solar radiation in winter (Fig. ESM3a). Snow depth was almost constant throughout the day in snow covered seasons. As suggested by previous studies, the cycle of Hg dynamics can be potentially influenced by the dominance of several factors on Hg concentrations that change by season and year. Indeed, the daytime atmospheric Hg concentrations (TGM or GEM) were systematically found lower than those in night-time, with averaged hourly values lower in winter than in summertime (Lan et al., 2012; Lee et al., 1998). In spring, during the snow cover season at high-elevation site and in polar and temperate region, the atmospheric Hg accumulates in the snowpack as Hg^{II} because it is scavenged from the air during the snow making process (Lalonde et al., 2002), can be released later as elemental Hg at night-time (Faïn et al., 2013). It starts to increase after sunset as consequence of radicals (e.g.

hydroperoxyl radical, $HO_2\cdot$) in the reduction reaction which prevails over the Hg oxidation process that resulted more active during the day (Ferrari et al., 2004). In summer, the atmospheric gaseous Hg lowest concentration was reached when solar radiation (i.e., air temperature) reached its maximum, while the highest one was measured during dark hours before sunrise. This behaviour has been observed in different locations such as mountainous (Lin et al., 2019) and urban sites (Prete et al., 2018). Other studies described a greater diurnal variability characterized by daily minima before sunrise and maximum level near solar noon, especially in summer with the possible contribution of different factors including greater insolation and higher temperature (Kellerhals et al., 2003). Carpi and Lindberg (1998) and Scholtz et al. (2003) investigated the effect of solar radiation and temperature on atmospheric Hg concentration and its diurnal variability. Light, soil temperature and ozone also resulted in key factors in Hg evasion from the earth's surface (Poissant and Casimir, 1998; Engle et al., 2005; Xin and Gustin, 2007). TGM and O_3 showed similar diel variability over different seasons (Fig. 5a) and this, O_3 variability, can be used to understand processes able to also affect TGM. They both registered lower values in winter with a small variation along the 24 hours. Instead, in spring and summer the amplitude of the daily cycle is higher, with the lowest values during the daytime when solar radiation (Fig. 5b) (and temperature) reached its maximum.

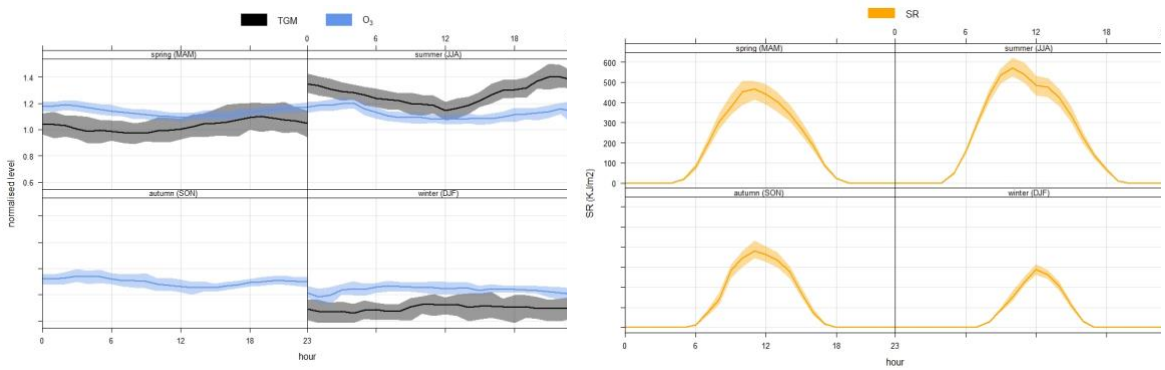

(a) **(b)**

Figure 5. Diurnal variation of TGM (black line) and O_3 (blue line) (a). The variables are normalised, i.e. they are divided by their mean values, to compare the shape of diurnal trends for variables on different scales; solar radiation (orange line) for different seasons during 2018 (b). The TGM values for autumn 2018 are missing.

For O_3, this "reversal" diurnal variation is indicative of the vertical transport from the PBL of air-masses still poor in O_3 as well as to dry deposition processes occurring along the

mountain slopes during the central part of the day. Other phenomena that should be considered are on one side the removal via aqueous-phase chemistry by fog droplets (Ou Yang et al., 2012) or by reacting with locally produced nitrogen oxides (i.e. emitted by soil) (see Wang et al., 2006; Crowley et al., 2010; Warneck, 2000). Conversely, during night-time the higher O_3 values are indicative of a stronger impact of air masses which are more representative of the free troposphere or the regional baseline conditions (see e.g. Cooper et et al., 2020). It is thus conceivable that TGM diel variability at MRG can be affected by the same process. With the aim of specifically evaluating the possibility that the diurnal and the seasonal variability of the regional PBL height affected the atmospheric observations at MRG, we analysed PBL height derived by ERA5. The difference in TGM concentration levels on a seasonal and diurnal basis at MRG could be partially interpreted by the evolution in the height of the PBL. Fig. 6a shows the averaged diurnal variation of PBL height during the winter. In spring and in summer 2018 the height of PBL reached highest levels (Fig. 6b, 6c). On the other hand, comparing the spring 2018 and 2019 there was no marked difference in the PBL height, and this factor failed to provide the reason for different measured mean concentrations of TGM (Fig. 6b, 6d).

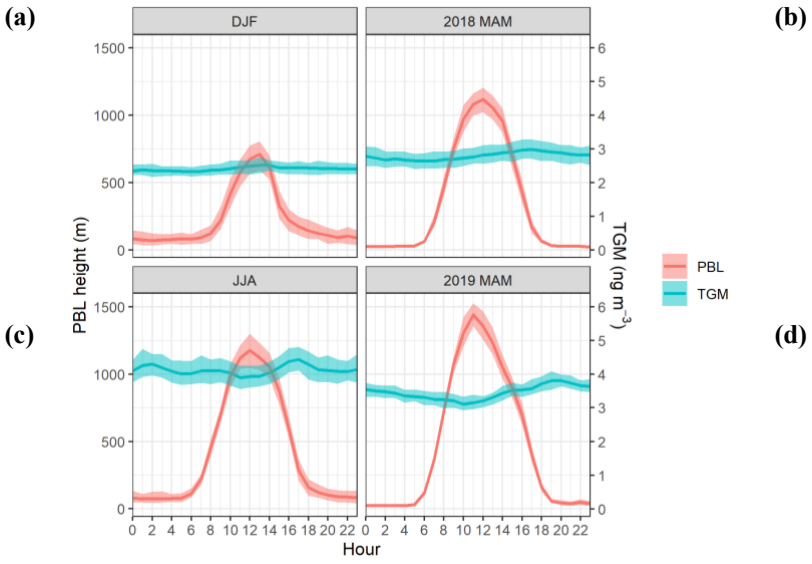

Figure 6. Diurnal variation of PBL and TGM in the different seasons.

As expected, for each season, the atmospheric mixing height showed a diurnal profile, reaching its maximum at around midday (ranging from >500 m a.g.l. during the winter up

to 1200 m a.g.l. in spring and summer) and minimum levels during the dark, with transitions from boundary layer to free tropospheric air. Therefore, we may argue that during spring and summer a potential contribution from anthropogenic and natural sources related to transport of air masses from the PBL is likely for MRG (Obrist et al., 2008). The change in the height of the atmospheric boundary layer, regional and local point sources, in addition to local meteorology, were considered the main factors affecting the diurnal Hg patterns, besides contaminated surfaces and volatilization of previously deposited Hg (Faïn et al., 2009; Prete et al., 2018). Emission by vegetation and water bodies and photochemical reactions are possible reasons for stronger diurnal variation of TGM (Kellerhals et al., 2003). Therefore, the whole effect of chemical and physical processes, that act as both sources and sinks of Hg species, was reflected on the temporal variation of atmospheric gaseous Hg species. The differences in the levels and profiles of the diurnal variation of atmospheric Hg that we registered, suggest the peculiar characteristics of our remote monitoring site (Mao et al., 2008). Additional explanations on different seasonal level of TGM can be possibly drawn analyzing the path of the back-trajectories as well as the relationship between TGM and the ancillary parameters and potential reemission of gaseous Hg from earth surfaces (i.e. snow or soil) (Faïn et al, 2007; Gustin et al., 2006).

3.1.3 Influence of synoptic-scale air mass transport

Fig. 7a shows the density map for the back-trajectories originated at MRG over the whole period of study, with superimposed the mean trajectories for each cluster (see Sect. 2.2.4). Cluster 1 accounted for 15.5% of back-trajectories and it was characterized by air masses originating in eastern Europe, east of the measurement site. Cluster 2 was the most dominant one (35.7%) and it comprised trajectories originating mainly in continental Europe; these air masses were also characterized by relatively low travel altitudes, with respect to the other clusters. Cluster 3, 4, and 5 all represented different types of transport from the west. While cluster 3 showed the second highest occurrence (24.4%) and still some “continental” features, clusters 4 and 5 occurred less frequently (17.7% and 6.7%, respectively), and indicated long-range transport from North America through the Atlantic Ocean, coupled with higher travel altitudes with respect to other clusters. The detailed density maps for the different clusters can be found in the Supplementary Material (Fig. ESM4). We then analyzed the TGM concentrations based on the different air mass transport regimes. Fig. 7b shows the histograms and probability density functions of the TGM measurements, as a function of the clusters shown in Fig. 7a. Since 5 possible cluster attributions characterized

each set of back-trajectories (i.e., 5 back-trajectories at 00, 06, 12, and 18 UTC each day), the mode of cluster values was chosen as representative of each set. The related TGM concentrations at those specific hours were then selected for calculating the histograms. A sensitivity test by calculating the average of the hourly concentrations around each set value (e.g., the average between 21 and 3 UTC as representative of the 00 UTC value, and so on) did not show any significant difference. Cluster 1 was characterized by the highest TGM values on average (dashed lines), thus possibly indicating pollution from largely industrialized areas in Eastern Europe. Values for this cluster were quite equally distributed around all bins, with maximum density between 3 and 4 ng m^{-3}, and a secondary peak between 6 and 7 ng m^{-3}. Cluster 2 was characterized by a slightly lower average value than cluster 1 (3.4 ng m^{-3}), which was also close to the peak of the distribution. Also in this case, air masses from continental Europe or from the Po Valley nearby likely contribute to the high TGM values. Clusters 3, 4, and 5 were characterized by the lowest averages (below 2.8 ng m^{-3}), and for all clusters the distribution density peaked at ~2 ng m^{-3}, thus indicating the arrival of cleaner air masses from the west.

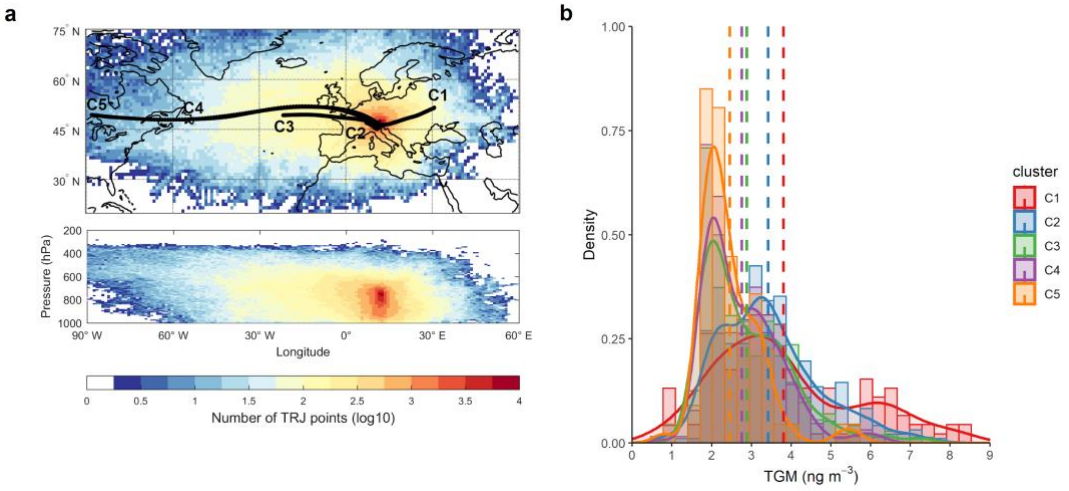

Figure 7. a) Concentration field (vertical cross section included) for back-trajectories starting at MRG, together with the mean trajectories for each cluster; b) probability density function of TGM measurements for each cluster, together with the average values (dashed lines).

For further analyzing the TGM variability as a function of the different air masses, we also deployed the potential source contribution function (PSCF) approach, by using the function implemented in the "openair" R package (Carslaw and Ropkins, 2012). This is a widely used

technique for locating the sources of a pollutant, depending on the back-trajectory positions (see, e.g., Hopke et al., 1995). For each grid cell ij, if n_{ij} is the total number of back-trajectory points falling in that cell during the whole observation period, and m_{ij} is the number of back-trajectory points that fall in the ij-th cell during a certain event (e.g., TGM concentrations higher than a certain threshold), the PSCF is computed as $n_{ij} = \frac{n_{ij}}{n_{nij}}$. The PSCF values can be interpreted as the conditional probability that the TGM concentration at the measurement site exceeds the specific threshold if the air masses passed through the ij-th cell before reaching the station. To account for the uncertainties due to cells with low n_{ij} occurrence, which can lead to unexpected high PSCF values, the PSCF values in this work were scaled by a weighting function W_{ij} (implemented into the "openair" function):

$$W(n_{ij}) = \begin{cases} 1.00, & n_{ij} > 2\overline{n} \\ 0.75, & \overline{n} < n_{ij} \leq 2\overline{n} \\ 0.50, & \overline{n}/2 < n_{ij} \leq \overline{n} \\ 0.15, & n_{ij} \leq \overline{n}/2 \end{cases}$$

where $\underline{n}$ is the average number of endpoints per cell, computed on every cell with at least one endpoint. To retain only "acute pollution events", the threshold was set as the 90th percentile of TGM concentrations. Fig. ESM5 shows the PSCF maps divided in the different seasons, to investigate potential source regions. Since no data for autumn are present, the corresponding map is not shown. On the other hand, to point out the differences already shown in Sect. 3.1.1, maps concerning spring are produced for the two separate years. By considering the two years together, spring was characterized by almost half of the episodes (49.8%), almost equally spaced between years (23.4% for 2018 and 26.4% for 2019). Mainly because of the different values, the PSCF patterns sensibly differ. While 2018 showed only high PSCF values for some air masses originating south of Greenland, 2019 showed the highest contribution from eastern Europe, as already identified by the density functions shown in Fig. 7b. Another important contribution for 2019 was from northern Africa. The elevated contribution from eastern Europe appeared constant also in winter and summer, which showed less occurrence of events (31.5% and 18.7%, respectively). Nevertheless, some limitations of the PSCF approach have to be taken into account: (i) since all trajectories converge to MRG, it is rather difficult to identify possible local sources, (ii) the PSCF field indicates the geographic origin of the air-masses, but does not necessarily indicate a source location (which can effectively occur upwind or downwind of the high PSCF region, especially when dealing with secondary pollutants or with regions crossed by a low number of back-trajectories), (iii) regions with high PSCF values and a low frequency of back-

trajectory occurrence likely provide only a limited integral contribution to the overall observed TGM variability, and (iv) these results can be considered valid for MRG only, and not extended to other measurement sites.

3.1.4 Spatial patterns of TGM

In order to study the potential sources and influence on TGM concentrations observed at MRG, several polar plots have been created and included in Fig. 8: in the left column the concentrations of TGM (ng m^{-3}) are shown as a function of wind speed and direction, on the right column the frequency of wind speed and direction are visualized; each line is referred to a different time period. Fig. 8a depicts that high TGM concentrations are inversely proportional to wind speed, as they were recorded at wind speed < 5 m s^{-1} that accounts for the 80% of the total wind speed values in the study period. This suggests that local sources are significant for this site. In general, the prevalent wind directions at MRG were west and east-southeast (Fig. 8b). The lowest TGM concentrations were measured in relation to air flowing from south west and wind speed up to 25 m s^{-1}, but these events were quite rare (Fig. 8a). The same analysis performed at seasonal level confirms the differences in seasonal trends (see section 3.1.1). In particular, in winter low TGM concentrations were associated with high wind speed and west/southwest wind direction (Fig. ESM3a). In summer high TGM values were related to wind speed up to 15 m s^{-1} blowing from the north eastern sector, thus confirming the potential source emissions over eastern Europe detected by the back-trajectory analysis. The comparison between spring 2018 and 2019 shows that in 2018 there was one prevailing wind direction associated with low wind speed, i.e. the west-east axis, while 2019 was characterized by a wider range of values and directions quite uniformly distributed in the south sector. As already reported in Section 3.11, the TGM values in 2018 were lower than in 2019, when the highest TGM values were associated with wind speed lower than 5 m s^{-1} (Fig. ESM.3b). In the following, we further elaborate on the attribution of the differences observed in TGM between spring 2018 and 2019.

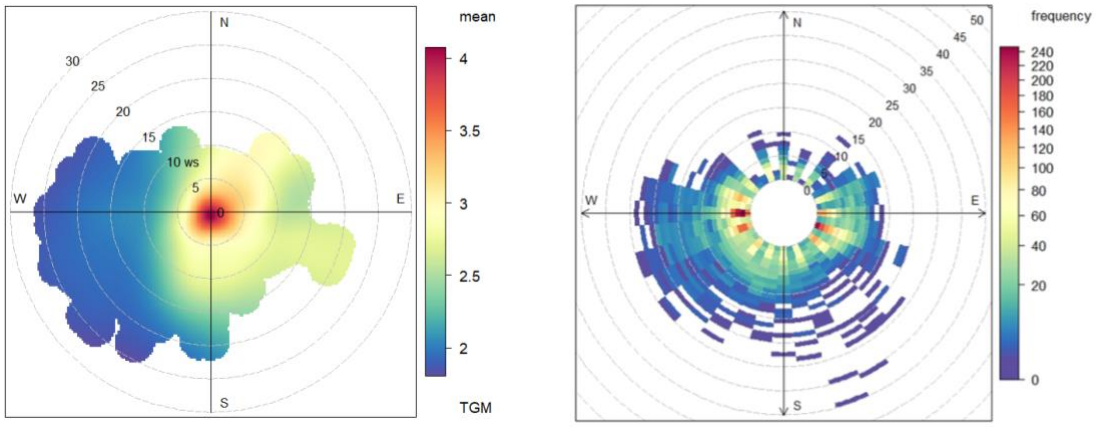

(a) **(b)**

Figure 8. Polar plots (a) of mean TGM (ng m^{-3}), showing the variation in concentration by wind speed (m s^{-1}) and direction (°N), and polar frequency plot (b) of wind speed and direction, referred to the whole investigated period. Plots generated using OpenAir in R.

3.2 The difference between spring 2018 and 2019: investigation of the relation between TGM and meteorological factors at different scales

The relation between atmospheric Hg species and meteorological variables has been already explored in literature, but few data are available for mountain sites (Berg et al., 2013; Diéguez et al., 2019; Fain et al., 2009; Fu et al., 2012a, 2012b; Wan et al., 2009). In particular, wind speed and direction played an important role in the identification of TGM sources and transport patterns (Zhang et al., 2015, 2016), while temperature, solar radiation and wind speed were often related to TGM diurnal cycle (Yin et al. 2018). The seasonal analysis at MRG showed quite different TGM concentrations in spring 2018 and 2019, therefore the relation between TGM and the meteorological variables was investigated more in depth, to try identifying the processes mainly responsible for this difference. Firstly, a correlation chart of the daily averages of all the variables was produced. Daily averages were used to remove any bias from diurnal variability and the analysis was carried out separately for the two springs. The most remarkable difference was the strong correlation between TGM and snow depth (SD) and the anti-correlation between TGM and wind speed in spring 2019. The positive correlation with SD and the negative correlation with wind speed indicates a likely re-emission process from the snow cover. April 2019 was characterized by a very high precipitation amount (326 mm), reaching the levels of October 2018 (340 mm).

Moreover, SD showed a decreasing trend from March to May 2018, while in spring 2019 it gradually increased and reached the highest value of the whole monitoring period in May, i.e. about 160 cm. The LAGRANTO back-trajectories analysis suggested significant differences in synoptic-scale air mass circulation between spring 2018 and spring 2019 (Fig. ESM5). While a dominant westerly contribution was evident for spring 2018, important contributions from eastern Europe and northern Africa were evident for spring 2019. In particular, eastern Europe is a well-known source of anthropogenic Hg. These different synoptic-scale atmospheric transport regimes are supported by local wind observations: the prevalent monthly wind direction in spring 2018 was south-west, while in spring 2019 it changed to south-east. This is consistent with the significantly different atmospheric transport regimes diagnosed by the LAGRANTO analyses: in spring 2019 air masses mainly from eastern Europe were likely transported by the atmospheric long-range circulation at MRG, possibly contributing to the high TGM high concentration. This interpretation is also in accordance with the monthly average wind speed, that was around 2.5 m/s in spring 2018, it reached values up to 7 m/s in January 2019, favouring the long-range transport, then it dropped at 4 m/sec in May, enhancing the contribution of the main local source, i.e. the re-emission from the snow cover, thus resulting anti-correlated with TGM.

In conclusion, the differences in TGM concentrations between the two springs were likely attributed to the combination of different factors: (i) synoptic-scale atmospheric circulations more favourable for the transport of polluted air-masses from eastern Europe in spring 2019; (ii) high amount of snow precipitation in winter and spring 2019; (iii) re-emission process of Hg from the snowpack in spring 2019. Anyhow, these preliminary findings suggest that further data are required to investigate better the sources and the transport processes at local and large scales that are responsible for the TGM behaviour at MRG, due to the high amount of inter-annual variability.

4. Analysis of some episodic high or low TGM concentration events

Some peculiar profiles in the TGM concentrations have been observed over a short period of time, usually lasting a few hours. The behaviour of atmospheric Hg has been examined in a time slot around these particular events, considering also other variables such as surface ozone and meteorological parameters. These events were characterized by an average TGM hourly concentration at least 5% above or below the average concentration of the previous or following 24 hours. A similar approach was used by other authors (Ci et al., 2011; Han et al., 2014; Mao et al., 2016).

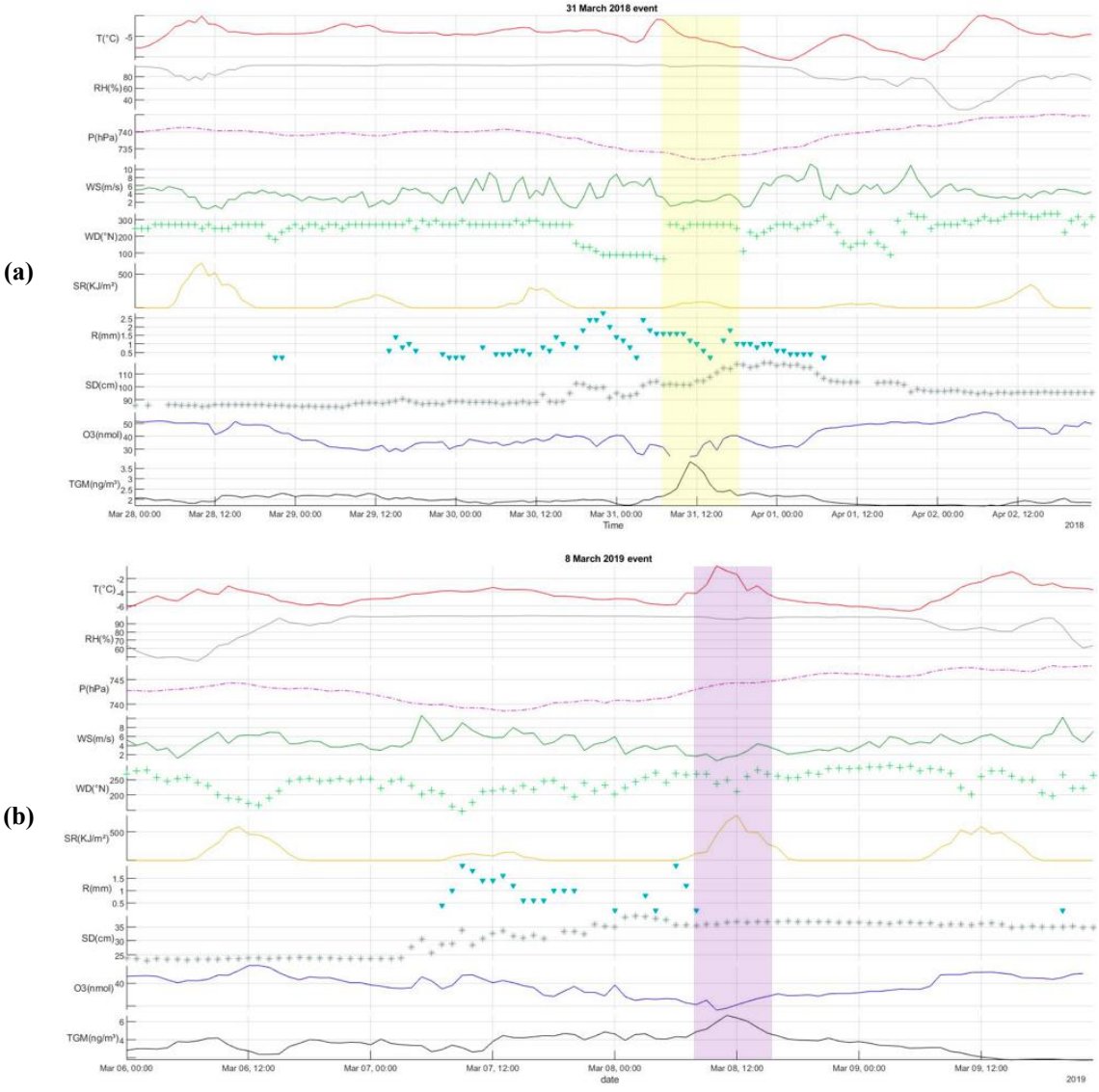

Figure 9. Summary of the profile of hourly measured parameters during the a) event#1, b) event#2. From the bottom to the top: TGM concentrations (black line), O_3 (blue line), snow depth (SD) (grey asterisk), snowy deposition (R) (turquoise triangle), solar radiation (SR) (orange line), wind direction (WD) (°N, light green cross), wind speed (WS) (dark green line), atmospheric pressure (P) (pink dashed line), relative humidity (RH) (grey line), air temperature (T) (red line). Event#1 and event#2 ranges are highlighted by the yellow and pink shading, respectively. Grey dashed vertical lines indicate midday and midnight.

781 The event #1 occurred on 31 March 2018, with a peak between 06:00 UTC (08:00 LST, local
782 standard time) and 18:00 UTC that reached a maximum TGM concentration of 3.81 ng m^{-3}
783 at 11:00 UTC, while the ozone concentration reached its lowest value for the entire spring
784 and summer of 2018, i.e. 24.5 nmol mol^{-1}. At the same time, the values of other parameters
785 were: air T=-5.2 °C, P=732 hPa, RH=98%, and wind blowing from west with speed < 2.0 m
786 s^{-1}. In addition, solar radiation was significantly lower than the value registered the day
787 before at the same hour, of the TGM peak, i.e. 66.1 and 302 KJ m^{-2}, respectively. Moreover,
788 SD increased by 14 cm and about 32 mm of wet precipitation (snow deposition) were
789 registered (Fig. 9a). A similar event (event #2) occurred on 8 March 2019, recording a rapid
790 rise in TGM concentrations (6.65 ng m^{-3} at 11:00 UTC), a few hours after 24 hours of
791 snowfall (SD > 4.5 cm). At that time the levels of the following parameters were: T = - 0.9
792 °C, wind speed < 1.5 m s^{-1}, RH up to 95%, Solar Radiation about 700 KJ m^{-2} and ozone
793 again at its lowest value (29 nmol mol^{-1}) (Fig. 9b). Both sudden increases in hourly TGM
794 were registered after significant snow deposition. Therefore, the snow surface that
795 accumulated Hg, could have released it within 24/36 hours, contributing to a TGM peak that
796 recycled Hg between the snow and the lower atmosphere (Spolaor et al., 2018). Indeed, snow
797 is considered a wet deposition vector and an active substrate for transferring Hg from the
798 atmosphere to the surface and visa versa (Faïn et al., 2007, 2009; Spolaor et al., 2019).
799 Moreover, the sudden increase of TGM in both events occurred under particular weather
800 conditions of (i) sub-zero temperature (< -0.8°C), (ii) high relative humidity, (iii) low wind
801 speed (< 2.0 m s^{-1}) and in the daytime. These TGM peaks can be interpreted as the release
802 into the ambient air of Hg^0 after photoreduction during daytime of the Hg^{2+} deposited onto
803 the snow surface via wet (and dry) deposition (Subir et al., 2012; Swartzendruber et al.,
804 2006). Indeed, we suppose that Hg^{2+} (Hg^{II} in both gaseous and particulate form) underwent
805 a photoreduction process that usually takes place in aquatic media (wet or frozen such as the
806 snow surface) (Weiss-Penzias et al., 2015). The change in the wind direction from west to
807 east (event #1) favoured the mixing of two air masses of different origins, the low wind
808 speed conditions also favoured fast increases in TGM concentrations as the Hg remained
809 above the surface instead of being transported away. This, combined with the wind direction
810 effect, suggests a switch between local and regional influences and sources (Fu et al., 2010,
811 2012a, 2012b; Kentisbeer et al., 2014, 2015; Swartzendruber et al., 2006). Several events
812 (e.g. event #3 that occurred between 8-10 April 2018, not shown), depicted a Hg pattern
813 strongly related to the wind speed. In this case, the TGM concentrations varied from > 3 ng
814 m^{-3} to < 2 ng m^{-3}, and a minimum was reached when wind speed changed from values < 2.0
815 m s^{-1} to > 7.5 m s^{-1} (9 April, 11.00 UTC). The influence of wind speed, wind direction and

other meteorological parameters on atmospheric Hg levels has been observed also in the events #1 and #2, and by other authors in other sites (Fu et al., 2009, 2010, Prete et al., 2018; Swartzendruber et al., 2006; Wan et al., 2009; Yin et al., 2018).

5. Conclusion

In this work, TGM was monitored continuously at Col Margherita site, the highest observatory for the study of atmospheric Hg in Italy. The mean TGM concentration at MRG based on a year-round measurement (March 2018 to May 2019) was 3.14 ±1.29 ng m^{-3}, which resulted considerably higher than other long-term averaged values observed in remote and rural sites of mountainous, continental and coastal locations of Europe and North America, but lower than those registered at some elevated remote and rural stations in China. Differences in seasonal mean TGM levels showed an increasing tendency from cold to warm season similarly to some remote sites located in the Northern and Southern Hemisphere. Diurnal variability of TGM exhibited a similar pattern over different seasons with an amplitude larger in summer than winter. The spatial patterns of TGM noticeably varied seasonally and low TGM concentrations were related with high wind speeds. Low winter values were associated with west/southwest wind direction and summer high TGM values to the northeast sector. Considering the whole measurement period, high TGM concentrations were likely associated with low wind speed and no prevalence in wind direction, indicating a significant contribution of local sources (e.g. re-emission from snow and soil surface). Some events were identified during which hourly peaks of TGM were registered in peculiar weather conditions, such as T below 0°C, sunlight and abundant snow deposition. These quick increases of TGM may be attributed to photochemical reduction of gaseous and/or particulate Hg^{II} previously deposited onto snow surfaces. The correlation analysis applied to the whole dataset did not provide any relevant correlation between TGM and the other ancillary variables (meteorological parameters and ozone). Contrariwise, considering separately springs 2018 and 2019, strong correlation was found between TGM and temperature, whilst the correlation between TGM and P was notable only in spring 20. In addition, TGM was strongly correlated with snow depth and anti-correlated with wind speed in spring 2019. The PBL analysis at MRG showed diurnal variation with lower height during the dark, reaching the maximum at midday. Seasonal change of PBL height provided higher values following the order: summer>spring (2018 and 2019)>winter. The PBL height of two springs was comparable and no conclusions could be drawn considering only this factor. Different seasonal levels of TGM found an explanation in the analysis of the back-

trajectories, that displayed higher TGM level with air masses that originated over Eastern Europe and passed from continental Europe, while low TGM concentrations were associated with long-range transport of cleaner air masses from west sector originating in North America and Atlantic Ocean. As observed the levels and temporal trends of TGM suggest the specificity of the remote site of MRG. Furthermore, the comparison of the two different springs resulted not comparable in terms of concentration and profiles. Hence, the results of this year-round investigation showed that the behavior of atmospheric Hg is potentially caused by multiple environmental factors. In order to understand the effect of air pollution and the potential impact of climate change, further investigations are needed in terms of a longer TGM monitoring activity, and additional measurements of Hg in atmospheric deposition, snow and soil will be performed. The future goal will be to improve the knowledge of Hg behavior and its deposition/reemission processes to/from the earth's surface that can play an important role as a sink and source of Hg at remote alpine regions.

Acknowledgments

The Hg measurements of this study were supported by ERA-PLANET (www.era-planet.eu), trans-national project iGOSP - Integrated Global Observing Systems for Persistent Pollutants (www.igosp.eu), funded under the EU Horizon 2020-SC5-15-2015 “Strengthening the European Research Area in the domain of Earth Observation”, type of action: ERA-NET-Cofund Grant, (Grant Agreement N. 689443). The authors are grateful for financial support by the National Project of Interest Next-Data (http://www.nextdataproject.it/) by the Italian Ministry for Education, University and Research (MIUR), for ozone and meteorological measurements. The authors would like to thank Dr. Federico Scoto (CNR-ISAC) and Dr. Ilaria Crotti (Ca’ Foscari University of Venice) for providing the Col Margherita location maps and additional graphs using QGis open-source software and MATLAB, respectively. The authors are grateful to Dr. Michael Sprenger at the atmospheric dynamics group at IAC-ETH, Zurich, for help in using the LAGRANTO.FTP tool for calculating the backward trajectories. This work includes modified Copernicus Atmosphere Monitoring Service information [2020].
The ERA5 PBL dataset has been downloaded from the Climate Data Store (https://cds.climate.copernicus.eu/#!/home). We also thank Meteotrentino for providing the solar radiation and precipitation data from the weather station of the Passo Valles (Trento, Italy) (https://www.meteotrentino.it). Finally, authors would like to cordially thank Renzo Minella and Loris Scola, director of the “Ski area San Pellegrino” (https://www.ski area sanpellegrino.it) and head of the cable car service, respectively, and all technical staff for their appreciated cooperation and support during field activities at the Col Margherita Observatory.

Data availability

All the data presented in this work are available for scientific purposes upon request to the corresponding authors

Declaration of competing interest

The authors declare that they have no known competing financial interests or personal relationships that could have appeared to influence the work reported in this paper.

Appendix A. List of abbreviations and acronyms used in the paper and supplementary material

AAS – Atomic absorption spectrometry
AFS – Atomic fluorescence spectrometry
AMNET – American Atmospheric Mercury Network
AMS – Automated measuring system
APMMN – Asia Pacific Mercury Monitoring Network
ARPA – Regional Agencies for Environmental Protection
ATSDR – Agency for Toxic Substances and Disease Registry
CAMNet – Canadian Atmospheric Mercury Network
CARIBIC – Civil Aircraft for Regular Investigation of the Atmosphere Based on an Instrumented Container
CEMS – Continuous Emissions Monitoring System
CEN – European Committee for Standardization
DQM – Data Quality Management
EMEP – European Monitor Observations and Evaluation Programme
ECV –Essential Climate Variables
EN – European Standard
EPA – Environmental Protection Agency
GAW – Global Atmosphere Watch
GEM – Gaseous elemental mercury
GMOS – Global Mercury Observation System
GOM – Gaseous oxidized mercury
iGOSP – Integrated Global Observing Systems for Persistent Pollutants
ISO – International Organization for Standardization
ISS – Italian National Institute of Health
ISPRA – Institute for Environmental Protection and Research
LOAEL – Lowest-observed-adverse-effect level
LOD – Limit Of Detection
LST – Local Standard Time
MATTM – Ministry for Environment, Land and Sea Protection of Italy
MIUR – Ministry of Education, University and Research
MRG – Col Margherita Observatory
MRLs – Minimal Risk Levels
NRT – Near Real Time
PBL – Planet Boundary Layer
PBM2.5 – Particulate Bounded Mercury (<2.5μm)
PSCF – Potential Source Contribution Function
QA – Quality Assurance

QC – Quality Control
RfC – Reference concentration for Chronic inhalation exposure
RGM - Reactive Gaseous Mercury
SDI – Spatial Data Infrastructure
SOP – Standard Operating Procedure
TC – Technical Committee
TGM – Total gaseous mercury
UNEP – United Nations Environment Programme
UNESCO – United Nations Educational, Scientific and Cultural Organization
WHO – World Health Organization
WMO – World Meteorological Organization

References

Angot, H., Dastoor, A., De Simone, F., Gårdfeldt, K., Gencarelli, C. N., Hedgecock, I. M., Langer, S., Magand, O., Mastromonaco, M. N., Nordstrøm, C., Pfaffhuber, K. A., Pirrone, N., Ryjkov, A., Selin, N. E., Skov, H., Song, S., Sprovieri, F., Steffen, A., Toyota, K., Travnikov, O., Yang, X., and Dommergue, A.: Chemical cycling and deposition of atmospheric mercury in polar regions: review of recent measurements and comparison with models, Atmos. Chem. Phys., 16, 10735–10763, 2016. https://doi.org/10.5194/acp-16-10735-2016

Arpav, Agenzia Regionale per la Prevenzione e Protezione Ambientale del Veneto, 2018, https://www.arpa.veneto.it/arpavinforma/comunicati-stampa/archivio/comunicati-2018/incendio-boschivo-a-taibon-agordino-aggiornamenti/?searchterm=incendio%20taibon (in Italian)

Bagnato, E., Aiuppa, A., Parello, F., Calabrese, S., D'Alessandro, W., Mather, T.A., McGonigle, A.J.S., Pyle, D.M., Wängberg, I., Degassing of gaseous (elemental and reactive) and particulate mercury from Mount Etna volcano (Southern Italy), Atmos. Environ., 41(35), 7377-7388, 2007, https://doi.org/10.1016/j.atmosenv.2007.05.060

Bagnato, E., Parello, F., Valenza, M., Caliro, S., Mercury content and speciation in the Phlegrean Fields volcanic complex: Evidence from hydrothermal system and fumaroles, J. Volcanol. Geotherm. Res., 187(3-4), 250-260, 2009, https://doi.org/10.1016/j.jvolgeores.2009.09.010

Bagnato, E., Sprovieri, M., Barra, M., Bitetto, M., Bonsignore, M., Calabrese, S., Di Stefano, V., Oliveri, E., Parello, F., Mazzola, S., The sea-air exchange of mercury (Hg) in the marine boundary layer of the Augusta basin (southern Italy): Concentrations and evasion flux, Chemosphere, 93(9), 2024-2032, 2013, https://doi.org/10.1016/j.chemosphere.2013.07.025

973 Bagnato, E., Barra, M., Cardellini, C., Chiodini, G., Parello, F., Sprovieri, M., First combined flux chamber
974 survey of mercury and CO_2 emissions from soil diffuse degassing at Solfatara of Pozzuoli crater, Campi Flegrei
975 (Italy): Mapping and quantification of gas release, J. Volcanol. Geotherm. Res., 289, 26-40, 2014,
976 http://doi.org/10.1016/j.jvolgeores.2014.10.017
977
978 Bagnoli, A., and Gartner, I., Monitoraggio delle aree geotermiche toscane: Concentrazioni di H_2S e Hg nelle
979 aree geotermiche toscane. Monitoraggi ARPAT e validazione dati Enel (Area Vasta Sud. Report anno 2017.
980 Arpa Toscana 2018, Prot. n° 0046235, 1-41 (Technical Report), 2018 (in Italian).
981 Barbaro, E., Morabito, E., Gregoris, E., Feltracco, M., Gabrieli, J., Vardè, M., Cairns, W.R.L., Dallo, F., De
982 Blasi, F., Zangrando, R., Barbante, C., Gambaro, A., Col Margherita Observatory: A background site in the
983 Eastern Italian Alps for investigating the chemical composition of atmospheric aerosols, Atmos. Environ., 221,
984 117071, 2020, https://doi.org/10.1016/j.atmosenv.2019.117071
985
986 Blanchard, P., Froude, F.A., Martin, J.B., Dryfhout-Clark, H., Woods, J.T., Four years of continuous total
987 gaseous mercury (TGM) measurements at sites in Ontario, Canada, Atmos. Environ., 36(23), 3735-3743, 2002,
988 https://doi.org/10.1016/S1352-2310(02)00344-8
989
990 Beniston, M., Diaz, H.F., Bradley, R.S., Climatic Change at High Elevation Sites: an overview, Clim. Change,
991 36(3-4), 233-251, 1997, https://doi.org/10.1023/A:1005380714349
992
993 Berg, T., Pfaffhuber, K.A., Cole, A.S., Engelsen, O., Steffen, A., Ten-year trends in atmospheric mercury
994 concentrations, meteorological effects and climate variables at Zeppelin, Ny-Ålesund, Atmos. Chem. Phys.,
995 13, 6575-6586, 2013, https://doi.org/10.5194/acp-13-6575-2013
996
997 Bigi, A., and Ghermandi, G.: Trends and variability of atmospheric PM2.5 and PM10–2.5 concentration in the
998 Po Valley, Italy, Atmos. Chem. Phys., 16, 15777–15788, 2016. https://doi.org/10.5194/acp-16-15777-2016
999
1000 Bonasoni, P., Giovanelli, G., Colombo, T., and Cundari, V., Surface ozone observations at Mt. Cimone
1001 Observatory, Italy, Proc. SPIE 2047, Atmospheric Ozone, November, 2 1993,
1002 https://doi.org/10.1117/12.163483
1003
1004 Bonasoni, P., Stohl, A., Cristofanelli, P., Calzolari, F., Colombo, T., and Evangelisti, F.: Background ozone
1005 variations at Mt. Cimone Station, Atmos. Environ., 34, 5183–5189, 2000, https://doi.org/10.1016/S1352-
1006 2310(00)00268-5
1007
1008 Breder, R., Flucht, R., Mercury levels in the atmosphere of various regions and locations in Italy, Sci. Total
1009 Environ., 40, 231–244, 1984, https://doi.org/10.1016/0048-9697(84)90353-X
1010
1011 Cabassi, J., Tassi, F., Venturi, S., Calabrese, S., Capecchiacci, F., D'Alessandro, W., Vaselli, O., A new
1012 approach for the measurement of gaseous elemental mercury (GEM) and H_2S in air from anthropogenic and
1013 natural sources: Examples from Mt. Amiata (Siena, Central Italy) and Solfatara Crater (Campi Flegrei,
1014 Southern Italy), J. Geochem. Explor., 175, 48-58, 2017, https://doi.org/10.1016/j.gexplo.2016.12.017

Cairns, W.R.L., Vardé, M., Dallo, F., de Blasi, F., Maffezzoli, N., Gabrieli, J., Cozzi, G., Barbante, C., Cristofanelli, P., Naitza, L., Calzolari, F., Busetto, M., Davolio, S., Bonasoni, P., (2019). Total Gaseous Mercury (TGM) and ozone (O_3) over spring - summer 2018 and winter 2019 at the Col Margherita Atmospheric Observatory (2543 m a.s.l.). In Proceedings of the ICMGP 2019, The 14th International Conference on Mercury as a Global Pollutant, September 7-13, 2019. Krakow, Poland, pp 109-110.

Carslaw, D., and Ropkins, K., Openair – an R package for air quality data analysis, Environ. Model. Softw., 27–28, 52–61, 2012. https://doi.org/10.1016/j.envsoft.2011.09.008

Carpi, A., and Lindberg, S.E., Sunlight-mediated emission of elemental mercury from soil amended with municipal sewage sludge, Environ. Sci. Technol., 31 1997, 2085-2091. https://doi.org/10.1021/es960910+

Chen, L., Liu, M., Xu, Z., Fan, R., Tao, J., Chen, D., Sun, J., Variation trends and influencing factors of total gaseous mercury in the Pearl River Delta - a highly industrialized region in South China influenced by seasonal monsoons. Atmos. Environ., 77, 757-766, 2013. https://doi.org/10.1016/j.atmosenv.2013.05.053

Chen, W.K., Li,T.C., Sheu, G.R., Lin, N.H., Chen, L.Y., Yuan, C.S., Correlation analysis, transportation mode of atmospheric mercury and criteria air pollutants, with meteorological parameters at two remote sites of mountain and offshore island in Asia, Aerosol Air Qual. Res., 16, 2692-2705, 2016. https://doi.org/10.4209/aaqr.2015.07.0455

Ci, Z., Zhang, X., Wang, Z., Niu, Z., Atmospheric gaseous elemental mercury (GEM) over a coastal/rural site downwind of East China: Temporal variation and long-range transport, Atmos. Environ., 45(15), 2480-2487, 1352-2310, 2011, https://doi.org/10.1016/j.atmosenv.2011.02.043

Cooper, O.R., Schultz, M.G., Schroeder, S., Chang, K.-L., Gaudel, A., Benítez, G.C., Cuevas, E., Fröhlich, M., Galbally, I.E., Molloy, S., Kubistin, D., Lu, X., McClure-Begley, A., Nédélec, P., O'Brien, J., Oltmans, S.J., Petropavlovskikh, I., Ries, L., Senik, I., Sjöberg, K., Solberg, S., Spain, G.T., Spangl, W., Steinbacher, M., Tarasick, D., Thouret, V. and Xu, X., Multi-decadal surface ozone trends at globally distributed remote locations. Elem Sci Anth, 8(1), 1-23, 2020. http://doi.org/10.1525/elementa.420

Carvalho, A., Monteiro, A., Ribeiro, I., Tchepel, O., Miranda, A.I., Borrego, C., Saavedra, S., Souto, J.A., Casares, J.J., High ozone levels in the northeast of Portugal: Analysis and characterization, Atmos. Environ., 44(8), 1020-1031 2010. https://doi.org/10.1016/j.atmosenv.2009.12.020

Cole, A.S., and Steffen, A., Trends in long-term gaseous mercury observations in the Arctic and effects of temperature and other atmospheric conditions, Atmos. Chem. Phys., 10, 4661-4672, 2010, https://doi.org/10.5194/acp-10-4661-2010

Cristofanelli, P., Fierli, F., Marinoni, A., Calzolari, F., Duchi, R., Burkhart, J., Stohl, A., Maione, M., Arduini, J., and Bonasoni, P., Influence of biomass burning and anthropogenic emissions on ozone, carbon monoxide and black carbon at the Mt. Cimone GAW-WMO global station (Italy, 2165 m a.s.l.), Atmos. Chem. Phys., 13, 15–30, 2013a, https://doi.org/10.5194/acp-13-15-2013

Cristofanelli, P., di Carlo, P., Altorio, A.D. et al. Analysis of Summer Ozone Observations at a High Mountain Site in Central Italy (Campo Imperatore, 2388 m a.s.l.). Pure Appl. Geophys. 170, 1985–1999, 2013b. https://doi.org/10.1007/s00024-012-0630-1

Cristofanelli, P., Scheel, H.-E., Steinbacher,M., Saliba, M., Azzopardi, F., Ellul, R., Fröhlich,M., Tositti, L., Brattich, E., Maione, M., Calzolari, F., Duchi, R., Landi, T.C., Marinoni, A., Bonasoni, P., Long-term surface ozone variability at Mt. Cimone WMO/GAW global station (2165 m a.s.l., Italy), Atmos. Environ., 101, 23-33, 2015. https://doi.org/10.1016/j.atmosenv.2014.11.012

Cristofanelli, P., Landi, T.C., Calzolari, F., Duchi, R., Marinoni, A., Rinaldi, M., Bonasoni, P., Summer atmospheric composition over the Mediterranean basin: Investigation on transport processes and pollutant export to the free troposphere by observations at the WMO/GAW Mt. Cimone global station (Italy, 2165 m a.s.l.). Atmos. Environ., 141, 139–152, 2016. https://doi.org/10.1016/j.atmosenv.2016.06.048

Cristofanelli, P., Brattich, E., Decesari, S., Landi, T.C., Maione, M., Putero, D., Tositti, L., Bonasoni, P., High-mountain atmospheric research the Italian Mt. Cimone WMO/GAW global station 2165 m asl, Springer Briefs in Meteorology, 2018, https://doi.org/10.1007/978-3-319-61127-3978-3-319-61126-6

Crowley, J. N., Schuster, G., Pouvesle, N., Parchatka, U., Fischer, H., Bonn, B., Bingemer, H., and Lelieveld, J.: Nocturnal nitrogen oxides at a rural mountain-site in south-western Germany, Atmos. Chem. Phys., 10, 2795–2812, 2010. https://doi.org/10.5194/acp-10-2795-2010

Crutzen, P.J., The influence of nitrogen oxides on the atmospheric ozone content. Quart. J. Roy. Meteor. Soc. 96, 320-325, 1970. https://doi.org/10.1002/qj.49709640815

D'Amore, F., Bencardino, M., Cinnirella, S., Sprovieri, F., Pirrone, N., Data quality through a web-based QA/QC system: implementation for atmospheric mercury data from the global mercury observation system, Environ. Sci.: Process. Impacts, 17(8), 1482-1491, 2015, https://doi.org/10.1039/c5em00205b

Denzler, B., Bogdal, C., Henne, S., Obrist, D., Steinbacher, M., and Hungerbühler, K.: Inversion Approach to Validate Mercury, Emissions Based on Background Air Monitoring at the High Altitude Research Station Jungfraujoch (3580 m), Environ. Scie. Technol., 51, 2846–2853, 2017. https://doi.org/10.1021/acs.est.6b05630

Diao, C., Li, J., Zhang, B., Tang, S., Characteristics of total gaseous mercury concentrations at a coastal area of the Yangtze Delta. China, J. Air. Waste. Manage., 67(3), 341-351, 2017, http://dx.doi.org/10.1080/10962247.2015.1054529

Diéguez, M.C., Bencardino, M., García, P.E., D'Amore, F., Castagna, J., De Simone, F., Soto Cárdenas, C., Ribeiro Guevara, S., Pirrone, N., Sprovieri, F., A multi-year record of atmospheric mercury species at a background mountain station in Andean Patagonia (Argentina): temporal trends and meteorological influence, Atmos. Environ., 214, 116819, 2019. https://doi.org/10.1016/j.atmosenv.2019.116819

Diémoz, H., Barnaba, F., Magri, T., Pession, G., Dionisi, D., Pittavino, S., Tombolato, I. K. F., Campanelli, M., Della Ceca, L. S., Hervo, M., Di Liberto, L., Ferrero, L., and Gobbi, G. P.: Transport of Po Valley aerosol pollution to the northwestern Alps – Part 1: Phenomenology, Atmos. Chem. Phys., 19, 3065–3095, 2019. https://doi.org/10.5194/acp-19-3065-2019

Dommergue, A., Sprovieri, F., Pirrone, N., Ebinghaus, R., Brooks, S., Courteaud, J., and Ferrari, C. P.: Overview of mercury measurements in the Antarctic troposphere, Atmos. Chem. Phys., 10, 3309–3319, 2010, https://doi.org/10.5194/acp-10-3309-2010

Dorling, S. R., Davies, T. D., and Pierce, C.E., Cluster analysis: a technique for estimating the synoptic meteorological conditions on air and precipitation chemistry – method and applications, Atmos. Environ, 26 (14), 2575–2581, 1992. https://doi.org/10.1016/0960-1686(92)90110-7

Ebinghaus, R., Kock, H.H., Jennings, S.G., McCartin, P., Orren, M.J., Measurements of atmospheric mercury concentrations in Northwestern and Central Europe - Comparison of experimental data and model results. Atmos. Environ. 29(22), 3333-3344, 1995, https://doi.org/10.1016/1352-2310(95)00229-R

Ebinghaus, R., Kock, H.H., Temme, C., Einax, J.W. Löwe, A.G., Richter, A., Burrows, J.P., Schroeder, W.H., Antarctic springtime depletion of atmospheric mercury, Environ. Sci. Technol., 36(6), 1238-1244, 2002, https://doi.org/10.1021/es015710z

Ebinghaus, R., Slemr, F., Brenninkmeijer, C.A.M., van Velthoven, P., Zahn, A., Hermann, M., O'Sullivan, D.A., Oram, D.E., Emissions of gaseous mercury from biomass burning in South America in 2005 observed during CARIBIC flights, Geophysical Research Letters, 34(8), L08813, 1-5, 2007, https://doi.org/10.1029/2006GL028866

EN 14625:2012, Ambient Air - Standard Method for the Measurement of the concentration of O_3 by Ultraviolet Photometry, Comité Européen de Normalisation, 2012

Engle, M.A., Gustin, M.S., Lindberg, S.E., Gertler, A.W., Ariya, P.A., The influence of ozone on atmospheric emissions of gaseous elemental mercury and reactive gaseous mercury from substrates, Atmos. Environ., 39, 7506-7517, 2005. https://doi.org/10.1016/j.atmosenv.2005.07.069

Faïn, X., Grangeon, S., Bahlmann, E., Fritsche, J., Obrist, D., Dommergue, A., Ferrari, C. P., Cairns, W., Ebinghaus, R., Barbante, C., Diurnal production of gaseous mercury in the alpine snowpack before snowmelt, J. Geophys. Res., 112, D21311, 1-12, 2007, https://doi.org/10.1029/2007JD008520

Faïn, X., Obrist, D., Hallar, A. G., Mccubbin, I., and Rahn, T.: High levels of reactive gaseous mercury observed at a high elevation research laboratory in the Rocky Mountains, Atmos. Chem. Phys., 9, 8049–8060, 2009, https://doi.org/10.5194/acp-9-8049-2009

Faïn, X., Helmig, D., Hueber, J., Obrist, D., Williams, M.W., Mercury dynamics in the Rocky Mountain, Colorado, snowpack, Biogeosciences, 10, 3793-3807, 2013, https://doi.org/10.5194/bg-10-3793-2013

Ferrara, R, Maserti, B.E., Atmospheric mercury levels in the Mount Etna volcanic area after an eruptive phase, Environ Technol., 11(1), 51-56, 1990, https://doi.org/10.1080/09593339009384838

Ferrara, R., Maserti, B.E., De Liso, A., Cioni, R., Raco, B., Taddeucci, G. Edner, H., Ragnarson, P., Svanberg, S., Wallinder, E., Atmospheric mercury emission at Solfatara volcano (Pozzuoli, Phlegraean Fields - Italy), Chemosphere, 29(7), 1421-1428, 1994, https://doi.org/10.1016/0045-6535(94)90275-5

Ferrara, R., Mazzolai, B., Edner, H., Svanberg, S., Wallinder, E., Atmospheric mercury sources in the Mt. Amiata area, Italy, Sci. Total Environ., 213(1-3), 13-23, 1998, https://doi.org/10.1016/S0048-9697(98)00067-9

Ferrara, R., Mazzolai, B., Lanzillotta, E., Nucaro, E., Pirrone, N., Volcanoes as emission sources of atmospheric mercury in the Mediterranean basin, Sci. Total Environ., 259 (1-3), 115-121, 2000, https://doi.org/10.1016/S0048-9697(00)00558-1

Ferrari, C.P., Dommergue, A., Boutron, C.F., Skov, H., Goodsite, M., Jensen, B., Nighttime production of elemental gaseous mercury in interstitial air of snow at Station Nord, Greenland, Atmos. Environ., 38(17), 2727-2735, 2004, https://doi.org/10.1016/j.atmosenv.2004.02.023

Fisher, J.A., Jacob, D.J., Soerensen, A.L, Amos, H.A., Alexandra Steffen, A., and Sunderland, E.S., Riverine source of Arctic Ocean mercury inferred from atmospheric observations. Nature Geosci 5, 499–504, 2012. https://doi.org/10.1038/ngeo1478

Fleming, Z.L., Doherty, R.M., von Schneidemesser, E., Malley, C.S., Cooper, O.R., Pinto, J.P., Colette, A., Xu, X., Simpson, D., Schultz, M.G., Lefohn, A.S., Hamad, S., Moolla, R., Solberg, S. and Feng, Z., Tropospheric Ozone Assessment Report: Present-day ozone distribution and trends relevant to human health. Elem Sci Anth, 6(1), 1-12, 2018, http://doi.org/10.1525/elementa.273

Fu, X., Feng, X., Zhu, W., Wang, S., Lu, J., Total gaseous mercury concentrations in ambient air in the eastern slope of Mt. Gongga, South-Eastern fringe of the Tibetan plateau, China, Atmos. Environ., 42(5), 970-979, 2008, https://doi.org/10.1016/j.atmosenv.2007.10.018

Fu, X., Feng, X., Wang, S., Rothenberg, S., Shang, L., Li, Z., and Qiu, G.: Temporal and spatial distributions of total gaseous mercury concentrations in ambient air in a mountainous area in southwestern China: Implications for industrial and domestic mercury emissions in remote areas in China, Sci. Total Environ., 407, 2306–2314, 2009. https://doi.org/10.1016/j.scitotenv.2008.11.053

Fu, X.W., Feng, X., Dong, Z.Q., Yin, R.S., Wang, J.X., Yang, Z.R., Zhang, H., Atmospheric gaseous elemental mercury (GEM) concentrations and mercury depositions at a high-altitude mountain peak in south China, Atmos. Chem. Phys., 10, 2425-2437, 2010, https://doi.org/10.5194/acp-10-2425-2010

Fu, X. W., Feng, X., Liang, P., Deliger, Zhang, H., Ji, J., and Liu, P.: Temporal trend and sources of speciated atmospheric mercury at Waliguan GAW station, Northwestern China, Atmos. Chem. Phys., 12, 1951–1964, 2012a, https://doi.org/10.5194/acp-12-1951-2012

Fu, X. W., Feng, X., Shang, L. H., Wang, S. F., and Zhang, H.: Two years of measurements of atmospheric total gaseous mercury (TGM) at a remote site in Mt. Changbai area, Northeastern China, Atmos. Chem. Phys., 12, 4215–4226, 2012b, https://doi.org/10.5194/acp-12-4215-2012

Fu, X., Marusczak, N., Heimbürger, L.-E., Sauvage, B., Gheusi, F., Prestbo, E.M., Sonke, J. E., Atmospheric mercury speciation dynamics at the high-altitude Pic du Midi Observatory, southern France, Atmos. Chem. Phys., 16, 5623-5639, 2016, https://doi.org/10.5194/acp-16-5623-2016

Gay, D.A., Schmeltz, D., Prestbo, E., Olson, M., Sharac, T., Tordon, R., The Atmospheric Mercury Network: measurement and initial examination of an ongoing atmospheric mercury record across North America, Atmos. Chem. Phys., 13, 11339-11349, 2013, https://doi.org/10.5194/acp-13-11339-2013

Gallardo, L., Carrasco, J., and Olivares, G., An analysis of ozone measurements at Cerro Tololo (30°S, 70°W, 2200 m.a.s.l.) in Chile, Tellus B: Chemical and Physical Meteorology, 52:1, 50-59, 2000. https://doi.org/10.3402/tellusb.v52i1.16081

Gaudel, A., Cooper, O.R., Ancellet, G., Barret, B., Boynard, A., Burrows, J.P., Clerbaux, C., Coheur, P.-F., Cuesta, J., Cuevas, E., Doniki, S., Dufour, G., Ebojie, F., Foret, G., Garcia, O., Granados Muños, M.J., Hannigan, J.W., Hase, F., Huang, G., Hassler, B., Hurtmans, D., Jaffe, D., Jones, N., Kalabokas, P., Kerridge, B., Kulawik, S.S., Latter, B., Leblanc, T., Le Flochmoën, E., Lin, W., Liu, J., Liu, X., Mahieu, E., McClure-Begley, A., Neu, J.L., Osman, M., Palm, M., Petetin, H., Petropavlovskikh, I., Querel, R., Rahpoe, N., Rozanov, A., Schultz, M.G., Schwab, J., Siddans, R., Smale, D., Steinbacher, M., Tanimoto, H., Tarasick, D.W., Thouret, V., Thompson, A.M., Trickl, T., Weatherhead, E., Wespes, C., Worden, H.M., Vigouroux, C., Xu, X., Zeng, G. and Ziemke, J., Tropospheric Ozone Assessment Report: Present-day distribution and trends of tropospheric ozone relevant to climate and global atmospheric chemistry model evaluation. Elem Sci Anth, 6(1), 1-39, 2018. http://doi.org/10.1525/elementa.291

Gilge, S., Plass-Duelmer, C., Fricke, W., Kaiser, A., Ries, L., Buchmann, B., Steinbacher, M., Ozone, carbon monoxide and nitrogen oxides time series at four alpine GAW mountain stations in central Europe, Atmos. Chem. Phys., 10, 12295-12316, 2010, https://doi.org/10.5194/acp-10-12295-2010

GMOS Standard Operational Procedure, Methods for the determination of TGM and GEM, 2011. http://www.gmos.eu/download/gmos-sop-tgm-gem/ (last access july 2020)

Gustin, M.S., Engle, M., Ericksen, J., Lyman, S., Stamenkovic, J., Xin, M., Mercury exchange between the atmosphere and low mercury containing substrates. Appl. Geochem, 21, 1913–1923, 2006. https://doi.org/10.1016/j.apgeochem.2006.08.007

Gustin, M.S., Lindberg, S.E., Weisberg, P.E., An update on the natural sources and sinks of atmospheric mercury, Appl. Geochem, 23(3), 482-493, 2008. https://doi.org/10.1016/j.apgeochem.2007.12.010.

Han, Y.-J., Kim, J.-E., Kim, P.-R., Kim, W.-J., Yi, S.-M., Seo, Y.-S., Kim, S.-H., General trends of atmospheric mercury concentrations in urban and rural areas in Korea and characteristics of high-concentration events, Atmos. Environ., 94, 754-764, 2014, https://doi.org/10.1016/j.atmosenv.2014.06.002

Hersbach, H., Bell, B., Berrisford, P., Hirahara, S., Horányi, A., Muñoz-Sabater, J., Nicolas, J., Puebey, C., Radu, R., Schepers, D., Simmons, A., Soci, C., Abdalla, S., Abellan, X., Balsamo, G., Bechtold, P., Biavati, G., Bidlot, J., Bonavita, M., De Chiara, G., Dahlgren, P., Dee, D., Diamantakis, M., Dragani, R., Flemming, J., Forbes, R., Fuentes, M., Geer, A., Haimberger, L., Healy, S., Hogan, R. J., Hólm, E., Janisková, M., Keeley, S., Laloyaux, P., Lopez, P., Lupu, C., Radnoti, G., de Rosnay, P., Rozum, I., Vamborg, F., Villaume, S., and Thépaut, J.-N, The ERA5 global reanalysis, Q. J. R. Meteorol. Soc., 146, 1999–2049, 2020. https://doi.org/10.1002/qj.3803

Hopke, P. K., Barrie, L. A., Li, S.-M., Cheng, M.-D., Li, C., and Xie, Y., Possible sources and preferred pathways for biogenic and non-sea-salt sulphur for the high Arctic, J. Geophys. Res., 100, 16, 595–616, 1995. https://doi.org/10.1029/95JD01712

Huang, J., Choi, H.-D., Hopke, P.K., Holsen, T.M., Ambient mercury sources in Rochester, NY: results from principal components analysis (PCA) of mercury monitoring network data, Environ. Sci. Technol., 44, 8441-8445, 2010. https://doi.org/10.1016/j.scitotenv.2018.09.040

Kaiser, A., Scheifinger, H., Spangl, W., Weiss, A., Gilge, S., Fricke, W., Ries, L., Cemas, D., Jesenovec, B., Transport of nitrogen oxides, carbon monoxide and ozone to the Alpine Global Atmosphere Watch stations Jungfraujoch (Switzerland), Zugspitze and Hohenpeissenberg (Germany), Sonnblick (Austria) and Mt. Krvavec (Slovenia), Atmos. Environ., 41(40), 9273-9287, 2007. https://doi.org/10.1016/j.atmosenv.2007.09.027

Kang, S., Zhang, Q., Qian, Y., Ji, Z., Li, C., Cong, Z., Zhang, Y., Guo, J., Du, W., Huang, J., You, Q., Panday, A.K., Rupakheti, M., Chen, D., Gustafsson, Ö., Thiemens, M.H., Qin, D., Linking atmospheric pollution to cryospheric change in the Third Pole region: current progress and future prospects, Natl. Sci. Rev., 6(4), 796-809, 2019, https://doi.org/10.1093/nsr/nwz031

Karthik, R., Paneerselvam, A., Ganguly, D., Hariharan, G., Srinivasalu, S., Purvaja, R., Temporal variability of atmospheric Total Gaseous Mercury and its correlation with meteorological parameters at a high-altitude station of the South India, Atmos. Pollut. Res., 8, 164-173, 2017. https://doi.org/10.1016/j.apr.2016.08.010

Kellerhals, M., Beauchamp, S., Belzer, W., Blanchard, P., Froude, F., Harvey, B., McDonald, K., Pilote, M., Poissant, L., Puckett, K., Temporal and spatial variability of total gaseous mercury in Canada: results from the Canadian Atmospheric Mercury Measurement Network (CAMNet), Atmos. Environ., 37, 1003-1011, 2003, https://doi.org/10.1016/S1352-2310(02)00917-2

Kentisbeer, J., Leeson, S. R., Malcolm, H. M., Leith, I. D., Braban, C. F., and Cape, J. N., Patterns and source analysis for atmospheric mercury at Auchencorth Moss, Scotland, Environ. Sci. Process. Imp., 16, 1112–1123, 2014, https://doi.org/10.1039/C3EM00700F

Kentisbeer, J., Leeson, S. R., Clark, T., Malcolm, H. M., Cape, J.N., Influences on and patterns in total gaseous mercury (TGM) at Harwell, England, Environ. Sci. Process. Imp., 17, 586-595, 2015, https://doi.org/10.1039/C3EM00700F

Kim, K.H., Ebinghaus, R., Schroeder, W.H., Blanchard, P., Kock, H.H., Steffen, A., Froude, F. A., Kim, M.Y., Hong, S., Kim, J.H., Atmospheric Mercury Concentrations from Several Observatory Sites in the Northern Hemisphere. J Atmos Chem 50, 1–24, 2005. https://doi.org/10.1007/s10874-005-9222-0

Klausen, J., Zellweger, C., Buchmann, B., and Hofer, P.: Uncertainty and bias of surface ozone measurements at selected Global Atmosphere Watch sites, J. Geophys. Res.-Atmos., 108, 4622, 2003, https://doi.org/10.1029/2003JD003710

Kock, H.H., Bieber, E., Ebinghaus, R., Spain, T.G., Thees, B., Comparison of long-term trends and seasonal variations of atmospheric mercury concentrations at the two European coastal monitoring stations Mace Head, Ireland, and Zingst, Germany, Atmos. Environ., 39(39), 7549-7556, 2005, https://doi.org/10.1016/j.atmosenv.2005.02.059

Kottek, M., J. Grieser, C. Beck, B. Rudolf, F. Rubel, World map of the Köppen-Geiger climate classification updated. – Meteorol. Z. 15, 259–263, 2006. https://doi.org/10.1127/0941-2948/2006/0130

Lalonde, J. D., Poulain, A. J., and Amyot, M.: The Role of Mercury Redox Reactions in Snow on Snow-to-Air Mercury Transfer, Environ. Sci. Technol., 36, 174–178, 2002. https://doi.org/10.1021/es010786g

Lan, X., Talbot, R., Castro, M., Perry, K., and Luke, W.: Seasonal and diurnal variations of atmospheric mercury across the US determined from AMNet monitoring data, Atmos. Chem. Phys., 12, 10569–10582, 2012. https://doi.org/10.5194/acp-12-10569-2012

Lee, D.S., Dollard, G.J. Pepler, S., Gas-phase mercury in the atmosphere of the United Kingdom, Atmos. Environ., 32(5), 855-864, 1998. https://doi.org/10.1016/S1352-2310(97)00316-6

Lefohn, A.S., Malley, C.S., Smith, L., Wells, B., Hazucha, M., Simon, H., Naik, V., Mills, G., Schultz, M.G., Paoletti, E., De Marco, A., Xu, X., Zhang, L., Wang, T., Neufeld, H.S., Musselman, R.C., Tarasick, D., Brauer, M., Feng, Z., Tang, H., Kobayashi, K., Sicard, P., Solberg, S., Gerosa, G., Tropospheric ozone assessment report: Global ozone metrics for climate change, human health, and crop/ecosystem research. Elem Sci Anth 6(1): 28. University of California Press, 2018. http://doi.org/10.1525/elementa.279

Lin, H., Tong, Y., Yin, X., Zhang, Q., Zhang, H., Zhang, H., Chen, L., Kang, S., Zhang, W., Schauer, J., de Foy, B., Bu, X., and Wang, X.: First measurement of atmospheric mercury species in Qomolangma Natural Nature Preserve, Tibetan Plateau, and evidence of transboundary pollutant invasion, Atmos. Chem. Phys., 19, 1373–1391, 2019. https://doi.org/10.5194/acp-19-1373-2019

Lindberg, S.E., Brooks, S., Lin, C.-J., Scott, K., Meyers, T., Chambers, L. Landis, M., & Stevens, R., Formation of Reactive Gaseous Mercury in the Arctic: Evidence of Oxidation of Hg° to Gas-Phase Hg-II Compounds after Arctic Sunrise. Water, Air, & Soil Pollution: Focus 1, 295-302, 2001. https://doi.org/10.1023/A:1013171509022

Loewen, M. D., Sharma, S., Tomy, G., Wang, F., Bullock, P., Wania, F.: Persistent organic pollutants and mercury in the Himalaya, Aqua. Ecosyst. Health Manage., 8(3), 223–233, 2005. https://doi.org/10.1080/14634980500220924

Lu, J.Y., and Schroeder, W.H., Annual time-series of total filterable atmospheric mercury concentrations in the Arctic, Tellus B, 56 (3), 213-222, 2004, https://doi.org/10.3402/tellusb.v56i3.16432

Mao, H., Talbot, R. W., Sigler, J. M., Sive, B. C., and Hegarty, J. D.: Seasonal and diurnal variations of Hg° over New England, Atmos. Chem. Phys., 8, 1403–1421, 2008. https://doi.org/10.5194/acp-8-1403-2008

Mao, H., Cheng, I., Zhang, L., Current understanding of the driving mechanisms for spatiotemporal variations of atmospheric speciated mercury: a review, Atmos. Chem. Phys., 16, 12897-12924, 2016. https://doi.org/10.5194/acp-16-12897-2016

Munthe, J., Wängberg, I., Pirrone, N., Iverfeldt, Å., Ferrara, R., Ebinghaus, R., Feng, X., Gårdfeldt, K., Keeler, G., Lanzillotta, E., Lindberg, S.E., Lu, J., Mamane, Y., Prestbo, E., Schmolke, S., Schroeder, W.H., Sommar, J., Sprovieri, F., Stevens, R.K., Stratton, W., Tuncel, G., Urba, A., Intercomparison of methods for sampling and analysis of atmospheric mercury species, Atmos. Environ., 35, 3007-3017, 2001. https://doi:10.1016/S1352-2310(01)00104-2

Naitza, L., Cristofanelli, P., Marinoni, A., Calzolari, F., Roccato, F., Busetto, M., Sferlazzo, D., Aruffo, E., Di Carlo, P., Bencardino, M., D'Amore, F., Sprovieri, F., Pirrone, N., Dallo, F., Gabrieli, J., Vardè, M., Resci, G., Barbante, C., Bonasoni, P., Davide Putero, D., Increasing the maturity of measurements of essential climate variables (ECVs) at Italian atmospheric WMO/GAW observatories by implementing automated data elaboration chains, Comput. Geosci., 137, 104432, 2020. https://doi.org/10.1016/j.cageo.2020.104432

Obrist, D., Hallar, A.G., Mccubbin, I., Stephens, B.B., Rahn, T., Atmospheric mercury concentrations at Storm Peak Laboratory in the Rocky Mountains: evidence for long-range transport from Asia, boundary layer contributions, and plant mercury uptake, Atmos. Environ., 42, pp. 7579-7589, 2008. https://doi.org/10.1016/j.atmosenv.2008.06.051

Okamoto, S., Tanimoto, H. A review of atmospheric chemistry observations at mountain sites. Prog. in Earth and Planet. Sci. 3, 34, 2016. https://doi.org/10.1186/s40645-016-0109-2

Ou Yang, C.-F., O., Lin, N.-H., Sheu, G.-R., Lee, C.-T., Wang, J.L., Seasonal and diurnal variations of ozone at a high-altitude mountain baseline station in East Asia, Atmos. Environ 46, 279-288, 2012. https://doi.org/10.1016/j.atmosenv.2011.09.060

Pacyna, E.G., Pacyna, J.M., Fudala, J. Strzelecka-Jastrzab, E., Hlawiczka, S., Panasiuk, D., Mercury emissions to the atmosphere from anthropogenic sources in europe in 2000 and their scenarios until 2020, Sci. Total Environ., 370 (1), 147-156, 2006. https://doi.org/10.1016/j.scitotenv.2006.06.023

Parisi, M.L., Ferrara, N., Torsello, L., Basosi, R., Life cycle assessment of atmospheric emission profiles of the Italian geothermal power plants, J. Clean. Prod., 234, 881-894, 2019. https://doi.org/10.1016/j.jclepro.2019.06.222

Pirrone, N., Costa, P., Pacyna, J.M., Ferrara, R., Mercury emissions to the atmosphere from natural and anthropogenic sources in the Mediterranean region, Atmos. Environ., 35(17), 2997-3006, 2001. https://doi.org/10.1016/S1352-2310(01)00103-0

Poissant, L., Casimir, A., Water-air and soil-air exchange rate of total gaseous mercury measured at background sites, Atmos. Environ., 32 (1998), pp. 883-893. https://doi.org/10.1016/S1352-2310(97)00132-5

Prete, D., Davis, M., Lu, J., Factors affecting the concentration and distribution of gaseous elemental mercury in the urban atmosphere of downtown Toronto, Atmos. Environ., 192, 24-34, 2018. https://doi.org/10.1016/j.atmosenv.2018.08.041

Read, K.A., Neves, L.M., Carpenter, L.J., Lewis, A.C., Fleming, Z.L., Kentisbeer, J., Four years (2011-2015) of total gaseous mercury measurements from the Cape Verde Atmospheric Observatory, Atmos. Chem. Phys., 17, 5393-5406, 2017. https://doi.org/10.5194/acp-17-5393-2017

Reiter, R., The ozone trend in the layer of 2 to 3 km a.s.l. since 1978 and the typical time variations of the ozone profile between ground and 3 km a.s.l., Meteorl. Atmos. Phys. 42, 91–104, 1990. https://doi.org/10.1007/BF01030581

Schmolke, S.R., Schroeder, W., Kock, H., Schneeberger, D., Munthe, J., Ebinghaus, R., Simultaneous measurements of total gaseous mercury at four sites on a 800 km transect: spatial distribution and short-time variability of total gaseous mercury over central Europe, Atmos. Environ., 33, 1725-1733, 1999. https://doi.org/10.1016/S1352-2310(98)00238-6

Scholtz, M.T., Van Heyst, B.J., Schroeder, W.H., Modelling of mercury emissions from background soils, Sci. Total Environ., 304, 2003, 185-207, 2003. https://doi.org/10.1016/S0048-9697(02)00568-5

Schroeder, W. H., Anlauf, K. G., Barrie, L. A., Lu, J. Y., Steffen, A., Schneeberger, D. R., and Berg, T.: Arctic springtime depletion of mercury, Nature, 394, 331–332, 1998. https://doi.org/10.1038/28530

Schultz, M.G., Akimoto, H., Bottenheim, J., Buchmann, B., Galbally, I.E., Gilge, S., Helmig, D., Koide, H., Alastair, C., Lewis, A.C., Novelli, P.C., Plass-Dülmer, C., Ryerson, T.B., Steinbacher, M., Steinbrecher, R., Tarasova, O., Tørseth, K., Thouret, V., Zellweger, C., The Global Atmosphere Watch reactive gases measurement network, Elem. Sci. Anth., 3, 000067, 2015. http://doi.org/10.12952/journal.elementa.000067

Schultz, M.G., Schröder, S., Lyapina, O., Cooper, O., Galbally, I., Petropavlovskikh, I., von Schneidemesser, E., Tanimoto, H., Elshorbany, Y., Naja, M., Seguel, R., Dauert, U., Eckhardt, P., Feigenspahn, S., Fiebig, M., Hjellbrekke, A.-G., Hong, Y.-D., Christian Kjeld, P., Koide, H., Lear, G., Tarasick, D., Ueno, M., Wallasch, M., Baumgardner, D., Chuang, M.-T., Gillett, R., Lee, M., Molloy, S., Moolla, R., Wang, T., Sharps, K., Adame, J.A., Ancellet, G., Apadula, F., Artaxo, P., Barlasina, M., Bogucka, M., Bonasoni, P., Chang, L., Colomb, A., Cuevas, E., Cupeiro, M., Degorska, A., Ding, A., Fröhlich, M., Frolova, M., Gadhavi, H., Gheusi, F., Gilge, S., Gonzalez, M.Y., Gros, V., Hamad, S.H., Helmig, D., Henriques, D., Hermansen, O., Holla, R., Huber, J., Im, U., Jaffe, D.A., Komala, N., Kubistin, D., Lam, K.-S., Laurila, T., Lee, H., Levy, I., Mazzoleni, C., Mazzoleni, L., McClure-Begley, A., Mohamad, M., Murovic, M., Navarro-Comas, M., Nicodim, F., Parrish, D., Read, K.A., Reid, N., Ries, L., Saxena, P., Schwab, J.J., Scorgie, Y., Senik, I., Simmonds, P., Sinha, V., Skorokhod, A., Spain, G., Spangl, W., Spoor, R., Springston, S.R., Steer, K., Steinbacher, M., Suharguniyawan, E., Torre, P., Trickl, T., Weili, L., Weller, R., Xu, X., Xue, L. and Zhiqiang, M., Tropospheric Ozone Assessment Report: Database and Metrics Data of Global Surface Ozone Observations. Elem Sci Anth, 5, 1-58, 2017. http://doi.org/10.1525/elementa.244

Sheu, G.-R., Lin, N.-H., Wang, J.-L., Lee, C.-T., Ou Yang, C.-F., Wang, S.-H., Temporal distribution and potential sources of atmospheric mercury measured at a high-elevation background station in Taiwan, Atmos. Environ., 44(20), 2393–2400, 2010. https://doi.org/10.1016/j.atmosenv.2010.04.009

Sheu, G.-R., Gay, D.A., Schmeltz, D., Olson, M., Chang, S.-C., Lin, D.-W., Nguyen, L.S.P, A New Monitoring Effort for Asia: The Asia Pacific Mercury Monitoring Network (APMMN), Atmosphere, 10(9), 481, 2019. https://doi.org/10.3390/atmos10090481

Skov, H., Christensen, J.H., Goodsite, M.E., Heidam, N.Z., Jensen, B., Wåhlin, P., Geernaert, G., Fate of Elemental Mercury in the Arctic during Atmospheric Mercury Depletion Episodes and the Load of Atmospheric Mercury to the Arctic, Environ. Sci. Technol., 38(8), 2373-2382, 2004. https://doi.org/10.1021/es030080h

Slemr. F., Trends in atmospheric mercury concentrations over the Atlantic Ocean and at the Wank summit, and the resulting constraints on the budget of atmospheric mercury. In Global and Regional Cycles: Sources, Fluxes and Mass Balances, eds. W. Baeyens, R. Ebinghaus, and O. Vasiliev, NATO-ASI-Series, Kluwer Academic Publishers, Dordrecht, The Netherlands, 33-84, 1996.

Slemr, F. and Scheel, H. E., Trends in atmospheric mercury concentrations at the summit of the Wank mountain, Southern Germany, Atmos. Environ., 32 (5), 845-853, 1998. https://doi.org/10.1016/S1352-2310(97)00131-3

Slemr, F., Brunke, E.-G., Labuschagne, C., and Ebinghaus, R.: Total gaseous mercury concentrations at the Cape Point GAW station and their seasonality, Geophys. Res. Lett., 35, L11807, 2008. https://doi:10.1029/2008GL033741

Slemr, F., Ebinghaus, R., Brenninkmeijer, C.A.M., Hermann, M., Kock, H.H., Martinsson, B.G., Schuck, T., Sprung, D., van Velthoven, P., Zahn, A., Ziereis, H., Gaseous mercury distribution in the upper troposphere and lower stratosphere observed onboard the CARIBIC passenger aircraft, Atmos. Chem. Phys., 9, 1957-1969, 2009. https://doi.org/10.5194/acp-9-1957-2009

Slemr, F., Brunke, E.-G., Ebinghaus, R., and Kuss, J.: Worldwide trend of atmospheric mercury since 1995, Atmos. Chem. Phys., 11, 4779–4787, 2011. https://doi.org/10.5194/acp-11-4779-2011

Slemr, F., Weigelt, A., Ebinghaus, R., Kock, H. H., Bödewadt, J., Brenninkmeijer, C. A. M., Rauthe-Schöch, A., Weber, S., Hermann, M., Becker, J., Zahn, A., Martinsson, B., Atmospheric mercury measurements onboard the CARIBIC passenger aircraft, Atmos. Meas. Tech., 9, 2291-2302, 2016. https://doi.org/10.5194/amt-9-2291-2016

Spolaor, A., Angot, H., Roman, M., Dommergue, A., Scarchilli, C., Vardè, M., Del Guasta, M., Pedeli, X., Varin, C., Sprovieri, F., Magand, O., Legrand, M., Barbante, C., and Cairns, W. R. L.: Feedback mechanisms between snow and atmospheric mercury: Results and observations from field campaigns on the Antarctic plateau, Chemosphere, 197, 306–317, 2018. https://doi.org/10.1016/j.chemosphere.2017.12.180

Spolaor, A., Barbaro, E., Cappelletti, D., Turetta, C., Mazzola, M., Giardi, F., Björkman, M. P., Lucchetta, F., Dallo, F., Pfaffhuber, K. A., Angot, H., Dommergue, A., Maturilli, M., Saiz-Lopez, A., Barbante, C., and Cairns, W. R. L.: Diurnal cycle of iodine, bromine, and mercury concentrations in Svalbard surface snow, Atmos. Chem. Phys., 19, 13325–13339, 2019. https://doi.org/10.5194/acp-19-13325-2019

Sprenger, M., and Wernli, H.: The LAGRANTO Lagrangian analysis tool – version 2.0, Geosci. Model Dev., 8, 2569–2586, 2015. https://dx.doi.org/10.5194/gmd-8-2569-2015

Sprovieri, F., Pirrone, N., Bencardino, M., D'Amore, F., Carbone, F., Cinnirella, S., Mannarino, V., Landis, M., Ebinghaus, R., Weigelt, A., Brunke, E.-G., Labuschagne, C., Martin, L., Munthe, J., Wängberg, I., Artaxo, P., Morais, F., Barbosa, H.D.M. J., Brito, J., Cairns, W., Barbante, C., Diéguez, M.D.C., Garcia, P.E., Dommergue, A., Angot, H., Magand, O., Skov, H., Horvat, M., Kotnik, J., Read, K.A., Neves, L. M., Gawlik, B.M., Sena, F., Mashyanov, N., Obolkin, V., Wip, D., Feng, X. B., Zhang, H., Fu, X., Ramachandran, R., Cossa, D., Knoery, J., Marusczak, N., Nerentorp, M., Norstrom, C., Atmospheric mercury concentrations observed at ground-based monitoring sites globally distributed in the framework of the GMOS network, Atmos. Chem. Phys., 16, 11915–11935, 2016, https://doi.org/10.5194/acp-16-11915-2016

Sprovieri, F., Pirrone, N., Bencardino, M., D'Amore, F., Angot, H., Barbante, C., Brunke, E.-G., Arcega-Cabrera, F., Cairns, W., Comero, S., Diéguez, M.D.C., Dommergue, A., Ebinghaus, R., Feng, X.B., Fu, X., Garcia, P.E., Gawlik, B.M., Hageström, U., Hansson, K., Horvat, M., Kotnik, J., Labuschagne, C., Magand, O., Martin, L., Mashyanov, N., Mkololo, T., Munthe, J., Obolkin, V., Ramirez Islas, M., Sena, F., Somerset, V., Spandow, P., Vardè, M., Walters, C., Wängberg, I., Weigelt, A., Yang, X., Zhang, H., Five-year records of mercury wet deposition flux at GMOS sites in the Northern and Southern hemispheres, Atmos. Chem. Phys., 17, 2689-2708, 2017, https://doi.org/10.5194/acp-17-2689-2017

Stamenkovic, J., Lyman, S., and Gustin, M. S., Seasonal and diel variation of atmospheric mercury concentrations in the Reno (Nevada, USA) airshed, Atmos. Environ., 41, 6662–6672, 2007. https://doi.org/10.1016/j.atmosenv.2007.04.015

Steffen, A., Lehnherr, I., Cole, A., Ariya, P., Dastoor, A., Durnford, D., Kirk, J., Pilote, M., Atmospheric mercury in the Canadian Arctic. Part I: A review of recent field measurements, Sci. Total Environ., 509-510, 3–15, 2015. https://doi.org/10.1016/j.scitotenv.2014.10.109

Stocker, T., Qin, D., Plattner, G., Tignor, M., Allen, S., Boschung, J., Nauels, A., Xia, Y., IPCC Summary for Policymakers in Climate Change 2013: the Physical Science Basis, Contribution of Working Group I to the Fifth Assessment Report of the Intergovernmental Panel on Climate Change, Cambridge University Press, Cambridge, New York, USA. 2013.

Subir, M., Ariya, P.A., Dastoor, A.P., A review of the sources of uncertainties in atmospheric mercury modeling II. Mercury surface and heterogeneous chemistry – A missing link, Atmos. Environ., 46, 1-10, 2011. https://doi.org/10.1016/j.atmosenv.2011.07.047

Swartzendruber, P.C., Jaffe, D.A., Prestbo, E.M., Weiss-Penzias, P., Selin, N.E., Park, R., Jacob, D.J., Strode, S., Jaeglé, L., Observations of reactive gaseous mercury in the free troposphere at the Mount Bachelor Observatory, J. Geophys. Res., 111, D24301, 1-12, 2006. https://doi.org/10.1029/2006JD007415

Taurino, E., Bernetti, A., De Lauretis, R., Cordella, M., D'Elia, I., Di Cristofaro, E., Gagna, A., Gonella, B., Lena, F., Moricci, F., Pantaleoni, M., Peschi, E., Romano, D., Vitullo, M., Italian Emission Inventory 1990-2017, Informative Inventory Report 2019, ISPRA Institute for Environmental Protection and Research Environmental Assessment, Control and Sustainability Department Emissions, Prevention of Atmospheric Impacts and Climate Change Area Air Emission Inventory Unit, Rapporti 306/2019, 1-198, 2019.

Tekran, model 2537B Ambient Mercury Vapor Analyzer, User Manual, Rev 3.12, July 2012

Temme, C., Blanchard, P., Steffen, A., Banic, C., Beauchamp, S., Poissant, L., Tordon, R., Wiens, B., Trend, seasonal and multivariate analysis study of total gaseous mercury data from the Canadian atmospheric mercury measurement network (CAMNet), Atmos. Environ., 41(26), 5423-5441, 2007. https://doi.org/10.1016/j.atmosenv.2007.02.021

Thermo Environmental Instruments Inc, Model 49C UV, photometric O_3 analyzer instruction manual P/N 9999. Franklin, MA, 1–3, 2000.

Tørseth, K., Aas, W., Breivik, K., Fjæraa, A. M., Fiebig, M., Hjellbrekke, A. G., Lund Myhre, C., Solberg, S., Yttri, K. E., Introduction to the European Monitoring and Evaluation Programme (EMEP) and observed atmospheric composition change during 1972–2009, Atmos. Chem. Phys., 12, 5447–5481, 2012. https://doi.org/10.5194/acp-12-5447-2012

Travnikov, O., and Iluyin, I., Regional model MSCE-HM of heavy metal transboundary air pollution in Europe, MSC-E technical report 6/2005, Meteorological Synthesizing Centre-East, Moscow, Russia, 2005.

Travnikov, O., Angot, H., Artaxo, P., Bencardino, M., Bieser, J., D'Amore, F., Dastoor, A., De Simone, F., Diéguez, M. D. C., Dommergue, A., Ebinghaus, R., Feng, X. B., Gencarelli, C. N., Hedgecock, I. M., Magand, O., Martin, L., Matthias, V., Mashyanov, N., Pirrone, N., Ramachandran, R., Read, K. A., Ryjkov, A., Selin, N. E., Sena, F., Song, S., Sprovieri, F., Wip, D., Wängberg, I., and Yang, X.: Multi-model study of mercury dispersion in the atmosphere: atmospheric processes and model evaluation, Atmos. Chem. Phys., 17, 5271–5295, 2017. https://doi.org/10.5194/acp-17-5271-2017

UNEP and WMO, Integrated Assessment of Black Carbon and Tropospheric Ozone. Nairobi Kenya: United Nations Environment Programme, 2011.

Vaselli, O., Higueras, P., Nisi, B., Esbríc, J.M., Cabassi, J., Martínez-Coronado, A., Tassi, F., Rappuoli, D., Distribution of gaseous Hg in the Mercury mining district of Mt. Amiata (Central Italy): A geochemical survey prior the reclamation project, Environ. Res., 125, 179-187, 2013. https://doi.org/10.1016/j.envres.2012.12.010

Vardè, M., Dallo, F., Cairns, W.R.L., de Blasi, F., Maffezzoli, N., Gabrieli, J., Cozzi, G., Cristofanelli, P., Naitza, L., Calzolari, F., Busetto, M., Davolio, S., Bonasoni, P., Barbante, C., (2019). A survey of total gaseous mercury and ozone during spring and summer 2018 after characterization of air masses at the Col Margherita Atmospheric Observatory (2543 m a.s.l.) in the Italian Dolomites. In Proceedings of the EGU General Assembly 2019, Vienna (Austria) 7–12 April 2019, Geophysical Research Abstracts Vol. 21, EGU2019-17017-4, 2019.

Vecchi, R., Valli, G., Ozone assessment in the southern part of the Alps, Atmos. Environ., 33(1), 97-109, 1998. https://doi.org/10.1016/S1352-2310(98)00133-2.

Wahsha, M., Bini, C., Zilioli, D., Spiandorello, M., Gallo, M., Potentially harmful elements in terraced agroecosystems of NE Italy: Geogenic vs anthropogenic enrichment, J. Geochem. Explor, 144(B), 355-362, 2014. https://doi.org/10.1016/j.gexplo.2014.01.012

Wan, Q., Feng, X., Lu, J., Zheng, W., Song, X., Han, S., and Xu, H.: Atmospheric mercury in Changbai Mountain area, northeastern China I. The seasonal distribution pattern of total gaseous mercury and its potential sources, Environ. Res., 109, 201–206, 2009. https://doi.org/10.1016/j.envres.2008.12.001

Wang, T., Wong, H. L. A., Tang, J., Ding, A., Wu, W. S., and Zhang, X. C., On the origin of surface ozone and reactive nitrogen observed at a remote mountain site in the northeastern Qinghai-Tibetan Plateau, western China, J. Geophys. Res.-Atmos., 111, D08303, 2006. https://doi.org/10.1029/2005jd006527

Wängberg, I., Munthe, J., Berg, T., Ebinghaus, R., Kock, H.H., Temme, C., Bieber, E., Spain, T.G., Stolk, A., Trends in air concentration and deposition of mercury in the coastal environment of the North Sea Area, Atmos. Environ., 41, 2612-2619, 2007. https://doi.org/10.1016/j.atmosenv.2006.11.024

Wängberg, I., Nerentorp Mastromonaco, M. G., Munthe, J., Gårdfeldt, K., Airborne mercury species at the Råö background monitoring site in Sweden: distribution of mercury as an effect of long-range transport, Atmos. Chem. Phys., 16, 13379-13387, 2016. https://doi.org/10.5194/acp-16-13379-2016

Warneck, P., Chemistry of the Natural Atmosphere, 2nd ed., Elsevier, New York, 2000.

Weiss-Penzias, P., Amos, H. M., Selin, N. E., Gustin, M. S., Jaffe, D. A., Obrist, D., Sheu, G.-R., and Giang, A., Use of a global model to understand speciated atmospheric mercury observations at five high-elevation sites, Atmos. Chem. Phys., 15, 1161–1173, 2015. https://doi.org/10.5194/acp-15-1161-2015

Wernli, B.H., and Davies, H.C.: A Lagrangian-based analysis of extratropical cyclones. I: the method and some applications, Q. J. Roy. Meteorol. Soc. 123, 467–489, 1997. http://dx.doi.org/10.1002/qj.49712353811

Witt, E.L., Kolka, R.K., Nater, E.A., Wickman, T.R., Forest fire effects on mercury deposition in the boreal forest, Environ. Sci. Technol., 43(6), 1776-1782, 2009. https://doi.org/10.1021/es802634y

World Meteorological Organization (WMO), Guidelines for Continuous Measurements of Ozone in the Troposphere, 2013, GAW Report 209, WMO No 1110, 2013. https://library.wmo.int/doc_num.php?explnum_id=7814

Xin, X., and Gustin, M.S., Gaseous elemental mercury exchange with low mercury containing soils: Investigation of controlling factors, Appl. Geochem., 22, 1451-1466, 2007. https://doi.org/10.1016/j.apgeochem.2007.02.006

Yin, X., Kang, S., de Foy, B., Cong, Z., Luo, J., Zhang, L., Ma, Y., Zhang, G., Rupakheti, D., Zhang, Q., Surface ozone at Nam Co in the inland Tibetan Plateau: variation, synthesis comparison and regional representativeness, Atmos. Chem. Phys., 17, 11293-11311, 2017. https://doi.org/10.5194/acp-17-11293-2017

Yin, X., Kang, S., de Foy, B., Ma, Y., Tong, Y., Zhang, W., Wang, X., Zhang, G., Zhang, Q.: Multi-year monitoring of atmospheric total gaseous mercury at a remote high-altitude site (Nam Co, 4730 m a.s.l.) in the inland Tibetan Plateau region, Atmos. Chem. Phys., 18, 10557-10574, 2018. https://doi.org/10.5194/acp-18-10557-2018

Zhang, H., Fu, X. W., Lin, C.-J., Wang, X., Feng, X. B.: Observation and analysis of speciated atmospheric mercury in Shangri-La, Tibetan Plateau, China, Atmos. Chem. Phys., 15, 653-665, 2015. https://doi.org/10.5194/acp-15-653-2015

Zhang, H., Fu, X., Lin, C.-J., Shang, L., Zhang, Y., Feng, X., and Lin, C.: Monsoon-facilitated characteristics and transport of atmospheric mercury at a high-altitude background site in southwestern China, Atmos. Chem. Phys., 16, 13131-13148, 2016. https://doi.org/10.5194/acp-16-13131-2016

Supplementary Material

Atmospheric total gaseous mercury at a remote high-elevation site (Col Margherita observatory, 2543 m a.s.l.) in the Italian Alps: Trend, seasonal variation and diurnal pattern

Massimiliano Vardè[1,2,3], Carlo Barbante[1,3], Elena Barbaro[1,3], Francesca Becherini[1], Maurizio Busetto[4], Paolo Bonasoni[4], Francescopiero Calzolari[4], Paolo Cristofanelli[4], Federico Dallo[1,3], Fabrizio De Blasi[1,3], Jacopo Gabrieli[1,3], Andrea Gambaro[3,1], Davide Putero[5], Andrea Spolaor[1,3], and Warren R.L. Cairns[1,3]

[1]Institute of Polar Sciences, National Research Council of Italy (CNR-ISP), Venice-Mestre, 30172, Italy
[2]Department of Chemical and Pharmaceutical Sciences, University of Ferrara (DipSCF-UniFE), Ferrara, 44121, Italy
[3]Department of Environmental Sciences, Informatics and Statistics, Ca' Foscari University of Venice (DAIS-UniVE), Venice-Mestre, 30172, Italy
[4]Institute of Atmospheric Sciences and Climate, National Research Council of Italy (CNR-ISAC), Bologna, 40129, Italy
[5]Institute of Atmospheric Sciences and Climate, National Research Council of Italy (CNR-ISAC), Torino, 10133, Italy

Correspondence to: Massimiliano Vardè (massimiliano.varde@cnr.it) and Warren R.L. Cairns (warrenraimondlee.cairns@cnr..it)

Keywords:
Atmospheric mercury; Background ozone; High-altitude station; Meteorological condition; Air masses trajectories; Planet boundary layer; South Eastern Dolomites; Italy.

Supplement to Section 1 Introduction:

Legal framework and standards

According to the Directive 2004/107/EC the measurements of mercury in the atmosphere have to comply with the European Committee for Standardization (CEN) reference method based on automated atomic fluorescence spectrometry (AFS) or atomic absorption spectrometry (AAS). In alternative national and international (i.e. International Organization for Standardization, ISO) standards can be followed or other methods if demonstrated equivalent. The Technical Committee CEN/TC 264 "Ambient Air Quality" prepared in 2010 the standard methods for the determination of total gaseous mercury (EN 15852:2010) and of mercury deposition (EN 15853:2010). It is important to point out that currently there are no European or national limit values for mercury in ambient air and atmospheric deposition, although recent European Directive and Italian Legislative Decree (D.Lgs 155/2010) both mention mercury as a hazardous pollutant for humans and the environment. Thus, ambient air quality guidelines for mercury are essential for the control of the atmospheric Hg emissions and for the reduction of Hg impacts on human health and biota in Europe (Pirrone 2001). Nevertheless, a daily emission limit value has been set at 50 µg m^{-3} (D.Lgs 133/2005, Allegato 1) to monitor mercury and its compounds expressed as total mercury from stationary sources by automated measuring system (AMS) using reference method (EN 14884:2005). Other guideline values, both based on yearly average, are: i) 0.2 µg m^{-3} as minimal risk level (MRL) for hazardous substances by the US Agency for Toxic Substances and Disease Registry (ATSDR); ii) 0.3 µg m^{-3} as reference concentration for chronic inhalation exposure (RfC) to elemental mercury by US Environmental Protection Agency (EPA). Finally, WHO established 1 µg m^{-3} the lowest-observed-adverse-effect level (LOAEL) for inorganic mercury vapour (WHO 2012). Notwithstanding, quality

guidelines for ambient air Hg have not been established yet in Italy and only a limit value for Hg and its airborne inorganic divalent compounds has been set at 20 ng m^{-3} per 8 hours, exclusively for professional exposure in workplaces (Ministerial Decree D.M. 6 August 2012, Allegato XXXVIII, 2012).

Air mercury measurements in Italy and current National regulations

Nevertheless in the last years the Italian Regional Agencies for Environmental Protection (ARPA) coordinated by the Institute for Environmental Protection and Research (ISPRA) carried out at local scale mercury measurements in areas of particular environmental interest such as near geothermal power plants (Bagnoli and Gartner, 2017), coal-fired thermal power plant, incinerator and in rural area using both a continuous emissions monitoring system (SME) and an automated Hg analyser (Fontana et al., 2018). Other Hg measurements in atmosphere were carried out in suburban/rural zones by research teams of Universities and Research Agencies (Munthe et al., 2001; Sprovieri et al., 2016; Vardè et al. 2014) and coastal/open seawater (Bagnato et al., 2013; Barago et al., 2020; Castagna et al., 2018; Fantozzi et al., 2013), volcanic/geothermal and mining areas (Bagnato et al., 2009; Barghigiani et al., 1990; Cabassi et al., 2017; Dedeurwaerder et al., 1982; Ferrara et al. 1994; Ferrara et al. 1998; Ferrara et al. 2000). In Europe, the Directive 2008/50/CE (transposed in Italy into Legislative Decree D.Lgs. 155/2010) on ambient air quality and cleaner air for European countries, set for ozone target value, long-term value and thresholds to protect human health, vegetation and forest through a network of monitoring stations. According to the macro-scale sitting criteria, stations can be classified as urban, suburban, rural and background rural. To better understand the mechanisms of formation and transport of particulate and gaseous pollutants such as $PM_{2.5}$, PAHs, metals, ozone and its precursors, an improvement of monitoring stations network has been established by Ministerial Decree (D.M. 5 May 2015) implementing the provisions of previous regulations, providing reference methods for sampling and analysis (i.e. concentrations of total mass of particulate matter and chemical speciation of PM10 and PM2.5), and setting supplementary monitoring stations for additional measurements (e.g. total gaseous mercury in air and total mercury in bulk deposition). The Directive (UE) 2015/1480 transposed into Ministerial Decree (D.M. 26 January 2017) amends certain parts relating to reference methods, data validation and the location of sampling points for the assessment of ambient air quality reported in the annexes of both previous Directives 2004/107/EC and 2008/50/EC.

Some authors provided proposals on mercury measurements in air and deposition, and research activities in the European Union, suggesting a fruitful accomplishment of a European network of monitoring stations considered important for more integrated and in-depth investigations of mercury (and its compounds). Voluntary observation network for mercury species in ambient air was also suggested and encouraged by each member state of the EU (Pirrone and Wichmann-Fiebig 2003). In Italy, the agreement between the Ministry for Environment, Land and Sea Protection (MATTM), research agencies (CNR and ENEA) and the Italian National Institute of Health (ISS), established a Special Network pursuant to the Italian Legislative Decree 155/2010 for the measurements of various air pollutants (i.e. PAHs, As, Cd, Ni, Hg, ozone and its precursors, PM2.5 mass concentration and its chemical characterization). Background and rural sites have been selected, running from north to south of Italy, to contribute and improve the knowledge of the formation and transport phenomena of atmospheric contaminants, to effective enhance the emission reduction strategies and to improve air quality for environment and health protection.

Supplement to Section 3 Results and discussion

3.1 Temporal trends of TGM

3.1.1 Annual and seasonal pattern

Table.ESM1 Atmospheric gaseous mercury concentrations from other elevated monitoring sites. Concentrations are reported in ng m^{-3} as mean ± standard deviation or as range.

Country	Location	Station	Altitude (m a.s.l.)	Coordinate	Species TGM (or GEM)	Mean concentration [or range]	Site classification	Sampling period	Instruments	Reference
China	Qinghai-Tibet Plateau	Mt. Gogga Moxi base station	1640	Lat 29.40 °N Lon 102.07 °E	TGM	3.98	remote	May 2005 - Jun 2006	Tekran 2537A	Fu et al. (2008)
China	Qinghai-Tibet Plateau	Mt. Gogga Moxi base station	1640	Lat 29.40 °N Lon 102.07 °E	TGM	3.91 ± 1.20	remote	Apr 2006 - Jun 2007	Tekran 2537A	Fu et al. (2009)
China	Qinghai–Xizang Tibet Plateau	Mt. Waliguan Baseline Observatory-WLG	3816	Lat 36.287 °N Lon 100.898 °E	TGM	1.98 ± 0.98	remote	Sep 2007 - Sep 2008	Tekran 2537A	Fu et al. (2012)a
China	Qinghai–Xizang Tibet Plateau	Mt. Waliguan Baseline Observatory-WLG	3816	Lat 36.287 °N Lon 100.898 °E	GEM	(2.05 ± 0.96)	remote	Oct 2007 - Sep 2009	Tekran 2537A/B	Fu et al. (2015)
China	Southeast Guizhou province	Mt. Leigong	2178	Lat 26.39 °N Lon 108.20 °E	GEM	(2.80 ± 1.51)	remote	May 2008 - May 2009	Tekran 2537A	Fu et al. (2010)
China	Northeastern China	Mt. Changbai	741	Lat 41.94 °N Lon 128.08 °E	TGM	1.60 ± 0.51	remote	Oct 2008 - Oct 2010	Tekran 2537A	Fu et al. (2012)b
China	Guangdong province	Mt. Dinghu monitoring site-DH	90	Lat 23.17 °N Lon 112.50 °E	TGM	5.07 ± 2.89	rural	Oct 2009 - Apr 2010	Tekran 2537B	Chen et al. (2013)
China	Hengduan Mountains Tibet Plateau	The Shangri-La station-SAWRS	3580	Lat 28.017 °N Lon 99.733 °E	TGM	2.55 ± 0.73	remote	Nov 2009 - Nov 2010	Tekran 2537A	Zhang et al. (2015)
China	Hengduan Mountains Tibet Plateau	The Shangri-La station-XGL	3580	Lat 28.017 °N Lon 99.733 °E	GEM	(2.52 ± 0.70)	remote	Jul 2010 - Oct 2010	Tekran 2537A/B	Fu et al. (2015)

China	Zhejiang province	Mt. Damei Dameishan Atmospheric Observatory-DAO	550	Lat 29.632 °N Lon 121.565 °E	TGM	3.31 ± 1.44	rural	Apr2011 - Apr 2013	Tekran 2537B	Yu et al. (2015)
China	Central Yunnan province	Mt. Ailao station-MAL	2450	Lat 24.533 °N Lon 100.017 °E	GEM	(2.09 ± 0.63)	remote	May 2011-May 2012	Tekran 2537A	Zhang et al. (2016)
China	Central Yunnan province	Mt. Ailao station-MAL	2450	Lat 24.533 °N Lon 100.017 °E	GEM	(2.05 ± 0.67)	remote	Sep 2011-Mar 2013	Tekran 2537A/B	Fu et al. (2015)
China	Damxung, Lhasa, Tibet	Nam Co	4730	Lat 30.77 °N Lon 90.98 °E	TGM	1.33 ± 0.24	remote	Jan 2012 - Oct 2014	Tekran 2537B	Yin et al. (2018)
China	Qomolangma National Nature Preserve (QNNP), Tibet	Mt. Qomolangma	4276	Lat 28.36 °N Lon 86.95 °E	GEM	(1.42 ± 0.37)	remote	Apr 2016-Aug 2016	Tekran 2537B	Lin et al. (2019)
Taiwan	Central Taiwan	Mt. Lulin station	2862	Lat 23.46 °N Lon 120.87 °E	TGM	[1.0 - 2.0]	remote	Mar 2011 - Feb 2012	n.a.	Chen et al., (2016)
USA	Central Oregon	Mount Bachelor Observatory-MBO	2763	Lat 43.98 °N Lon 121.69 °W	GEM	(1.77 ± 0.12)	remote	Mar 2004 - May 2004	Tekran 2537A	Weiss-Penzias et al. (2006)
USA	Central Oregon	Mount Bachelor Observatory-MBO	2763	Lat 43.98 °N Lon 121.69 °W	TGM	[1.4 - 1.8]	remote	Mar 2004 - Sep 2005	Tekran 2537A	Weiss-Penzias et al. (2007)
USA	Central Oregon	Mount Bachelor Observatory-MBO	2763	Lat 43.98 °N Lon 121.69 °W	GEM	(1.54 ± 0.18)	remote	May 2005 - Aug 2005	Tekran 2537A	Swartzendruber et al. (2006)
USA	Colorado	Storm Peak Laboratory-SPL	3210	Lat 40.45 °N Lon 106.73 °W	GEM	1.51 ± 0.12	remote	Oct 2006 - May 2007	Tekran 2537A	Obrist et al. (2008)
USA	Colorado	Storm Peak Laboratory-SPL	3210	Lat 40.45 °N Lon 106.73 °W	GEM	(1.6 ± 0.3)	remote	Apr 2008 - Jul 2008	Tekran 2537A	Faïn et al. (2009)
USA	Hawaii	Mauna Loa Observatory (MLO)	3397	Lat 19.53 °N Lon 155.59 °W	GEM	(1.4 ± 0.4)	remote	2002-2010	Tekran 2537A	Landis et al. (2013)
Germany	Bavarian Alps	Wank Mountain - WNK	1780	Lat 47.50 °N Lon 11.14 °E	TGM	[1.82 - 2.97]	remote	Mar 1990 - May 1996	AAS or AFS instruments	Slemr & Scheel (1998)
France	Central Pyrenees mountains	Pic du Midi-PDM	2877	Lat 42.937 °N Lon 0.142 °E	GEM	(1.86 ± 0.27)	remote	Nov 2011-Nov 2012	Tekran 2537A	Fu et al. (2016)
Italy	Southern Apennine	Longobucco Station-LON	1379	Lat 39.39408 °N Lon 16.61348 °E	TGM	1.43 ± 0.33	remote	Jan 2013 - Dec 2013	Tekran 2537B	Sprovieri et al. (2016)

Italy	Southeastern Dolomites	Col Margherita Observatory-MRG	2543	Lat 46.36683 °N Lon 11.79192 °E	TGM	1.69 ± 0.29	remote	Jan 2014 - Dec 2014	Tekran 2537B	Sprovieri et al. (2016)
Italy	Southeastern Dolomites	Col Margherita Observatory-MRG	2543	Lat 46.36683 °N Lon 11.79192 °E	TGM	1.73 ± 0.34	remote	Dec 2013 - Jul 2015	Tekran 2537B	This study
Italy	Southeastern Dolomites	Col Margherita Observatory-MRG	2543	Lat 46.36683 °N Lon 11.79192 °E	TGM	3.14 ± 1.29	remote	Mar 2018 - May 2019	Tekran 2537B	This study

92

Table.ESM2 Results (p-value) of post-hoc tests applied to data separated by year/seasons

Season	p-value		
	Conover	Dunn	Nemenyi
SP18-SP19	< 2.22e-16	< 2.22e-16	< 2.22e-16
S18-SP18	< 2.22e-16	< 2.22e-16	< 2.22e-16
W18/19-SP18	< 2.22e-16	< 2.22e-16	< 2.22e-16
S18-SP19	3.5629e-11	3.249e-08	30.553 1.0558e-06
W18/19-SP19	< 2.22e-16	< 2.22e-16	< 2.22e-16
W18/19-S18	< 2.22e-16	< 2.22e-16	< 2.22e-16

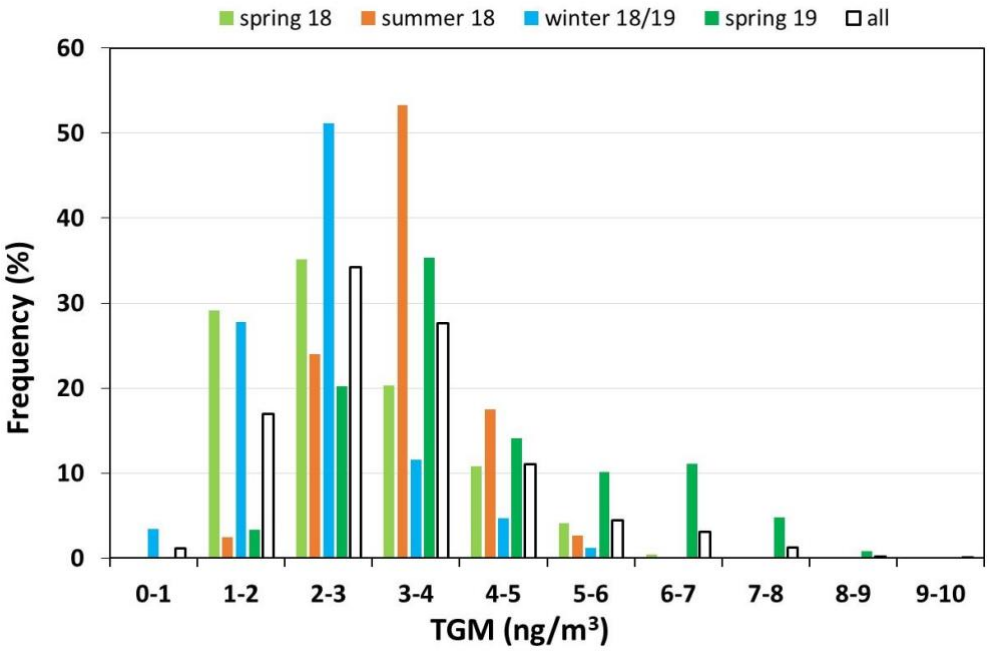

Fig.ESM1 Frequency distribution of TGM in the whole measurement periods, separating the seasons.

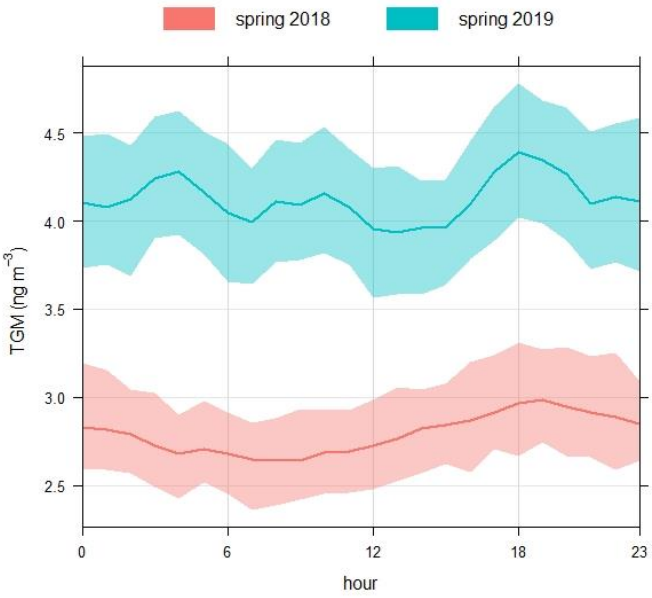

Fig.ESM2 Comparison between hourly variation of TGM in spring 2018 and 2019.

3.1.2 Daily trend of TGM

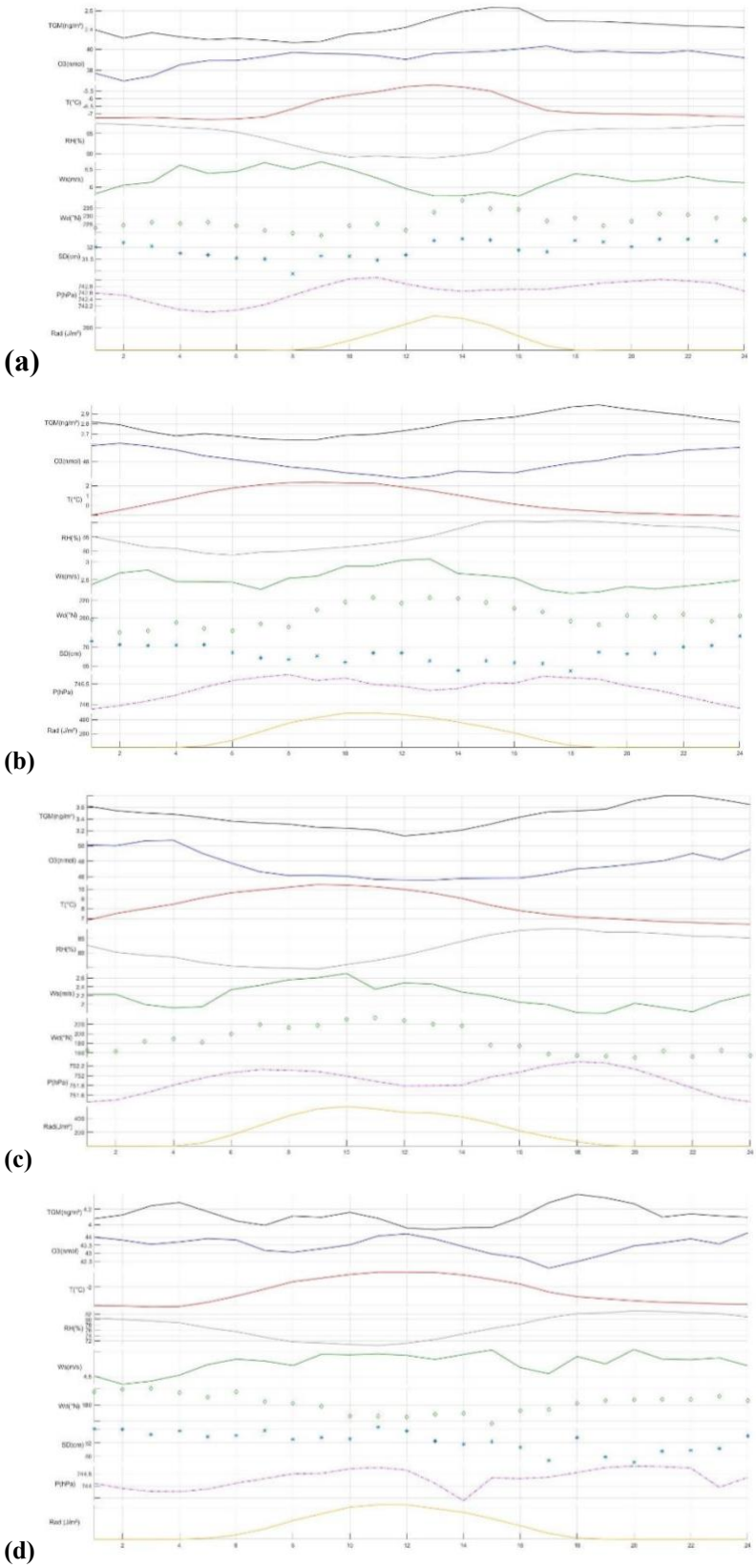

Fig.ESM3 Diurnal variation of meteorological parameters in a) winter 2018-2019; b) spring 2018; c) summer 2018; d) spring 2019.

3.1.3 Back-trajectory results

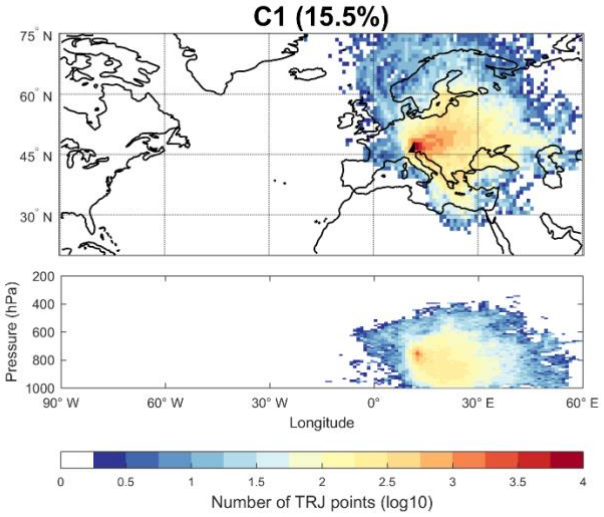

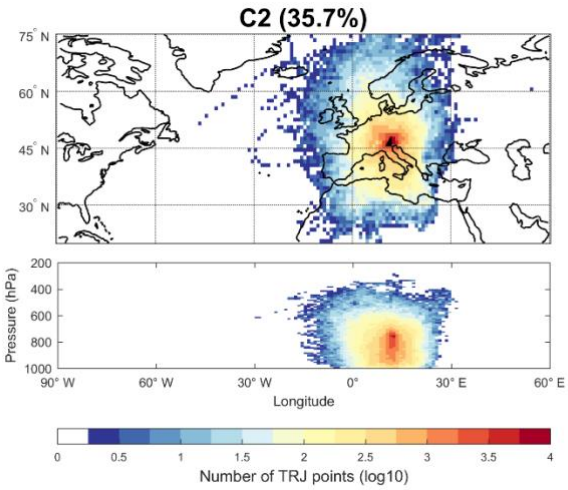

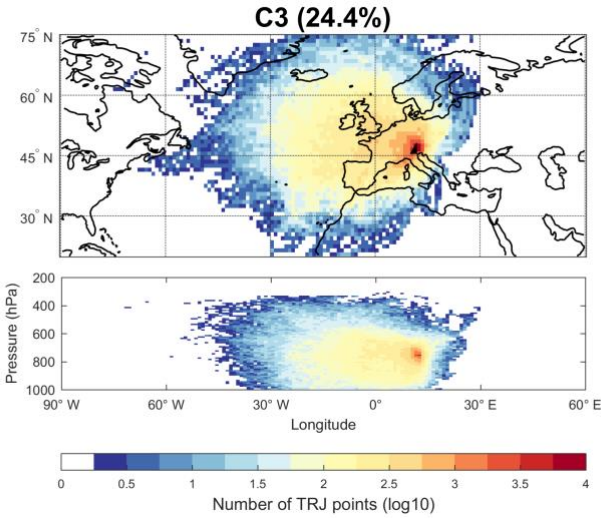

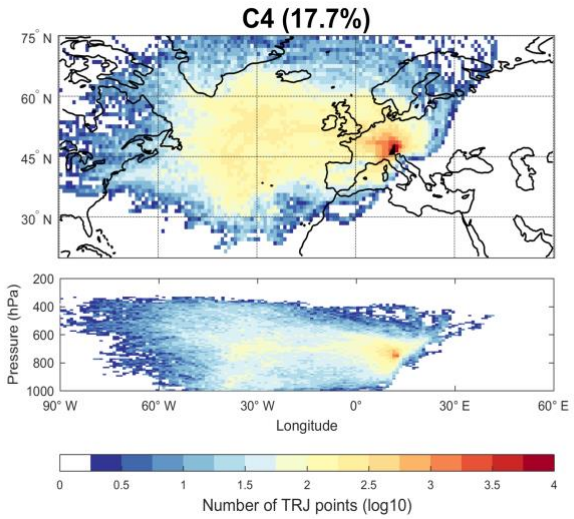

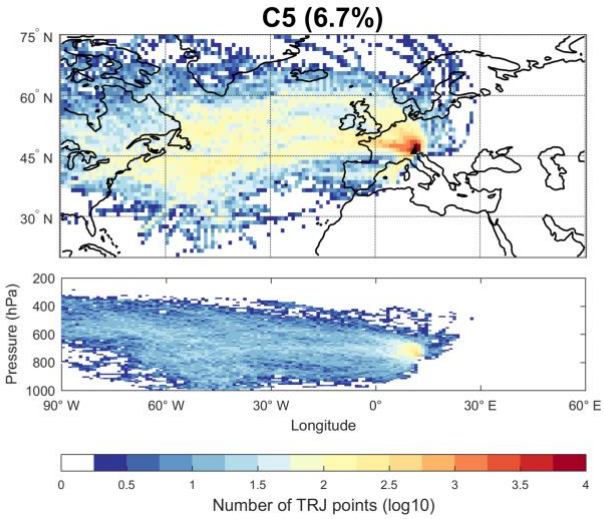

Fig.ESM4 Concentration field (vertical cross section included) for back-trajectories starting at MRG and belonging to the different clusters (from cluster 1 to cluster 5).

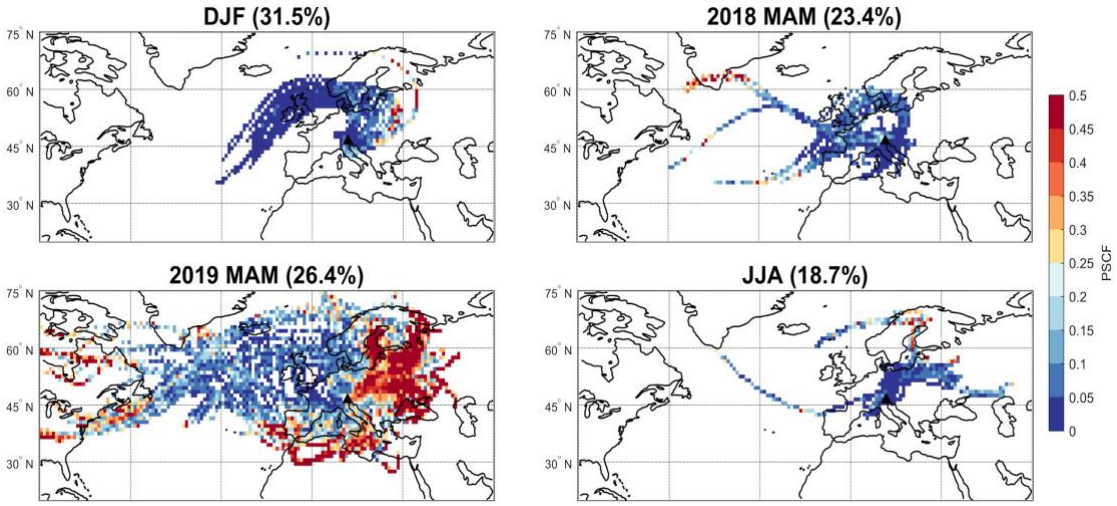

Fig.ESM5 Seasonal potential source contribution function (PSCF) density maps. The numbers in parentheses indicate the percentage of available data for each season. The threshold used for calculating the PSCF was the 90th percentile of the whole TGM distribution.

3.3 Spatial patterns of TGM

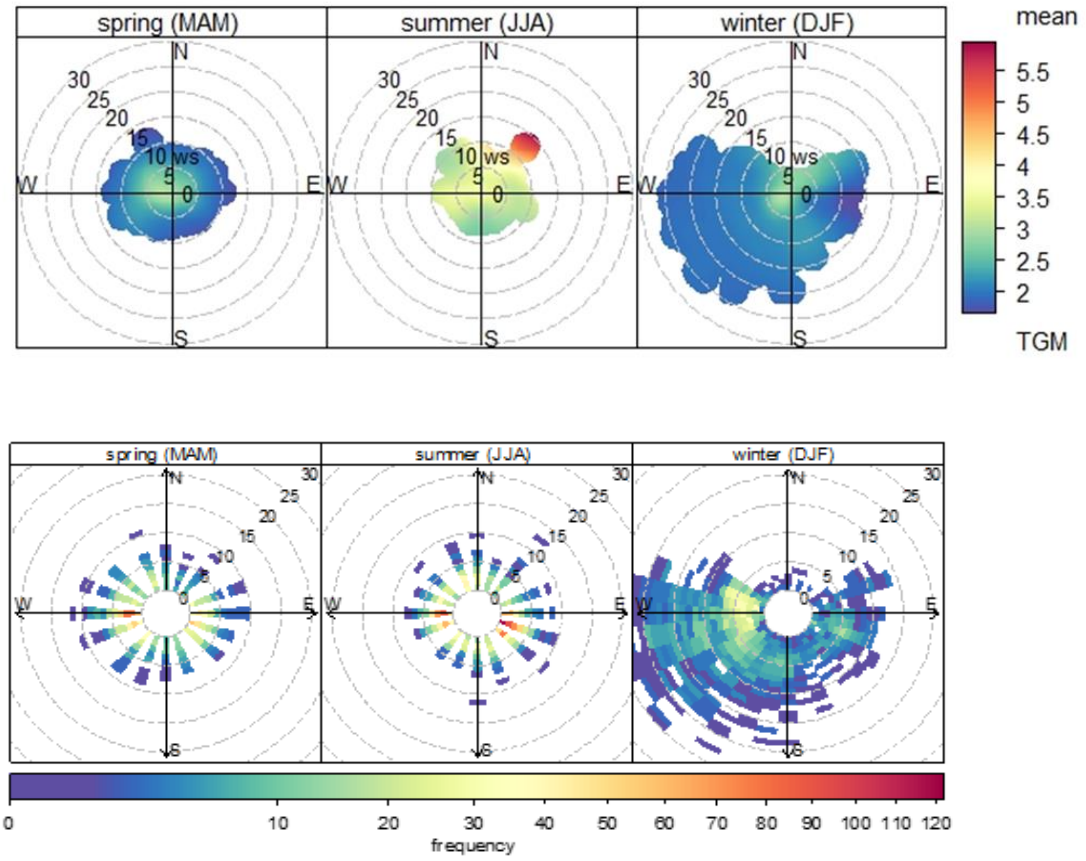

(a)

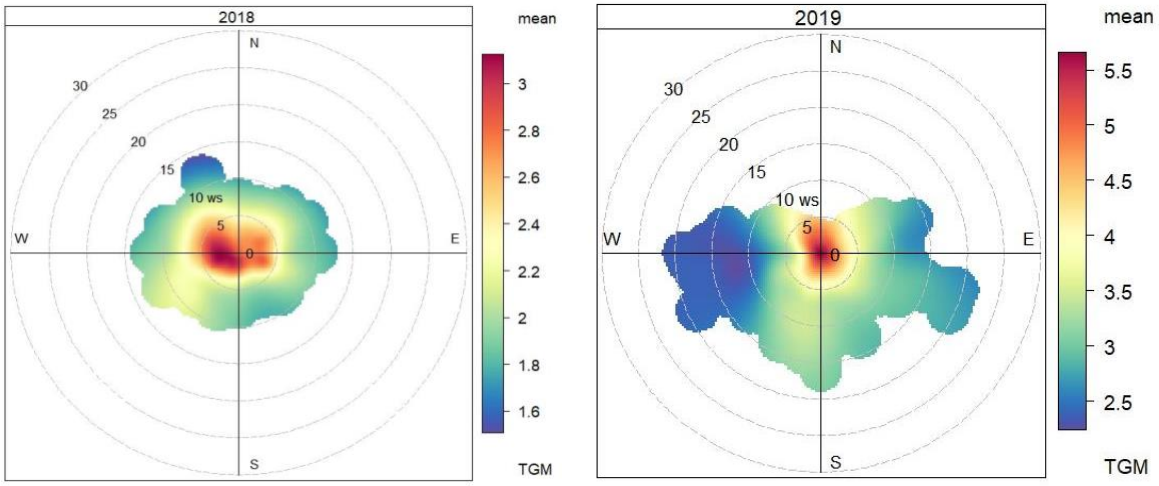

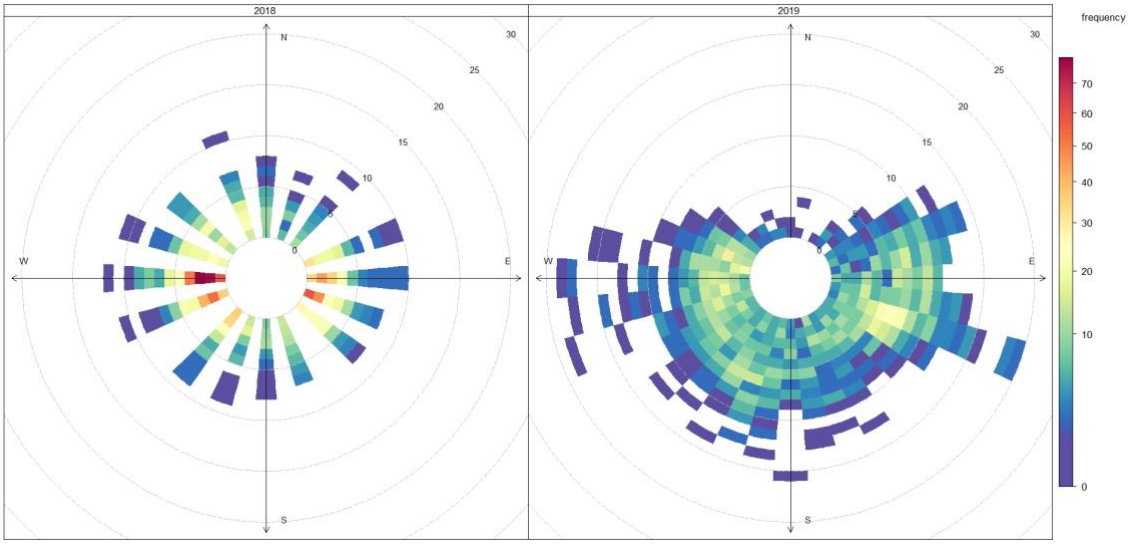

(b)

Fig.ESM6 Polar plots (left column) of mean TGM, showing the variation in concentration by wind speed (m/sec) and direction, and polar frequency plot (right column) of wind speed (m/sec) and direction, referred to: (a) different seasons of 2018; (b) spring 2018 and 2019. Plots generated using OpenAir in R.

References

Bagnato, E., Parello, F., Valenza, M., Caliro, S., (2009). *Mercury content and speciation in the Phlegrean Fields volcanic complex: Evidence from hydrothermal system and fumaroles*, J. Volcanol. Geotherm. Res., 187(3-4), 250-260, https://doi.org/10.1016/j.jvolgeores.2009.09.010.

Bagnato, E., Sprovieri, M., Barra, M., Bitetto, M., Bonsignore, M., Calabrese, S., Di Stefano, V., Oliveri, E., Parello, F., Mazzola, S., (2013). *The sea-air exchange of mercury (Hg) in the marine boundary layer of the Augusta basin (southern Italy): Concentrations and evasion flux*, Chemosphere, 93(9), 2024-2032, https://doi.org/10.1016/j.chemosphere.2013.07.025.

Bagnoli, A., and Gartner, I., *Monitoraggio delle aree geotermiche toscane: Concentrazioni di H2S e Hg nelle aree geotermiche toscane. Monitoraggi ARPAT e validazione dati Enel (Area Vasta Sud. Report anno 2017)*, Arpa Toscana 2018, Prot. n° 0046235, 1-41 (Technical Report), 2018 (in Italian).

Barago, N., Floreani, F., Acquavita, A., Covelli, S., Higueras, P., (2020). *Spatial and Temporal Trends of Gaseous Elemental Mercury over a Highly Impacted Coastal Environment (Northern Adriatic, Italy)*, Atmosphere, 11(9), 935; https://doi.org/10.3390/atmos11090935.

Barghigiani, C., Bargagli, R., Siegel, B.Z., Siegel, S.M., (1990). *A comparative study of mercury distribution on the aeolian volcanoes, vulcano and Stromboli*, Water Air Soil Pollut., 53, 179-188, https://doi.org/10.1007/BF00155002.

Cabassi, J., Tassi, F., Venturi, S., Calabrese, S., Capecchiacci, F., D'Alessandro, W., Vaselli, O., (2017). *A new approach for the measurement of gaseous elemental mercury (GEM) and H2S in air from anthropogenic and natural sources: Examples from Mt. Amiata (Siena, Central Italy) and Solfatara Crater (Campi Flegrei, Southern Italy)*, J. Geochem. Explor., 175, 48-58, https://doi.org/10.1016/j.gexplo.2016.12.017.

Castagna, J., Bencardino, M., D'Amore, F., Esposito, G., Pirrone, N., Sprovieri, F., (2018). *Atmospheric mercury species measurements across the Western Mediterranean region: Behaviour and variability during a 2015 research cruise campaign*, Atmos. Environ., 173, 108-126, https://doi.org/10.1016/j.atmosenv.2017.10.045.

Dedeurwaerder, H., Decadt, G. & Baeyens, W., (1982). *Estimations of mercury fluxes emitted by Mount Etna Volcano*, Bull Volcanol 45, 191–196, https://doi.org/10.1007/BF02597729.

Directive 2004/107/EC of the European Parliament and of the Council of 15 December 2004 relating to arsenic, cadmium, mercury, nickel and PAH in ambient air. Official Journal of the European Union (2004) L 23, 1-14, 26.1.2005.

Directive 2008/50/EC of the European parliament and of the council of 21 May 2008 on ambient air quality and a cleaner air for Europe. Official Journal of the European Union (2008) L 152, 1-44, 11.06.2008.

Directive (EU) 2015/1480 amending several annexes to Directives 2004/107/EC and 2008/50/EC of the European Parliament and of the Council laying down the rules concerning reference methods, data validation and location of sampling points for the assessment of ambient air quality. Official Journal of the European Union (2015) L 226/4, 1-8, 28.08.2015.

EN 14884:2005, Air quality - Stationary source emissions - Determination of total mercury: automated measuring systems, 2005.

EN 15852:2010, Ambient Air Quality - Standard Method for The Determination of Total Gaseous Mercury, Comite Europeen de Normalisation, 2010.

EN 15853:2010, Ambient air quality - Standard method for the determination of mercury deposition, , Comite Europeen de Normalisation, 2010.

Fantozzi, L., Manca, G., Ammoscato, I., Pirrone, N., Sprovieri, F., (2013). *The cycling and sea-air exchange of mercury in the waters of the Eastern Mediterranean during the 2010 MED-OCEANOR cruise campaign*, Sci. Total Environ., 448, 151-162, https://doi.org/10.1016/j.scitotenv.2012.09.062.

Ferrara, R., Maserti, B.E., De Liso, A., Cioni, R., Raco, B., Taddeucci, G. Edner, H., Ragnarson, P., Svanberg, S., Wallinder, E., (1994). *Atmospheric mercury emission at Solfatara volcano (Pozzuoli, Phlegraean Fields - Italy)*, Chemosphere, 29(7), 1421-1428, https://doi.org/10.1016/0045-6535(94)90275-5.

Ferrara, R., Mazzolai, B., Edner, H., Svanberg, S., Wallinder, E., (1998). *Atmospheric mercury sources in the Mt. Amiata area, Italy*, Sci. Total Environ., 213(1-3), 13-23, https://doi.org/10.1016/S0048-9697(98)00067-9.

Ferrara, R., Mazzolai, B., Lanzillotta, E., Nucaro, E., Pirrone, N., (2000). *Volcanoes as emission sources of atmospheric mercury in the Mediterranean basin*, Sci. Total Environ., 259(1-3), 115-121, https://doi.org/10.1016/S0048-9697(00)00558-1.

Fontana, M., Possamai, S., Spagnolo, P., Cappa, C., Bussi, C., Lollobrigida, F., Sacco, M., Milizia, L., Milingo, M., (2018). *Rapporto di sintesi sui dati prodotti dalla stazione di monitoraggio della qualità dell'aria ubicata nel Comune di Beinasco – Giardino Pubblico Aldo Mei, di proprietà di TRM S.p.A. Anno 2017*, Prot. n° 27947 Rapporto Tecnico pp 1-64. http://www.cittametropolitana.torino.it/cms/ambiente/qualita-aria/dati-qualita-aria/relazioni-annuali. (in Italian).

Ministerial Decree D.M. 6 August 2012, Recepimento della direttiva 2009/161/UE della Commissione del 17 dicembre 2009 che definisce il Terzo elenco di valori indicativi di esposizione professionale in attuazione della direttiva 98/24/CE del Consiglio e che modifica la direttiva 2009/39/CE della Commissione. Allegato XXXVIII, valori limite di esposizione professionale, mercurio e composti inorganici divalenti del mercurio compresi ossido mercurico e cloruro di mercurio (misurati come mercurio). (12A09782) (GU Serie Generale n.218 del 18-09-2012) (in Italian).

Ministerial Decree D.M. 5 May 2015, Metodi di valutazione delle stazioni di misurazione della qualita' dell'aria di cui all'articolo 6 del decreto legislativo 13 agosto 2010, n. 155. (15A04273) (GU Serie Generale n.128 del 05-06-2015) (in Italian).

Ministerial Decree D.M. 26 January 2017, Attuazione della direttiva (UE) 2015/1480 del 28 agosto 2015, che modifica taluni allegati delle direttive 2004/107/CE e 2008/50/CE nelle parti relative ai metodi di riferimento, alla convalida dei dati e all'ubicazione dei punti di campionamento per la valutazione della qualità' dell'aria ambiente. (17A00999) (GU Serie Generale n.33 del 09-02-2017) (in Italian).

Legislative Decree D.Lgs 133/2005, Allegato 1, Norme tecniche e valori limite di emissione per gli impianti di incenerimento di rifiuti, valori di emissione in atmosfera, Gazzetta ufficiale serie generale n.163 (in Italian).

Legislative Decree D.Lgs. 155/2010, Decreto Legislativo 13 agosto 2010, n.155, Attuazione della direttiva 2008/50/CE relativa alla qualità dell'aria ambiente e per un'aria più pulita in Europa. Gazzetta Ufficiale n. 216 del 15 settembre 2010-Suppl. Ordinario n. 217 (in Italian).

Munthe, J., Wängberg, I., Pirrone, N., Iverfeldt, Å., Ferrara, R., Ebinghaus, R., Feng, X., Gårdfeldt, K., Keeler, G., Lanzillotta, E., Lindberg, S.E., Lu, J., Mamane, Y., Prestbo, E., Schmolke, S., Schroeder, W.H., Sommar, J., Sprovieri, F., Stevens, R.K., Stratton, W., Tuncel, G., Urba, A., (2001). *Intercomparison of methods for sampling and analysis of atmospheric mercury species*, Atmos. Environ., 35, 3007-3017, https://doi:10.1016/S1352-2310(01)00104-2.

Pirrone, N., (2001). *Mercury research in Europe: towards the preparation of the EU air quality directive*, Atmospheric Environment, 35(17), 2979-2986, https://doi.org/10.1016/S1352-2310(01)00101-7.

Pirrone, N., Wichmann-Fiebig, M., (2003). *Some recommendations on mercury measurements and research activities in the European Union*, Atmospheric Environment, 37(1), 3-8, https://doi.org/10.1016/S1352-2310(03)00234-6.

Sprovieri, F., Pirrone, N., Bencardino, M., D'Amore, F., Carbone, F., Cinnirella, S., Mannarino, V., Landis, M., Ebinghaus, R., Weigelt, A., Brunke, E.-G., Labuschagne, C., Martin, L., Munthe, J., Wängberg, I., Artaxo, P., Morais, F., Barbosa, H.D.M. J., Brito, J., Cairns, W., Barbante, C., Diéguez, M.D.C., Garcia, P.E., Dommergue, A., Angot, H., Magand, O., Skov, H., Horvat, M., Kotnik, J., Read, K.A., Neves, L. M., Gawlik, B.M., Sena, F., Mashyanov, N., Obolkin, V., Wip, D., Feng, X. B., Zhang, H., Fu, X., Ramachandran, R., Cossa, D., Knoery, J., Marusczak, N., Nerentorp, M., Norstrom, C., (2016). *Atmospheric mercury concentrations observed at ground-based monitoring sites globally distributed in the framework of the GMOS network*, Atmos. Chem. Phys., 16, 11915–11935, https://doi.org/10.5194/acp-16-11915-2016.

Vardè, M., Servidio, A., Cofone, F., Rosselli, A., Sprovieri, F., (2014). *First measurements of Total Mercury (THg) in wet deposition at high altitude site in Southern Italy (1379m a.s.l.)*, In Proceedings of the XXV Congresso Nazionale della Società Chimica Italiana, Arcavacata di Rende, 7-12 september 2014.

World Health Organization (WHO), Air quality guidelines (AQGs) for Europe - Second edition, 2000 WHO Regional Publications, European Series, No. 91, ISBN 9289010827.

Applied Geochemistry 107 (2019) 19–33

Contents lists available at ScienceDirect

Applied Geochemistry

journal homepage: www.elsevier.com/locate/apgeochem

Comparative geochemical study between the tap waters and the bottled mineral waters in Calabria (Southern Italy) by compositional data analysis (CoDA) developments

Carmine Apollaro[a,1], Antonella Buccianti[b,c,1], Giovanni Vespasiano[a,*], Massimiliano Vardè[d,e], Ilaria Fuoco[a], Donatella Barca[a], Andrea Bloise[a], Domenico Miriello[a], Franco Cofone[f], Alessandro Servidio[f], Rosanna De Rosa[a]

[a] Department of Biology, Ecology and Earth Sciences (DiBEST), University of Calabria (UniCAL), Via P. Bucci 4, cubo 15B, I-87036, Arcavacata di Rende (CS), Italy
[b] Department of Earth Sciences, University of Florence (UniFI), Via G. La Pira 4, I-50121, Florence, Italy
[c] Institute of Geosciences and Earth Resources (CNR-IGG), Via G. La Pira 4, I-50121, Florence, Italy
[d] Institute for the Dynamics of Environmental Processes (CNR-IDPA), Via Torino 155, I-30172, Venice, Mestre, Italy
[e] Department of Chemical and Pharmaceutical Sciences (DipSCF), University of Ferrara (UniFE), Via Luigi Borsari 46, I-44121, Ferrara, Italy
[f] Institute of Nanotechnology (CNR-NANOTEC), Via P. Bucci 4, cubo 31C, I-87036, Arcavacata di Rende (CS), Italy

ARTICLE INFO

Editorial handling by Prof. M. Kersten

Keywords:
Drinking waters
Natural mineral waters
Major ions
Trace elements
Mercury
Geochemistry
Compositional data analysis
Southern Italy

ABSTRACT

This work focuses on comparing the inorganic content of tap and bottled mineral waters in the Calabria region (Southern Italy) performed by using robust Compositional Data Analysis (CoDA) methods and related new developments associated with a classical graphical-numerical approach.

Thirty-one samples of tap waters scattered throughout the Calabrian territory and twenty-one bottled natural mineral waters of various Calabrian brands were analyzed for major and trace inorganic components. In addition, a very sensitive method based on cold vapour atomic fluorescence spectrometry (CV-AFS) has been employed to determine total mercury (Hg_T) concentrations.

Compositional data analysis was used to identify the main interrelationships among physico-chemical parameters, highlighting the differences between the tap waters and the bottled mineral waters. Some elements, such as Al, Mn, Fe, Zn, and Pb resulted particularly enriched in the tap waters. This group of enriched elements was probably controlled by corrosion processes from metal pipes, asking for more monitoring on the state of the public distribution water network. Li, Ca, Cr, Ni, and Cd, on the other hand, appear to be mostly contributed by natural sources affecting the overall variability of the bottled mineral waters. In this context, Cr, Cu, Hg, and Pb are mainly enriched in the sparkling bottled mineral waters.

Innovative compositional indices did not highlight great differences from the Maximum Allowed Concentrations (MAC) in the two types of water, so that for the health of the consumer it is indifferent to drink tap or bottled mineral water. The results represent a fundamental base to develop monitoring plans in time to check for the maintenance of quality standards.

1. Introduction

In recent years the study of water resources is particularly increased due to continuously society developing that need of a good quality water for the different uses; notwithstanding this effort the new World Health Organization/United Nations International Children's Emergency Fund (WHO/UNICEF) Joint Monitoring Program (JMP) reports that 2.1 billion people worldwide lack access to safe, readily available water at home, and 4.4 billion lack safely managed sanitation (www.unicef.org/wash/). Safe and sufficient drinking water is essential for life but more than half of the river and lake water bodies in Europe are reported to be in less than good ecological status and about 25% of groundwater across Europe is in poor chemical status (water-protect.eu). Periodic quality controls in terms of physico-chemical parameters and microbiological aspects are carried out for bottled mineral waters and tap waters supplied by the municipal drinking water systems from

* Corresponding author.
E-mail address: giovanni.vespasiano@unical.it (G. Vespasiano).
[1] These authors have contributed equally to this work.

https://doi.org/10.1016/j.apgeochem.2019.05.011
Received 17 March 2019; Received in revised form 16 May 2019; Accepted 17 May 2019
Available online 22 May 2019
0883-2927/

relevant public authorities, at least in developed countries. Despite this, the bottled water use is increased compared to that of water supplied by municipal drinking water systems because the bottled mineral water is considered “free” by harmful elements to human health (Vardè et al., 2019). In this perspective, Italy is considered one of the main producers and consumers of bottled natural mineral water (Beverfood, 2016).

Water is a vulnerable resource and its chemistry is governed by several factors such as water-rock interaction, that plays the main role, together with others environmental factors and human activities (Mukate et al., 2018; Apollaro et al., 2019a; Biddau et al., 2019; Ghezzi et al., 2019).

It is known that waters contain elements that can be divided into essential and not-essential nutrients for human alimentation (Felici, 2005). It is also known that long times of exposure and consumption of some elements can cause negative effects on human health. For these hazard elements the WHO has established the guideline values (WHO, 2011) which, although not mandatory, are taken into account by the various government authorities. Based on these guidelines, the different authorities set national water quality limits based on specific environmental issues and economic aspects. In Italy, the EU directive 98/83/EC (98/83/EC, 1998) for drinking water and EU directive, 2003/40/EC for mineral water (2003/40/EC), have been incorporated in the national legislation, as legislative decree D.Lgs 31/2001 (D.Lgs 31/2001, 2001) and ministerial decree D.M. 29/12/2003 (D.M. 29/12/2003, 2003) and further modifications. Instead, into D.Lgs 152/2006 (D.Lgs.152/2006, 2006), the quality standards for groundwater are defined. Table 1 summarizes the current limit values established for drinking water, mineral water and groundwater by Italian law and the WHO threshold values that could be different in other countries.

Nevertheless, bottled waters are subject to less restrictive quality controls than those of drinking water and on bottle labels are not reported important information such as concentration of trace elements (Versari et al., 2002). Moreover, peculiar waters, defined therapeutic waters, are normally advertised by the market but often they are not suitable for daily consumption (Varrica et al., 2013).

Furthermore, the release of potential pollutants from polyethylene terephthalate (PET) and/or glass, colored or not, is possible (Reimann et al., 2010). The leaching of some potentially harmful elements from the bottles could depend from the storage time between bottling and consumption (Shotyk et al., 2006; Shotyk and Krachler, 2007a) and storage conditions (Keresztes et al., 2009).

The tap waters, often constituted by the mixing of several sources (different groundwaters and/or surface waters) are treated following different steps (coagulation, flocculation, sedimentation, filtration and disinfection) before being introduced into the water distribution system (Gray, 2008; Dinelli et al., 2012a). Despite these treatments, the waters that reside for a long time in autoclaves or similar, can change their organoleptic properties such as smell and taste, resulting of low quality to the consumer (Varrica et al., 2013).

Potential pollutants could be released by the pipes of the distribution system (Gonzalez et al., 2013 and reference in therein). The corrosion of the pipelines is undoubtedly one of the causes that favors the enrichment of some harmful elements. Indeed, the pipelines are generally very old, and maintenance is poor.

In recent works the chemical compositions of tap waters and/or bottled mineral waters and the comparisons between them were studied in some places of the world (Reimann et al., 2003; Desideri et al., 2007; Zamberlan da Silva et al., 2008; Birke et al., 2010a, 2010b; Bityukova and Petersell, 2010; Fugedi et al., 2010; Peh et al., 2010; Bertoldi et al., 2011) and also in Italy (e.g. Naddeo et al., 2008; Avino et al., 2010; Cicchella et al., 2010; Cidu et al., 2011; Dinelli et al., 2012a, 2012b; Veschetti et al., 2010; Varrica et al., 2013; Vardè et al., 2019), highlighting different aspects such as natural radioactivity, microbiological issues and enrichment in trace elements including Hg (Dinelli et al., 2010, 2012a,b; Caridi et al., 2017; Vardè et al., 2019). By considering Calabria Region more authors have investigated the content of major, minor and trace elements of natural waters (springs, stream waters, wells) in various areas with different geological features (Apollaro

Table 1
In the table are reported the limit values do not be exceeded in the tap waters, mineral waters and groundwaters (according to the Italian law D.Lgs. 31/2001; D.M. 10/02/2015; D.Lgs. 152/2006 and the World Health Organization drinking water guidelines 2011). (* = infants limit value).

Parameters (μg L^{-1})	D.Lgs 31/2001 tap water	D.M. 10/02/2015 mineral water	D.Lgs 152/2006 groundwater	WHO guideline value (2011)
Aluminium (Al)	200	–	200	200*
Ammonium (NH_4^+)	500	–	–	
Antimony (Sb)	5	5	5	20
Arsenic (As)	10	10	10	10
Barium (Ba)	–	1000	–	700
Beryllium (Be)	–	–	4	–
Boron (B)	1000	5000	1000	2400
Bromine (Br^-)	10	–	–	–
Cadmium (Cd)	5	3	5	3
Chromium (Cr Tot)	50	50	50	50
Chromium (Cr VI)	–	–	5	–
Cloride (Cl^-)	250000	–	–	250000*
Cobalt (Co)	–	–	50	–
Copper (Cu)	1000	1000	1000	20000
Fluoride (F^-)	1500	5000/1500*	1500	1500
Iron (Fe)	200	–	200	–
Lead (Pb)	10	10	10	10
Manganese (Mn)	50	500	50	400
Mercury (Hg)	1	1	1	6
Molybdenum (Mo)	–	–		70
Nickel (Ni)	20	20	20	70
Nitrate (NO_3^-)	50000	45000/10000*	–	50000
Nitrite (NO_2^-)	500	20	500	3000
Selenium (Se)	10	10	10	40
Silver (Ag)	–	–	10	–
Sulfate (SO_4^{2-})	250000	–	250000	500000
Tallium (Tl)	–	–	2	–
Uranium (U)	–	–	–	30
Vanadium (V)	50	–	–	–
Zinc (Zn)	–	–	3000	4000*

et al., 2007, 2009; 2011, 2012; Vespasiano et al., 2012a, 2012b; Apollaro et al., 2013a, 2013b; Protano et al., 2014; Vespasiano et al., 2014; Critelli et al., 2015a, 2015b; Vespasiano et al., 2015a, 2015b; 2015c; Apollaro et al., 2016; Vespasiano et al., 2016a, 2016b; 2017; Apollaro et al. 2019b; 2019c; Gaglioti et al., 2019). These works showed a substantial compositional variability of waters linked to complex regional geological setting, however highlighting a good quality status of the local water resources.

In this paper data for the comparison were collected for the first time in the Calabria Region (Southern Italy) and, notwithstanding the limited number of samples, the data set represents a reference framework for developing further monitoring plans. The data set in fact contains information about the main physico-chemical parameters, major ions and trace elements reporting a complete chemical analysis. On the contrary, data from the public regional agencies are often limited to some species determined for specific purposes (Nisi et al., 2016).

The CoDA (Compositional Data Analysis) approach was used to compare the tap waters (TW - from public drinking fountains and apartments) and the bottled mineral waters (BW - still and sparkling) including the proposal of new multivariate comparison indices. This analysis was associate to a complete geochemical characterization of the water by using classical geochemical diagrams currently adopted by the scientific community. The results have allowed to expand the knowledge on local resources and potential environmental issues, raising awareness the competent authorities on quality control. Moreover, data collection will represent a useful starting point for consumer who can be guided in choosing the water to use for his needs.

2. Geological and hydrogeological setting

The Calabrian Peloritan Orogen (*CPO*) represents a fragment of the European margin, which was thrust onto the Maghrebian-Sicilian and Appennine thrust and-fold belts during the Europe-Apulia collision in Oligocene-Early Miocene (e.g., Amodio Morelli et al., 1976; Cirrincione et al., 2015 and references therein). The *CPO* has been divided into two sectors, a Northern one and a Southern one, which are separated by a strikeslip tectonic line running along the Catanzaro trough (Boccaletti et al., 1984; Tansi et al., 2007).

The Northern and Southern sectors represent, respectively, two domains characterized by a different paleogeographic evolution carried out during middle Miocene.

In detail, the northern one extends from Sangineto tectonic line to the Capo Vaticano-Soverato alignment. This is a nappe pile, which can be described as the superposition of three major structural elements that represent different paleogeographic domains: (i) The Apennine Units (Iannace et al., 2007) that represents the lower portion made up of Mesozoic sedimentary and metasedimentary successions (Trias-Miocene). Mesozoic sedimentary successions are constituted by calcareous rocks. These lithotypes, due the fragile characters and the sin- and post-orogenetic tectonic evolution, are generally very fractured. Furthermore, because of their typical chemical composition, they are subject of karst phenomena through which the action of dissolving rainwater tends to expand and develop the network of pre-existing fractures. Mesozoic sedimentary successions, due to their peculiar hydrogeological characteristics, on a regional scale, represent the wide "*carbonate-dolomitic complex*". The carbonate complex can be considered as a wide reservoir, in which groundwater circulation is conditioned by the geometric relationships with the surrounding geological units, as well as by the great inner structural discontinuities. In general, this represents one of the main sources of drinking water supplies in Calabria and Southern Italy (Allocca et al., 2007).

(ii) The structurally intermediate allochthonous Alpine Liguride nappe (Liberi and Piluso, 2009) (Tithonian-Neocomian) made up of a series of Alpine metamorphic units including a Cretaceous-Paleogene metapelitic-ophiolitic-carbonate assemblage. The complex is divided in four subunits (Amodio Morelli et al., 1976), from the bottom to the top: (i) Frido Unit; (ii) Diamante-Terranova Unit; (iii) Malvito Unit; (iv) Gimigliano-Monte Reventino Unit (Liberi and Piluso, 2009; Bloise et al., 2012, 2017).

(iii) The Calabride Complex constituted by Hercynian and pre-Hercynian gneiss, granite and metapelite. The Calabride complex comprises three major Paleozoic tectono-metamorphic units: (a) the Bagni Unit (metapelite, metarenite and metabasite); (b) the Castagna Unit (paragneiss and schist); (c) the Sila Unit (metamorphic and plutonic rocks and a Mesozoic cover) (Van Dijk et al., 2000).

The Calabride and Liguride complexes could be grouped, from a general point of view, in the "*Crystalline-Metamorphic Hydrogeological Complex*" of Northern Calabria as proposed by Allocca et al. (2007).

The latter, compared with the Mesozoic carbonate aquifers, characterizes a less important hydrogeological system representative of a very complex hydrogeological setting in which porous shallow aquifers, characterized by the weathering profile coexist and interact with the intermediate aquifer, represented by the fissured rock basement. The resources linked to the crystalline-metamorphic aquifers, although considerably less extensive than those of the carbonate complex, can be considered interesting for local supply issues. Inside them, groundwater circulation and recharge are mainly conditioned by the degree of rocks alteration, which varies according to the depth and fracturing degree (Allocca et al., 2007).

The southern sector of the CPO develops to the south of the alignment that extends from Capo Vaticano to Soverato, including the Serre, the Aspromonte and the Peloritani massifs. In the southern sector the following structural elements can be recognized (Tortorici, 1982): (i) Longi-Taormina Unit; (ii) Mandanici Unit; (iii) Aspromonte Unit; (iv) Stilo Unit. These, with the exclusion of sedimentary coverings, can be incorporated into the crystalline-metamorphic complex defining the "*crystalline-metamorphic complex of Southern Calabria*".

From a hydrogeological point of view, in addition to the two-macro carbonate-dolomitic and crystalline-metamorphic complexes, a key role is played by the systems linked with the terrigenous and alluvial successions. Among the aquifers that have been the object of research and studies, there are the porous-quaternary ones, in which fall alluvial plains and coastal plains deposits. The high interest of these aquifers is mainly correlated with the high groundwater request for anthropic activities (Vespasiano et al. 2015d, 2016c). The alluvial and coastal deposits are the ones most represented in outcrop in the Calabrian Region. These terrains constitute continuous/heterogeneous and anisotropic aquifers (Allocca et al., 2007).

Both tap and bottled mineral waters were sampled in all Calabrian territory. Indeed, the sampling sites fall into main recognized hydrogeological complexes which are exploited to regional water supply. The chemical composition of each sampling point is linked to water-rock processes occurred in each investigation area. Thus, the geochemical features of the whole dataset (TW and BW) can be considered representative of the heterogeneous regional geological setting.

3. Materials and methods

3.1. Sample collection

Thirty-one samples of tap waters (TW) scattered throughout the Calabrian territory and twenty-one natural mineral waters (BW) of thirteen Calabrian brands were considered. The location of water samples is shown in Fig. 1. TW were collected during the months of October and November 2015 from public drinking fountains throughout the Calabrian region. BW were purchased at supermarkets during the same sampling period of drinking waters. Bottle containers were made in PET. Thirteen samples were still waters and seven sparkling waters.

The methodology of water sampling was already described by Apollaro et al. (2019c).

For total Hg determination purpose, sampling of TW has been

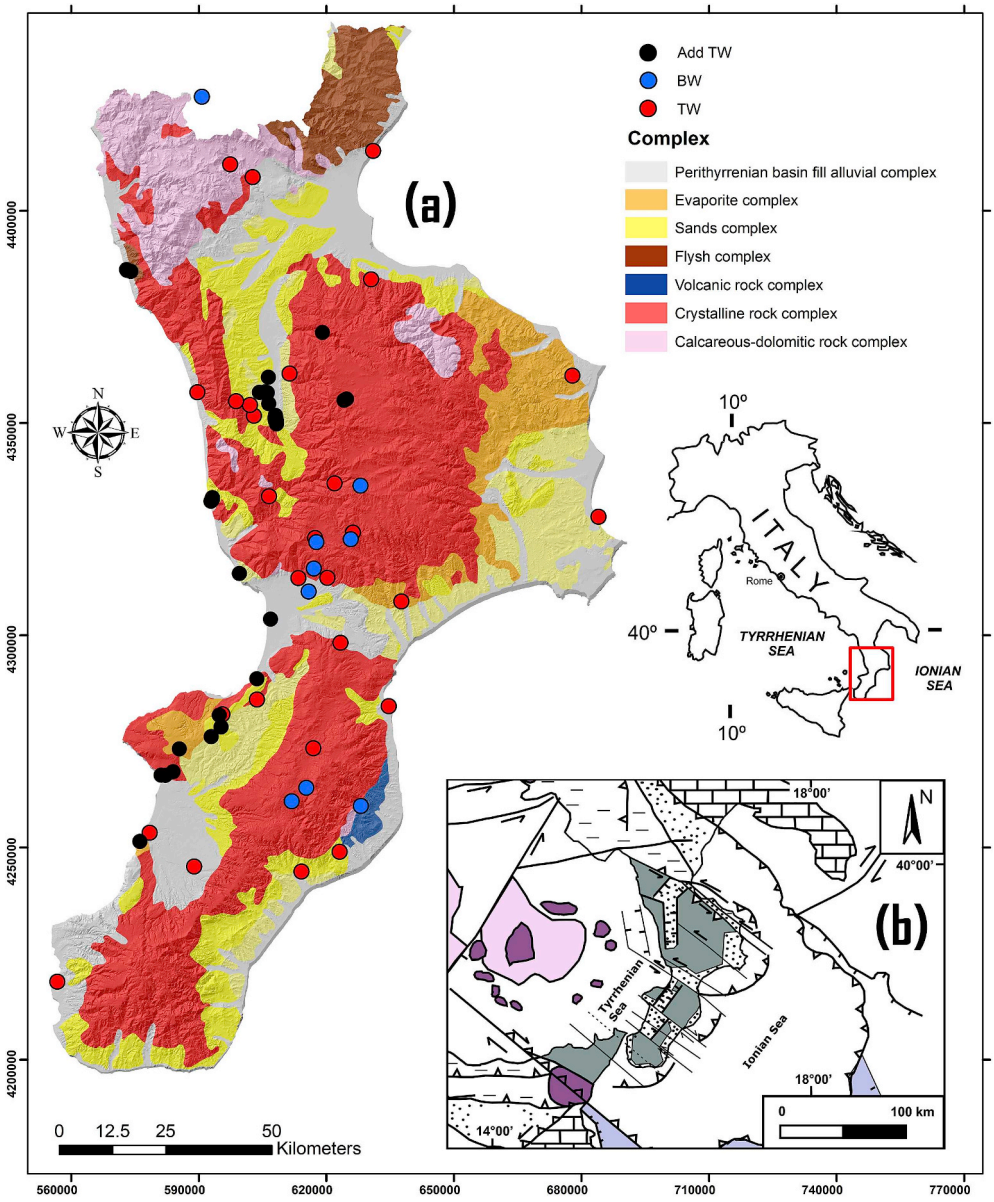

Fig. 1. (a) Simplified hydrogeological map of Calabria and (b) structural framework of the Calabrian Peloritan Orogen (modified by Tripodi et al., 2018). **TW:** tap waters, **BW:** bottled mineral waters. **Add TW** are additional samples for Hg measurements.

performed through (i) collection procedure using polypropylene (PP) gloves (ii) PP vials suitable for the determination of trace metals (VWR, Radnor, PA, USA) contained in a double zip-lock bag to minimize contamination (iii) stabilization of the Hg present in the sample with addition of hydrochloric acid (HCl 33–36% ultra-pure quality, UpA, Romil, Cambridge, UK) to a final concentration of 0.5% (v/v) (iiii) transport in a refrigerated bag to the laboratory. Once in the laboratory the TW samples are kept in the refrigerator at 4 °C and in the dark until the Hg analyses. For each selected sampling point, TW samples were collected in triplicate in 50 mL PP vials, previously cleaned in the laboratory with nitric acid diluted at 3.5% (v/v) and after chemical analysis that confirmed no Hg contamination. Once it was established that for each batch of used container the Hg content in the laboratory blank was below the detection limit, the vials could be used for taking water samples from public drinking fountains and for laboratory activities. The procedure followed for the storage, preparation and treatment of the material used in the laboratory and samples of BW, has been described in detail in a previous work (Vardè et al., 2019). Finally, an additional sampling (TW 32/60, $n = 29$) of TW samples was considered for mercury measurements (see Table 3) to verify if Hg concentrations were confirmed at ultra-trace levels.

3.2. Analytical methods

Total alkalinity and dissolved silica (SiO_2) were directly determined in the field by acidimetric titration using HCl 0.01 N as titrating agent and methyl orange as indicator and using a portable spectrophotometer. In the laboratory, the concentrations of major cations and anions were determined by high performance liquid chromatography (HPLC, Dionex DX 1100, Sunnyvale, CA, USA), whereas those of several trace elements (Li, Be, B, Al, V, Cr, Mn, Fe, Co, Ni, Cu, Zn, As, Se, Rb, Sr, Mo, Cd, Ba, Pb, and U) were determined by a quadrupole inductively coupled plasma-mass spectrometer (ICP-MS, PerkinElmer/SCIEX, Elan DRCe, Concord, ON, Canada) with a collision reaction cell capable of reducing or avoiding the formation of polyatomic spectral interferences. All the chemical data were produced in the laboratory of the Department of Earth Sciences of the University of Calabria. Data quality for metal and trace elements was checked by running the SRM

Table 2
Summary statistics for the two groups of data (left columns tap waters, cases = 31, right columns bottled mineral waters, cases = 21).

	Tap waters					Bottled waters				
	Minimum	Maximum	Median	Kurtosis	Skewness	Minimum	Maximum	Median	Kurtosis	Skewness
pH	6.50	7.96	7.46	0.39	−0.97	6.23	7.87	7.39	−1.26	−0.50
Ca^{2+}	3540	164050	23910	10.39	2.66	1350	53730	13520	−1.40	0.68
Mg^{2+}	1760	30110	8630	0.58	1.07	1050	18450	4660	−1.07	0.63
K^+	340	13890	1320	15.01	3.64	590	2150	1290	−1.37	0.23
Na^+	3010	212460	9410	23.57	4.64	3210	24540	13500	−0.14	0.38
Cl^-	3000	398330	9880	28.77	5.29	4500	27050	9180	−1.25	0.63
SO_4^{2-}	3410	108120	10430	6.40	2.44	3590	37200	7180	−0.25	1.14
HCO_3^-	18310	465250	106780	2.86	1.42	9150	221190	64070	−1.31	0.63
F^-	30	730	150	0.65	1.09	30	440	110	1.14	1.37
NO_3^-	240	33230	2540	8.67	2.98	120	11070	2500	−0.73	0.82
SiO_2	3400	26800	18200	−1.04	−0.39	3400	42300	21000	−0.30	0.09
Li	0.17	10.75	0.90	6.41	2.32	0.20	11.29	3.16	−1.28	0.39
B	6.94	119	6.94	5.18	2.36	6.94	43.30	6.94	2.03	1.73
Al	0.44	117	1.17	25.77	4.93	0.44	24.05	0.44	13.68	3.66
V	0.06	3.58	0.75	3.27	1.53	0.06	8.41	1.22	2.25	1.68
Cr	0.09	1.10	0.20	2.84	1.89	0.09	13.07	0.23	5.04	2.19
Mn	0.01	99.6	0.36	29.80	5.42	0.10	3.36	0.10	2.01	1.75
Ni	0.21	3.57	0.93	2.30	1.58	0.09	1.95	0.52	−0.74	0.55
Cu	0.14	78.8	4.88	14.73	3.61	0.14	8.11	1.40	1.20	1.58
Zn	0.55	153	22.69	3.33	1.70	0.55	23.60	0.55	7.55	2.95
Sr	34.89	1998	93.3	7.83	2.65	12.96	1039	67.3	−0.08	1.24
Se	0.29	4.82	2.52	−0.51	−0.21	0.29	0.91	0.29	4.17	2.35
Rb	0.46	3.03	0.46	1.89	1.54	0.46	2.20	0.46	−0.35	1.02
Mo	0.16	64.7	0.76	30.42	5.49	0.16	3.02	0.16	1.93	1.77
U	0.01	6.98	0.68	2.09	1.63	0.01	4.32	0.08	6.31	2.62
Pb	0.01	2.05	0.15	10.41	2.83	0.01	0.13	0.01	9.74	2.98
As	0.59	3.02	0.59	3.14	1.81	0.59	1.91	0.59	−0.54	1.16
Cd	0.01	0.17	0.02	14.13	3.38	0.00	0.09	0.01	3.25	2.03
Ba	3.47	90.9	11.54	2.84	1.78	0.70	26.00	6.93	−1.26	0.65
Fe	0.49	620	12.93	16.73	3.89	0.45	5.83	2.09	−0.43	0.74

Table 3
Concentration of Hg expressed in ng L^{-1} respectively, from tap waters (column 1), additional tap waters (column 2) and bottled mineral waters (column 3).

ID	Hg_T (ng L^{-1})	ID	Hg_T (ng L^{-1})	ID	Hg_T (ng L^{-1})
TW01	1.36	TW32	0.29	BW01-1	< 0.09
TW02	1.06	TW33	0.47	BW01-2	< 0.09
TW03	1.02	TW34	0.22	BW02	0.16
TW04	0.28	TW35	0.49	BW03	0.12
TW05	0.68	TW36	0.28	BW04	0.16
TW06	1.48	TW37	0.14	BW05-1	< 0.09
TW07	0.88	TW38	0.18	BW05-2	0.10
TW08	0.75	TW39	0.44	BW06-1	0.37
TW09	0.47	TW40	0.66	BW06-2	0.91
TW10	0.51	TW41	0.25	BW07	0.14
TW11	0.39	TW42	0.87	BW08-1	< 0.09
TW12	0.51	TW43	0.21	BW08-2	0.13
TW13	3.68	TW44	0.23	BW09	0.14
TW14	0.37	TW45	0.39	BW10-1	0.10
TW15	0.46	TW46	0.48	BW10-2	0.11
TW16	1.22	TW47	0.55	BW11	0.15
TW17	0.96	TW48	0.19	BW12	< 0.09
TW18	1.10	TW49	0.68	BW13-1	0.40
TW19	0.42	TW50	1.95	BW13-2	0.32
TW20	0.70	TW51	0.40	BW14-1	0.12
TW21	0.97	TW52	0.87	BW14-2	0.11
TW22	0.66	TW53	0.36		
TW23	1.61	TW54	0.29		
TW24	0.99	TW55	0.59		
TW25	1.14	TW56	0.38		
TW26	0.92	TW57	1.76		
TW27	1.79	TW58	1.33		
TW28	0.91	TW59	0.30		
TW29	3.46	TW60	1.23		
TW30	0.67				
TW31	5.57				

NIST1643e standard reference solution (Trace Elements in Water, National Institute of Standards and Technology, USA). For trace elements, deviations from the certified concentrations were found to be lower than 7% whereas for major elements the deviation from the ionic balance condition was always less than ± 5%. No contamination was detected from analyses of blank field solutions.

Total Hg was measured after addition of a 0.5% (v/v) bromochloride solution to all water samples, with the aim to oxide process of all mercury forms to Hg^{2+} until a complete yellow staining (indicating complete Hg oxidation) of the solution is observed. The Hg analyses were performed following the optimized the United States Environmental Protection Agency method (US-EPA) 1631 version E (US-EPA, 2002) by cold-vapour atomic fluorescence spectrometry (CV-AFS), that allowed authors the quantitation of mercury with high sensitivity up to sub-nanogram per litre. Operating and maintenance costs were less expensive compared to other instruments such as cold-vapour atomic absorption spectrometry (CV-AAS) and ICP-MS. The analytical method employed provided for a strict analytical control procedure through a calibration curve in the range 0.17–0.25 ng L^{-1} ($R^2 > 0.9995$) with percentage recoveries in the range between 90.27 and 111.75 (average 101.02%), the use of initial and ongoing IPR and OPR precision standards, matrix spikes and duplicates, and three reference material having certified Hg content with average percentage recovery of 101.17% ($n = 16$) for the BCR-579 (Hg in coastal seawater, IRMM, Belgium), 105.96% ($n = 8$) for the ORMS-5 (Hg in river-water, NRCC, Canada) and 105.63% ($n = 4$) for the ERM-CA615 (Hg in groundwater, IRMM, Belgium), respectively. The limit of detection (LOD) and the limit of quantification (LOQ) calculated according to US-EPA 1631 method were equal to 0.03 and 0.09 ng L^{-1} respectively.

Field data and compositional features of all water samples considered, in terms of main physico-chemical parameters, major ions and trace elements, are listed in Tables 1Sa and 1Sb (Supplementary material).

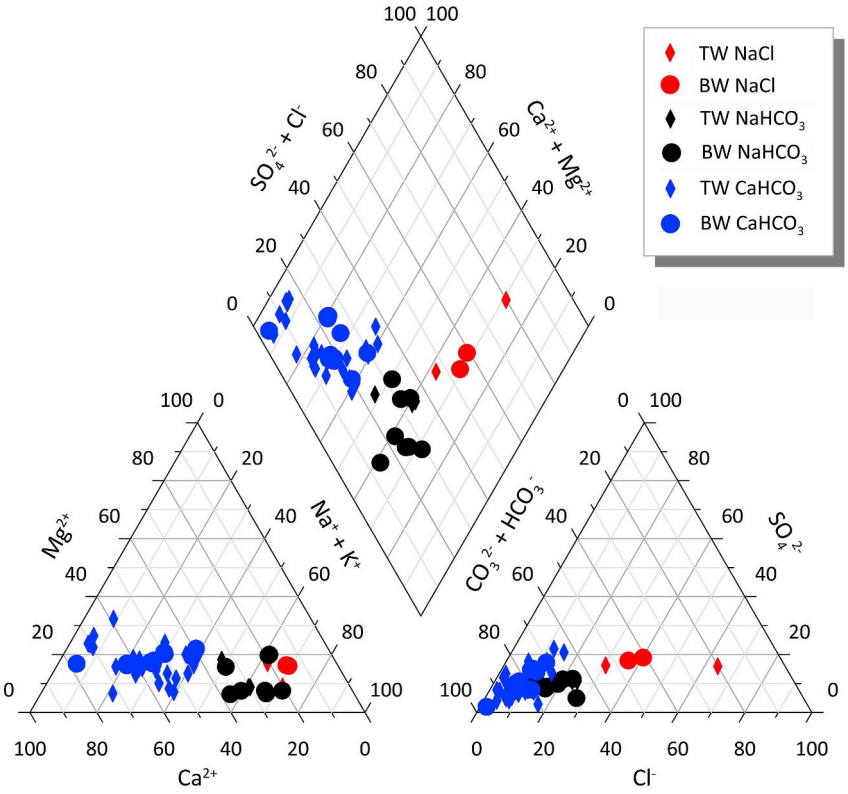

Fig. 2. Piper Diagram of major cations and anions for the tap water and bottled mineral water samples of the Calabria Region.

4. Statistical analysis

Concentrations of elements and/or chemical species in water are compositional data that need to be expressed in log-ratio coordinates before applying the traditional statistical tools (Aitchison, 1982; Buccianti and Pawlowsky-Glahn, 2005). It is in fact well known that the sample space of compositions is not the usual Euclidean space, but the simplex governed by the Aitchison geometry (Pawlowsky-Glahn et al., 2015). There are different possibilities to transform the data, and in our case the log-centered (clr, centered log-ratio) transformation was used since it works successfully in multivariate investigations as cluster analysis (see Supplementary material).

The data sets are given by 31 tap waters and 21 bottled mineral waters. Variables as NH_4^+, PO_4^{3-}, Be, Co and Bi were eliminated by the analysis since most of the data (> 60%) where below the detection limits while Hg was not included since determined with a very different experimental method, related to a different sampling strategy and characterized by very low concentrations. For all the other variables (Ca^{2+}, Mg^{2+}, K^+, Na^+, Cl^-, SO_4^{2-}, HCO_3^-, F^-, NO_3^-, SiO_2, Li, Be, B, Al, V, Cr, Mn, Fe, Co, Ni, Cu, Zn, As, Se, Rb, Sr, Mo, Cd, Ba, Pb, and U), before to calculate the clr coordinates, data below the detection limits were substituted by using the compositional approach proposed by Martin-Fernandez et al. (2015) based on a Bayesian-multiplicative replacement.

In a first attempt, simple statistics were determined for each data-set (minimum, maximum and median) together with the values of skewness and kurtosis able to highlight the presence of anomalous values and/or plurimodality. Box-plots were used as a robust graphical tool to compare the concentrations of the major components and the trace elements. The same plots were realized also after to have clr-transformed the data with the aim to visualize important shifts from the compositional barycenter for each variable. Independent samples Kruskas-Wallis and median tests (Corder and Foreman, 2014) were applied on raw and clr-data to probe for each variable the presence of statistically significant differences between the data sets.

Subsequently, from a multivariate point of view a cluster analysis was performed on clr-variables, by using the Ward method as linkage tool and the Euclidean distance as similarity measure, with the aim to evaluate the presence of natural groups to cross-correlate with the original membership. Significance of the natural groups was also tested by using robust procedures (Verboven and Hubert, 2005; García-Escudero et al., 2010).

Comparative study between tap and bottled mineral water in Italy has been discussed by Dinelli et al. (2012a,b).

Comparing spread between datasets is an important step since high differences might be related to suspected different behavior and or to the presence of anomalous cases (see Supplementary material). In our case we propose a comparative index compatible with the compositional nature of the data. The index is the ratio between the contribution to the whole variance of the data set given by each clr-variable in the two different groups, TW and BW (Daunis-I-Estadella et al., 2006). Associated with the comparison between group medians when the ratio for a given variable is equal to 1 the contribution to variability is similar in the two datasets and the variable cannot be suspected as the source for potential differences. When the ratio is > 1 the source of variability of natural processes is dominant, the contrary when the ratio is < 1. If the ratio values are plotted in decreasing order versus the ranked element/chemical species, it is possible to visualize immediately where the contribution to variance is chemically located, highlighting the behavior of single variables with respect to the compositional barycenter.

In the evaluation of water quality also the comparison with the MAC (Maximum Allowed Concentration) guidelines is important so that Tamasi and Cini (2004) proposed a metal index MI also used in Varrica et al. (2013) (see Supplementary material).

In this case too, it is possible to substitute the index with another compatible with the compositional nature of the data. The MAC values ($\mu g\ L^{-1}$) for the two datasets were considered for B, Al, V, Cr, Mn, Fe, Ni, Cu, Zn, As, Se, Mo, Cd, Ba, Pb, and U, thus generating two new compositions. The robust Mahalanobis distance between each composition pertaining to BW or TW groups and the corresponding MAC

values was determined by using the robust covariance structure of each dataset. In this context the robust Mahalanobis distance represents a new index of compositional difference with respect to the MAC compositions (Gozzi et al., 2018). When the differences are high and show homogeneous values with respect to the MAC composition the nearness to warning thresholds is not suspected. The two proposed "compositional" indices wish to contribute in the diffusion of the use of correct statistical practices in the management of environmental data.

5. Results and discussion

Geochemical data for both tap waters and bottled mineral waters were interpreted following a consolidated classical procedure which comprises: (i) Piper diagram, (ii) binary graph of SO_4^{2-} vs. $HCO_3^- + Cl^-$, in which iso-salinity lines are drawn for reference and (iii) binary plots of Cl^- vs. elements to obtain information about processes possibly occurring during groundwater circulation. These information were discussed together with results of the statistical analysis (box-plots, cluster analysis) and statistical considerations of detected Hg ultra-trace concentrations.

5.1. Water chemistry

Bottled mineral waters and tap waters showed different physicochemical characteristics and composition in terms of major and trace elements. BW have shown mean pH values of 7.18 ± 0.57 (min 6.23, max 7.87), comparable with that detected for TW (mean 7.40, min 6.50, max 7.90). Electrical conductivity (EC) is lower for BW with mean values of 223 μS cm^{-1} (min 52, max 475) respect to 351 μS cm^{-1} (min 109, max 1570) detected for TW, these ones also showing a larger spread of values. To be noticed here is the presence of high values in TW in some sampling places in proximity of coastal areas.

Piper diagram (Fig. 2) highlighted three main compositional groups for waters: NaCl (4 samples), Na–HCO_3 (11 samples) and Ca–HCO_3 (38 samples). Both the considered groups (TW and BW) present at least one sample in each geochemical family. These compositions reflect a typical groundwater evolution starting from a meteoric NaCl end-member that, through water-rock interaction, acquires initially a Na–HCO_3 composition and then come to terms more evolved as Ca–HCO_3.

$$NaCl \rightarrow NaHCO_3 \rightarrow CaHCO_3$$

This process leads to an increase in salinity from NaCl to Ca–HCO_3 groups (Appelo and Postma, 1996; Vespasiano et al., 2015d).

This trend is not sufficiently clear through the only elaboration of the diagram in Fig. 2. To retrieve this kind of information is convenient to refer to the correlation diagram SO_4^{2-} vs $HCO_3^- + Cl^-$ (Fig. 3). Overall, the diagram highlights low Total Ionic Salinity (TIS) values, attested below 16 meq L^{-1} iso-salinity line, with a larger spread of salinity for the TW which recorded the highest values. Furthermore, as previously anticipated, on the diagram is evident an increase in salinity from NaCl to Ca–HCO_3 group with the exception of the TW23 sample showing high salinity and NaCl composition. This composition reflects probably a sea water contamination.

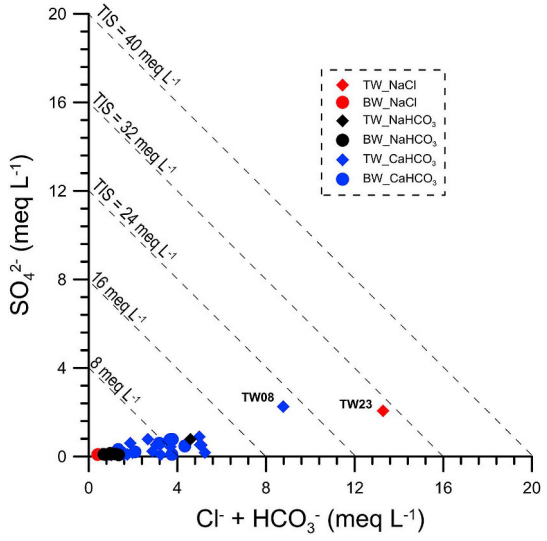

Fig. 3. Correlation diagram of SO_4^{2-} vs. $HCO_3^- + Cl^-$ showing the tap waters and bottled mineral waters of the Calabria Region. Iso-salinity lines are drawn for reference.

Chloride plots (Fig. 4) were useful for appraising mixing and other processes occurring in the aquifers, such as calcite precipitation and water-rock interactions. Each diagram was characterized by the presence of the hypothetical dilution line realized by starting from the composition of sea water (Nordstrom et al., 1979).

In general, major anions and cations like Cl^-, SO_4^{2-}, NO_3^-, Na^+, Mg^{2+}, K^+, and Ca^{2+} are slightly more enriched in TW respect then BW.

As reported in Fig. 4a, b, c, and e, all samples showed Ca^{2+}, Mg^{2+}, K^+ and SO_4^{2-} enrichment probably from water-rock interactions with calcite, dolomite, K-Feldspar and/or Mg-enriched minerals as biotite and olivine (e.g. Apollaro et al., 2009, 2011, 2019b; Perri et al., 2016). The SO_4^{2-} probably derives from the dissolution of minerals like pyrite (oxidative dissolution) and gypsum.

The Cl^- vs. Na^+ plot (Fig. 4d) shows that most of samples fall in proximity to the seawater dilution line, indicating that takes place a negligible water-rock interaction with Na-bearing phases.

A particular detailed analysis is to be destined to the NO_3^- as extremely harmful if present in high concentrations (Fig. 4f). It is of fundamental importance that water intended for human consumption complies with the MAC of 45 mg L^{-1} and 10 mg L^{-1} for water proposed for infants and toddlers (D.M. 10/02/2015 and further modifications).

There are four tap waters and two bottled mineral waters above the maximum limit of 10 mg L^{-1}, therefore these six waters are not recommended for infants' consumption. Nevertheless, all 52 samples, including BW and TW, have values less than the maximum permissible concentration (45 mg L^{-1}).

5.2. Compositional statistical data analysis

In Table 2 the summary statistics of the pH values and of the concentrations of the analyzed variables (μg L^{-1}) are reported for tap (left columns, 31 cases) and bottled mineral waters (right columns, 21 cases).

In Fig. 5 (main chemical components) and Fig. 6 (trace elements) the box plots visualize the variability of each raw variable as well as the presence of skewness and/or anomalous cases. In Fig. 7 all the variables for the two data sets are compared by considering their shift with respect to the compositional barycenter (the geometric mean of the composition) by using the log-centered transformation of Aitchison (1982). As we can see for the main components NO_3^- is characterized by the highest variability in both the datasets testifying a homogenization of the sources contributing to this chemical species. On the whole, besides NO_3^- and SO_4^{2-}, main components in tap waters show a lower variability compared with bottled mineral water, a result that appears to well characterize the comparison of the datasets as the number of anomalous cases is only lightly higher for TW. By considering the trace elements (Fig. 6), Sr is the element showing the highest variability in BW, Zn in TW, the two elements well representing the natural contribution from weathering reactions and corrosion pipe, respectively. On the whole, trace elements in TW show higher variability indicating that, possibly, several processes affect the final concentrations. Increasing variance often tend to generate alternative states and contribute to the developing of plurimodality (Carpenter and Brock, 2006; Dakos et al., 2012; Dai et al., 2015) representing a less stable geochemical system in time or space, subjected to possible

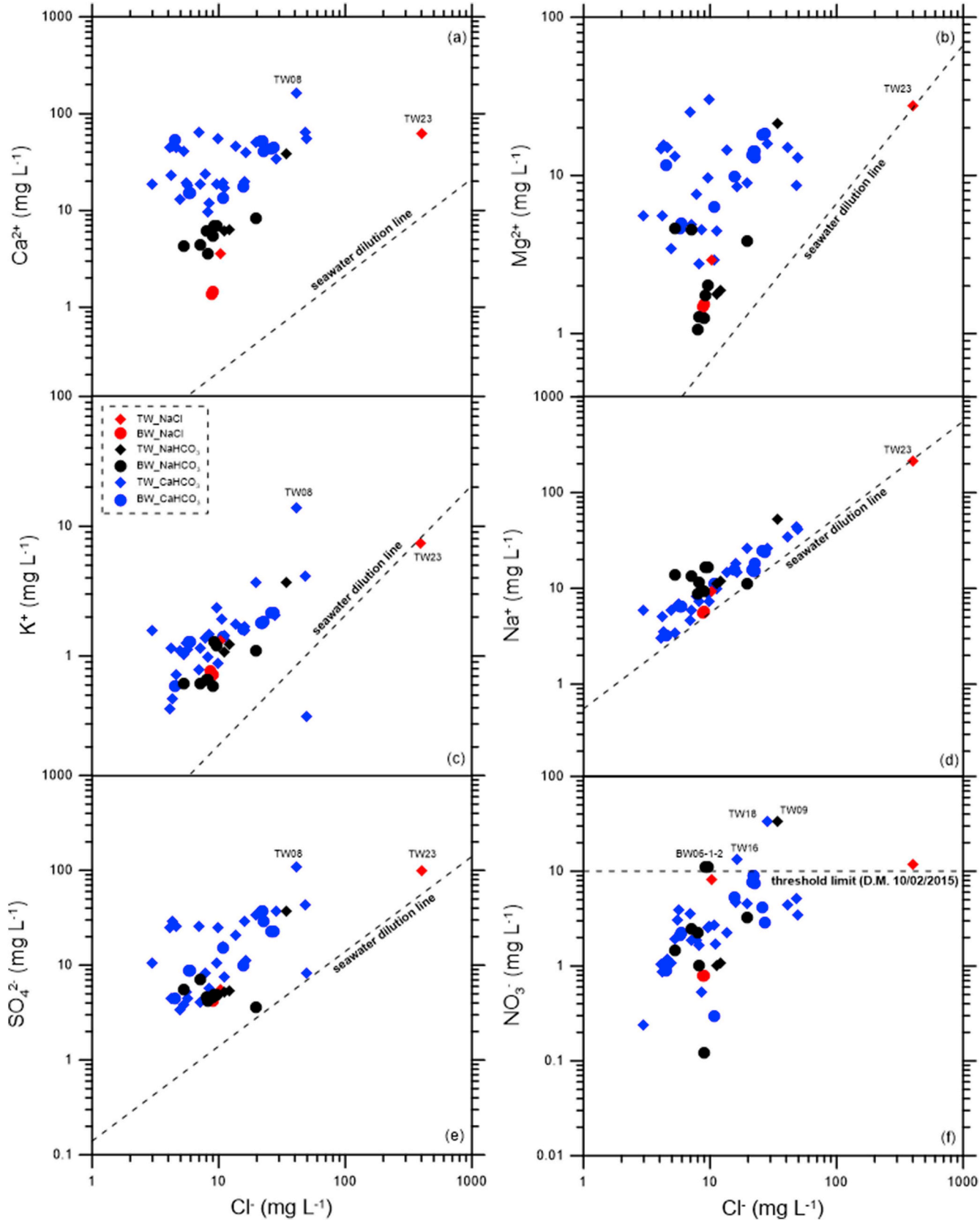

Fig. 4. Correlation diagram of Na^+, Mg^{2+}, K^+, Ca^{2+}, SO_4^{2-} and NO_3^- vs. Cl^- where are plotted bottled mineral and tap waters of the Calabria Region.

regime shifts.

The pattern in Fig. 7 shows that for BW, Cr and U are the species that present cases highly moving from the compositional barycenter followed by Sr, a behavior that could indicates the well traced contribution of different lithologies by these elements (Kabata-Pendias and Szteke, 2015). A similar behavior for U and Sr also characterizes the

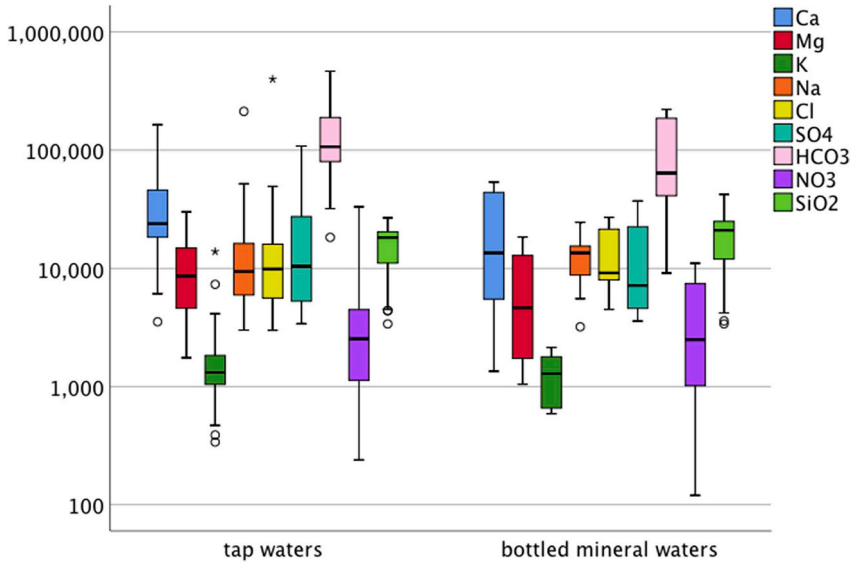

Fig. 5. Box-plots of tap waters and bottled mineral waters (μg L^{-1}) for the main chemical components (o = oultiers; * = estreme values).

TW, perhaps yet revealing the signal of their original natural sources. Cr is an element showing strong lithophic tendencies and can be found from ultramafic rocks to the sedimentary ones. Mobility of U depend from the host minerals and by dissolution processes that control precipitation of oxides, carbonates, phosphates and other compounds. Dispersion of these elements thus highly depends from the source and the Eh-pH conditions of the environment. Sr is a relatively common element in the lithosphere from mafic rocks to calcareous sediments and during weathering is easily mobile then absorbed by clay minerals and organic matter. It is possible that the clr-behavior of all these elements reflects their resilience in maintaining their original fingerprint when comparing BW and TW. It is not possible to draw the same conclusions for Mn, Fe, Zn and Pb, whose variability from the compositional barycenter appears to be attributable mainly to the corrosion pipes.

To be noticed here is that these results could not be so clearly highlighted if only classical box-plots were analyzed.

Results of the independent samples Kruskas-Wallis and median tests applied on raw data indicate that Al, Fe, Cu, Zn, Se, Mo, Cd, and Pb, present significant differences in median values ($p < 0.01$) while for Li, Al, Fe, Cu, Zn, Se, Mo, Cd, Ba, Pb, and U, and there are significant differences in the shape of the frequency distributions ($p < 0.01$). The same tests applied on log-centered variables indicate that the hypothesis of similarity in the shape of the frequency distribution and/or median values has to be rejected ($p < 0.01$) in several cases. In particular, variables as Na^+, Cl^-, NO_3^-, SiO_2, Li, B, V, Cr, Zn, As, Se, Rb, Pb, and U do not present a similar behavior in moving variability around the compositional barycenter in the two analyzed groups of data while for Na^+, Cl^-, NO_3^-, Li, B, Cr, Fe, Zn, As, Se, and Pb, also the hypothesis of similar median clr-values has to be rejected ($p < 0.01$).

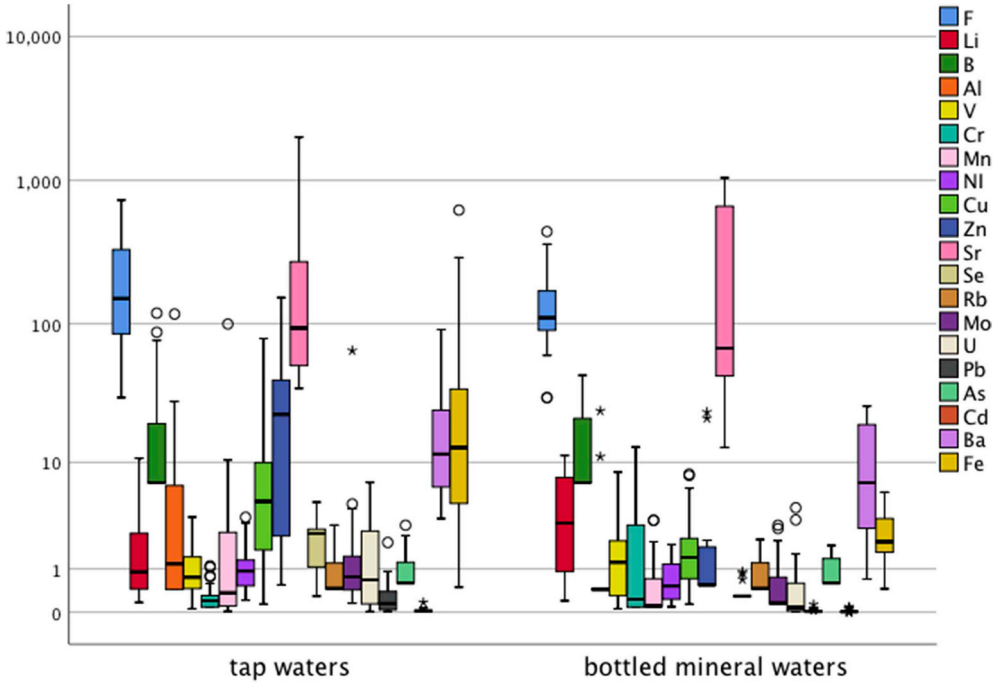

Fig. 6. Box-plots of tap waters and bottled mineral waters (μg L^{-1}) for trace elements (o = oultiers; * = estreme values).

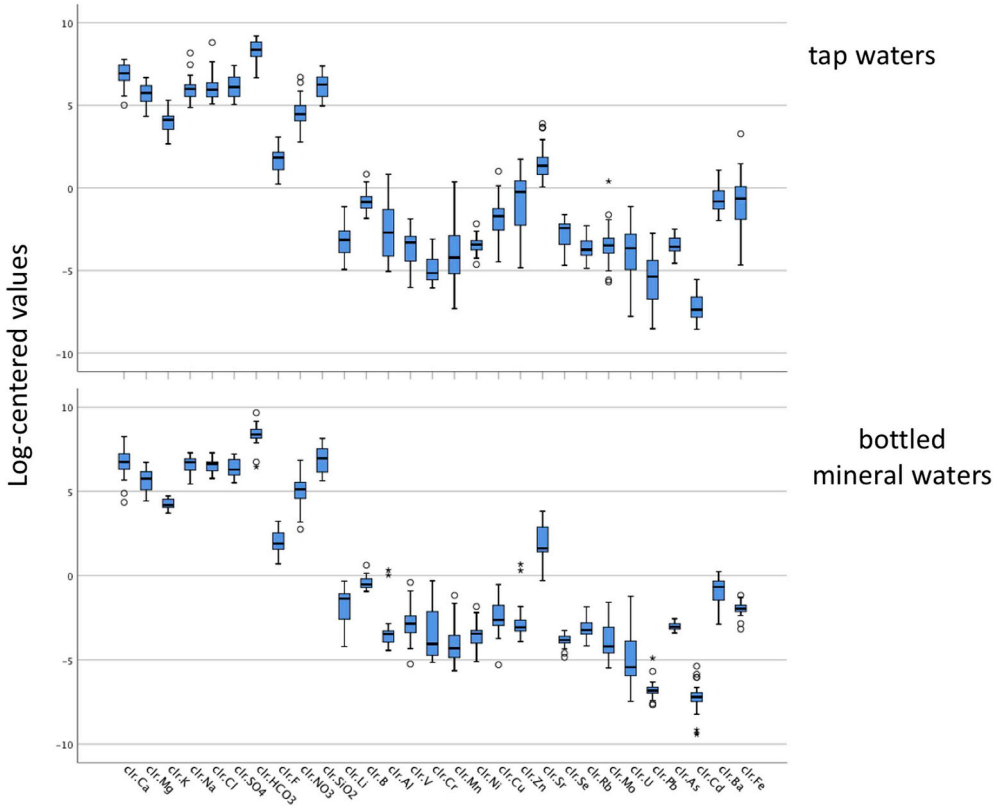

Fig. 7. Box-plots of tap waters and bottled mineral waters (μg L^{-1}) for main chemical components and trace elements, both clr-transformed. (o = oultiers; * = estreme values).

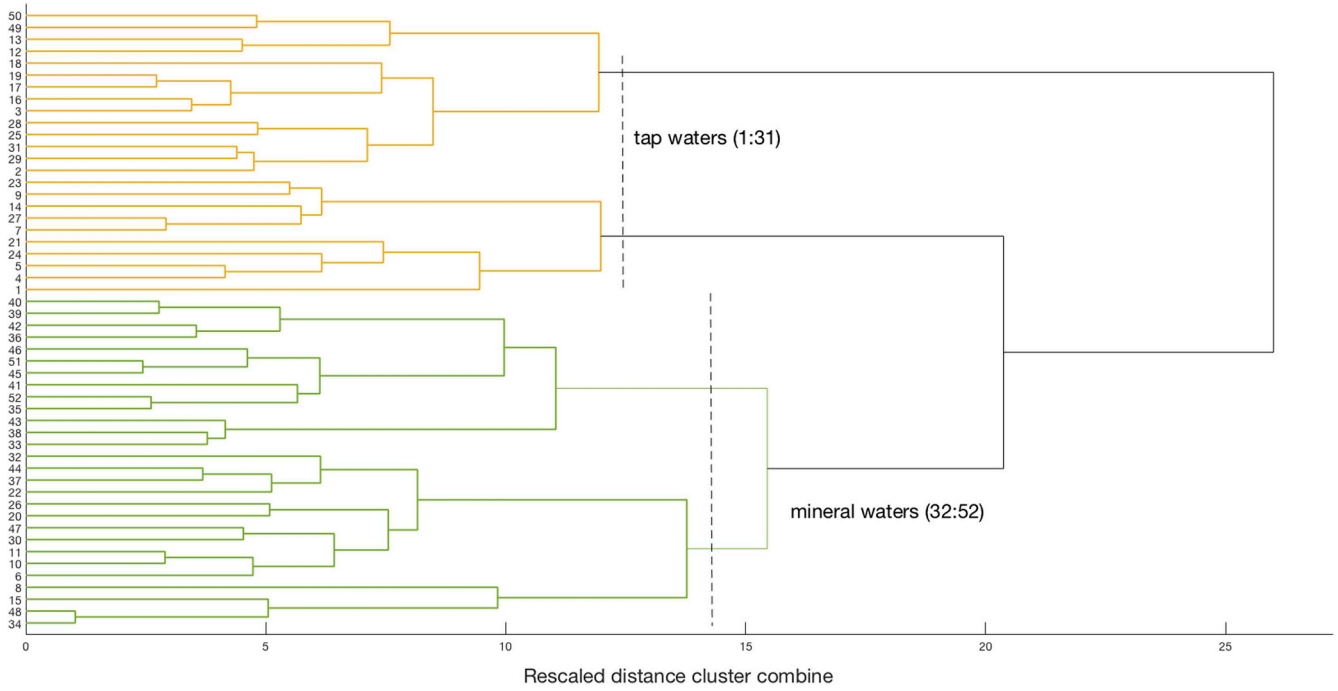

Fig. 8. Dendrogram for the cluster analysis of the clr-variables (similarity measure = Euclidean distance; linkage = Ward's method); cases 1/31 tap waters (yellow lines), cases 32/52 bottled mineral waters (green lines). Cases 50 and 49 contaminate the cluster of the tap waters; cases 15, 8, 22, 20, 26, 30, 10, 11, 6 contaminate the cluster of bottled mineral waters. (For interpretation of the references to color in this figure legend, the reader is referred to the Web version of this article.)

This result could indicate that the original signature of the source of the elements is maintained and yet mark the difference between BW and TW or the influence of non-natural processes mainly affecting TW.

In Fig. 8 is reported the dendrogram obtained by applying the cluster analysis algorithm on clr-variables by using the Ward method as linkage tool and the Euclidean distance as similarity measure (Kaufman and Rousseeuw, 1990; Everitt et al., 2001; Verboven and Hubert, 2005; García-Escudero et al., 2010; De Amorim, 2015). The cross tabulation

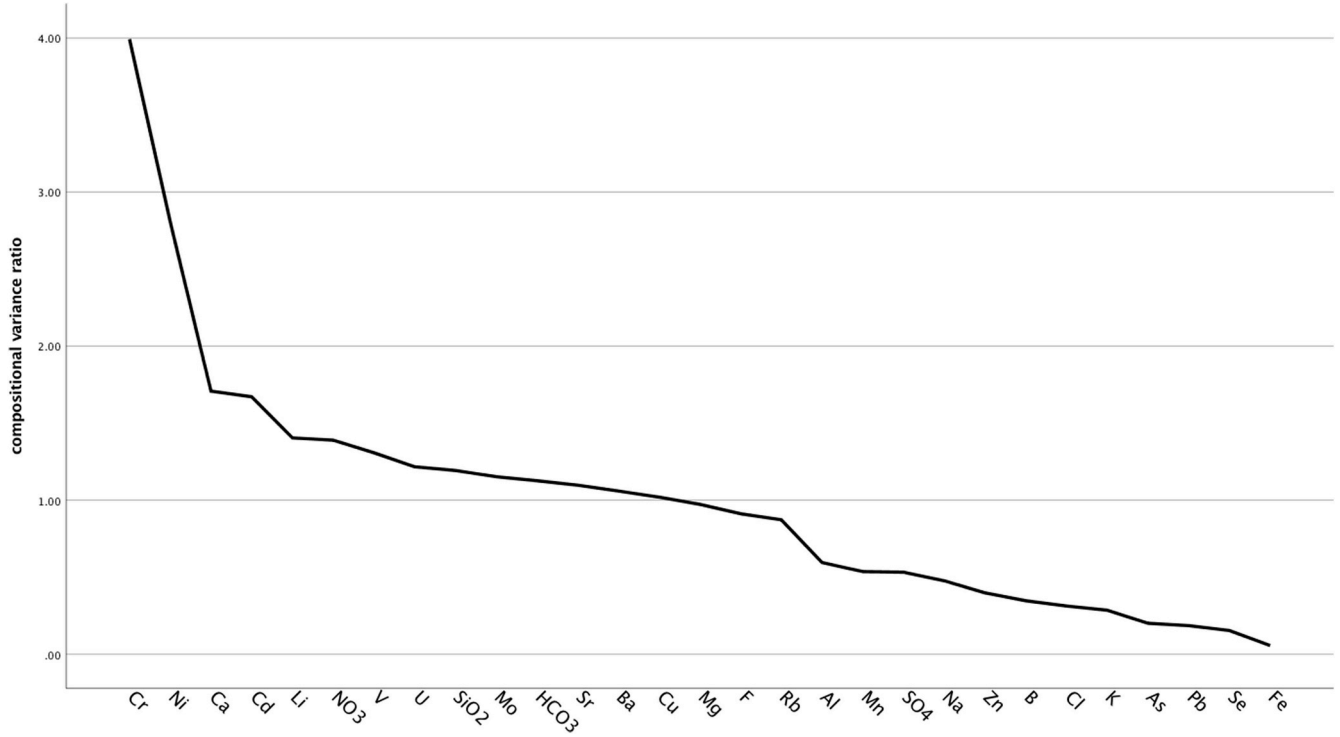

Fig. 9. Ratio of the contribution of each variable to the whole clr-variance in the two data sets, tap waters versus bottled mineral waters; variables in decreasing order of the ratio.

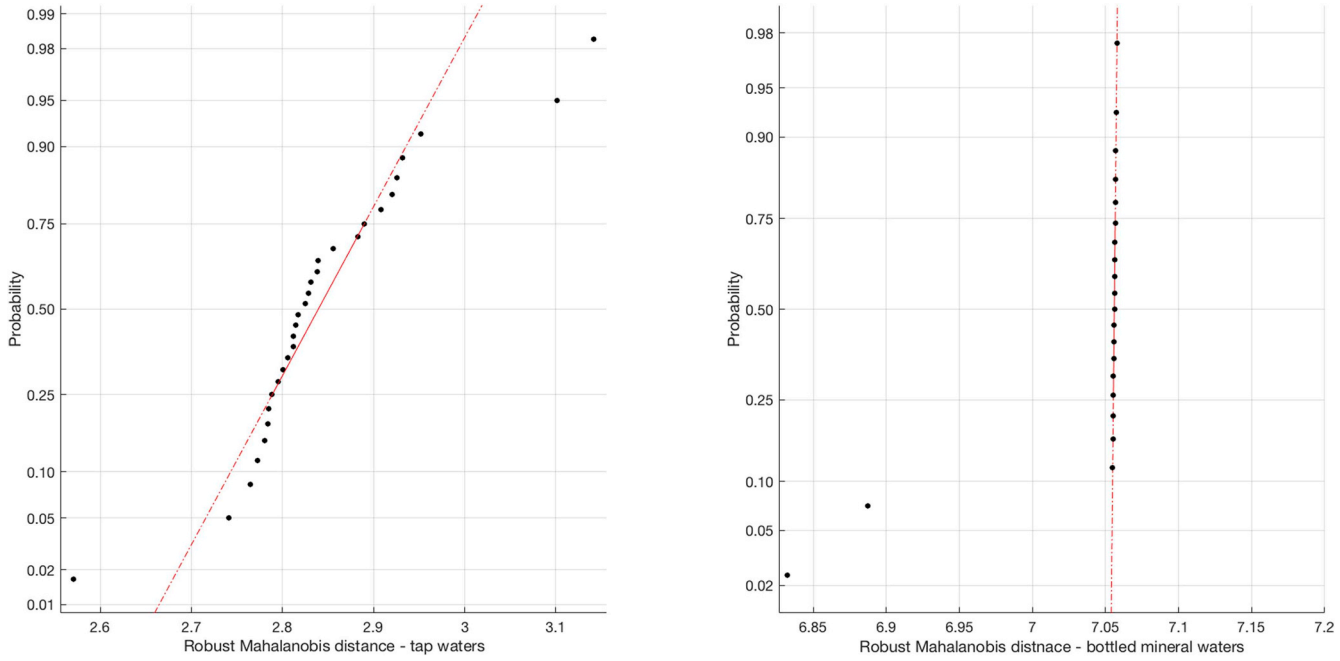

Fig. 10. Probability plots of the robust Mahalanobis distance (log values) of the composition of each sample with reference to the threshold compositions.

between the original case membership (TW and BW) and the two main natural groups obtained by the clustering procedure is significant (Chi-square test and Cramer's V, $p < 0.02$) indicating that the two groups of data, with few exceptions, are clearly different and sufficiently homogeneous inside them. The cluster represented by TW is particularly homogeneous with the exception of the cases 49 and 50 (BW13-1 and BW13-2) that originally pertained to BW set.

The cluster represented by BW is more contaminated by the presence of some samples of TW with which present high similarity as the cases 15, 8, 22, 20, 26, 30, 10, 11, 6 (TW15, TW08, TW22, TW20, TW26, TW30, TW10, TW11, TW06).

Combining the results of the clustering procedure with the previous statistical analysis it is possible to summarize that the difference between the two main clusters, that practically coincide with the original sets of data, appears to be attributable to the different behavior of As, B, Cl^-, Cr, Fe, Li^+, Na^+, NO_3^-, Pb, Se and Zn, both in median values, in the shape of the frequency distribution as well as in the distances of values from the compositional barycenter of the corresponding composition, as testified by the comparative box-plots (Figs. 5–7) and by the Kruskas-Wallis and median tests. The additional contribution of cluster

analysis, beside the previous investigations, lies in the multivariate structure of the procedure that also investigates the joint relationships among the elements facilitating the identification of common processes affecting their behavior.

The ratio of the contribution of each variable to the whole clr-variance of the composition for each data set is analyzed in a graphical way in Fig. 9 as a compositional alternative to the magnitude spread (Dinelli et al. 2012a,b). This tool represents an innovative way to characterize differences between datasets by considering the compositional nature of the data (Daunis-I-Estadella et al., 2006) and can be associated with the tests on median values. When the ratio is equal to 1 the contribution to variability is similar in the two datasets and the variable could not be affected by perturbations responsible for differences. On the other hand, when the ratio is > 1 the source of the variability of natural processes is dominant (numerator pertaining to BW), the contrary when the ratio is < 1. As we can see in Fig. 9 on the left, for metals as Cr and Ni, followed by Cd, V, U and Mo the ratio is higher than 1 so that the behavior of these elements governs the variability of BW with respect to TW. On the other hand, TW are mainly affected by variability in Al, Mn, Zn, As, Pb, Se and Fe, characterized by the ratio < 1 on the right of the plot. The results are in agreement with the data provided by Dinelli et al. 2012a,b, in particular, regarding some transition metals distribution. However, the comparison remains partial due to the not homogeneity of the two datasets concerning the scale of the investigation, national versus regional one.

With the aim to compare the concentrations of the chemical species with the Maximum Allowed Concentrations (MAC) (Tamasi and Cini, 2004; Varrica et al., 2013) the robust Mahalanobis distance between compositions was used for variables where the law limits were available. It was calculated for B, Al, V, Cr, Mn, Fe, Ni, Cu, Zn, As, Se, Mo, Cd, Ba, Pb, and U, thus representing a new index of compositional difference with respect to the MAC compositions (De Maesschalck and Massart, 2000; Varmuza and Filzmoser, 2009; Buccianti, 2018; Buccianti et al., 2018; Gozzi et al., 2018). When the differences are high and show homogeneous values with respect to the corresponding MAC composition, the nearness to warning thresholds is not suspected as well as the presence of processes able to shift the geochemical conditions.

For tap water the robust Mahalanobis distance varies from 14.68 to 26.43 while for bottled mineral water from 927 to 1162 thus pointing out that in both cases there is a considerable compositional distance from the respective thresholds. In Fig. 10 the probability plots of the difference values are reported with the aim to evaluate their distribution and homogeneity.

5.3. Hg distribution in bottled mineral waters and tap waters

In this work, Hg concentration has been processed in a dedicated section because (i) it was determined by a different technique (CV-AFS), (ii) it has shown concentrations of different orders of magnitude lower than the remaining constituents and (iii) it was characterized by a non-homogeneous dataset compared to the waters previously considered.

Of the total of 31 TW samples from public drinking fountains (TW 01/31) the mean concentration of Hg was 1.19 ng L^{-1} while the median 0.92 ng L^{-1} (std. dev. 1.12), with minimum and maximum values of 0.28 and 5.57 ng L^{-1} respectively. The mean Hg content in Calabrian bottled water (BW 01/014, 1–2) was found to be 0.19 ng L^{-1}, the median value 0.12 ng L^{-1} (std. dev. 0.19), with the Hg concentration ranged from < LOD (< 0.09 ng L^{-1}) to 0.91 ng L^{-1}.

All samples of TW and BW (still and sparkling) were analyzed in triplicate with the same analytical procedure. Concentration of the element were well below the European and national drinking water limit of 1 μg L^{-1} ranging from sub-nanogram to few nanogram per litre (Table 3) (Vardè et al., 2015a, 2015b, 2017, 2018, 2019). Indeed, 61% of TW samples ($n = 19$) had Hg concentration below 1.00 ng L^{-1}, 29% of drinking water samples ($n = 9$) had Hg content above 1.00 ng L^{-1} and below 2.00 ng L^{-1}, and finally only for 10% of water samples Hg was above 2.00 ng L^{-1} and below the highest observed Hg concentration of 5.57 ng L^{-1} found for TW31 water sample.

Hg content was found at or below the LOD for the 24% of the BW samples ($n = 5$), while for the 52% of the bottled samples ($n = 11$) Hg was below 0.30 ng L^{-1}, and finally for 14% of BW samples ($n = 3$) Hg was in the range between 0.30 and 0.40 ngL^{-1}. The highest observed concentration for Hg was at 0.91 ng L^{-1}, (BW06-2) sparkling typology, while the still sample (BW06-1) showed Hg concentration of 0.37 ng L^{-1}. This difference in Hg content between the two typologies (sparkling and still) for about 60% should be probably attributable to the quality of CO_2 artificially added and/or to the leaching of metals from the tank/bulk CO_2 storage-injection system.

As anticipated, for comparison, an additional sampling of TW was considered for mercury measurements (see Table 3). Hg determination on these additional TW samples (TW 32/60, were TW 32/41 public fountain, TW 42/60 household water) showed mean Hg concentration value of 0.34 and 0.69 ng L^{-1}, respectively, median value 0.28 and 0.48 ng L^{-1}, with minimum 0.14 and 0.19 ng L^{-1} and maximum of 0.66 and 1.95 ng L^{-1} (std. dev. 0.17 and 0.52). Values have confirmed that Hg was found at ultra-trace levels also for these additional samples taken from different sampling sites (Fig. 1S – Supplementary material).

Considering whole TW dataset (TW 01/60), the mean Hg value was found 0.74 ng L^{-1} and median equal to 0.48 ng L^{-1} with the minimum and maximum concentrations of 0.14 and 5.57 ng L^{-1}. Hg concentrations measured in this study showed that TW provided Hg mean, median, minimum and maximum concentrations higher than those detected from bottled water. The difference can be attributed due to the fact that TW coming from different water reservoirs (river waters, lake waters, groundwaters) mixed in variable proportions by the aqueduct manager and by physico-chemical processes treated to improve drinking water quality before the distribution through piped networks. Bottled water not undergoing any of these processes give a clear indication that the presence of Hg at ultra-traces is attributable to the lithology of the aquifer.

With the aim to assess the potential contribution of Hg_T in drinking water (TW) due to chlorination as a chemical process of water disinfection, in this study a generic sodium hypochlorite solution (SHS) used in an Italian aqueduct was investigated. Analysis of the SHS sample was conducted in triplicate and confirmed a total Hg concentration of 233.90 ng L^{-1}. The SHS analyzed (12% solution in volume, equal to ~10% by weight of active chlorine, specific weight of 1.2 kg L^{-1}) was diluted up to the recommended value of 0.2 mg L^{-1} for residual disinfectant following the Italian legislation for drinking water (D.Lgs. 31/2001, Annex 1, c). Using a dilution factor of about 1:6,000,000 the calculated contribution of sodium hypochlorite solution to Hg_T content in TW was found equal to 3.90E-05 ng L^{-1}, confirming that mercury levels in Calabrian TW are not directly affected to SHS disinfection product.

6. Conclusions

Storing data about the chemical composition of water increases our knowledge about the processes that modify its quality, particularly when public institutions, as regional environmental agencies, often check only some parameters for defined aims. In this paper a geochemical and statistical approach oriented on a compositional base was carried out to compare new data related to the tap waters (TW) and the bottled mineral waters (BW) (still and sparkling) sampled in the Calabrian Region (Southern Italy).

The multidisciplinary approach allowed to assert that the dataset (TW and BW) is composed of three main compositional groups of waters recognizable in (i) NaCl, (ii) Na–HCO_3 and (iii) Ca–HCO_3 types, characterized by low TIS values attested below 16 meq L^{-1}, with a greater enrichment in major elements like Cl^-, SO_4^{2-}, NO_3^-, Na^+, Mg^{2+}, K^+, and Ca^{2+} observed in TW with respect to BW. In this

context, the classical correlation diagrams between Cl^- vs. Ca^{2+}, Mg^{2+}, Na^+, K^+ and SO_4^{2} show a typical water-rocks interaction trends linked to dissolution of main minerals that compose the Calabrian aquifers. These minerals can be summarized in calcite, dolomite, K-feldspar, Na-bearing phases, Mg-enriched minerals as biotite and olivine, pyrite, gypsum that can found in different geological setting.

The different enrichment in some elements into the two groups of waters and the typical chemical features have been highlighted by the compositional statistical analysis. Cluster analysis and a new compositional index based on the contribution of each log-centered variable to the whole variance have evidenced variables mainly related to natural processes versus those associated to an anthropic origin, as well as variables prone to alternative states (multimodality). Al, Mn, Fe, Zn, and Pb are particularly enriched in the TW probably linked to leaching of pipelines that in many cases are very old, whereas Li, Ca, Cr, Ni, and Cd, are the variables that most contribute to the overall variability of BW. In particular, Cr, Cu and Pb are mainly enriched in sparkling BW probably attributable to the quality of CO_2 artificially added and/or to leaching of metals from the tank/bulk CO_2 storage-injection system. Hg concentrations in TW are also higher than those detected in bottled water, but the levels do not appear to be related to SHS disinfection product. Thus, the difference can be attributed to other physico-chemical treatment processes developed to improve drinking water quality before the distribution through piped networks and/or for corrosion of solids containing Hg and other hazardous metals inside the drinking water pipes (Renner, 2008; Schock et al., 2008; Peng et al., 2010; Peng and Korshin, 2011; Liu et al., 2017). However, the presence of Hg in surface waters could be attributable also to atmospheric wet and dry deposition pathways (Lynam et al., 2014).

Ultra-traces concentrations of Hg_T detected in BW are instead attributable to water-rock interaction although higher concentrations were detected in sparkling waters compared to natural ones, asking again for contributions due the artificial addition of CO_2 and to the processes related to the storage-injection system.

The comparison between the whole compositions of the two datasets with the corresponding Maximum Allowed Concentrations (MAC) performed by using the robust Mahalanobis distance pointed out that there is for TW and BW a considerable distance from the respective thresholds testifying the good quality of the resource. Moreover, as reported in this work and as evidenced by Vardè et al. (2018, 2019), the hazard quotient (HQ) is very low so that Hg concentrations in Calabrian BW should not cause any adverse health effects.

On the whole, the data set realized in this work as well as the considerations about the interpretation of the experimental results represent a fundamental base to develop monitoring plans in time and space with the aim to check for the maintenance of quality standards.

Acknowledgements

The authors are particularly grateful to Dr. Geologist Domenico Burello for his help in collecting and analysing tap waters and bottled waters. Finally, the authors are grateful to the Institute of Atmospheric Pollution Research-National Research Council (CNR-IIA) for giving us the opportunity to carried out Hg analyses at their laboratory in Arcavacata di Rende.

Appendix A. Supplementary data

Supplementary data to this article can be found online at https://doi.org/10.1016/j.apgeochem.2019.05.011.

References

Aitchison, J., 1982. The statistical analysis of compositional data (with discussion). J. Royal Stat. Soc., Series B (Stat. Methodol.) 44 (2), 139–160. https://doi.org/10.1111/j.2517-6161.1982.tb01195.x.

Allocca, V., Celico, F., Celico, P., De Vita, P., Fabbrocino, S., Mattia, S., Monacelli, G., Musilli, I., Piscopo, V., Scalise, A.R., Summa, G., Tranfaglia, G., 2007. Note illustrative della Carta idrogeologica dell'Italia meridionale. Istituto Poligrafico e Zecca dello Stato ISBN 88-448-0215-5, p. 211, con carte allegate, ISBN 88-448-0223-6.

Amodio Morelli, L., Bonardi, G., Colonna, V., Dietrich, D., Giunta, G., Ippolito, F., Liguori, V., Lorenzoni, S., Paglionico, A., Perrone, V., Piccareta, G., Russo, M., Scandone, P., Zanettin-Lorenzoni, E., Zuppetta, A., 1976. L'arco Calabro- Peloritano nell'orogene Appenninico Maghrebide. Mem. Soc. Geol. It. 17, 1–60.

Appelo, C.A.J., Postma, D., 1996. Geochemistry, groundwaters and pollution. A. A. Balkema, Rotterdam 536 pp.

Apollaro, C., Marini, L., De Rosa, R., 2007. Use of reaction path modelling to predict the chemistry of stream water and groundwater: a case study from the Fiume Grande valley (Calabria, Italy). Environ. Geol. 51 (7), 1133–1145. https://doi.org/10.1007/s00254-006-0404-0.

Apollaro, C., Accornero, M., Marini, L., Barca, D., De Rosa, R., 2009. The impact of dolomite and plagioclase weathering on the chemistry of shallow groundwaters circulating in a granodiorite-dominated catchment of the Sila Massif (Calabria, Southern Italy). Appl. Geochem. 24, 957–979. https://doi.org/10.1016/j.apgeochem.2009.02.026.

Apollaro, C., Marini, L., Critelli, T., Barca, D., Bloise, A., De Rosa, R., Liberi, F., Miriello, D., 2011. Investigation of rock-to-water release and fate of major, minor, and trace elements in the metabasalt-serpentinite shallow aquifer of Mt. Reventino (CZ, Italy) by reaction path modeling. Appl. Geochem. 26, 1722–1740. https://doi.org/10.1016/j.apgeochem.2011.04.028.

Apollaro, C., Dotsika, E., Marini, L., Barca, D., Bloise, A., De Rosa, R., Doveri, M., Lelli, M., Muto, F., 2012. Chemical and isotopic characterization of the thermo mineral water of Terme Sibarite springs (Northern Calabria, Italy). Geochem. J. 46 (2), 117–129. https://doi.org/10.2343/geochemj.1.0166.

Apollaro, C., Marini, L., Critelli, T., De Rosa, R., Bloise, A., Miriello, D., Catalano, M., Armano, V., 2013a. Modeling of the impact of dolomite and biotite dissolution on vermiculite composition in a gneissic shallow aquifer of the Sila Massif (Calabria, Italy). Appl. Geochem. 35, 297–311. https://doi.org/10.1016/j.apgeochem.2013.05.004.

Apollaro, C., Marini, L., Critelli, T., De Rosa, R., 2013b. The standard thermodynamic properties of vermiculites and prediction of their occurrence during water-rock interaction. Appl. Geochem. 35, 264–278. https://doi.org/10.1016/j.apgeochem.2013.04.018.

Apollaro, C., Vespasiano, G., Muto, F., De Rosa, R., Barca, D., Marini, L., 2016. Use of mean residence time of water, flowrate, and equilibrium temperature indicated by water geothermometers to rank geothermal resources. Application to the thermal water circuits of Northern Calabria. J. Volcanol. Geotherm. Res. 328, 147–158. https://doi.org/10.1016/j.jvolgeores.2016.10.014.

Apollaro, C., Fuoco, I., Brozzo, G., De Rosa, R., 2019a. Release and fate of Cr (VI) in the ophiolitic aquifers of Italy: the role of Fe (III) as a potential oxidant of Cr (III) supported by reaction path modelling. Sci. Total Environ. 660, 1459–1471. https://doi.org/10.1016/j.scitotenv.2019.01.103.

Apollaro, C., Perri, F., Le Pera, E., Fuoco, I., Critelli, T., 2019b. Chemical and mineropetrographical changes on granulite rocks affected by weathering processes. Front. Earth Sci. https://doi.org/10.1007/s11707-018-0745-5.

Apollaro, C., 2019c. Geochemical Modeling of Water-Rock Interaction in the Granulite Rocks of Lower Crust in the Serre Massif (Southern Calabria, Italy). Geofluids. https://doi.org/10.1155/2019/5602648.

Avino, P., Capannesi, G., Diaco, L., Rosada, A., 2010. Multivariate analysis applied to trace and ultra-trace elements in Italian potable waters determined by INAA. Curr. Anal. Chem. 6 (1), 26–36. https://doi.org/10.2174/157341110790069646.

Bertoldi, D., Bontempo, L., Larcher, R., Nicolini, G., Voerkelius, S., Lorenz, G.D., Ueckermann, H., Froeschl, H., Baxter, M.J., Hoogewerff, J., Brereton, P., 2011. Survey of the chemical composition of 571 European bottled mineral waters. J. Food Compos. Anal. 24 (3), 376–385. https://doi.org/10.1016/j.jfca.2010.07.005.

Beverfood, 2016. Bevitalia Acque Minerali, Bibite e Succhi 2016-2017. Beverfood srl 1-389.

Biddau, R., Cidu, R., Da Pelo, S., Carletti, A., Ghiglieri, G., Pittalis, D., 2019. Source and fate of nitrate in contaminated groundwater systems: assessing spatial and temporal variations by hydrogeochemistry and multiple stable isotope tools. Sci. Total Environ. 647, 1121–1136. https://doi.org/10.1016/j.scitotenv.2018.08.007.

Birke, M., Rauch, U., Harazim, B., Lorenz, H., Glatte, W., 2010a. Major and trace elements in German bottled water, their regional distribution, and accordance with national and international standards. J. Geochem. Explor. 107 (3), 245–271. https://doi.org/10.1016/j.gexplo.2010.06.002.

Birke, M., Reimann, C., Demetriades, A., Rauch, U., Lorenz, H., Harazim, B., Glatte, W., 2010b. Determination of major and trace elements in European bottled mineral water—analytical methods. J. Geochem. Explor. 107 (3), 217–226. https://doi.org/10.1016/j.gexplo.2010.05.005.

Bityukova, L., Petersell, V., 2010. Chemical composition of bottled mineral waters in Estonia. J. Geochem. Explor. 107 (3), 238–244. https://doi.org/10.1016/j.gexplo.2010.07.006.

Bloise, A., Belluso, E., Critelli, T., Catalano, M., Apollaro, C., Miriello, D., Barrese, E., 2012. Amphibole asbestos and other fibrous minerals in the meta-basalt of the Gimigliano-Mount Reventino Unit (Calabria, south-Italy). Rend. Online Soc. Geol. It 21 (2), 847–848.

Bloise, A., Catalano, M., Critelli, T., Apollaro, C., Miriello, D., 2017. Naturally occurring asbestos: potential for human exposure, san Severino Lucano (Basilicata, southern Italy). Environ. Earth Sci. 76 (19), 648.

Boccaletti, M., Nicolich, R., Tortorici, L., 1984. The Calabrian Arc and the Ionian Sea in the dynamic evolution of the central Mediterranean. Mar. Geol. 55, 219–245.

Buccianti, A., Pawlowsky-Glahn, V., 2005. New perspectives on water chemistry and

compositional data analysis. Math. Geol. 37 (7), 703–727. https://doi.org/10.1007/s11004-005-7376-6.
Buccianti, A., 2018. Water chemistry: are new challenges possible from CoDA (compositional data analysis) point of view? In: Daya Sagar, B., Cheng, Q., Agterberg, F. (Eds.), Handbook of Mathematical Geosciences. Springer International Publishing, Cham, pp. 299–311. Springer. https://doi.org/10.1007/978-3-319-78999-6_16.
Buccianti, A., Lima, A., Albanese, S., De Vivo, B., 2018. Measuring the change under compositional data analysis (CoDA): insight on the dynamics of geochemical systems. J. Geochem. Explor. 189, 100–108. https://doi.org/10.1016/j.gexplo.2017.05.006.
Caridi, F., Messina, M., D'Agostino, M., 2017. An investigation about natural radioactivity, hydrochemistry, and metal pollution in groundwater from Calabrian selected areas, southern Italy. Environ. Earth Sci. https://doi.org/10.1007/s12665-017-7031-9.
Carpenter, S.R., Brock, W.A., 2006. Rising variance: a leading indicator of ecological transition. Ecol. Lett. 9 (3), 311–318.
Cicchella, D., Albanese, S., De Vivo, B., Dinelli, E., Giaccio, L., Lima, A., Valera, P., 2010. Trace elements and ions in Italian bottled mineral waters: identification of anomalous values and human health related effects. J. Geochem. Explor. 107 (3), 336–349. https://doi.org/10.1016/j.gexplo.2010.04.004.
Cidu, R., Frau, F., Tore, P., 2011. Drinking water quality: comparing inorganic components in bottled water and Italian tap water. J. Food Compos. Anal. 24 (2), 184–193. https://doi.org/10.1016/j.jfca.2010.08.005.
Cirrincione, R., Fazio, E., Fiannacca, P., Ortolano, G., Pezzino, A., Punturo, R., 2015. The Calabria-Peloritani Orogen, a composite terrane in Central Mediterranean; its overall architecture and geodynamic significance for a pre-Alpine scenario around the Tethyan basin. In: "Progresses In Deciphering Structures and Compositions of Basement Rocks". Periodico di Mineralogia 84. pp. 701–749. https://doi.org/10.2451/2015PM0446. 3B (Special Issue).
Corder, G.W., Foreman, D.I., 2014. Nonparametric Statistics: A Step-by-step Approach. Wiley ISBN: 978-1-118-84031-3.
Critelli, T., Vespasiano, G., Apollaro, C., Muto, F., Marini, L., De Rosa, R., 2015a. Hydrogeo- chemical study of an ophioltic aquifer: a case study of Lago (Southern Italy, Calabria). Environ. Earth Sci. 74, 533–543. https://doi.org/10.1007/s12665-015-4061-z.
Critelli, T., Apollaro, C., Vespasiano, G., De Rosa, R., 2015b. Geochemical modeling as a tool to investigate the release and fate of Cr in the ophilitic aquifers of Northern Calabria (S-Italy). Rend. Online Soc. Geol. Ital. 33, 28–30. https://doi.org/10.3301/ROL.2015.07.
D.Lgs. 31, 2001. Decreto legislativo 2 febbraio 2001, n. 31, Attuazione della Direttiva 98/83/CE relativa alla qualità delle acque destinate al consumo umano. Gazzetta Ufficiale n. 52 del 03-03-2001. Supplemento Ordinario n. 41.
D.Lgs.152, 2006. Decreto Legislativo 3 aprile 2006, n. 152, Norme in materia ambientale. Gazzetta Ufficiale n. 88 del 14 aprile 2006. Supplemento Ordinario n. 96.
D.M. 29/12, 2003. Decreto Ministero della Salute 29 dicembre 2003, Attuazione della Direttiva n. 2003/40/CE nella parte relativa ai criteri di valutazione delle caratteristiche delle acque minerali naturali di cui al Decreto Ministeriale 12 .11.1992, n. 542, e successive modificazioni, nonché alle condizioni di utilizzazione dei trattamenti delle acque minerali naturali e delle acque di sorgente. Gazzetta Ufficiale n. 302 del 31-12-2003.
D.M. 10/02, 2015. Decreto Ministero della Salute 10 febbraio 2015. Criteri di valutazione delle caratteristiche delle acque minerali naturali. Gazzetta Ufficiale n.50 del 02-03-2015.
Dai, L., Korolev, K.S., Gore, J., 2015. Relation between stability and resilience determines the performance of early warning signals under different environmental drivers. Proc. Natl. Acad. Sci. Unit. States Am. 112 (32), 10056–10061. https://doi.org/10.1073/pnas.1418415112.
Dakos, V., Van Nes, E.H., D'Odorico, P., Scheffer, M., 2012. Robustness of variance and autocorrelation as indicators of critical slowing down. Ecology 93 (2), 264–271. https://doi.org/10.1890/11-0889.1.
Daunis-I-Estadella, J., Barceló-Vidal, C., Buccianti, A., 2006. Exploratory compositional data analysis. In: In: Buccianti, A., Mateu-Figueras, G., Pawlowsky-Glahn (Eds.), Compositional Data Analysis in the Geosciences: from Theory to Practice, vol 264. Geological Society, London, Special Publications, pp. 161–174.
De Amorim, R.C., 2015. Feature relevance in ward's hierarchical clustering using the L_p norm. J. Classif. 32 (1), 46–62. https://doi.org/10.1007/s00357-015-9167-1.
De Maesschalck, R., Jouan-Rimbaud, D., Massart, D.L., 2000. The Mahalanobis distance. Chemometr. Intell. Lab. Syst. 50 (1), 1–18. https://doi.org/10.1016/S0169-7439(99)00047-7.
Desideri, D., Meli, A.M., Feduzi, L., Roselli, C., Rongoni, A., Saetta, D., 2007. ^{238}U, ^{234}U, ^{226}Ra, ^{210}Po concentrations of bottled mineral waters in Italy and their dose contribution. J. Environ. Radioact. 94 (2), 86–97. https://doi.org/10.1016/j.jenvrad.2007.01.005.
Dinelli, E., Lima, A., De Vivo, B., Albanese, S., Cicchella, D., Valera, P., 2010. Hydrogeochemical analysis on Italian bottled mineral waters: effects of geology. J. Geochem. Explor. 107, 317–335.
Dinelli, E., Lima, A., Albanese, S., Birke, M., Cicchella, D., Giaccio, L., Valera, P., De Vivo, B., 2012a. Major and trace elements in tap water from Italy. J. Geochem. Explor. 112, 54–75. https://doi.org/10.1016/j.gexplo.2011.07.009.
Dinelli, E., Lima, A., Albanese, S., Birke, M., Cicchella, D., Giaccio, L., Valera, P., De Vivo, B., 2012b. Comparative study between bottled mineral and tap water in Italy. J. Geochem. Explor. 112, 368–389. https://doi.org/10.1016/j.gexplo.2011.11.002.
EU Directive 2003/40/EC, 2003. Council Directive of 16 May 2003 establishing the list, concentration limits and labeling requirements for the constituents of natural mineral waters and the conditions for using ozone-enriched air for the treatment of natural mineral waters and spring waters. Off. J. Euro. Union L126/34 22/05/2003.
EU Directive 98/83/EC, 1998. Council directive of 3 November 1998 on the quality of water intended for human consumption. Off. J. Euro. Union L 330 32 5.12.1998.
Everitt, B.S., Landau, S., Leese, M., 2001. Cluster Analysis, fourth ed. Oxford University Press, Inc., London, 0340761199 New York; Arnold.
Felici, M.L., 2005. Fattori ambientali e salute: il ruolo degli elementi in traccia nella salute umana. Geologia Ambientale Anno XIII n. 3/2005.
Fugedi, U., Kuti, L., Jordan, G., Kerek, B., 2010. Investigation of the hydrogeochemistry of some bottled mineral waters in Hungary. J. Geochem. Explor. 107 (3), 305–316. https://doi.org/10.1016/j.gexplo.2010.10.011.
Gaglioti, S., Infusino, E., Caloiero, T., Callegari, G., Guagliardi, I., 2019. Geochemical characterization of spring waters in the crati river basin, Calabria (southern Italy). Geofluids 2019 Article ID 3850148, 16 pages, 2019. https://doi.org/10.1155/2019/3850148.
Garcia-Escudero, L.A., Gordaliza, A., Matrán, C., Mayo-Iscar, A., 2010. A review of robust clustering method. Adv. Data Anal. Classif. 4 (2–3), 89–109. https://doi.org/10.1007/s11634-010-0064-5.
Ghezzi, L., D'Orazio, M., Doveri, M., Lelli, M., Petrini, R., Giannecchini, R., 2019. Groundwater and potentially toxic elements in a dismissed mining area: thallium contamination of drinking spring water in the Apuan Alps (Tuscany, Italy). J. Geochem. Explor. 197, 84–92. https://doi.org/10.1016/j.gexplo.2018.11.009.
Gonzalez, S., Lopez-Roldan, R., Cortina, J.-L., 2013. Presence of metals in drinking water distribution networks due to pipe material leaching: a review. Toxicol. Environ. Chem. 95 (6), 870–889. https://doi.org/10.1080/02772248.2013.840372.
Gozzi, C., Sauro Graziano, R., Frondini, F., Buccianti, A., 2018. Innovative monitoring tools for the complex spatial dynamics of river chemistry: case study for the Alpine region. Environ. Earth Sci. 77 (16), 579. https://doi.org/10.1007/s12665-018-7756-0.
Gray, N., 2008. Drinking Water Quality: Problems and Solutions, second ed. Cambridge University Press, Cambridge, UK ISBN: 9780521702539.
Iannace, A., Vitale, S., D'Errico, M., Mazzoli, S., Di Staso, A., Macaione, E., Messina, A., Reddy, S.M., Somma, R., Zamparelli, V., Zattin, M., Bonardi, G., 2007. The carbonate tectonic units of northern Calabria (Italy): a record of Apulian palaeomargin evolution and Miocene convergence, continental crustal subduction, and exhumation of HP-LT rocks. J. Geol. Soc., London 164, 1165–1186. https://doi.org/10.1144/0016-76492007-017.
Kabata-Pendias, A., Szteke, B., 2015. Trace Elements in Abiotic and Biotic Environments, first ed. CRC Press, Boca Raton, pp. 1–468. https://doi.org/10.1201/b18198.
Kaufman, L., Rousseeuw, P.J., 1990. Finding Groups in Data: an Introduction to Cluster Analysis. Wiley-Interscience, New York (Series in Applied Probability and Statistics). ISBN 0-471-87876-6.
Keresztes, S., Tatar, E., Mihucz, V.G., Virag, I., Majdik, C., Zaray, G., 2009. Leaching of antimony from polyethylene terephthalate (PET) bottles into mineral water. Sci. Total Environ. 407 (16), 4731–4735. https://doi.org/10.1016/j.scitotenv.2009.04.025.
Liberi, F., Piluso, E., 2009. Tectonometamorphic evolutionof the ophiolitic sequences from Northern Calabrian Arc. Ital. J. Geosci. (Boll. Soc. Geol. It.) 128, 483–493.
Liu, G., Zhang, Y., Knibbe, W.-J., Feng, C., Liu, W., Medema, G., Van der Meer, W., 2017. Potential impacts of changing supply-water quality on drinking water distribution: a review. Water Res. 116 (1), 135–148. https://doi.org/10.1016/j.watres.2017.03.031.
Lynam, M.M., Dvonch, J.T., Hall, N.L., Morishita, M., Barres, J.A., 2014. Spatial patterns in wet and dry deposition of atmospheric mercury and trace elements in central Illinois, USA. Environ. Sci. Pollut. Res. 21 (6), 4032–4043. https://doi.org/10.1007/s11356-013-2011-4.
Martín-Fernández, J.A., Hron, K., Templ, M., Filzmoser, P., Palarea-Albaladejo, J., 2015. Bayesian-multiplicative treatment of count zeros in compositional data sets. Stat. Model. 15 (2), 134–158.
Mukate, S., Panaskar, D., Wagh, V., Muley, A., Jangam, C., Pawar, R., 2018. Impact of anthropogenic inputs on water quality in Chincholi industrial area of Solapur, Maharashtra, India. Groundwater Sustain. Dev. 7, 359–371. https://doi.org/10.1016/j.gsd.2017.11.001.
Naddeo, V., Zarra, T., Belgiorno, V., 2008. A comparative approach to the variation of natural elements in Italian bottled waters according to the national and international standard limits. J. Food Compos. Anal. 21 (6), 505–514. https://doi.org/10.1016/j.jfca.2008.02.010.
Nisi, B., Buccianti, A., Raco, B., Battaglini, R., 2016. Analysis of complex regional databases and their support in the identification of background/baseline compositional facies in groundwater investigation: developments and application examples. J. Geochem. Explor. 164, 3–17. https://doi.org/10.1016/j.gexplo.2015.06.019.
Nordstrom, D.K., Plummer, L.N., Wigley, T.M.L., Wolery, T.J., Ball, J.W., Jenne, E.A., Bassett, R.L., Crerar, D.A., Florence, T.M., Fritz, B., Hoffmann, M., Holdren, G.R., Lafon, G.M., Mattigod, S.V., McDuff, R.E., Morel, F., Reddy, M.M., Sposito, G., Thrailkill, J., 1979. A comparison of computerized chemical models for equilibrium calculations in aqueous systems. In: Chemical Modeling of Aqueous Systems: Speciation, Sorption, Solubility, and Kinetics. ACS Symposium Series. No.93. American Chemical Society, Washington, DC, pp. 857–892 ISBN 9780841204799.
Pawlowsky-Glahn, V., Egozcue, J.J., Tolosana-Delgado, R., 2015. Modeling and Analysis of Compositional Data. John Wiley & Sons 247 pp. isbn: 978-1-118-44306-4.
Peh, Z., Šorša, A., Halamić, J., 2010. Composition and variation of major and trace elements in Croatian bottled waters. J. Geochem. Explor. 107 (3), 227–237. https://doi.org/10.1016/j.gexplo.2010.02.002.
Peng, C.Y., Korshin, G.V., Valentine, R.L., Hill, A.S., Friedman, M.J., Reiber, S.H., 2010. Characterization of elemental and structural composition of corrosion scales and deposits formed in drinking water distribution systems. Water Res. 44 (15), 4570–4580. https://doi.org/10.1016/j.watres.2010.05.043.
Peng, C.Y., Korshin, G.V., 2011. Speciation of trace inorganic contaminants in corrosion scales and deposits formed in drinking water distribution systems. Water Res. 45

(17), 5553–5563. https://doi.org/10.1016/j.watres.2011.08.017.
Perri, F., Ietto, F., Le Pera, E., Apollaro, C., 2016. Weathering processes affecting granitoid profiles of Capo Vaticano (Calabria, southern Italy) based on petrographic, mineralogic and reaction path modeling approaches. Geol. J. 51 (3), 368–386.
Protano, C., Zinnà, L., Giampaoli, S., Romano Spica, V., Chiavarini, S., Vitali, M., 2014. Heavy metal pollution and potential ecological risks in rivers: a case study from Southern Italy. Bull. Environ. Contam. Toxicol. 92 (1), 75–80. https://doi.org/10.1007/s00128-013-1150-0.
Reimann, C., Bjorvatn, K., Frengstad, B., Melaku, Z., Tekle-Haimanot, R., Siewers, U., 2003. Drinking water quality in the Ethiopian section of the East African Rift Valley I–data and health aspects. Sci. Total Environ. 311 (1–3), 65–80. https://doi.org/10.1016/S0048-9697(03)00137-2.
Reimann, C., Birke, M., Filzmoser, P., 2010. Bottled drinking water: water contamination from bottle materials (glass, hard PET, soft PET), the influence of colour and acidification. Appl. Geochem. 25 (7), 1030–1046. https://doi.org/10.1016/j.apgeochem.2010.04.009.
Renner, R., 2008. Pipe scales release hazardous metals into drinking water. Environ. Sci. Technol. 42 (12). https://doi.org/10.1021/es087143m. 4241–4241.
Shotyk, W., Krachler, M., Chen, B., 2006. Contamination of Canadian and European bottled waters with antimony from PET containers. J. Environ. Monit. 8 (2), 288–292. https://doi.org/10.1039/b517844b.
Shotyk, W., Krachler, M., 2007a. Contamination of bottled waters with antimony leaching from polyethylene terephthalate (PET) increases upon storage. Environ. Sci. Technol. 41 (5), 1560–1563. https://doi.org/10.1021/es061511+.
Schock, M.R., Hyland, R.N., Welch, M.M., 2008. Occurrence of contaminant accumulation in lead pipe scales from domestic drinking-water distribution systems. Environ. Sci. Technol. 42 (12), 4285–4291. https://doi.org/10.1021/es702488v.
Tamasi, G., Cini, R., 2004. Heavy metals in drinking waters from Mount Amiata (Tuscany, Italy). Possible risk from arsenic for public health in the Province of Siena. Sci. Total Environ. 327 (1–3), 41–51. https://doi.org/10.1016/j.scitotenv.2003.10.011.
Tansi, C., Muto, F., Critelli, S., Iovine, G., 2007. Neogene-Quaternary strike-slip tectonics in the central Calabrian Arc (southern Italy). J. Geodyn 43, 393–414.
Tortorici, L., 1982. Lineamenti geologico-strutturali dell'arco calabro-peloritano. Rendiconti SIMP 38, 927–940.
Tripodi, V., Muto, F., Brutto, F., Perri, F., Critelli, S., 2018. Neogene-Quaternary evolution of the forearc and backarc regions between the Serre and Aspromonte Massifs, Calabria (southern Italy). Mar. Pet. Geol. 95, 328–343. https://doi.org/10.1016/j.marpetgeo.2018.03.028.
US-EPA Method 1631, 2002. Revision E: Mercury in Water by Oxidation, Purge and Trap, and Cold Vapor Atomic Fluorescence Spectrometry. United States Environmental Protection Agency.
Van Dijk, J.P., Bello, M., Brancaleoni, G.P., Cantarella, G., Costa, V., Frixia, A., Golfetto, F., Merlini, S., Riva, M., Torricelli, S., Toscano, C., Zerilli, A., 2000. A regional structural model for the northern sector of the Calabrian Arc (southern Italy). Tectonophysics 324, 267–320.
Vardè, M., Cofone, F., Servidio, A., Rosselli, A., Mannarino, V., Di Traglia, M., 2015a. Determination of Ultra-Trace Total Mercury in Bottled Waters Produced in Calabria (Southern Italy). XV Congresso Nazionale di Chimica dell'Ambiente e dei Beni Culturali. Società Chimica Italiana (SCI), 14-18 June 2015, Bergamo, Italy, pp. 177.
Vardè, M., Rosselli, A., Servidio, A., Cofone, F., Mannarino, V., Di Traglia, M., 2015b. Mercury at picomole L^{-1} (pM) level in drinking water by cold vapor atomic fluorescence spectrometry (CV-AFS) along four provinces in Southern Italy (Calabria). XV Congresso Nazionale di Chimica dell'Ambiente e dei Beni Culturali. Società Chimica Italiana (SCI), 14-18 June, Bergamo, Italy, pp. 178.
Vardè, M., Cofone, F., Rosselli, A., Servidio, A., Di Traglia, M., Vespasiano, G., Apollaro, C., 10-14 September 2017. Quanto Mercurio nelle Acque Minerali Naturali della Campania? XXVI Congresso Nazionale Società Chimica Italiana (SCI). Paestum (Salerno), Italy, pp. 36.
Vardè, M., Servidio, A., Vespasiano, G., Cofone, F., Rosselli, A., Di Traglia, M., Apollaro, C., Pasti, L., Cavazzini, A., 17 December 2018. Mercury in Bottled Water from Emilia-Romagna and Veneto: Ultra-trace amount determination and evaluation of intake using a health risk assessment approach. XVIII Giornata Della Chimica dell'Emilia Romagna. Società Chimica Italiana (SCI) Sezione Emilia-Romagna. pp. 90 Parma, Italy.
Vardè, M., Servidio, A., Vespasiano, G., Pasti, L., Cavazzini, A., Di Traglia, M., Rosselli, A., Cofone, F., Apollaro, C., Cairns, W.R.L., Scalabrin, E., De Rosa, R., Procopio, A., 2019. Ultra-trace determination of total mercury in Italian bottled waters. Chemosphere 219, 896–913. https://doi.org/10.1016/j.chemosphere.2018.12.020.
Varmuza, K., Filzmoser, P., 2009. Introduction to Multivariate Statistical Analysis in Chemometrics, first ed. CRC Press, Boca Raton, pp. 1–336. https://doi.org/10.1201/9781420059496.
Varrica, D., Tamburo, E., Dongarrà, G., 2013. Sicilian bottled natural waters: major and trace inorganic components. Appl. Geochem. 34, 102–113. https://doi.org/10.1016/j.apgeochem.2013.02.017.
Verboven, S., Hubert, M., 2005. LIBRA: a MATLAB library for robust analysis. Chemometr. Intell. Lab. Syst. 75, 127–136.
Versari, A., Parpinello, G.P., Galassi, S., 2002. Chemometric survey of Italian bottled mineral waters by means of their labelled physico-chemical and chemical composition. J. Food Compos. Anal. 15 (3), 251–264. https://doi.org/10.1006/jfca.2002.1058.
Veschetti, E., Achene, L., Ferretti, E., Lucentini, L., Citti, G., Ottaviani, M., 2010. Migration of trace metals in Italian drinking waters from distribution networks. Toxicol. Environ. Chem. 92 (3), 521–535. https://doi.org/10.1080/02772240903036139.
Vespasiano, G., Muto, F., Apollaro, C., De Rosa, R., 2012a. Preliminary hydrogeochemical and geological characterization of the thermal aquifer in the Guardia Piemontese area (Calabria, south Italy). Rend. Online Soc. Geol. Ital. 21, 841–842.
Vespasiano, G., Apollaro, C., Muto, F., De Rosa, R., 2012b. Geochemical and hydrogeological characterization of the metamorphic-serpentinitic multiaquifer of the Scala catchment, Amantea (Calabria, South Italy). Rend. Online Soc. Geol. Ital. 21, 879–880.
Vespasiano, G., Apollaro, C., Muto, F., Dotsika, E., De Rosa, R., Marini, L., 2014. Chemical and isotopic characteristics of the warm and cold waters of the Luigiane Spa near Guardia Piemontese (Calabria, Italy) in a complex faulted geological framework. Appl. Geochem. 41, 73–88. https://doi.org/10.1016/j.apgeochem.2013.11.014.
Vespasiano, G., Apollaro, C., Muto, F., De Rosa, R., Critelli, T., 2015a. Preliminary geochemical and geological characterization of the thermal site of Spezzano Albanese (Calabria, South Italy). Rend. Online Soc. Geol. Ital. 33, 108–110.
Vespasiano, G., Apollaro, C., Muto, F., De Rosa, R., Dotsika, E., Marini, L., 2015b. Preliminary geochemical characterization of the warm waters of the Grotta delle Ninfe near Cerchiara di Calabria (South Italy). Rend. Online Soc. Geol. Ital. 39, 130–133.
Vespasiano, G., Apollaro, C., De Rosa, R., Muto, F., Larosa, S., Fiebig, J., Mulch, A., Marini, L., 2015c. The small spring method (SSM) for the definition of stable isotope - elevation relationships in northern Calabria (southern Italy). Appl. Geochem. 63, 333–346. https://doi.org/10.1016/j.apgeochem.2015.10.001.
Vespasiano, G., Apollaro, C., Marini, L., Dominici, R., Cianflone, G., Romanazzi, A., Polemio, M., De Rosa, R., 2015d. Hydrogeological and isotopic study of the multi-aquifer system of the sibari plain (Calabria, southern Italy). Rend. Online Soc. Geol. Ital. 39, 134–137.
Vespasiano, G., Marini, L., Apollaro, C., De Rosa, R., 2016a. Preliminary geochemical characterization of the thermal waters of Caronte SPA springs (Calabria, South Italy). Rend. Online Soc. Geol. Ital. 39, 138–141.
Vespasiano, G., Apollaro, C., 2016b. Preliminary geochemical characterization of a carbonate aquifer: the case of Pollino massif (Calabria, South Italy). Rend. Online Soc. Geol. Ital. 38, 109–112.
Vespasiano, G., Cianflone, G., Cannata, C.B., Apollaro, C., Dominici, R., De Rosa, R., 2016c. Analysis of groundwater pollution in the Sant'Eufemia plain (Calabria – south Italy). Ital. J. Eng. Geol. Environ. https://doi:10.4408/IJEGE.2016-02.O-01.
Vespasiano, G., Notaro, P., Cianflone, G., 2017. Water-mortar interaction in a tunnel located in the southern Calabria (southern Italy). Environ. Eng. Geosci. 24 (3), 305–315. https://doi.org/10.2113/EEG-1978.
WHO, 2011. Guidelines for Drinking-Water Quality, fourth ed. World Health Organization.
Zamberlan da Silva, M.E., Santana, R.G., Guilhermetti, M., Camargo Filho, I., Endoc, E.H., Ueda-Nakamura, T., Vataru Nakamura, C., Dias Filho, B.P., 2008. Comparison of the bacteriological quality of tap water and bottled mineral water. Int. J. Hyg Environ. Health 211 (5–6), 504–509. https://doi.org/10.1016/j.ijheh.2007.09.004.

Supplementary material

S1. clr-transformation

The clr real coordinates (equation 1) are obtained by dividing the D components of each composition by the geometric mean $g(x) = (\prod_{i=1}^{D} x_i)^{\frac{1}{D}}$ of the parts and then taking the natural logarithm (Aitchison 1986):

$$clr(x) = \left[log\frac{x_1}{g(x)}, log\frac{x_2}{g(x)}, \ldots, log\frac{x_D}{g(x)}\right] \qquad (1)$$

S2. Comparison between data sets

Since the databases analyzed by Dinelli et al. (201), display a large spread of concentration values that span several orders of magnitude a "magnitude of spreading" (equation 2) was calculated defined as:

$$Magnitude\ of\ spreading = \frac{\frac{Max_{BW}}{Min_{BW}}}{\frac{Max_{TW}}{Min_{TW}}} \qquad (2)$$

where BW stands for bottled mineral water group and *TW* stands for tap water group. Using this mathematical expression, values > 1 indicate that the specific element has a larger spread in the mineral water data set and values < 1 indicate that the spread is larger in the tap water data set.

S3. Comparison of the data set values with Maximum Allowed Concentrations

Tamasi and Cini (2004) proposed a metal index MI also used in Varrica et al. (2013). The metal index MI (equation 3) is based on the largest possible number of trace metals and was defined as:

$$MI = \sum_{i=1}^{M} \frac{C_i}{(MAC)_i} \qquad (3)$$

where C is the concentration of each element in solution, i is the i^{th} sample and MAC the Maximum Allowed Concentration. Waters with *MI* values exceeding 1 are beyond a warning threshold requiring more attention.

Table 1Sa. Physico-chemical parameters and concentrations of major chemical components in the tap and bottled mineral waters from the Calabria Region. HCO_3^- represents alkalinity in mg HCO_3^- L^{-1}. **TW:** Tap water, **BW:** Bottled mineral water (**1**, still - **2**, sparkling).

ID	type	pH	EC	Ca^{2+}	Mg^{2+}	K^+	Na^+	NH_4^+	Cl^-	SO_4^{2-}	HCO_3^-	F^-	NO_3^-	PO_4^{3-}	SiO_2	Total Hardeness
			µS cm^{-1}	mg L^{-1}	mg L^{-1}	mg L^{-1}	mg L^{-1}	mg L^{-1}	mg L^{-1}	mg L^{-1}	mg L^{-1}	mg L^{-1}	mg L^{-1}	mg L^{-1}	mg L^{-1}	mg L^{-1}
TW01	Tap Water	7,43	332	44,4	14,9	0,7	3,2	< 0.05	4,6	25,8	186,1	0,5	1,2	< 0.5	4,5	17,2
TW02	Tap Water	7,46	115	6,1	1,8	1,1	11,2	0,12	11,2	5,3	32,0	0,1	1,0	< 0.5	11,1	2,3
TW03	Tap Water	7,66	170	19,1	4,8	1,3	6,7	< 0.05	5,5	5,2	85,4	0,1	3,1	< 0.5	21,7	6,7
TW04	Tap Water	7,88	346	46,2	15,6	0,5	3,5	< 0.05	4,3	29,2	184,6	0,5	1,1	< 0.5	4,5	17,9
TW05	Tap Water	7,44	486	63,7	24,9	0,8	4,7	< 0.05	7,0	25,4	294,4	0,2	3,6	< 0.5	5,9	26,2
TW06	Tap Water	7,90	177	18,8	5,6	1,6	5,9	< 0.05	3,0	10,4	82,4	< 0.1	0,2	< 0.5	22,2	7,0
TW07	Tap Water	7,81	384	45,6	14,4	1,8	14,6	< 0.05	13,7	21,0	201,4	0,2	2,3	< 0.5	11,1	17,3
TW08	Tap Water	6,82	1020	164,1	15,0	13,9	35,0	< 0.05	40,8	108,1	465,3	0,2	4,4	< 0.5	19,8	47,1
TW09	Tap Water	7,21	567	38,9	21,2	3,7	52,0	< 0.05	34,3	37,6	221,2	0,7	33,2	< 0.5	26,7	18,4
TW10	Tap Water	7,96	168	18,7	4,9	1,2	5,8	< 0.05	7,2	4,0	83,9	0,1	1,8	< 0.5	20,0	6,7
TW11	Tap Water	7,62	186	23,3	5,6	1,2	5,1	< 0.05	4,2	4,4	99,2	0,1	0,9	< 0.5	19,3	8,1
TW12	Tap Water	6,55	120	9,5	2,8	1,0	7,4	< 0.05	8,2	4,5	48,8	0,1	1,7	< 0.5	14,9	3,5
TW13	Tap Water	6,50	109	3,5	2,9	1,3	9,4	< 0.05	10,4	5,6	18,3	0,1	8,2	< 0.5	18,2	2,1
TW14	Tap Water	7,18	588	65,1	8,6	4,1	43,7	< 0.05	48,5	42,7	221,2	0,5	5,2	< 0.5	20,8	19,8
TW15	Tap Water	7,35	151	11,9	4,5	1,5	9,8	< 0.05	8,5	5,6	64,1	0,2	0,5	< 0.5	18,7	4,8
TW16	Tap Water	7,41	353	40,0	8,5	1,6	14,6	< 0.05	16,2	11,3	148,0	0,1	13,2	< 0.5	24,0	13,5
TW17	Tap Water	7,56	133	12,9	3,4	1,1	6,0	< 0.05	4,9	3,4	54,9	0,1	1,1	< 0.5	19,4	4,6
TW18	Tap Water	6,57	433	34,0	15,7	2,1	26,6	< 0.05	28,2	37,4	114,4	0,2	33,1	< 0.5	26,8	15,0
TW19	Tap Water	7,41	184	17,3	4,5	1,4	9,9	< 0.05	11,2	7,6	79,3	0,1	1,7	< 0.5	24,3	6,2
TW20	Tap Water	7,79	546	55,5	13,0	0,3	41,2	< 0.05	49,4	8,3	234,9	< 0.1	3,5	< 0.5	3,4	19,2
TW21	Tap Water	7,55	503	54,9	30,1	0,9	7,3	< 0.05	9,9	24,8	292,9	0,4	2,6	< 0.5	7,4	26,1
TW22	Tap Water	7,60	169	18,1	4,7	1,1	6,8	< 0.05	5,7	4,5	80,9	0,1	3,9	< 0.5	23,5	6,5
TW23	Tap Water	7,29	1570	62,5	27,7	7,3	212,5	< 0.05	398,3	99,1	125,1	0,3	11,9	< 0.5	12,9	27,0
TW24	Tap Water	7,82	332	44,1	14,8	0,4	3,0	< 0.05	4,1	25,2	178,5	0,3	1,0	< 0.5	4,4	17,1
TW25	Tap Water	7,50	261	19,6	9,8	1,7	18,1	< 0.05	15,9	29,0	87,0	0,4	4,7	< 0.5	17,7	8,9
TW26	Tap Water	7,70	227	18,9	9,6	2,4	8,8	< 0.05	9,7	10,4	105,3	0,1	2,5	< 0.5	19,4	8,7
TW27	Tap Water	7,11	429	50,3	9,0	3,7	26,1	< 0.05	19,7	34,2	187,6	0,5	4,6	< 0.5	19,7	16,3
TW28	Tap Water	7,54	222	23,9	7,5	1,4	8,3	0,06	7,9	8,3	106,8	0,2	1,9	< 0.5	12,9	9,1
TW29	Tap Water	6,90	191	19,2	2,9	1,9	11,3	< 0.05	10,7	15,8	62,5	0,3	2,7	< 0.5	16,3	6,0
TW30	Tap Water	7,46	315	41,2	13,3	1,0	3,4	0,06	5,3	3,8	189,2	0,1	1,9	< 0.5	4,4	15,8
TW31	Tap Water	7,60	124	6,4	1,9	1,2	11,8	0,14	12,2	5,3	32,0	0,1	1,1	< 0.5	11,6	2,4
BW01-1	Bottled Mineral Water	7,71	185	13,5	6,3	1,4	11,0	< 0.05	10,7	15,3	62,5	0,1	0,3	< 0.5	23,4	6,0
BW01-2	Bottled Mineral Water	7,74	138	8,2	3,8	1,1	11,2	< 0.05	19,6	3,6	48,8	0,1	3,3	< 0.5	27,2	3,6
BW02	Bottled Mineral Water	7,57	444	4,4	4,6	0,6	13,5	< 0.05	7,2	7,2	47,3	0,4	2,5	< 0.5	20,4	3,0
BW03	Bottled Mineral Water	6,23	98	52,2	14,1	1,8	15,2	0,35	22,3	37,2	192,2	0,1	8,9	< 0.5	36,7	18,9
BW04	Bottled Mineral Water	7,13	140	3,5	1,3	0,7	11,4	0,08	8,3	4,2	30,5	0,1	1,0	< 0.5	3,6	1,4
BW05-1	Bottled Mineral Water	7,28	160	15,1	5,0	1,3	6,5	< 0.05	6,0	8,8	67,1	0,1	2,3	< 0.5	22,2	5,8
BW05-2	Bottled Mineral Water	7,41	130	15,1	4,7	1,3	6,5	< 0.05	5,8	8,8	71,7	0,1	2,1	< 0.5	12,0	5,7
BW06-1	Bottled Mineral Water	6,24	144	7,0	2,0	1,2	16,6	< 0.05	9,6	4,9	44,2	0,1	11,0	< 0.5	42,3	2,6
BW06-2	Bottled Mineral Water	6,28	125,3	6,9	1,7	1,3	16,5	< 0.05	9,2	5,0	41,2	0,1	11,1	< 0.5	29,8	2,4
BW07	Bottled Mineral Water	7,87	475	44,1	18,5	2,1	24,3	< 0.05	27,1	23,0	218,1	0,3	2,9	< 0.5	24,1	18,6
BW08-1	Bottled Mineral Water	6,63	101	5,5	1,2	0,6	9,2	< 0.05	9,0	4,6	25,9	0,1	0,1	< 0.5	26,2	1,9
BW08-2	Bottled Mineral Water	6,57	82	6,2	1,1	0,7	8,8	< 0.05	8,0	4,6	27,5	0,1	2,2	< 0.5	25,0	2,0
BW09	Bottled Mineral Water	7,39	264	17,5	9,8	1,6	15,4	< 0.05	15,7	9,9	100,7	< 0.1	5,3	< 0.5	4,2	8,4
BW10-1	Bottled Mineral Water	7,71	401	41,1	12,9	1,8	18,4	< 0.05	22,4	29,0	155,6	0,2	7,4	< 0.5	23,1	15,6
BW10-2	Bottled Mineral Water	7,75	384	44,0	17,9	2,2	24,5	< 0.05	26,0	22,6	219,7	0,3	4,2	< 0.5	13,1	18,4
BW11	Bottled Mineral Water	7,51	371	53,7	11,7	0,6	3,2	< 0.05	4,5	4,5	221,2	< 0.1	0,9	< 0.5	5,1	18,2
BW12	Bottled Mineral Water	7,04	127	4,3	4,7	0,6	13,7	< 0.05	5,3	5,5	64,1	0,3	1,4	< 0.5	19,4	3,0
BW13-1	Bottled Mineral Water	6,67	69	1,4	1,5	0,7	5,7	< 0.05	9,0	4,3	9,2	0,1	0,8	< 0.5	3,4	1,0
BW13-2	Bottled Mineral Water	6,67	52	1,4	1,5	0,8	5,6	< 0.05	8,7	4,3	11,0	0,4	0,8	< 0.5	8,1	0,9
BW14-1	Bottled Mineral Water	7,58	435	52,0	14,1	1,8	15,3	< 0.05	22,3	37,0	186,1	0,1	8,9	< 0.5	20,1	18,8
BW14-2	Bottled Mineral Water	7,84	352	52,2	13,5	1,8	15,5	< 0.05	21,4	35,8	186,1	0,1	7,7	< 0.5	21,0	18,6

Table 1Sb. Concentrations of trace chemical components in the tap and bottled mineral waters from the Calabria Region. **TW:** Tap water, **BW:** Bottled mineral water (**1**, still - **2**, sparkling).

ID	type	Li	Be	B	Al	V	Cr	Mn	Co	Ni	Cu	Zn	Sr	Se	Rb	Mo	U	Pb	Bi	As	Cd	Ba	Fe	Hg
		µg L^{-1}	µg L^{-1}	µg L^{-1}	µg L^{-1}	µg L^{-1}	µg L^{-1}	µg L^{-1}	µg L^{-1}	µg L^{-1}	µg L^{-1}	µg L^{-1}	µg L^{-1}	µg L^{-1}	µg L^{-1}	µg L^{-1}	µg L^{-1}	µg L^{-1}	µg L^{-1}	µg L^{-1}	µg L^{-1}	µg L^{-1}	µg L^{-1}	ng L^{-1}
TW01	Tap Water	0,19	< 0.03	< 11.56	< 0.73	0,11	< 0.14	0,20	< 0.59	0,86	1,52	87,90	912	< 0.49	< 0.77	1,28	3,05	< 0.02	< 0.38	< 0.99	0,01	23,85	620	3,68
TW02	Tap Water	0,75	< 0.03	< 11.56	1,17	0,92	< 0.14	10,43	< 0.59	0,27	3,32	33,45	36,05	< 0.49	1,77	0,63	0,14	< 0.02	< 0.38	< 0.99	0,01	6,09	30,02	3,46
TW03	Tap Water	0,72	< 0.03	< 11.56	3,34	1,65	0,38	0,96	< 0.59	0,57	5,18	153,00	61,6	2,52	< 0.77	0,49	0,28	0,31	< 0.38	< 0.99	0,05	6,44	18,19	0,37
TW04	Tap Water	0,30	< 0.03	< 11.56	< 0.73	0,20	0,28	0,18	< 0.59	0,93	2,79	102,00	1001	< 0.49	< 0.77	1,13	3,11	0,50	< 0.38	< 0.99	0,03	24,79	15,28	1,36
TW05	Tap Water	0,24	< 0.03	< 11.56	< 0.73	1,19	0,21	0,18	< 0.59	2,30	11,40	25,30	354	< 0.49	< 0.77	4,65	1,90	2,05	< 0.38	< 0.99	0,02	19,09	4,89	1,06
TW06	Tap Water	0,71	< 0.03	< 11.56	1,83	0,55	< 0.14	0,22	< 0.59	0,58	1,67	1,24	75,2	2,45	< 0.77	0,57	0,23	0,11	< 0.38	< 0.99	0,02	9,04	1,69	0,46
TW07	Tap Water	3,24	< 0.03	27,36	< 0.73	0,50	< 0.14	< 0.17	< 0.59	0,97	7,41	6,71	106	< 0.49	< 0.77	1,37	1,03	0,33	< 0.38	< 0.99	0,01	41,04	10,24	1,61
TW08	Tap Water	10,75	< 0.03	76,4	< 0.73	0,42	0,17	99,56	< 0.59	3,57	1,31	< 0.91	740	3,88	3,03	2,30	5,21	< 0.02	< 0.38	1,83	0,02	45,61	290	0,97
TW09	Tap Water	2,10	< 0.03	60,6	7,41	0,39	0,21	0,71	< 0.59	1,25	3,38	22,69	240	3,23	1,78	1,77	2,37	0,07	< 0.38	< 0.99	0,02	72,81	11,94	1,02
TW10	Tap Water	0,47	< 0.03	< 11.56	0,77	1,00	0,18	< 0.17	< 0.59	0,42	0,65	< 0.91	58,0	2,38	< 0.77	0,34	0,14	< 0.02	< 0.38	< 0.99	0,02	9,57	< 0.82	0,28
TW11	Tap Water	0,98	< 0.03	< 11.56	< 0.73	0,59	< 0.14	< 0.17	< 0.59	0,51	< 0.23	< 0.91	49,9	2,42	< 0.77	0,36	0,75	< 0.02	< 0.38	< 0.99	0,04	8,78	< 0.82	0,66
TW12	Tap Water	2,76	< 0.03	< 11.56	4,29	0,51	0,19	6,60	< 0.59	1,49	78,75	34,95	41,36	2,65	1,35	0,33	0,10	0,35	< 0.38	1,61	0,06	8,22	15,02	1,22
TW13	Tap Water	1,23	< 0.03	12,14	9,08	< 0.10	< 0.14	4,46	< 0.59	2,69	14,33	39,63	42,41	2,56	1,74	< 0.26	0,01	0,38	< 0.38	1,59	0,07	7,84	10,05	0,96
TW14	Tap Water	5,42	< 0.03	118	< 0.73	0,87	0,21	0,28	< 0.59	1,31	16,70	24,00	1998	3,79	< 0.77	1,07	1,73	0,92	< 0.38	1,66	0,01	55,1	< 0.82	0,99
TW15	Tap Water	6,92	< 0.03	< 11.56	6,10	2,13	< 0.14	0,83	< 0.59	0,21	1,06	< 0.91	34,89	2,73	< 0.77	4,24	6,96	< 0.02	< 0.38	1,05	0,02	4,05	12,93	1,14
TW16	Tap Water	2,39	< 0.03	19,49	13,72	1,68	0,76	3,09	< 0.59	1,57	17,17	49,32	166	2,89	< 0.77	< 0.26	0,22	0,58	< 0.38	< 0.99	0,05	11,54	39,64	1,10
TW17	Tap Water	0,33	< 0.03	< 11.56	3,71	0,75	0,20	0,43	< 0.59	0,49	2,06	14,98	47,03	2,29	< 0.77	0,54	0,11	0,08	< 0.38	< 0.99	0,05	4,44	17,49	0,68
TW18	Tap Water	3,92	< 0.03	30,44	< 0.73	0,47	1,10	2,87	< 0.59	1,30	8,97	22,55	229	3,59	0,91	< 0.26	0,03	0,19	< 0.38	< 0.99	0,01	13,21	95,8	0,42
TW19	Tap Water	0,43	< 0.03	12,98	7,47	1,35	0,24	0,36	< 0.59	0,36	5,19	31,12	65,9	2,42	< 0.77	0,30	0,04	0,04	< 0.38	< 0.99	0,03	9,51	9,30	0,67
TW20	Tap Water	0,17	< 0.03	< 11.56	6,89	1,50	0,79	0,39	< 0.59	1,19	1,45	< 0.91	55,0	2,36	1,55	1,10	0,68	0,11	< 0.38	< 0.99	0,02	6,39	5,15	1,48
TW21	Tap Water	0,58	< 0.03	< 11.56	< 0.73	2,31	0,58	< 0.17	< 0.59	3,17	4,88	33,97	96,8	4,82	1,04	64,74	6,98	0,20	< 0.38	2,41	0,17	48,84	< 0.82	0,88
TW22	Tap Water	0,90	< 0.03	< 11.56	< 0.73	1,54	0,20	< 0.17	< 0.59	0,45	1,21	19,42	51,6	< 0.49	< 0.77	0,37	0,09	< 0.02	< 0.38	< 0.99	0,01	5,30	13,27	0,75
TW23	Tap Water	3,77	< 0.03	87,2	< 0.73	0,74	0,32	< 0.17	< 0.59	1,52	10,95	20,98	306	4,74	< 0.77	1,52	3,43	0,07	< 0.38	1,44	0,04	38,56	10,28	0,92
TW24	Tap Water	0,27	< 0.03	< 11.56	2,87	0,13	< 0.14	< 0.17	< 0.59	0,85	2,46	66,20	1029	2,59	< 0.77	1,30	3,07	0,22	< 0.38	< 0.99	0,01	22,88	< 0.82	0,47
TW25	Tap Water	2,05	< 0.03	19,35	117	0,33	0,29	2,33	< 0.59	1,30	18,77	70,20	93,3	2,82	0,81	0,81	0,50	0,77	< 0.38	< 0.99	0,02	19,28	151	0,51
TW26	Tap Water	0,67	< 0.03	11,61	15,55	3,58	1,05	< 0.17	< 0.59	0,60	1,75	< 0.91	85,1	2,56	1,89	0,53	0,22	0,04	< 0.38	1,23	0,01	3,47	14,88	0,39
TW27	Tap Water	1,84	< 0.03	41,09	< 0.73	1,53	0,16	< 0.17	< 0.59	1,01	4,32	4,11	222	< 0.49	< 0.77	0,70	0,81	0,12	< 0.38	< 0.99	0,01	91,0	4,52	0,70
TW28	Tap Water	2,49	< 0.03	< 11.56	28,11	1,11	< 0.14	1,63	< 0.59	0,68	41,82	10,69	39,15	2,33	< 0.77	2,00	2,97	0,41	< 0.38	3,02	0,02	5,09	43,77	1,79
TW29	Tap Water	2,57	< 0.03	13,54	1,16	0,45	< 0.14	3,23	< 0.59	0,54	6,84	72,70	142	< 0.49	1,05	0,51	0,28	0,62	< 0.38	1,22	0,01	12,72	133	0,91
TW30	Tap Water	0,40	< 0.03	< 11.56	0,94	0,74	0,35	< 0.17	< 0.59	1,10	5,44	< 0.91	368	2,59	0,84	1,85	1,07	0,15	< 0.38	1,19	0,01	13,53	< 0.82	0,51
TW31	Tap Water	0,68	< 0.03	< 11.56	6,31	0,92	< 0.14	4,92	< 0.59	0,35	7,26	40,21	39,11	2,56	2,23	0,76	0,14	0,67	< 0.38	< 0.99	0,01	5,67	70,1	5,57
BW01-1	Bottled Mineral Water	0,44	< 0.03	< 11.56	< 0.73	8,41	< 0.14	< 0.17	< 0.59	0,40	0,30	< 0.91	54,4	< 0.49	1,84	2,14	0,28	< 0.02	< 0.38	< 0.99	0,01	0,70	1,37	< 0.09
BW01-2	Bottled Mineral Water	0,20	< 0.03	< 11.56	< 0.73	5,41	7,62	< 0.17	< 0.59	0,52	7,91	1,52	67,3	< 0.49	< 0.77	< 0.26	0,01	< 0.02	< 0.38	< 0.99	0,01	2,27	1,85	< 0.09
BW02	Bottled Mineral Water	5,11	< 0.03	< 11.56	< 0.73	1,22	< 0.14	2,05	< 0.59	< 0.15	0,55	< 0.91	28,33	< 0.49	< 0.77	2,81	3,38	< 0.02	< 0.38	< 0.99	0,01	2,77	2,05	0,16
BW03	Bottled Mineral Water	7,73	< 0.03	22,63	< 0.73	2,13	3,24	0,48	< 0.59	0,91	< 0.23	< 0.91	690	0,91	< 0.77	< 0.26	0,63	< 0.02	< 0.38	1,91	< 0.004	25,54	4,72	0,12
BW04	Bottled Mineral Water	2,73	< 0.03	< 11.56	< 0.73	0,29	< 0.14	< 0.17	< 0.59	< 0.15	2,26	< 0.91	34,62	< 0.49	< 0.77	< 0.26	0,03	< 0.02	< 0.38	< 0.99	< 0.004	3,98	1,42	0,16
BW05-1	Bottled Mineral Water	0,92	< 0.03	< 11.56	< 0.73	1,29	0,21	< 0.17	< 0.59	0,23	0,71	< 0.91	50,1	< 0.49	< 0.77	0,75	0,06	< 0.02	< 0.38	< 0.99	0,01	6,93	1,61	< 0.09
BW05-2	Bottled Mineral Water	0,92	< 0.03	< 11.56	< 0.73	4,86	13,07	< 0.17	< 0.59	0,52	8,11	2,16	50,0	< 0.49	< 0.77	0,83	0,06	0,06	< 0.38	< 0.99	0,01	6,89	2,47	0,10
BW06-1	Bottled Mineral Water	9,15	0,30	< 11.56	< 0.73	0,27	0,14	< 0.17	< 0.59	0,23	1,40	< 0.91	70,8	< 0.49	1,38	< 0.26	0,05	< 0.02	< 0.38	< 0.99	0,01	2,84	3,97	0,37
BW06-2	Bottled Mineral Water	8,27	0,28	< 11.56	< 0.73	0,23	< 0.14	0,71	< 0.59	0,30	2,31	< 0.91	68,1	< 0.49	< 0.77	< 0.26	0,02	< 0.02	< 0.38	< 0.99	0,01	2,75	1,37	0,91
BW07	Bottled Mineral Water	11,03	< 0.03	42,49	< 0.73	0,30	0,20	< 0.17	< 0.59	0,84	0,61	< 0.91	1040	< 0.49	2,20	0,37	0,10	< 0.02	< 0.38	1,36	< 0.004	19,09	3,20	0,14
BW08-1	Bottled Mineral Water	2,13	< 0.03	< 11.56	< 0.73	0,12	< 0.14	< 0.17	< 0.59	< 0.15	1,15	< 0.91	43,91	< 0.49	< 0.77	< 0.26	0,02	< 0.02	< 0.38	< 0.99	0,01	2,83	2,09	< 0.09
BW08-2	Bottled Mineral Water	1,61	< 0.03	< 11.56	< 0.73	0,92	2,86	< 0.17	< 0.59	< 0.15	1,79	1,66	42,90	< 0.49	< 0.77	< 0.26	0,01	< 0.02	< 0.38	< 0.99	0,01	3,01	1,72	0,13
BW09	Bottled Mineral Water	0,72	< 0.03	< 11.56	< 0.73	5,89	0,23	< 0.17	< 0.59	1,18	0,60	< 0.91	144	< 0.49	< 0.77	0,54	0,08	< 0.02	< 0.38	< 0.99	0,01	13,81	2,76	0,14
BW10-1	Bottled Mineral Water	7,63	< 0.03	25,46	< 0.73	1,12	0,67	< 0.17	< 0.59	1,16	1,84	1,87	736	< 0.49	1,01	< 0.26	0,26	0,03	< 0.38	1,59	0,07	21,43	4,86	0,10
BW10-2	Bottled Mineral Water	11,29	< 0.03	43,30	< 0.73	2,16	6,85	1,08	< 0.59	1,06	6,29	1,84	1028	< 0.49	2,02	0,38	0,10	0,06	< 0.38	1,56	0,01	19,61	3,47	0,11
BW11	Bottled Mineral Water	0,28	< 0.03	< 11.56	< 0.73	0,62	0,28	< 0.17	< 0.59	1,36	1,02	< 0.91	71,0	< 0.49	1,20	1,72	1,54	< 0.02	< 0.38	< 0.99	0,01	17,95	2,61	0,15
BW12	Bottled Mineral Water	5,32	< 0.03	< 11.56	< 0.73	1,35	< 0.14	2,09	< 0.59	< 0.15	0,98	< 0.91	25,44	< 0.49	< 0.77	3,02	4,32	< 0.02	< 0.38	< 0.99	0,01	2,77	1,75	< 0.09
BW13-1	Bottled Mineral Water	2,75	< 0.03	< 11.56	11,05	< 0.10	< 0.14	3,36	< 0.59	1,72	1,05	21,27	13,14	< 0.49	1,71	< 0.26	0,01	< 0.02	< 0.38	< 0.99	0,05	7,34	0,45	0,40
BW13-2	Bottled Mineral Water	3,16	< 0.03	< 11.56	24,05	0,59	2,15	3,34	< 0.59	1,95	5,97	23,60	12,96	< 0.49	0,95	< 0.26	0,01	0,13	< 0.38	< 0.99	0,05	7,78	1,01	0,32
BW14-1	Bottled Mineral Water	7,49	< 0.03	23,88	< 0.73	2,02	3,03	0,58	< 0.59	1,27	1,94	2,05	669	0,69	1,17	< 0.26	0,59	0,04	< 0.38	1,79	0,09	26,00	5,83	0,12
BW14-2	Bottled Mineral Water	7,58	< 0.03	21,18	< 0.73	1,94	3,08	0,59	< 0.59	1,01	1,62	1,11	660	0,86	< 0.77	< 0.26	0,61	< 0.02	< 0.38	1,82	< 0.004	25,14	5,06	0,11

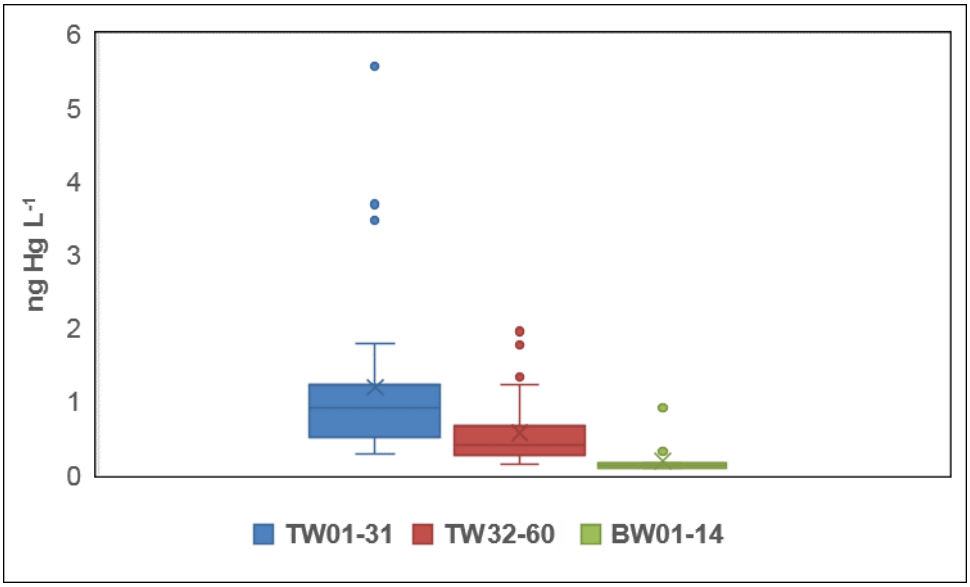

Fig. 1S. Box-plot comparison of Hg_T concentration in tap waters and bottled mineral waters.

Chemosphere 219 (2019) 896–913

Contents lists available at ScienceDirect

Chemosphere

journal homepage: www.elsevier.com/locate/chemosphere

Ultra-trace determination of total mercury in Italian bottled waters

Massimiliano Vardè [a, b, *], Alessandro Servidio [c], Giovanni Vespasiano [d, g], Luisa Pasti [b], Alberto Cavazzini [b], Mario Di Traglia [e], Annalisa Rosselli [f], Franco Cofone [c], Carmine Apollaro [g], Warren R.L. Cairns [a], Elisa Scalabrin [h], Rosanna De Rosa [g], Antonio Procopio [i]

[a] Istituto per la Dinamica dei Processi Ambientali – Consiglio Nazionale delle Ricerche (CNR-IDPA), Via Torino 155, I-30172, Venezia-Mestre, Italy
[b] Dipartimento di Scienze Chimiche e Farmaceutiche (DipSCF), Università degli Studi di Ferrara (Unife), Via Luigi Borsari 46, I-44121, Ferrara, Italy
[c] Istituto di Nanotecnologia – Consiglio Nazionale delle Ricerche (CNR-NANOTEC), Via P. Bucci 4, cubo 31C, I-87036, Arcavacata di Rende (CS), Italy
[d] EalCUBO (Environment, Earth, Engineering), Università della Calabria (Unical), Via P. Bucci 4, cubo 15B, I-87036, Arcavacata di Rende (CS), Italy
[e] Dipartimento di Sanità Pubblica e Malattie Infettive (DSPMI), Sapienza Università di Roma, Piazzale Aldo Moro 5, I-00185, Roma, Italy
[f] Dipartimento di Medicina Sperimentale, Università degli Studi della Campania "Luigi Vanvitelli", Via Santa Maria di Costantinopoli 16, I-80138, Napoli, Italy
[g] Dipartimento di Biologia, Ecologia e Scienze della Terra (DiBEST), Università della Calabria (Unical), Via P. Bucci 4, cubo 15B, I-87036, Arcavacata di Rende (CS), Italy
[h] Dipartimento di Scienze Ambientali, Informatica e Statistica (DAIS), Università Ca' Foscari Venezia, Via Torino 155, I-30172, Venezia-Mestre, Italy
[i] Dipartimento di Scienze della Salute, Università degli Studi "Magna Graecia" di Catanzaro (UMG), Viale Europa, Località Germaneto, I-88100, Catanzaro, Italy

HIGHLIGHTS

- First measurements of mercury at ultratrace levels in a large population of Italian bottled water.
- 244 bottled waters corresponding to 136 Italian springs were analysed.
- 86% of the Italian bottled waters analysed were at concentration above the calculated LOQ.
- Daily and weekly intake of Hg from Italian bottled water were estimated for three population groups.

GRAPHICAL ABSTRACT

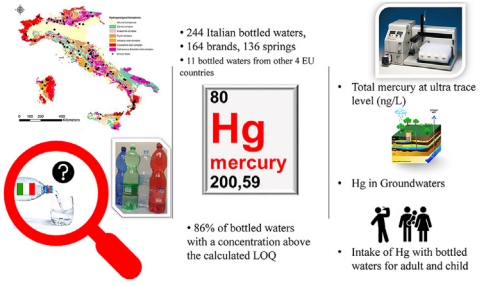

ARTICLE INFO

Article history:
Received 30 May 2018
Received in revised form
23 November 2018
Accepted 2 December 2018
Available online 7 December 2018

Handling Editor:

Keywords:
Natural mineral waters
CV-AFS
Water chemistry

ABSTRACT

Mercury (Hg) is a widespread, highly toxic persistent pollutant with adverse health effects on humans. So far, concentrations below the method detection limit have always been reported by studies on the concentration of mercury in bottled water when determined using instrumental analytical methods. These are often very expensive and are unaffordable for many laboratories. In this work, a less expensive method based on cold vapour atomic fluorescence spectrometry has been employed to determine total mercury (Hg_T) concentrations in bottled natural mineral waters. In all, 255 waters representing 164 different typologies were analysed. They came from 136 springs located in 18 Italian regions. In all samples, Hg_T concentrations were found in the range of sub-nanogram to a few nanograms per litre, well below the National and European regulatory limit (1 $\mu g\,L^{-1}$). Differences in Hg_T concentrations were related not only to the environmental characteristics of the springs but also to the extent and impact of human activities. Higher concentrations were found in waters coming from regions with former mining and/or natural thermal and volcanic activity. These data allowed us to estimate the mercury intake by

* Corresponding author. Istituto per la Dinamica dei Processi Ambientali – Consiglio Nazionale delle Ricerche (CNR-IDPA), Via Torino 155, I-30172, Venezia-Mestre, Italy.
E-mail address: massimiliano.varde@cnr.it (M. Vardè).

https://doi.org/10.1016/j.chemosphere.2018.12.020

Daily intake
Risk assessment
Italy

population (adults, children and toddlers) from drinkable mineral waters consumption. The mean mercury daily intake was found to be remarkably lower, not only than the provisional tolerable value (1 μg L^{-1} according to European and Italian legislation) but also than the estimated provisional tolerable weekly intake (PTWI) value (4 μg kg^{-1} body weight) recommended by the Joint FAO/WHO Expert Committee on Food Additives (JECFA).

1. Introduction

The bottled water industry is growing and is steadily becoming an important economic and public health factor. The estimated global consumption of bottled water in 2005 was around 165 billion litres, which means an annual per capita consumption of 25–26 L (Cicchella et al., 2010; Naddeo et al., 2008). Italy is both one of the largest producers (over 13 billion L per year) and consumers of bottled water in the world, with a consumption of 208 L per capita per year (Beverfood, 2016). Several market surveys show that, in an era characterized by a heavy chemical pollution, consumers still consider bottled water pure, pristine and a symbolic of good health (Allen et al., 1989; D'Ascenzo et al., 1997; Dinelli et al., 2012; Falahee and MacRae, 1995; Saad et al., 1998; Versari et al., 2002). However, only major element concentrations are reported on water labels, whereas trace elements and other potentially harmful substances that can be naturally present in water sources are ignored (2009/54/EC, 2009). Since the severity of adverse health effects are time- and dose-dependent, this may raise concerns due to the high consumption rates of mineral waters (Pokras, 2005). World Health Organization (WHO) guidelines for drinking water derive from internationally agreed procedures for health risk assessment (Graham, 1999; WHO - World Health Organization, 2011). These should in principle be used by national authorities as a basis for establishing their own water quality standards. Both the European and Italian legislations (98/83/EC, 1998) and (D.Lgs. (Legislative Decree) 2/2/2001, 2001) provide detailed quality control criteria for potentially harmful contaminants in water intended for human consumption, but, bottled waters are not subjected to the comprehensive analyses as tap water (2003/40/EC, 2003; Ministerial Decree, D.M. 29/12/2003, 2003). This opens the question of whether bottled waters should be more strictly regulated, with additional and more detailed information on the label (Hussain et al., 1997). Among potential contaminants, heavy metals are highly relevant to water quality. Their concentration depends on many factors, including the source, typology, storage and transportation conditions as well as (possible) release from the packaging bottles. Mercury is one of the more harmful and undesirable contaminants (Eisler, 2004), since in the aquatic environment inorganic mercury may be transformed by biological and chemical and/or abiotic processes to the more toxic, organometallic methylmercury form, making Hg contamination a worldwide concern (Morel et al., 1998). One of the routes of exposure to Hg for humans is drinking water (Clifton, 2007). There is a considerable body of experimental evidence on the toxic effects due to exposure to various types of mercury compounds during short- (acute) or prolonged-term (chronic) incidents (Ratcliffe et al., 1996). Hg has no beneficial biological function, and its presence in living organisms is associated with various degenerative diseases (Bhan and Sarkar, 2005; Valko et al., 2005). Previous studies indicated that Hg induces adverse effects on the central nervous system of foetuses, children and adults (Ask et al., 2002; Snyder, 1971). Moreover, mercury exposure, even at low doses, results in significant renal and liver toxicity (Dieguez-Acuña et al., 2004), fertility decrease (Ernst and Lauritsen, 1991; Harada, 1968), immune system alterations (Soleo et al., 1997) and damage to the cardiovascular system (Sørensen et al., 1999). To ensure the safety of consumers, the European Directive 98/83/EC translated nationally into a legislative decree (D.Lgs. 31/2001 (Legislative Decree), 2001) on the quality of drinking water sets a maximum level of mercury in water of 1 μg L^{-1} (or 1 ppb). This limit has been also adopted by the Directives 2003/40/EC for mineral water (D.M. 29/12/2003 (Ministerial Decree), 2003). For comparison, a number of national and international standards for mercury in drinking water are listed in Table 1. To satisfy the low detection limit required to quantitatively determine Hg in drinking water, specific methods and suitable instrumentations are required. Different analytical techniques have been used for mercury determination in environmental matrices and other media at low concentrations, including the flow injection mercury system (FIMS) - cold vapour atomic absorption spectrometry (CV-AAS) (Pourreza and Ghanemi, 2009; Rivaro et al., 2007), cold vapour atomic fluorescence spectrometry (CV-AFS) (Bloom and Fitzgerald, 1988; Fitzgerald and Gill, 1979; Geng et al., 2008; Gill and Fitzgerald, 1987; Wu et al., 2006; Yu and Yan, 2004) as well as flow injection analysis systems coupled to atomic fluorescence spectrometry (FIA-AFS) (Leopold et al., 2009). Other common instruments include inductively coupled plasma atomic emission spectrometry (ICP-AES) and electrothermal atomic absorption spectrometry (ET-AAS) (Arpadjan et al., 1997), ICP optical emission spectrometry (OES) and ICP mass spectrometry (MS) (Cairns et al., 2008; de Wuilloud et al., 2002; Minnich et al., 2008; Passariello et al., 1996) and thermal desorption (TD) gas chromatography–mass spectrometry (GC-MS) (Ito et al., 2009). Various pre-treatment, pre-concentration and detection procedures have been applied for mercury speciation analysis in natural waters (Leopold et al., 2010). ICP-MS with isotope dilution (ID) and cold vapour generation has a high sensitivity, high selectivity, and high sample throughput, however, the cost of such instrumentation and the isotopic standards may still be prohibitive to many laboratories (Mann et al., 2003). As an alternative, CV-AFS is less expensive, and it has been used extensively to determine mercury

Table 1
Comparison of the national and international standards for Hg in mineral waters and drinking waters.

Italian Standards for Mineral Waters (I-BW) and Drinking Water (I-DW) μg L^{-1}		
I-BW	1.0	Ministerial Decree D.M. 29/12/2003
I-DW	1.0	Legislative Decree D.Lgs. 31/2001
European Standards for Mineral Waters (EU-BW) and Drinking Water (E-DW)		
EU-MW	1.0	EU Directive 2003/40/EC
EU-DW	1.0	EU Directive 1998/83/EC
International Standards for Mineral Waters (BW) and Drinking Waters		
Chinese BW	1.0	Ministry of Environmental Protection (MEP) GB 2762-2012
Chinese DW	1.0	Ministry of Environmental Protection (MEP) GB 5749-2006
Canadian BW	1.0	Health Canada. Food and Drug Regulations
Canadian DW	1.0	Australian Drinking Water Guidelines
US-EPA BW	2.0	Safe Drinking Water Act (SDWA), 40 CFR 141.62
US-EPA DW	2.0	Food and Drug Administration (FDA). 21 CFR 103.35
WHO	6,0	WHO 2005, WHO/SDE/WSH/05.08/10

due to its low interferences, high sensitivity and relatively low sample consumption (Knox et al., 1995; Zi et al., 2009). In Europe, water brands are recognized by the EU Commission (OJEC, 1996; OJEC, 2010). The list of natural mineral waters is regularly updated and can change year to year. From 2010 to 2014, more than 400 Italian brands were registered by the EU (Ciotoli and Guerra, 2016). Despite the large number of brands on the Italian market, eight companies account for about 71.5% of production (Beverfood, 2016; Bono and Boni, 2001). The remaining fraction of the market is made of small companies with local plants and distribution. The aim of this study is to investigate with very sensitive analytical methods the total mercury (Hg_T) concentrations in Italian bottled waters to understand if a relationships exists between the presence of mercury, the physico-chemical parameters of waters, and the lithology of the aquifer. In addition, these data will be useful in evaluating the potential mercury daily intake from bottled drinking water.

2. Geological and hydrogeological setting

The geology of Italy is characterized by the presence of three major orogenic belts: the Alps, the Apennines and the Calabria-Peloritani Arc (CPA). From a geological point of view, there are significant differences among these three belts. A Pre-Alpine basement crops out essentially in Sardinia, Calabria and locally in the Alps. It is composed of metamorphosed sedimentary successions and Caledonian and Variscan magmatic rocks. Post-Variscan deposits consist mainly of sedimentary successions of Permian to Cretaceous age, which record the evolution of the passive margins developed around the Tethyan Ocean, with abundant carbonate deposits in both areas (Sardinia and Calabria). The metamorphic and crystalline Alpine and Hercynian rocks outcropping in Calabria constitute the so called “Calabrian basement Complex”. Carbonate mesozoic rocks occur in small tectonic windows below them. Eocene, Oligocene and Lower Miocene terrigenous sequences outcrop as remnants along the over thrust contacts between these basement units, and as tectonic wedges along major high-angle fault zones. Italy is also characterized by four main magmatic episodes, spanning in time from the Permian to recent times, which were related to different geodynamic settings. The most significant are the Permian volcanic episodes, in the Southern Alps, the Eocene–Oligocene rhyolitic–trachitic and basaltic episodes in the Southern Alps; the Tertiary calk-alkaline magmatism (Oligocene–Miocene) in Sardinia and the Plio-Quaternary volcanism in Sardinia, Central and Southern Italy and in Sicily (Beccaluva et al., 2004; Peccerillo, 2005). In this framework, the most important water resources are associated with the alluvial and Mesozoic (limestone and dolomitic limestone) successions characterizing the Alpine, Apennine and CPA areas (Civita, 2008). Volcanic areas mark out isolated groundwater resources, predominantly stored in the pyroclastic deposits. Local water resources are found in siliciclastic and flysch complexes (Civita, 2008). Other important hydrological complexes are associated with the carbonate sedimentary successions of the tertiary age. Although the hydrological complexes related to magmatic (plutonic) or metamorphic rocks outcropping in the Western and Central Alps, in Calabria, in north-eastern Sicily and in Sardinia, are less important from an extensional viewpoint, they can produce several high-quality springs and, as reported by Apollaro (Apollaro et al., 2016) and Vespasiano (Vespasiano, 2015; Vespasiano et al., 2015b, 2015a, 2014) they may be the site of important deep thermal systems.

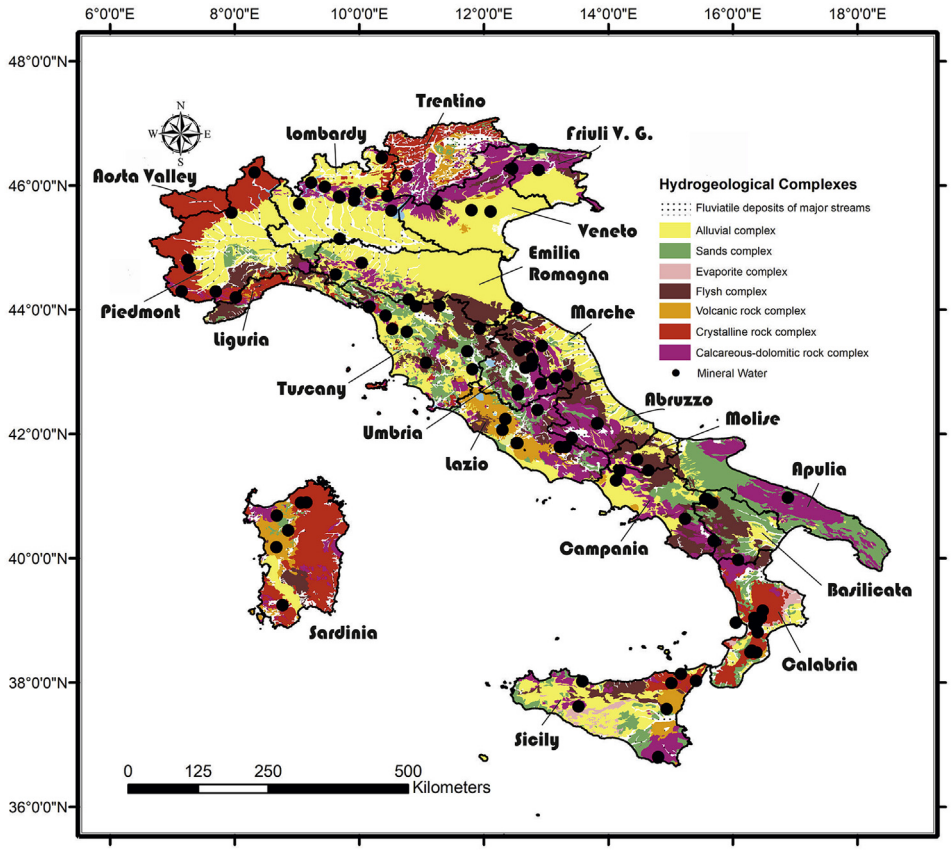

Fig. 1. Schematic hydrogeological map modified after Lithological Map of Italy (1:1.000.000) produced by the Servizio Geologico d'Italia, Istituto Superiore per la Protezione e la Ricerca Ambientale (ISPRA) where are reported the Italian mineral waters source locations. More sources were represented by the same dot.

Table 2
Summary of Hg concentration and other parameters for Italian bottled mineral waters considered in the study.

Sample ID	Hg (ng L^{-1})	Classification	Mineral content	Zone	Packaging	Bottle colour
ITA001-1	0.32	Non carbonated	Low	Central Italy	PET	Colourless
ITA001-2	0.16	Carbonated	Low	Central Italy	PET	Coloured (blue)
ITA001-3	0.42	Carbonated	Low	Central Italy	PET	Coloured (green)
ITA002-3	0.37	Carbonated	Low	Central Italy	PET	Coloured (green)
ITA003-1	0.20	Non carbonated	Low	Central Italy	PET	Colourless
ITA003-3	0.20	Carbonated	Low	Central Italy	PET	Coloured (green)
ITA004-1	0.83	Non carbonated	Low	Central Italy	PET	Coloured (blue)
ITA004-2	0.27	Carbonated	Low	Central Italy	PET	Coloured (blue)
ITA004-3	0.27	Carbonated	Low	Central Italy	PET	Coloured (blue)
ITA005-1	<0.09	Non carbonated	Low	Southern Italy	PET	Colourless
ITA006-1	<0.09	Non carbonated	Low	Southern Italy	PET	Colourless
ITA007-1	<0.09	Non carbonated	Low	Southern Italy	PET	Colourless
ITA008-1	0.19	Non carbonated	Low	Southern Italy	PET	Colourless
ITA009-1	<0.09	Non carbonated	Low	Southern Italy	PET	Colourless
ITA009-4	0.22	Carbonated	Low	Southern Italy	PET	Coloured (blue)
ITA010-2	0.71	Carbonated	Intermediate	Southern Italy	PET	Coloured (blue)
ITA010-4	0.09	Carbonated	Intermediate	Southern Italy	PET	Coloured (green)
ITA011-1	0.23	Non carbonated	Low	Southern Italy	PET	Colourless
ITA012-1	<0.09	Non carbonated	Low	Southern Italy	PET	Colourless
ITA012-4	0.09	Carbonated	Intermediate	Southern Italy	PET	Coloured (pink)
ITA012-4	0.13	Carbonated	High	Southern Italy	PET	Coloured (green)
ITA013-1	0.30	Non carbonated	Low	Southern Italy	PET	Colourless
ITA014-1	0.28	Non carbonated	Low	Southern Italy	PET	Colourless
ITA014-3	0.30	Carbonated	Low	Southern Italy	PET	Colourless
ITA015-1	0.15	Non carbonated	Low	Southern Italy	PET	Colourless
ITA016-4	<0.09	Carbonated	Intermediate	Southern Italy	PET	Coloured (green)
ITA017-4	<0.09	Carbonated	High	Southern Italy	PET	Coloured (green)
ITA018-1	<0.09	Non carbonated	Low	Southern Italy	PET	Colourless
ITA018-2	<0.09	Carbonated	Low	Southern Italy	PET	Colourless
ITA019-1	0.16	Non carbonated	Low	Southern Italy	PET	Colourless
ITA020-1	0.12	Non carbonated	Low	Southern Italy	PET	Colourless
ITA021-1	0.16	Non carbonated	Low	Southern Italy	PET	Colourless
ITA022-1	<0.09	Non carbonated	Low	Southern Italy	PET	Coloured (blue)
ITA022-2	0.10	Carbonated	Low	Southern Italy	PET	Coloured (blue)
ITA023-1	0.37	Non carbonated	Low	Southern Italy	PET	Colourless
ITA023-2	0.91	Carbonated	Low	Southern Italy	PET	Colourless
ITA024-1	0.14	Non carbonated	Low	Southern Italy	PET	Colourless
ITA025-1	<0.09	Non carbonated	Low	Southern Italy	PET	Colourless
ITA025-2	0.13	Carbonated	Low	Southern Italy	PET	Colourless
ITA026-1	0.14	Non carbonated	Low	Southern Italy	PET	Colourless
ITA027-1	0.10	Non carbonated	Low	Southern Italy	PET	Colourless
ITA027-2	0.11	Carbonated	Low	Southern Italy	PET	Coloured (blue)
ITA028-1	<0.09	Non carbonated	Low	Southern Italy	PET	Coloured (blue)
ITA029-1	0.40	Non carbonated	Very low	Southern Italy	PET	Coloured (blue)
ITA029-2	0.32	Carbonated	Very low	Southern Italy	PET	Coloured (blue)
ITA030-1	0.12	Non carbonated	Low	Southern Italy	PET	Colourless
ITA030-2	0.11	Carbonated	Low	Southern Italy	PET	Colourless
ITA031-1	0.23	Non carbonated	Intermediate	Southern Italy	PET	Colourless
ITA031-2	0.32	Carbonated	Intermediate	Southern Italy	PET	Colourless
ITA032-1	0.36	Non carbonated	Intermediate	Southern Italy	PET	Colourless
ITA032-3	0.30	Carbonated	Intermediate	Southern Italy	PET	Colourless
ITA033-4	1.24	Carbonated	Intermediate	Southern Italy	PET	Coloured (green)
ITA034-1	0.15	Non carbonated	Low	Southern Italy	PET	Colourless
ITA035-3	0.44	Carbonated	Low	Southern Italy	PET	Coloured (green)
ITA036-4	0.21	Carbonated	Intermediate	Southern Italy	PET	Coloured (green)
ITA037-1	0.18	Non carbonated	Low	Southern Italy	PET	Colourless
ITA037-2	0.23	Carbonated	Low	Southern Italy	Glass	Coloured (green)
ITA038-1	0.49	Non carbonated	Low	Southern Italy	PET	Coloured (green)
ITA039-1	0.11	Non carbonated	Low	Southern Italy	Glass	Coloured (green)
ITA040-1	0.44	Non carbonated	Low	Southern Italy	PET	Colourless
ITA040-2	0.43	Carbonated	Intermediate	Southern Italy	PET	Colourless
ITA041-4	0.30	Carbonated	Intermediate	Southern Italy	PET	Coloured (green)
ITA042-1	0.29	Non carbonated	Low	Southern Italy	PET	Colourless
ITA042-2	0.20	Carbonated	Low	Southern Italy	PET	Colourless
ITA043-1	0.36	Non carbonated	Low	Southern Italy	PET	Colourless
ITA043-3	0.36	Carbonated	Low	Southern Italy	PET	Colourless
ITA044-1	0.20	Non carbonated	Low	Northern Italy	PET	Colourless
ITA044-2	0.15	Carbonated	Low	Northern Italy	PET	Coloured (blue)
ITA044-3	0.26	Carbonated	Low	Northern Italy	PET	Colourless
ITA045-1	<0.09	Non carbonated	Low	Northern Italy	PET	Colourless
ITA046-1	0.58	Non carbonated	Intermediate	Northern Italy	Glass	Colourless
ITA046-2	0.35	Carbonated	Intermediate	Northern Italy	Glass	Colourless
ITA047-1	0.30	Non carbonated	Low	Northern Italy	PET	Colourless

(*continued on next page*)

Table 2 (*continued*)

Sample ID	Hg (ng L^{-1})	Classification	Mineral content	Zone	Packaging	Bottle colour
ITA048-1	0.41	Non carbonated	Low	Northern Italy	PET	Colourless
ITA048-2	0.39	Carbonated	Low	Northern Italy	PET	Colourless
ITA049-1	0.26	Non carbonated	Low	Northern Italy	PET	Colourless
ITA050-1	0.26	Non carbonated	Low	Northern Italy	PET	Colourless
ITA051-2	0.27	Carbonated	Low	Northern Italy	PET	Coloured (blue)
ITA052-4	0.44	Carbonated	Intermediate	Central Italy	PET	Coloured (green)
ITA053-4	0.89	Carbonated	Intermediate	Central Italy	PET	Coloured (green)
ITA054-2	0.27	Carbonated	Intermediate	Central Italy	PET	Coloured (green)
ITA054-4	0.21	Carbonated	Intermediate	Central Italy	PET	Coloured (green)
ITA055-1	0.44	Non carbonated	Low	Central Italy	PET	Coloured (blue)
ITA055-3	0.38	Carbonated	Low	Central Italy	PET	Coloured (blue)
ITA056-1	0.44	Non carbonated	Intermediate	Central Italy	PET	Coloured (green)
ITA056-2	0.18	Carbonated	Intermediate	Central Italy	PET	Coloured (green)
ITA056-4	<0.09	Carbonated	Intermediate	Central Italy	PET	Coloured (green)
ITA057-1	0.19	Non carbonated	Low	Central Italy	PET	Colourless
ITA057-3	0.14	Carbonated	Low	Central Italy	PET	Colourless
ITA058-1	<0.09	Non carbonated	Low	Central Italy	Glass	Coloured (green)
ITA058-3	0.21	Carbonated	Low	Central Italy	Glass	Coloured (green)
ITA059-4	0.86	Carbonated	Intermediate	Central Italy	PET	Coloured (green)
ITA060-4	0.27	Carbonated	Intermediate	Central Italy	PET	Colourless
ITA061-4	0.58	Carbonated	Intermediate	Central Italy	PET	Colourless
ITA062-1	0.15	Non carbonated	Low	Northern Italy	PET	Colourless
ITA063-1	0.25	Non carbonated	Intermediate	Northern Italy	Glass	Colourless
ITA064-1	0.23	Non carbonated	Low	Northern Italy	PET	Colourless
ITA064-2	0.26	Carbonated	Low	Northern Italy	PET	Colourless
ITA065-1	0.59	Non carbonated	Low	Northern Italy	Glass	Colourless
ITA065-2	0.40	Carbonated	Low	Northern Italy	Glass	Colourless
ITA066-2	0.18	Carbonated	Low	Northern Italy	PET	Colourless
ITA067-1	0.55	Non carbonated	High	Northern Italy	PET	Colourless
ITA068-1	0.52	Non carbonated	Low	Northern Italy	PET	Colourless
ITA069-1	0.16	Non carbonated	Low	Northern Italy	PET	Colourless
ITA069-2	0.39	Carbonated	Low	Northern Italy	PET	Coloured (blue)
ITA069-3	0.32	Carbonated	Low	Northern Italy	PET	Coloured (blue)
ITA070-1	0.12	Non carbonated	Low	Northern Italy	PET	Colourless
ITA070-2	0.13	Carbonated	Low	Northern Italy	PET	Colourless
ITA070-3	0.19	Carbonated	Low	Northern Italy	PET	Colourless
ITA071-1	0.39	Non carbonated	Very low	Northern Italy	PET	Colourless
ITA072-1	0.22	Non carbonated	Low	Northern Italy	PET	Colourless
ITA072-2	0.13	Carbonated	Low	Northern Italy	PET	Colourless
ITA073-1	0.30	Non carbonated	Low	Northern Italy	PET	Colourless
ITA074-1	0.14	Non carbonated	Low	Northern Italy	Glass	Colourless
ITA074-2	0.13	Carbonated	Low	Northern Italy	Glass	Colourless
ITA075-2	0.23	Carbonated	Intermediate	Northern Italy	PET	Coloured (green)
ITA076-1	0.33	Non carbonated	Low	Northern Italy	PET	Colourless
ITA076-2	0.45	Carbonated	Low	Northern Italy	PET	Colourless
ITA077-1	<0.09	Non carbonated	Low	Northern Italy	PET	Coloured (blue)
ITA078-1	0.24	Non carbonated	Low	Central Italy	PET	Colourless
ITA078-3	0.25	Carbonated	Low	Central Italy	PET	Coloured (green)
ITA079-1	0.35	Non carbonated	Low	Central Italy	PET	Colourless
ITA080-1	0.26	Non carbonated	Low	Central Italy	PET	Colourless
ITA080-3	0.21	Carbonated	Low	Central Italy	PET	Coloured (green)
ITA081-1	0.34	Non carbonated	Low	Central Italy	PET	Colourless
ITA082-3	0.25	Carbonated	Low	Central Italy	PET	Coloured (blue)
ITA083-1	0.33	Non carbonated	Low	Central Italy	PET	Colourless
ITA083-3	0.17	Carbonated	Low	Central Italy	PET	Colourless
ITA084-3	0.26	Carbonated	Low	Central Italy	PET	Coloured (blue)
ITA085-1	0.21	Non carbonated	Low	Southern Italy	PET	Coloured (blue)
ITA085-2	0.20	Carbonated	Low	Southern Italy	PET	Coloured (green)
ITA086-1	0.21	Non carbonated	Low	Southern Italy	PET	Colourless
ITA087-1	0.15	Non carbonated	Very low	Northern Italy	PET	Colourless
ITA088-1	0.23	Non carbonated	Very low	Northern Italy	Glass	Colourless
ITA088-2	0.25	Carbonated	Very low	Northern Italy	Glass	Colourless
ITA089-1	<0.09	Non carbonated	Low	Northern Italy	PET	Colourless
ITA089-2	0.21	Carbonated	Very low	Northern Italy	PET	Colourless
ITA090-1	0.26	Non carbonated	Very low	Northern Italy	PET	Colourless
ITA090-2	0.27	Carbonated	Very low	Northern Italy	PET	Colourless
ITA091-1	0.37	Non carbonated	Low	Northern Italy	PET	Colourless
ITA092-1	0.14	Non carbonated	Very low	Northern Italy	PET	Colourless
ITA092-2	0.18	Carbonated	Very low	Northern Italy	PET	Colourless
ITA093-1	0.79	Non carbonated	Very low	Northern Italy	PET	Colourless
ITA094-1	0.19	Non carbonated	Very low	Northern Italy	PET	Coloured (blue)
ITA095-1	<0.09	Non carbonated	Very low	Northern Italy	PET	Colourless
ITA096-1	<0.09	Non carbonated	Very low	Northern Italy	PET	Colourless
ITA096-2	<0.09	Carbonated	Very low	Northern Italy	PET	Colourless
ITA097-1	0.36	Non carbonated	Very low	Northern Italy	PET	Colourless

Table 2 (*continued*)

Sample ID	Hg (ng L^{-1})	Classification	Mineral content	Zone	Packaging	Bottle colour
ITA097-2	0.91	Carbonated	Very low	Northern Italy	PET	Colourless
ITA098-1	0.25	Non carbonated	Very low	Northern Italy	PET	Colourless
ITA099-1	0.24	Non carbonated	Very low	Northern Italy	PET	Colourless
ITA099-1	0.11	Non carbonated	Very low	Northern Italy	PET	Colourless
ITA099-2	0.28	Carbonated	Very low	Northern Italy	PET	Colourless
ITA099-3	0.19	Carbonated	Very low	Northern Italy	PET	Colourless
ITA100-1	0.38	Non carbonated	Very low	Northern Italy	PET	Colourless
ITA100-2	0.21	Carbonated	Very low	Northern Italy	PET	Colourless
ITA101-1	0.46	Non carbonated	Low	Southern Italy	PET	Colourless
ITA102-1	0.17	Non carbonated	Low	Southern Italy	PET	Colourless
ITA103-1	0.97	Non carbonated	Low	Southern Italy	PET	Colourless
ITA104-1	0.26	Non carbonated	Low	Southern Italy	PET	Colourless
ITA105-1	0.30	Non carbonated	Low	Southern Italy	PET	Colourless
ITA106-1	0.48	Non carbonated	Low	Southern Italy	PET	Colourless
ITA107-1	0.30	Non carbonated	Low	Southern Italy	PET	Colourless
ITA108-1	0.44	Non carbonated	High	Southern Italy	PET	Coloured (blue)
ITA109-2	0.82	Carbonated	Intermediate	Southern Italy	PET	Coloured (green)
ITA110-1	0.19	Non carbonated	Low	Southern Italy	PET	Colourless
ITA111-1	0.20	Non carbonated	Low	Southern Italy	PET	Coloured (green)
ITA112-1	0.13	Non carbonated	Low	Southern Italy	PET	Colourless
ITA113-1	0.22	Non carbonated	Low	Southern Italy	PET	Colourless
ITA114-1	<0.09	Non carbonated	Low	Southern Italy	PET	Colourless
ITA115-3	<0.09	Carbonated	Intermediate	Southern Italy	PET	Colourless
ITA116-1	<0.09	Non carbonated	Low	Southern Italy	PET	Colourless
ITA117-1	<0.09	Non carbonated	Low	Southern Italy	PET	Colourless
ITA118-1	<0.09	Non carbonated	Low	Southern Italy	PET	Colourless
ITA118-2	<0.09	Carbonated	Low	Southern Italy	PET	Colourless
ITA119-1	<0.09	Non carbonated	Low	Southern Italy	PET	Colourless
ITA120-1	<0.09	Non carbonated	Low	Southern Italy	PET	Colourless
ITA121-1	<0.09	Non carbonated	Low	Southern Italy	PET	Colourless
ITA122-1	<0.09	Non carbonated	Low	Southern Italy	PET	Colourless
ITA123-1	<0.09	Non carbonated	Low	Southern Italy	PET	Colourless
ITA124-1	<0.09	Non carbonated	Low	Southern Italy	PET	Colourless
ITA125-1	0.29	Non carbonated	Very low	Northern Italy	Glass	Colourless
ITA125-2	0.35	Carbonated	Very low	Northern Italy	Glass	Colourless
ITA126-1	0.10	Non carbonated	High	Central Italy	Glass	Colourless
ITA127-1	5.39	Non carbonated	Very low	Central Italy	Glass	Coloured (green)
ITA128-1	0.28	Non carbonated	Low	Central Italy	PET	Colourless
ITA128-2	0.48	Carbonated	Low	Central Italy	PET	Colourless
ITA129-1	0.14	Non carbonated	Low	Central Italy	PET	Colourless
ITA129-2	0.16	Carbonated	Low	Central Italy	PET	Colourless
ITA129-3	0.33	Carbonated	Low	Central Italy	PET	Coloured (green)
ITA130-1	0.37	Non carbonated	Low	Central Italy	PET	Colourless
ITA130-2	0.17	Carbonated	Low	Central Italy	PET	Colourless
ITA131-3	0.30	Carbonated	Low	Central Italy	Glass	Colourless
ITA132-1	0.29	Non carbonated	Low	Central Italy	PET	Colourless
ITA132-2	0.22	Carbonated	Low	Central Italy	PET	Colourless
ITA133-1	0.09	Non carbonated	Low	Central Italy	PET	Colourless
ITA134-1	0.35	Non carbonated	Intermediate	Central Italy	PET	Colourless
ITA134-2	0.32	Carbonated	Intermediate	Central Italy	PET	Colourless
ITA135-1	1.74	Non carbonated	Low	Central Italy	Glass	Coloured (green)
ITA136-1	<0.09	Non carbonated	Low	Central Italy	PET	Colourless
ITA137-1	0.16	Non carbonated	Intermediate	Central Italy	PET	Coloured (green)
ITA138-1	0.35	Non carbonated	Intermediate	Central Italy	PET	Coloured (green)
ITA139-1	0.24	Non carbonated	Low	Central Italy	PET	Colourless
ITA140-4	0.22	Carbonated	Low	Central Italy	PET	Coloured (green)
ITA141-1	0.20	Non carbonated	Low	Central Italy	PET	Colourless
ITA141-2	0.40	Carbonated	Low	Central Italy	PET	Colourless
ITA142-2	0.15	Carbonated	Low	Central Italy	PET	Coloured (blue)
ITA143-2	0.26	Carbonated	Low	Central Italy	PET	Coloured (blue)
ITA144-1	0.09	Non carbonated	Low	Central Italy	PET	Colourless
ITA145-1	<0.09	Non carbonated	Low	Central Italy	PET	Colourless
ITA145-2	0.60	Carbonated	Low	Central Italy	PET	Coloured (blue)
ITA146-1	0.47	Non carbonated	Low	Central Italy	PET	Colourless
ITA147-1	0.51	Non carbonated	Low	Central Italy	PET	Colourless
ITA147-2	0.19	Carbonated	Low	Central Italy	PET	Colourless
ITA148-1	0.23	Non carbonated	Low	Central Italy	PET	Colourless
ITA148-2	0.20	Carbonated	Low	Central Italy	PET	Colourless
ITA149-1	0.27	Non carbonated	Low	Central Italy	PET	Colourless
ITA149-2	0.45	Carbonated	Low	Central Italy	PET	Colourless
ITA150-4	0.91	Carbonated	Intermediate	Central Italy	PET	Coloured (green)
ITA151-1	0.32	Non carbonated	Low	Central Italy	PET	Colourless
ITA152-1	0.24	Non carbonated	Low	Central Italy	PET	Colourless
ITA153-1	0.34	Non carbonated	Low	Central Italy	PET	Coloured (green)
ITA153-2	0.11	Carbonated	Low	Central Italy	PET	Coloured (red)

(*continued on next page*)

Table 2 (*continued*)

Sample ID	Hg (ng L^{-1})	Classification	Mineral content	Zone	Packaging	Bottle colour
ITA153-2	0.38	Carbonated	Low	Central Italy	PET	Coloured (red)
ITA153-3	0.15	Carbonated	Low	Central Italy	PET	Coloured (blue)
ITA154-1	0.27	Non carbonated	Low	Central Italy	PET	Colourless
ITA154-3	0.26	Carbonated	Low	Central Italy	PET	Colourless
ITA155-1	0.38	Non carbonated	Intermediate	Central Italy	PET	Coloured (green)
ITA156-1	0.42	Non carbonated	Low	Central Italy	PET	Colourless
ITA156-3	0.35	Carbonated	Low	Central Italy	PET	Colourless
ITA157-1	0.37	Non carbonated	Low	Central Italy	PET	Colourless
ITA157-2	0.28	Carbonated	Low	Central Italy	PET	Colourless
ITA158-1	0.31	Non carbonated	Low	Central Italy	PET	Colourless
ITA158-3	0.21	Carbonated	Low	Central Italy	PET	Colourless
ITA159-2	0.31	Carbonated	Low	Northern Italy	PET	Colourless
ITA160-2	0.28	Carbonated	Low	Northern Italy	PET	Coloured (blue)
ITA161-1	0.21	Non carbonated	Low	Northern Italy	PET	Colourless
ITA162-1	0.14	Non carbonated	Low	Northern Italy	Glass	Colourless
ITA162-2	<0.09	Carbonated	Low	Northern Italy	PET	Colourless
ITA163-1	0.20	Non carbonated	Low	Northern Italy	PET	Colourless
ITA163-2	0.31	Carbonated	Low	Northern Italy	PET	Coloured (blue)
ITA163-3	0.25	Carbonated	Low	Northern Italy	PET	Coloured (green)
ITA164-1	0.22	Non carbonated	Low	Northern Italy	PET	Colourless
ITA164-2	0.19	Carbonated	Low	Northern Italy	PET	Coloured (green)

National and European regulatory limit of Hg in natural mineral bottled water set at 1 μg L^{-1}
Note: the last no. of the sample code indicates water typology: 1-still. 2-sparkling. 3-lightly sparkling. 4-naturally sparkling.

3. Materials and methods

3.1. Sample collection

Between January 2014 and March 2016, 244 bottles of water (mineral, springs and drinking) available on the Italian market were purchased in randomly selected shops from all over Italy. These bottled waters represent 164 brands of water and correspond to 136 springs located in 55 provinces from 18 out of the 20 Italian regions (Fig. 1). In addition, for comparison, 11 bottled waters from 5 brands from other European countries (Denmark, France, Slovenia and Spain) were analysed (see Table S1). For a given brand different water types were analysed; the total number of 255 bottles of water (244 from Italy and 11 from other European Country) consisted of 144 bottled mineral waters (still/not carbonated), 19 with a natural content of carbon dioxide (CO_2) notated as naturally sparkling, and 92 with artificially added CO_2, split between 63 sparkling and 29 lightly sparkling waters.

The bottled water samples collected in this study had two different container types, glass with a metal screw cap with a thin polyethylene (PE) film (21 samples) or polyethylene terephthalate (PET) packaging with a PE screw cap (234 samples). The colour of the bottle containers varied as follows: 78 containers were coloured (32 blue-bluish, 43 green-greenish and 3 red-reddish) and 177 were colourless.

Based on the dry residue content, the samples were classified as very low (28 samples), low (177 samples) and intermediate mineral content (34 samples). Only 5 brands had a concentration of total dissolved solids of up to 1500 mg L^{-1}. A list of samples based on their main chemical compositional parameters (carbonated, mineral content) is reported in Table 2. The geographical coordinates and elevation of springs of all analysed samples are summarized in Table S2.

3.2. Labware, chemicals and reagents

Ultrapure deionized water (Millipore, Milli-Q, 18 MΩ cm, Burlington, MA, USA) was used to rinse all containers, to prepare blank solutions, calibration standards and to dilute concentrated reagents. Laboratory plasticware used (Nalgene, Thermo Scientific, Waltham, (MA), USA) and metal-free tubes (VWR, Radnor, PA, USA) were of either fluorinated polyethylene (FPE) or polypropylene (PP) with high-density polyethylene (HDPE) caps. An alkaline detergent (Micro-90, Sigma-Aldrich Inc., Saint Louis, MO, USA) diluted in deionized water was used to clean the plasticware. Subsequently, all laboratory containers were then filled completely to the neck with a 3.5% (v/v) nitric acid solution (HNO_3, 67-69%, supra-pure quality, SpA, Romil, Cambridge, UK) and were immersed in a hot bath for 6 h at 65 °C. After rinsing a bromine monochloride (BrCl) 1% (v/v) solution was used to completely fill the bottles and tubes for 24 h. Between each step, bottles, tubes and caps were rinsed five times with ultrapure deionized water. Hydrochloric acid (HCl, 33-36%, ultra-pure quality, UpA, Romil, Cambridge, UK) was diluted to 0.5% (v/v) to stabilize samples before analysis. Tin (II) chloride ($SnCl_2 \bullet 2H_2O$), hydroxylammonium chloride ($NH_2OH \bullet HCl$) and BrCl solutions were prepared from high purity quality reagents (ACS, ISO, Reag. Ph Eur grade, Emsure, Merck KGaA, Darmstadt, Germany). Nitrogen (N_2) and argon (Ar) gases at ultra-high purity (UHP) (Grade 5.0, 99.9990%, Rivoira, Milan, Italy) were further purified using a gold-coated sand/bead trap to remove Hg before purging the reagent solutions and use as a carrier gas during sample analysis.

3.3. Analytical methods

Upon arrival in the laboratory, each bottled water was recorded, placed in a plastic zip-lock type bag and stored in a dark environment in the clean laboratory at room temperature (20 °C) to avoid contaminations as well as any temperature or light effects (Rahmanian et al., 2015). Once in the laboratory, water samples were analysed within less than two weeks. Unlike previous authors (Allen et al., 1989) the outer surfaces of the bottled samples were not washed. Mineral waters with carbon dioxide (natural or added) were treated following the same procedure for still waters. To reduce the blank levels, all handling procedures were carried out whilst wearing PP gloves, a clean lab coat and blue PP over shoes (Bertoldi et al., 2011). For each analysis, a 50 g aliquot of water from a newly opened bottle was transferred into a new 50 ml acid pre-cleaned PP tube, and HCl UpA was immediately added to final concentration of 0.5% (v/v) with the aim of minimizing Hg volatilization. All Hg forms were transformed to divalent Hg^{2+} by adding BrCl to a final concentration of 0.5% (v/v), 24-48 h before

analysis. To homogenize the sample and allow digestion at room temperature, each PP tube was sealed and agitated, the persistence of the yellow colour of the solution was checked to ensure a BrCl excess. One hour before analysis, $NH_2OH•HCl$, (0.2% v/v solution) was added to reduce any BrCl excess and destroy free halogens. Oxidized divalent mercury (Hg^{2+}) was reduced to elemental mercury (Hg^0) using $SnCl_2•2H_2O$ and purged from the sample in a gas-liquid separator with an Hg-free argon streams. From there it was concentrated onto a dual gold-coated bead traps, where Hg^0 was amalgamated in two stages, first onto a "sample" and then onto "analytical" traps (Gill and Fitzgerald, 1987). The elemental mercury was then thermally desorbed from the gold traps and carried to the cell for CV-AFS detection. After each single step, samples were stored in a refrigerator and kept at 4 °C until analysis (Tvermoes et al., 2014). Total mercury concentrations in mineral waters were measured by dual gold amalgamation cold vapour atomic fluorescence spectrometry (CV-AFS) using a Tekran Series 2600 system equipped with pump unit and autosampler (Tekran Corporation Inc., Toronto, (ON), Canada) according to the main procedures outlined in the U.S. EPA Method 1631 version E (US-EPA, 2002) and the European standard (European Committee for Standardization, 2010; ISO 17852, 2006). All water samples were analysed in duplicate, and replicate analysis of each sample was expressed as averaged value.

3.4. Quality assurance and quality control

Two different mercury stock standard solutions SRMs, (standard reference material) for ICP and for AAS, 1000 mg L^{-1} Hg in 12% nitric acid (TraceCERT, Sigma-Aldrich Inc., Saint Louis, MO, USA), were diluted to the required concentrations to prepare the standards for the calibration curve and the initial and ongoing recovery solutions (IPR, OPR), matrix spikes and duplicates (MS, MSD) respectively. Standard and reference solutions were analysed following the same procedures used for water samples. The method gave a linear response in the range of 0.1-100 ng Hg L^{-1} with an R^2 value higher than 0.9998, the average recovery ranged between 96 and 117%. Quality assurance and quality control (QA/QC) processes for Hg analyses were performed by using replicates, laboratory reagent blanks, IPR and OPR standards, and MS/MSD solutions. The mean values of the laboratory blanks measured at each analytical run (0.04 ng L^{-1}, RSD < 20% n = 7) were subtracted from the sample values to determine the sample mercury concentration. The method limit of detection (LOD) was calculated as the blank value plus three times the standard deviation of the 7 replicates of the blank solutions as suggested by US-EPA 2003. The method LOD and quantitation limits (LOQ) were estimated to be 0.03 and 0.09 ng Hg L^{-1} respectively. Such analytical performances are in good agreement with those indicated in U.S. EPA Method 1631 E and are comparable to those reported in recent studies (Sprovieri et al., 2017). The IPR and OPR solutions (about 5 ng L^{-1}) analysed prior sample analysis and subsequently after every 12 samples and gave an average recovery of 101% and 89%, respectively. These values were within the quality control acceptance criteria for method performance in the U.S. EPA Method 1631 E (IPR: 79–121% and OPR: 77–123%). Blank and matrix spiked solutions at different concentration levels were analysed. The results are reported in Table 3. Three Certified Reference Materials (CRMs) for Hg in water, BCR- 579 and ERM- CA615, obtained from the Institute for Reference Materials and Measurements of the European Joint Research Centre (IRMM-JRC) and ORMS-5 produced by the National Research Council of Canada (NRCC), were analysed for quality control purposes, to verify the accuracy and precision of method and to detect possible matrix interferences (Ricci et al., 2016, 2012). Recoveries for the CRMs measured during the analytical run ranged between 78 and 115% as can be seen in Table 4. The Relative Standard Deviations (%RSD) calculated from replicates of the lowest calibration standard as well as for the IPR and OPR, and for spiked BCR-579 solutions were within 10% and thus well below 21%, the limit value as indicated in U.S. EPA Method 1631 E (Quality Control Acceptance Criteria for Performance Tests), showing that the method precision was sactisfactory. Fruitful participation in a global inter-laboratory-comparison-exercises (Brooks Rand Inc., Seattle (WA), USA) for Hg in freshwater samples corroborated the high quality of the analytical data presented here (Sprovieri et al., 2017; Vardè et al., 2014).

3.5. Statistical analysis

Results for Hg are reported in the text both as median and mean values. Median values were used to compare different samples because they are less affected by outliers. Mean values were used to report replicates of the same sample (see Table 2). Pearson correlation coefficients were calculated to examine the possible relationship between Hg concentration and other parameters present on the labels of the bottled water samples (see Table 5). In calculations, Hg concentrations below LOQ were set equal to 0.09 ng L^{-1}. Pearson's correlation and Principal Component Analysis (PCA) were applied to Hg and another 16 parameters reported on bottle labels (T, pH, EC, TDS, CO_2, Na^+, K^+, Ca^{2+}, Mg^{2+}, HCO_3^-, Cl^-, NO_3^-, SO_4^{2-}, F^-, SiO_2, spring elevation). One-way ANOVA and Kruskal-Wallis

Table 4
Total mercury concentrations in Certified Reference Materials (CRMs).

CRM	Certified value ± 95% confidence interval [UoM]	Found ± SD
BCR® - 579 (Coastal seawater)	1.9 ± 0.5 [ng kg^{-1}]	[a]1.94 ± 0.20
ORMS - 5 (Elevated mercury in river water)	26.2 ± 1.3 [pg g^{-1}]	[b]27.44 ± 3.81
ERM® - CA615 (Groundwater)	37 ± 4 [µg L^{-1}]	[c]39.10 ± 3.84

Number of replicates [a]n = 62. [b]n = 8. [c]n = 4

Table 3
Total mercury concentrations in Recovery Solutions and Matrix Spikes.

Solutions	n. of replicates	Quantity of Hg added	Quantity of Hg found		Recovery (%)[a]
IPR (Initial Precision Recovery)	[n = 10]	5.00	5.05	ng L^{-1}	101.0
OPR (Ongoing Precision Recovery)	[n = 20]	5.48	4.89	ng L^{-1}	89.2
Matrix Spike					
Ultra Pure Water	[n = 6]	1.05	1.04	ng L^{-1}	99.0
Natural Mineral Water[b]	[n = 6]	1.12	1.09	ng L^{-1}	97.3
Rainwater[b]	[n = 6]	2.90	2.79	ng L^{-1}	96.2
Seawater[b]	[n = 6]	3.40	3.41	ng L^{-1}	100.3

[a] 100 x [(Found-base)/added].
[b] Base value of real samples has been not reported but subtracted from found value.

Table 5
Summary of Pearson correlation matrix for mercury and parameters considered in this study.

	Hg (ng L^{-1})	T (°C)	pH (20 °C)	EC (20 °C)	TDS (mg L^{-1})	CO_2 (mg L^{-1})	Na^+ (mg L^{-1})	K^+ (mg L^{-1})	Ca^{2+} (mg L^{-1})	Mg^{2+} (mg L^{-1})	HCO_3^- (mg L^{-1})	Cl^- (mg L^{-1})	SO_4^{2-} (mg L^{-1})	NO_3^- (mg L^{-1})	F^- (mg L^{-1})	SiO_2 (mg L^{-1})	Altitude a.s.l. (m)
Hg (ng L^{-1})	**1.00**																
T (°C)	−0.06	**1.00**															
pH (20°C)	−0.34	−0.48	**1.00**														
EC (20 °C)	0.02	0.66	−0.48	**1.00**													
TDS (mg L^{-1})	−0.01	0.64	−0.46	0.98	**1.00**												
CO_2 (mg L^{-1})	0.04	0.47	−0.72	0.71	0.64	**1.00**											
Na^+ (mg L^{-1})	0.19	0.32	−0.24	0.71	0.65	0.52	**1.00**										
K^+ (mg L^{-1})	0.07	0.41	−0.53	0.59	0.51	0.86	0.72	**1.00**									
Ca^{2+} (mg L^{-1})	−0.11	0.53	−0.45	0.79	0.83	0.53	0.16	0.16	**1.00**								
Mg^{2+} (mg L^{-1})	−0.18	0.68	−0.34	0.81	0.87	0.41	0.25	0.18	0.89	**1.00**							
HCO_3^- (mg L^{-1})	0.11	0.37	−0.41	0.88	0.83	0.74	0.83	0.66	0.58	0.49	**1.00**						
Cl^- (mg L^{-1})	0.18	0.51	−0.26	0.69	0.60	0.48	0.93	0.67	0.12	0.26	0.73	**1.00**					
SO_4^{2-} (mg L^{-1})	−0.17	0.60	−0.36	0.71	0.80	0.34	0.10	0.08	0.91	0.97	0.37	0.08	**1.00**				
NO_3^- (mg L^{-1})	0.15	−0.02	−0.16	−0.08	−0.12	0.04	−0.02	0.10	−0.17	−0.04	−0.12	0.09	−0.11	**1.00**			
F^- (mg L^{-1})	−0.12	0.72	−0.61	0.79	0.83	0.67	0.26	0.46	0.85	0.90	0.49	0.26	0.90	−0.01	**1.00**		
SiO_2 (mg L^{-1})	0.04	0.39	−0.72	0.25	0.20	0.78	0.05	0.67	0.23	0.17	0.19	0.09	0.16	0.35	0.52	**1.00**	
Altitude a.s.l. (m)	0.00	−0.66	0.29	−0.34	−0.27	−0.36	−0.24	−0.34	−0.19	−0.21	−0.30	−0.40	−0.11	−0.13	−0.26	−0.32	**1.00**

ANOVA were used to investigate possible differences in Hg concentration between bottled water samples based on their origin, mineral content, and typology, as well as any differences from due to container type (material and colour). A p value < 0.05 was considered as being statistically significant. Graphical and statistical analyses were performed using Statistica 8 software (2008).

4. Results and discussion

4.1. Physico-chemical parameters

Mineral waters showed different physico-chemical characteristics and composition in terms of major and trace elements. In general, the chemical content of bottled water is determined by the lithological composition of the reservoir rocks. Similar types of rock, however, may lead to different types of mineral water. Indeed, the chemical content depends on the amount of mineralizing agents, such as CO_2, redox conditions and complexants (Anke et al., 2009; Birke et al., 2010; Merkel and Planer-Friedrich, 2005; Siegel, 2002; Voigt, 1972). Physico-chemical features were obtained from the bottled water labels. In general, the examined mineral waters showed a mean temperature of 13.04 °C (min 3.20 °C, max 33.30 °C, median 12.35 °C), a mean pH of 7.18 (min 5.28, max 8.40, median 7.31) and a mean electrical conductivity (EC) of 497.67 μS cm^{-1} (min 15.20, max 3630.00, median 399.00).

4.2. Water classification

The water chemistry of bottled waters was initially examined by means of: (a) triangular plots involving major cations and anions expressed as in equivalent units (Fig. 2), as suggested by Zaporozec (1972); (b) correlation graphs of $Ca^{2+}+Mg^{2+}$ vs. $Na^+ + K^+$, where iso-salinity lines have been drawn for reference (see Fig. 3); and, finally, (c) chloride plots (Fig. 4). Some samples were not reported on these graphs due absence of data on their labels. Fig. 2 shows that: (i) roughly 130 mineral water samples belong to the Ca–HCO_3 chemical type. The exceptions are: 5 samples showing Na–Cl composition, 14 samples with Na–HCO_3 composition and 3 samples with Ca–SO_4 composition. Mineral waters showed Total Ionic Salinity (TIS) within the range of 0.28-105 meq L^{-1}, as indicated by the correlation plot $Ca^{2+}+Mg^{2+}$ vs. $Na^+ + K^+$ (Fig. 3). Most of samples (132) fell below the iso-salinity line of 20 meq L^{-1} and only 4 samples were characterized by TIS values higher than 40 meq L^{-1}, probably due to deep thermal conditions and a long residence time of the water in the reservoirs. Chloride plots (Fig. 4) were useful for appraising mixing and other processes occurring in the aquifers, such as calcite precipitation and water-rock interactions. Each diagram was characterized by the presence of the hypothetical dilution line created by starting from the composition of sea water (Nordstrom et al., 1979). The Cl^- vs. Na^+ plot (Fig. 4a) shows that most of samples fell in proximity to, or slightly above, the sea water dilution line, indicating a negligible water-rock interaction. In particular, Na–Cl waters are on the seawater dilution line, and their low salinity, allows them to be considered as immature waters and representative of the rainwater component. Some samples (6) fell slightly above the dilution line suggesting minor water rock interactions with Na-enriched phases, like Albite. Likewise, a Cl^- vs. K^+ plot (Fig. 4b) underlined that most of waters fell close to the sea water dilution line reinforcing the predominance of the rainwater component. In some cases, there were samples above the dilution line suggesting a prolonged water-rock interaction with K-enriched phases, like K-Feldspar, volcanic and evaporitic deposits, etc. Furthermore, all samples showed Ca^{2+}, Mg^{2+} and SO_4^{2-} enrichment (Fig. 4c, d and 4e) probably from water-rock interactions with calcite, dolomite and/or Mg-enriched minerals as biotite and olivine. The SO_4^{2-} probably derives from the dissolution of minerals

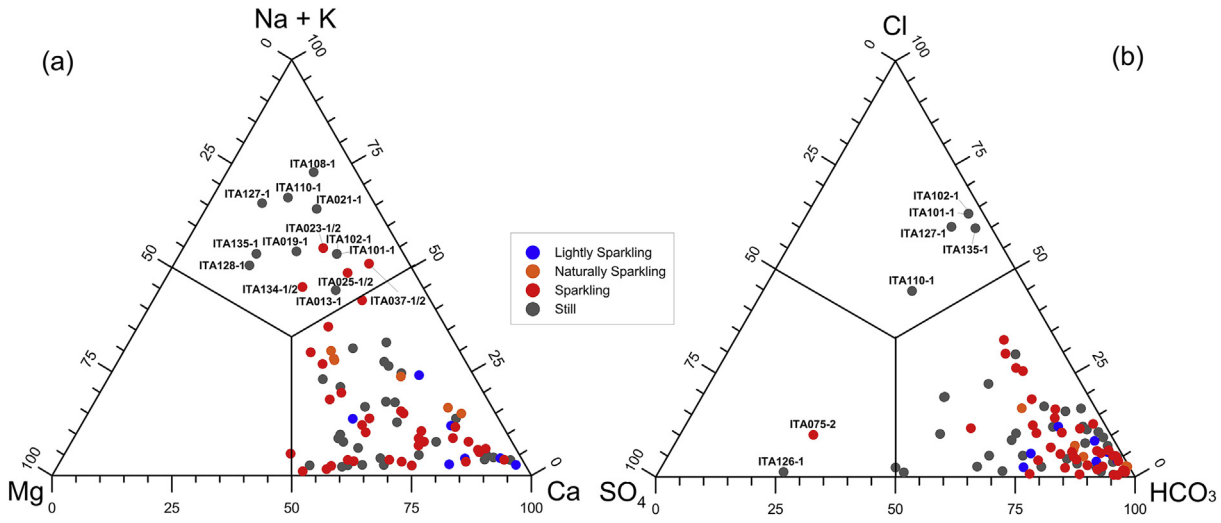

Fig. 2. Triangular plots of (a) major cations and (b) major anions (concentrations in equivalent units).

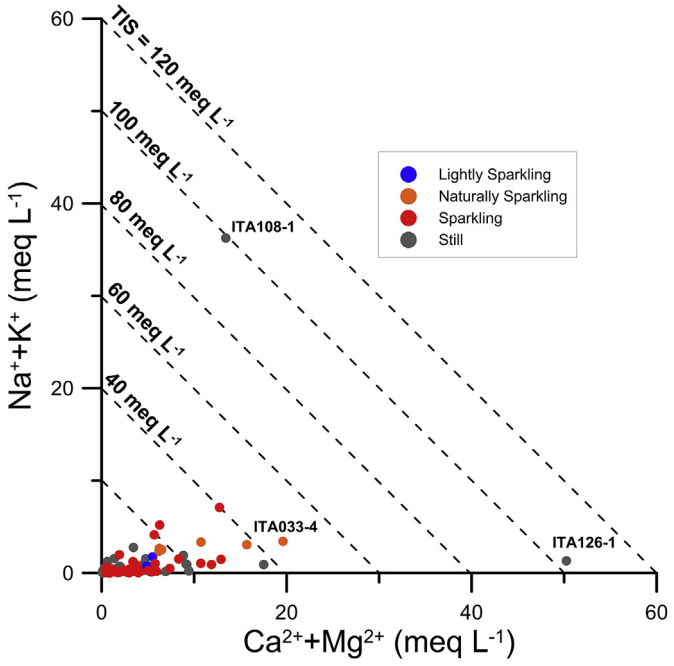

Fig. 3. Correlation diagram of $Na^+ + K^+$ vs. $Ca^{2+} + Mg^{2+}$ showing mineral water samples. Iso-salinity lines are drawn for reference.

like pyrite (oxidative dissolution) and gypsum (Fig. 5). In addition, the set of results summarized in the Pearson correlation table (Table 5) were graphically highlighted by a principal component analysis (PCA) reported in Fig. 6. The first two principal components account for 65.40% of the total data variability. There are very high correlations between groups of system variables (eg $Ca^{2+}+Mg^{2+}$, $Na^+ + K^+$, Cl^-, $CO_2+HCO_3^-$, EC+TDS). The variables of the second quadrant (K^+, Na^+, Cl^-, CO_2, HCO_3^-, SiO_2) are positively correlated to the two variables (Hg, NO_3^-) that characterize the second axis. The variables of the third quadrant ($Ca^{2+}+Mg^{2+}$, $Na^+ + K^+$, Cl^-, $CO_2+HCO_3^-$, EC+TDS) are positively linked to each other and show a slightly negative correlation with those of the second axis (Hg, NO_3^-). The SiO_2 variable is not related to the parameters of the second quadrant, while Fluoride (F^-) is positively tied to the third quadrant variables (excluding temperature) while having a negative relationship with second quadrant variables (excluding silica). In the 4th quadrant, pH and altitude have a weak positive relationship. In conclusion, by considering both the Pearson correlation table and PCA there are not any statistically significant relationships between total mercury concentration and the other considered parameters. However, a weakly positive correlation between Hg and NO_3^-, and (at least qualitatively) an inverse relationship between Hg and pH is suggested (Mann et al., 2003). The increasing Hg concentration with decreasing pH could be due to a prolonged interaction with Hg-bearing metal-sulfides that can induce pH decreases (Fig. 6), as suggested in previous studies (Boszke et al., 2002; Mann et al., 2003).

4.3. Mercury concentration in bottled waters

4.3.1. Sampling size

A total of 244 different bottled waters from Italy and 11 from other EU Countries were analysed to determine their Hg concentration. Three (or more) bottled waters were analysed for each water typology to check inter- and intra-sample variability, these were found to be lower than 5% and 1%, respectively. Hg_T was found at concentration above the LOD in 209 of 244 Italian bottled waters (86% of total). Results on mercury concentrations are summarized in Fig. 7 (Boxplot comparison of Hg concentrations), while all parameters reported on the bottle label (i.e. pH, EC, TDS etc.) are reported in Table S3. Total mercury was found at ultra trace levels in Italian bottled waters. Concentrations indeed ranged from <0.09 to 5.39 ng L^{-1}, with a mean of 0.33 ± 0.41 ng L^{-1}; the median was 0.26 ng L^{-1}. Preliminary results on Hg_T in Italian mineral natural waters were presented for bottled waters from Calabria and Campania (Vardè et al., 2015; Vardè et al., 2017). For 11 bottled waters from other EU countries, mercury was in the concentration range of 0.12-0.36 ng L^{-1}, with a mean of 0.22 ± 0.07 ng L^{-1}; and median of 0.22 ng L^{-1} (Fig. 7a). Thirty-eight bottle waters out of 255 (corresponding to 15%) had mercury concentrations below the LOQ; in 152 samples, mercury was in the range between < 0.09-0.26 ng L^{-1} (59.61%), while 100 bottle samples had Hg_T between 0.27 and 0.97 ng L^{-1} (39%). Only for three different italian brands (1.8%), had Hg_T values as high as 1.0 ng L^{-1}. Of these, two were from Tuscany, and the other from Campania. To evaluate differences in mercury concentrations in bottled waters considered in this study, samples were subdivided on the basis of (in parenthesis number of samples): i) national origin either Italy (244) or EU (11); ii) typology:

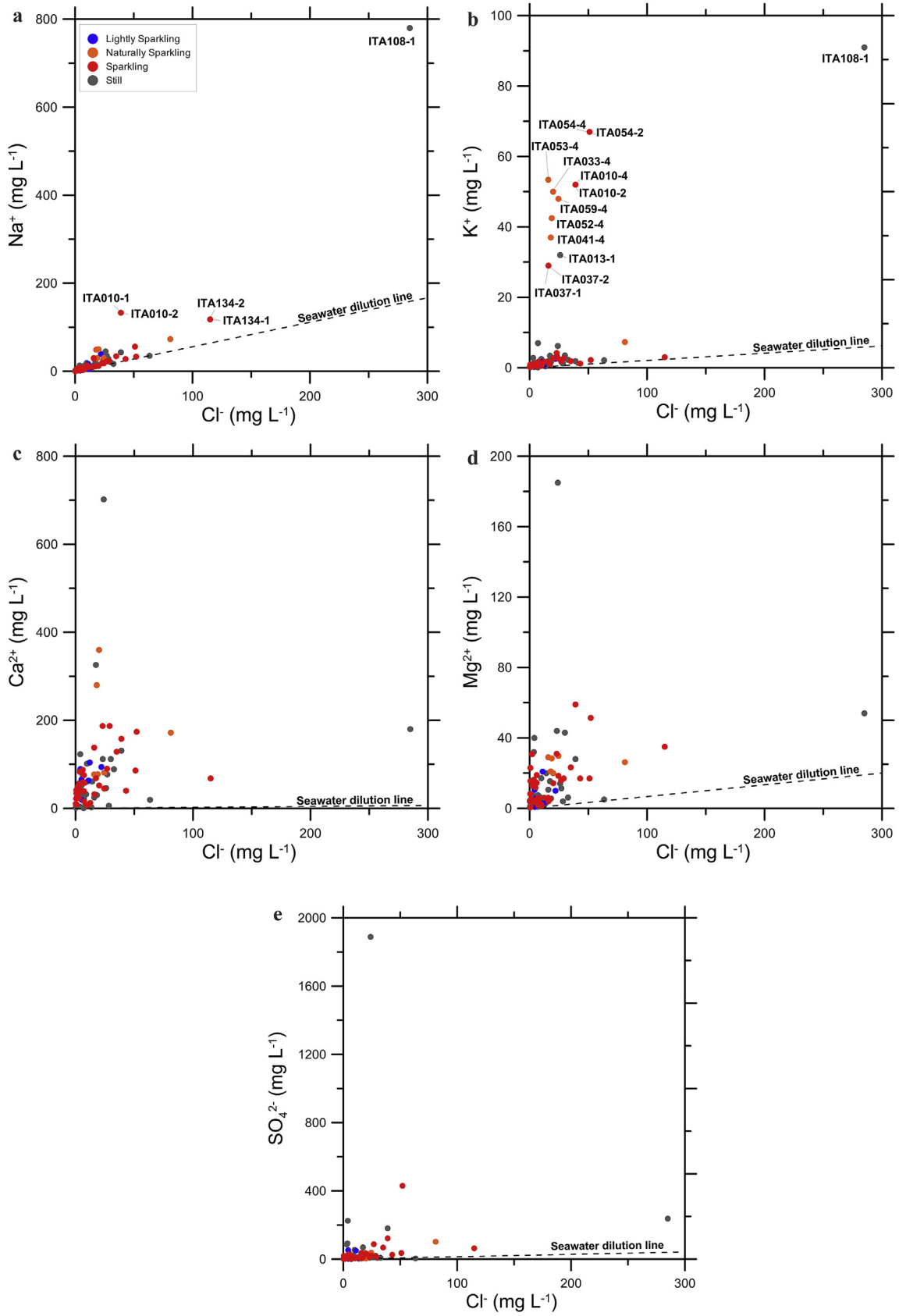

Fig. 4. Correlation diagram of Na^+ vs. Cl^- (a).K^+ vs. Cl^- (b).Ca^{2+} vs. Cl^- (c).Mg^{2+} vs. Cl^- and SO_4^{2-} vs. Cl^- (d) showing Italian mineral water samples.

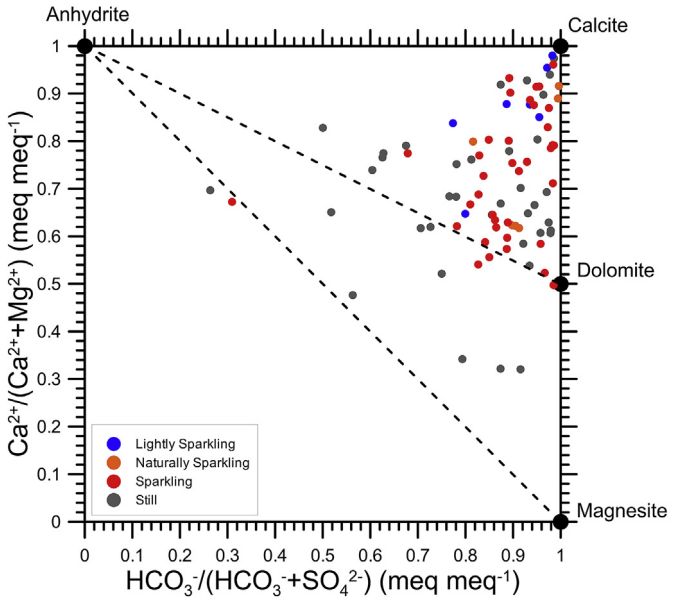

Fig. 5. Modified Langelier-Ludwig diagram where $HCO_3^-/(HCO_3^-/SO_4^{2-})$ (meq meq^{-1}) are plotted against $Ca^{2+}/(Ca^{2+}+Mg^{2+})$ (meq meq^{-1}).

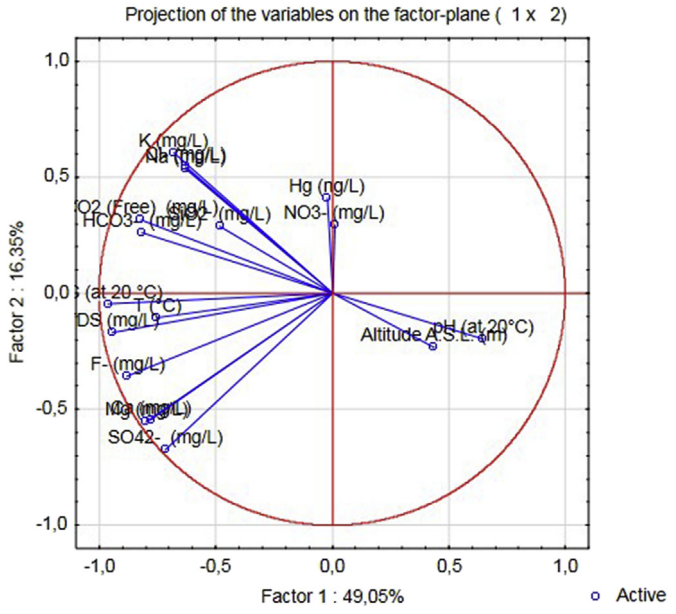

Fig. 6. Correlation circle graph for all variables of this study.

still (144), sparkling (63), lightly sparkling (29) and naturally sparkling (19); iii) mineral content: very low (28), low (184), intermediate (35) and high (7); iv) geographical zone: southern, central, northern and, finally, (v) region by region (see Table 2 and S1). Mean values of Hg_T were not statistically different between the different categories in which the samples were divided. Indeed, for non carbonated and carbonated waters (Fig. 7b) values of 0.31 ± 0.21 ng L^{-1} and 0.35 ± 0.53 ng L^{-1} were obtained, respectively; for still, sparkling, naturally sparkling and lightly sparkling waters, the following values were found: 0.35 ± 0.53 ng L^{-1}, 0.30 ± 0.19 ng L^{-1}, 0.44 ± 0.36 ng L^{-1} and 0.27 ± 0.08 ng L^{-1} (see Fig. 7c); for waters with different mineral content, Hg_T was 0.51 ± 1.03 ng L^{-1}, 0.28 ± 0.19 ng L^{-1}, 0.42 ± 0.28 ng L^{-1} and 0.31 ± 0.22 ng L^{-1} (see Fig. 7d). Analogous conclusions can be drawn for waters coming from different geographical zones such as southern, central, northern Italy (see Fig. 7e and f). A possible explanation for such low Hg_T concentrations in Italian mineral water can be found in light of the geological structure of the aquifers, the occurrence and amount of organic matter and clay fractions (Sposito, 1989), and the texture and pH of the soil, which altogether contribute to a low mobility for Hg, so it stays strongly adsorbed onto particle surfaces (Różański et al., 2016). To conclude this paragraph, in Fig. 8a, the elevation (m) vs. Hg_T (ng L^{-1}) plot is reported. Mean and median concentrations of Hg were reported for each altitude class. Four altitude classes have been grouped at around 500 m altitude intervals. Although, the correlation is not statistically significant, the qualitative decrease of Hg_T with increasing altitude could be due to evaporative effects and/or prolonged water rock interaction, which for low-altitude areas is evidenced by the higher concentration of mobile elements such as chloride (see Fig. 8b) (Boszke et al., 2002).

4.3.2. *Tuscany and Campania anomalies*

The highest Hg_T values were found for ITA127-1 and ITA135-1 samples (5.39 ng L^{-1} and 1.74 ng L^{-1} respectively). In both cases, they were still waters from springs located in the North-West of Tuscany (see Fig. 7c and f). A possible explanation can be found in past Tuscan mining activities (Levigliani, Tuscany). Mercury has been extracted in the past from the metamorphic basement (Hercynian basement) outcropping in the area and made up by phyllites, quartzites, calcschists, metalimestones, dolostones, graphitic shales and metavolcanic rocks. Local lithology and former mining activities for extraction and processing of Cinnabar (HgS) influenced Hg concentrations in groundwater system located in a large area of southern Tuscany close to Mt. Amiata as confirmed by recent studies (Vaselli et al., 2015). In a previous paper, bottled water samples from Tuscany had shown several different elements and ions above the Italian law thresholds which was explained by the authors as due to the presence of thermal sources (Naddeo et al., 2008). In addition, the water sample (naturally sparkling) from Roccamonfina, a volcanic aquifer in the province of Caserta, Campania, had a concentration of 1.24 ng L^{-1} (see Fig. 7e and f). This result is in agreement with that reported by (Bagnato et al., 2009).

4.3.3. *Packaging material and preservation influence on Hg measurements in environmental samples*

The use, preparation and storage of appropriate material containers for sampling environmental matrices for mercury has been evaluated in previous works. Contamination and losses of mercury have been reported for seawater samples, stored in PE bottles, due to the passage of gaseous Hg from ambient air to the sample or vice versa through the walls of the container (Bothner and Robertson, 1975). Hg contamination of water samples treated and preserved in different containers (of both glass and polymeric materials) has been verified even with different laboratory handling techniques using different oxidizing reagents (Cragin, 1979). In one study, the influence of containers materials (HDPE, PP, FEP and PFA) and acid treatment on the concentrations of 62 elements in water was investigated. Among all the metals considered, mercury (II) was recognized as having the characteristic of adsorbing on the bottle surface. Between the different types of polymeric materials used, and whether a pre and after washing-treatment had been carried out, the Hg concentration measured did not show any noticeable discrepancies (Reimann et al., 1999). To preserve the samples, and avoid blank problems we have used pre acid-cleaned on FEP containers with acidification of the samples with low Hg HCl (0.5% v/v) and the subsequent treatment with BrCl (Parker and Bloom, 2005). Under these conditions both Teflon and glass containers have been demonstrated to preserve aqueous samples containing Hg at ppt

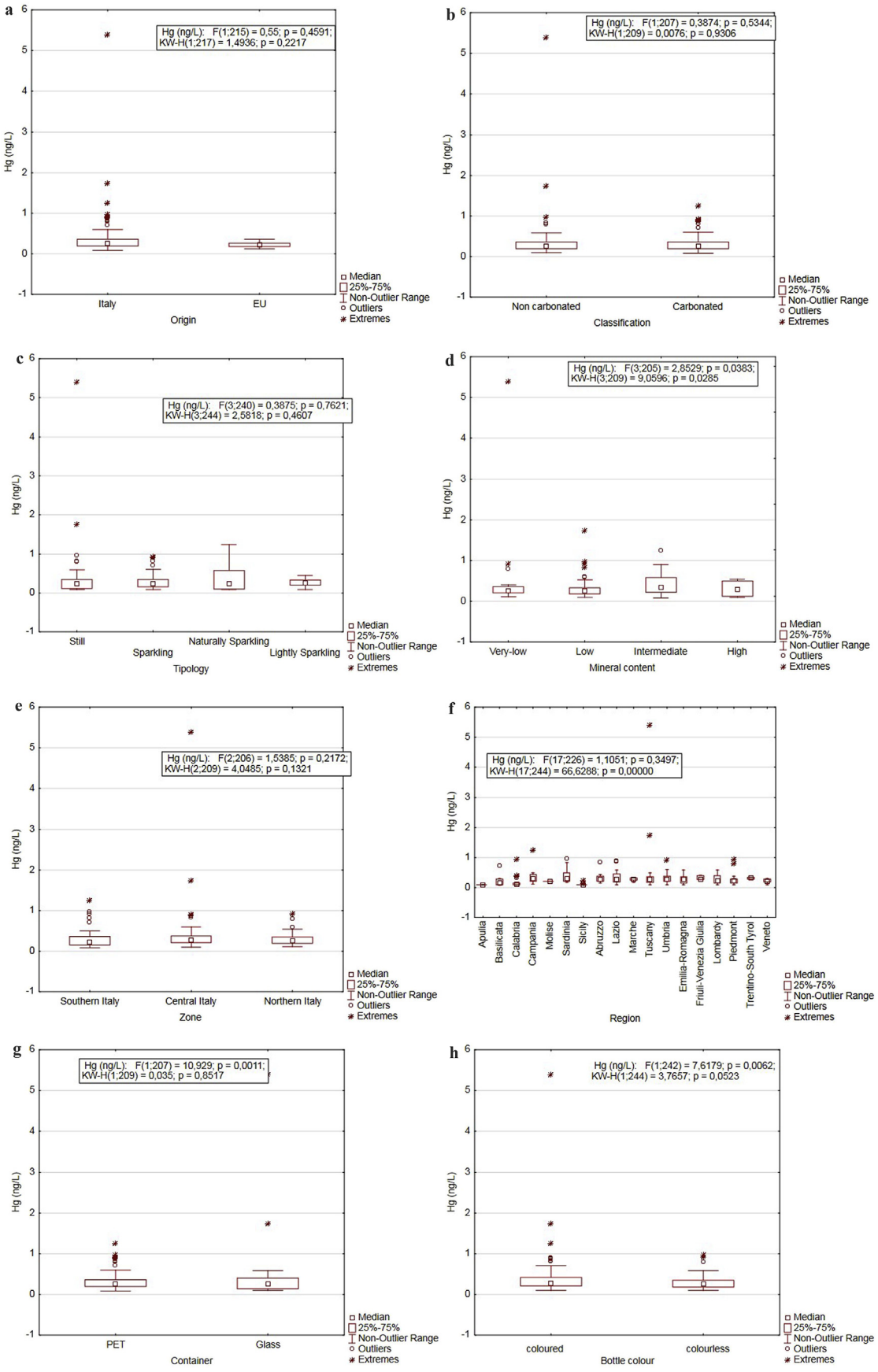

Fig. 7. a-h. Boxplot comparison of Hg concentration in (a) different bottle waters from Italy (n = 244) and EU (n = 11); (b) carbonated and non-carbonated bottled water samples from Italy; (c) different tipologies of bottled water samples from Italy; (d) bottled water samples with different mineral content from Italy; (e) different macro area of Italy; (f) Italian bottled waters region by region; (g) in different container; (h) different colour of bottled waters.

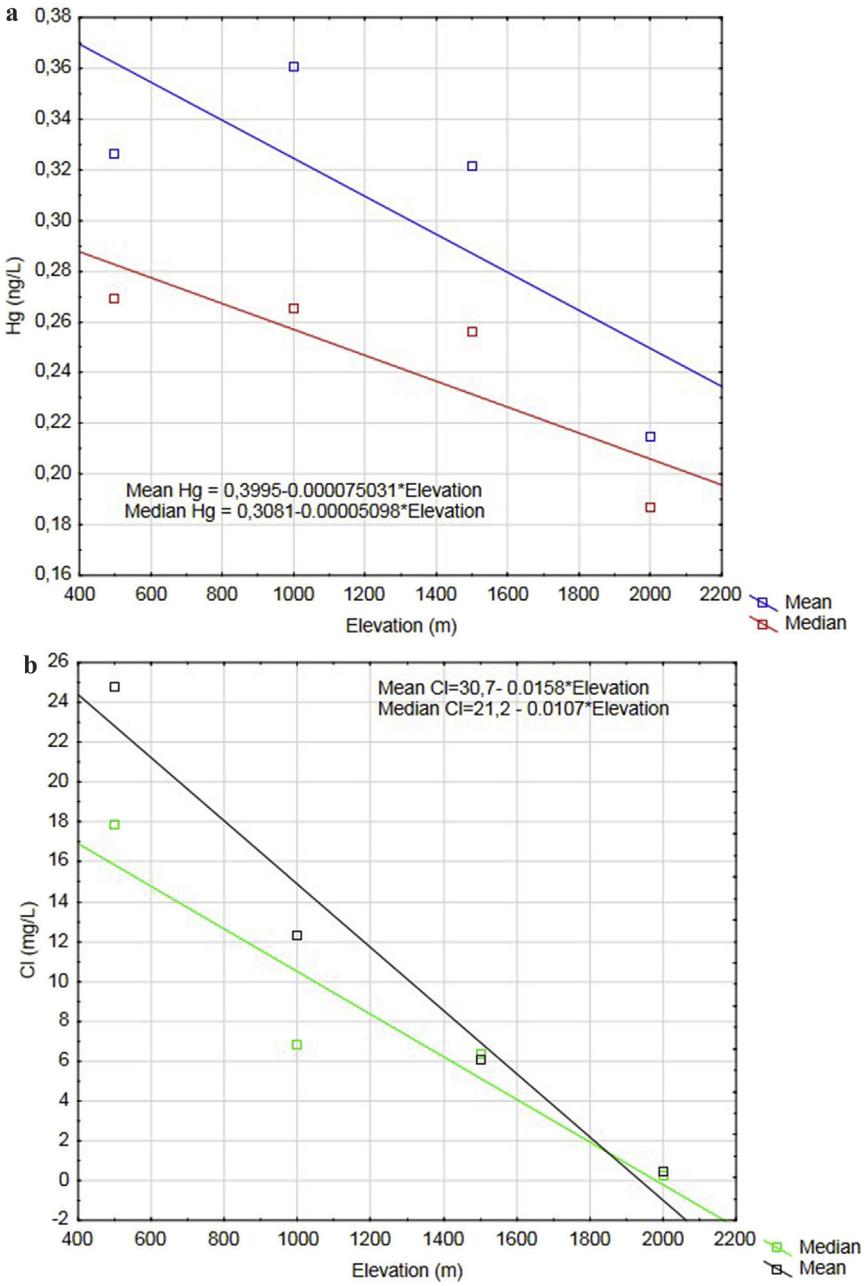

Fig. 8. Elevation spring (m) vs Hg (mean and median) concentration (ng L^{-1}) (a); vs Cl^- (mean and median) concentration (mg L^{-1}) (b).

concentrations for up to at least 1 year. Comparison of Hg_T levels in Italian bottled waters packaged either in glass (21) or in PET (234) are shown on box plot in Fig. 7g. As it can be seen, Hg_T median values between different containers (glass 0.62 ± 1.21 ng L^{-1}, PET 0.30 ± 0.18 ng L^{-1}) were not statistically significant. As previously mentioned, differences in a few outlier values are probably not attributable to different container materials. In addition, the colour of both type of containers, glass and PET, was evaluated. The bottle colour (coloured and not coloured) had no influence on the concentration of Hg_T in the two groups (Fig. 7h), such as reported in a previous study where authors described results on leaching of sixty chemicals, included Hg, for both coloured/non-coloured in both glass and PET bottles used as containers of natural mineral waters (Reimann et al., 2012).

5. Estimation of risk of human exposure to Hg from bottled waters

The major source of human exposure to mercury is through food, such as in fish and shellfish, as methyl mercury. Inorganic mercury Hg^{2+} is considered the main form of Hg in drinking water, in the absence of anthropogenic contamination. Only under particular conditions can it be transformed into more toxic organic compounds (Baldi, 1997; Ullrich et al., 2001). In 2005, the WHO estimated an average daily intake of 1 μg Hg from water, assuming a concentration of 0.5 μg L^{-1} in drinking water. This resulted in a guideline value of 6 μg L^{-1} of Hg in water, to keep the TDI (total daily intake) for a 60 kg adult, drinking 2 L of water a day, below 10% of the total TDI from food (2 μg kg^{-1}) (WHO - World Health Organization, 2005). Considering that the average intake of total

Table 6
Daily (D_T) and estimated weekly intake (EWI) and hazard quotient (HQ) for Hg_T calculated from bottled water concentrations for adults, children and toddlers.

	Calculated from bottled water concentrations (this work)			From literature values for fish[a], or fish and shellfish[b]		
Group of population	D_T	EWI	HQ [e]	EWI [a]	EWI [b, c]	EWI [b, d]
Adults	1.10E-05	7.70E-05	3.66E-05	0.45–1.35	0.8–3.2	n.d. – 4.6
Children	4.80E-05	3.36E-04	1.60E-04	n.a.	1.3–5.5	n.d. – 8.0
Toddlers	7.30E-05	5.11E-04	2.43E-04	n.a.	n.a.	n.a.

D_T and EWI were expressed as μg kg^{-1} (Bw) d^{-1}; μg kg^{-1} (Bw) w^{-1} respectively.
n.d. = not detected; n.a. = not available.
[a] Jinadasa et al. (2014).
[b] Spada et al. (2012).
[c] Hg_T from fish.
[d] Hg_T from shellfish.
[e] HQ < 1 suggests no health risk effect for a healthy exposed population; HQ > 1 indicates an increasing probability for the occurrence of harmful effects in the exposed population; HQ = 1 is the safe level limit value.

mercury assumed through food is in the range 2-20 μg d^{-1} with only 10% of the TDI allocated to drinking water, in 2011 the Committee has decided to set a provisional tolerable weekly intake (PTWI) for inorganic mercury of 4 μg kg^{-1} of body weight (Bw) lowering the previous value (5 μg kg^{-1} d^{-1}) fixed in 1972 by the Joint FAO/WHO Expert Committee on Food Additives (JECFA). Assuming that we only have inorganic mercury in drinking water, as per the indications by WHO (FAO et al., 2011; WHO - World Health Organization, 2011, 2008, 2005) and total mercury data obtained in this study, can be used to estimate the mercury intake from the consumption of bottled water in Italy. Following the approach proposed by previous authors (Ayedun et al., 2015; Batayneh, 2010), the Hg dose was calculated as follows using equation (1).

$$D_T = \frac{D_w \text{ x } C_{Hg}}{Bw} \quad (1)$$

where:

D_T is the calculated dose taken, from water (μg kg^{-1} d^{-1}), Dw represents the average volume of bottled water consumed every day (L d^{-1}), C_{Hg} is the average concentration of mercury (μg L^{-1}) and Bw represents the average body weight (kg). Considering that an adult has an average weight of 60 kg and 2 L daily water consumption, one gets a value of:

D_T (adults) = 1.10E-05 μg kg^{-1} (Bw) d^{-1}

However, children take 70–75% of their total liquid consumption from water and products prepared from drinking water, but mercury has the same limit values for adults and children/infants in agreement with the WHO (WHO, 2011), making them the subpopulation most sensitive to chemical contaminants (Balbus and Lang, 2001). On the Italian market 38 out of the 244 samples were sold as bottled water intended for consumption by infants. The mean Hg value in these was found to be 0.48 ng L^{-1}, so the Hg dose taken by children and toddlers was estimated by considering only these samples. Using equation (1), the following data were obtained for a child with an average weight of 10 kg with 1 L of daily water consumption, and for toddlers (infants) with an average weight of 5 kg with a water consumption of 0.75 L:

D_T (children) = 4.80E-05 μg kg^{-1} (Bw) d^{-1}

D_T (toddlers) = 7.3 E-05 μg kg^{-1} (Bw) d^{-1}

So, despite drinking waters suggested for consumption by infants and children, and in lower quantities than adults, the daily mean consumption of Hg from bottled water follows the trend: toddlers (infants) > children > adults.

For comparison, these values can be converted into an EWI (Estimated Weekly Intake) by multiplying by 7 the D_T values. The calculated results are reported in Table 6. In addition, a risk assessment can be performed by a comparative analysis between a reference dose (RfD) and the mean daily exposure to mercury (D_T) by calculating a hazard quotient (HQ) for the three age groups according to the following formula (equation (2)):

$$HQ = \frac{D_T}{RfD} \quad (2)$$

where RfD is the reference dose for $HgCl_2$, which has an established value of 3.00E-04 mg kg^{-1} d^{-1} (US-EPA, 1995). The HQ values obtained for adults, children and toddlers (infants) are reported in Table 6. The values found are several orders of magnitude under the value obtained if the reference dose is consumed, resulting in an HQ value of 1 and is indicative of the maximum concentration with an acceptable risk. The quantification of these HQs related to the average intake of mercury from bottled water should be useful when evaluating the total mercury exposure from food, so a mercury hazard index (HI) can be calculated for the entire population of Italy. These findings highlight the fact that the assumption of Hg from natural mineral water bottled in Italy is orders of magnitude lower than the Hg_T consumed from fish and seafood (Jinadasa et al., 2014; Spada et al., 2012), reported for comparison in Table 6. Our results obtained for both Hg concentrations in bottled waters on a national (Italian) scale and and the calculated daily dose of Hg taken by different groups of the Italian population confirmed that the mean mercury daily intake was widely lower than the provisional tolerable daily intake suggested by the JEFCA. Along with the EWI data and HQ data, this suggest that there is little or no risk for mercury consumption from Italian bottled waters at the present time.

6. Overview and conclusions

Hg is one of the more toxic hazardous trace elements and it is ubiquitous in the environment. Therefore, measuring Hg levels on a national scale in environmental matrices is very relevant. This is confirmed by the priorities established in the Minamata Convention which proposed controls on it's use in artisanal mining and industry, with the aim of reducing Hg release into the environment. This should protect human health as well as the environment. To date, for Hg, there are no systematic or comprehensive studies on its occurrence in natural mineral waters. Therefore, it was not possible to estimate mercury intake with drinking water (see Studies on bottled mineral waters in literature in Supplemenary Information). The bottled waters considered in our study showed quantities of mercury at ultra-trace levels from 0.09 to 5.39 ng L^{-1}. Despite considerable variability in the water sources, a low

variability of the Hg amount between water typologies (mineral content, carbonated and not carbonated samples), regional origins and packaging materials, suggests that the aquifers from which groundwater is drawn and bottled are not in general affected by anthropogenic contamination. However, we found a few brands from Tuscany and Campania with higher concentration of Hg compared to the mean and median values of all the other water samples. We ascribe this to the geological structure of the aquifer and thermal and volcanic activity as well as former metal extraction activities from mines. The data collected in this work on Hg concentrations in Italian bottled waters provides information missing from previous studies and confirms what was already known about Hg in bottled water, and generally in aquifers exploited for the potable water supply in Italy (ARPAV - Agenzia Regionale per la Prevenzione e Protezione Ambientale del Veneto, 2013). This hopefully will improve our understanding of the processes and mechanisms related to mobilisation of toxic elements. Our analytical results demonstrate a natural (geogenic) presence of this potentially harmful element at a very low level, which implies good water quality and a safe geological environment with respect to Hg contamination. Being one thousand times below the maximum allowable concentration (MAC) of EU and Italian legislation ($1\ \mu g\ L^{-1}$), mercury concentrations in Italian natural mineral waters should not cause for any adverse health effects as evidenced by the daily and weekly intake values found in this study resulting in very low HQ (hazard quotient) results.

Acknowledgements

This work was funded by the authors themselves. The mention of commercial products does not constitute approval or recommendation by the authors. We are very grateful to Dr. Mario Gensini and Mr. Valentino Mannarino that respectively helped us to collect samples and log bottled waters in the laboratory. We thank the Institute for Atmospheric Pollution Research of the Italian National Research Council (CNR-IIA) that allowed us to perform all the analytical steps and instrumental analysis in their laboratories at the unit in Calabria. Our thanks are due to Dr. Riccardo Ferrante, Department of Medicine, Epidemiology, Hygiene and Environment (DiMEILA), INAIL Research Centre, Monte Porzio Catone (Rome), Italy, for giving support in searching and selecting public health publications of our interest in this topic. The manuscript was reviewed, and helpful suggestions and language editing were provided by Dr. Maddalena Parafati, and Prof. Alessandro Scarso to whom that are acknowledged with gratitude.

Appendix A. Supplementary data

Supplementary data to this article can be found online at https://doi.org/10.1016/j.chemosphere.2018.12.020.

References

D'Ascenzo, F., Laureti, T., Troi, G., Vinci, G., 1997. Analisi statistica multivariata nel confronto tra acque di reti e acque minerali. Acqua - Ind. delle Bevande XXVI, 377–382.

Allen, H.E., Halley-Henderson, M.A., Hass, C.N., 1989. Chemical Composition of Bottled Mineral Water. Arch. Environ. Heal. AEHLEV 44 (9896), 18. https://doi.org/10.1080/00039896.1989.9934383.

Anke, M., Seeber, O., Müller, R., Schäfer, U., Zerull, J., 2009. Uranium transfer in the food chain from soil to plants, animals and man. Chemie der Erde - Geochemistry 69, 75–90. https://doi.org/10.1016/j.chemer.2007.12.001.

Apollaro, C., Vespasiano, G., Muto, F., De Rosa, R., Barca, D., Marini, L., 2016. Use of mean residence time of water, flowrate, and equilibrium temperature indicated by water geothermometers to rank geothermal resources. Application to the thermal water circuits of Northern Calabria. J. Volcanol. Geotherm. Res. 328, 147–158. https://doi.org/10.1016/j.jvolgeores.2016.10.014.

Arpadjan, S., Vuchkova, L., Kostadinova, E., 1997. Sorption of Arsenic, Bismuth, Mercury, Antimony, Selenium and Tinon Dithiocarbamate Loaded Polyurethane Foam as a Preconcentration Methodfor Their Determination in Water Samples by Simultaneous Inductively Coupled Plasma Atomic Emission Spectrometry and E. Analyst 122, 243–246.

ARPAV - Agenzia Regionale per la Prevenzione e Protezione Ambientale del Veneto, 2013. Monitoraggio d'indagine delle acque sotterranee in alcuni comuni della provincia di Treviso per lo studio delle modalità di propagazione del plume di inquinamento da mercurio (Hg) - MeMo. ARPAV - Relazione Conclusiva ottobre 2013, 1–27.

Ask, K., Akesson, A., Berglund, M., Vahter, M., 2002. Inorganic mercury and methylmercury in placentas of Swedish women. Environ. Health Perspect. 110, 523–526.

Ayedun, H., Gbadebo, A.M., Idowu, O.A., Arowolo, T.A., 2015. Toxic elements in groundwater of Lagos and Ogun States, Southwest, Nigeria and their human health risk assessment. Environ. Monit. Assess. 187. https://doi.org/10.1007/s10661-015-4319-7.

Bagnato, E., Parello, F., Valenza, M., Caliro, S., 2009. Mercury content and speciation in the Phlegrean Fields volcanic complex: Evidence from hydrothermal system and fumaroles. J. Volcanol. Geotherm. Res. 187, 250–260. https://doi.org/10.1016/j.jvolgeores.2009.09.010.

Balbus, J.M., Lang, M.E., 2001. Is the water safe for my baby? Pediatr. Clin. North Am. 48, 1129–1152. https://doi.org/Doi 10.1016/S0031-3955(05)70365-5.

Baldi, F., 1997. Microbial Tbansformation of Mercury Species and Their Importance in the Biogeochemical Cycle of Mercury. In: Sigel, A., Sigel, H. (Eds.), Metal Ions in Biological Systems: Mercury and Its Effects on Environmént and Biology. New York, USA, pp. 213–257 chp. 8.

Batayneh, A.T., 2010. Heavy metals in water springs of the Yarmouk Basin, North Jordan and their potentiality in health risk assessment. Int. J. Phys. Sci. 5, 997–1003.

Beccaluva, L., Bianchini, G., Siena, F., 2004. Tertiary–quaternary volcanism and tectonomagmatic evolution in Italy. In: Special Volume of the Italian Geological Society for the IGC 32 Florence, pp. 153–160.

Bertoldi, D., Bontempo, L., Larcher, R., Nicolini, G., Voerkelius, S., Lorenz, G.D., Ueckermann, H., Froeschl, H., Baxter, M.J., Hoogewerff, J., Brereton, P., 2011. Survey of the chemical composition of 571 European bottled mineral waters. J. Food Compos. Anal. 24, 376–385. https://doi.org/10.1016/j.jfca.2010.07.005.

Beverfood, 2016. Bevitalia Acque Minerali, Bibite e Succhi 2016-2017. Bervefood srl 1–389.

Bhan, A., Sarkar, N.N., 2005. Mercury in the Environment: Effect on Health and Reproduction. Rev. Environ. Health 20, 1161–1208. https://doi.org/10.1515/REVEH.2005.20.1.39.

Birke, M., Rauch, U., Harazim, B., Lorenz, H., Glatte, W., 2010. Major and trace elements in German bottled water, their regional distribution, and accordance with national and international standards. J. Geochemical Explor. 107, 245–271. https://doi.org/10.1016/j.gexplo.2010.06.002.

Bloom, N., Fitzgerald, W.F., 1988. Determination of volatile mercury species at the picogram level by low-temperature gas chromatography with cold-vapour atomic fluorescence detection. Anal. Chim. Acta 208, 151–161. https://doi.org/10.1016/S0003-2670(00)80743-6.

Bono, P., Boni, C., 2001. Mineral waters in Italy, LaMoreaux,. In: Springs and Bottled waters of the world. Springer Berlin Heidelberg, Berlin, Heidelberg. https://doi.org/10.1007/978-3-642-56414-7.

Boszke, L., Głosińska, G., Siepak, J., 2002. Some Aspects of Speciation of Mercury in a Water Environment. Polish J. Environ. Stud. 11, 285–298.

Bothner, M.H., Robertson, D.E., 1975. Mercury Contamination of Sea Water Samples Stored in Polyethylene Containers. Anal. Chem. 47, 592–595. https://doi.org/10.1021/ac60353a012.

Cairns, W.R.L., Ranaldo, M., Hennebelle, R., Turetta, C., Capodaglio, G., Ferrari, C.F., Dommergue, A., Cescon, P., Barbante, C., 2008. Speciation analysis of mercury in seawater from the lagoon of Venice by on-line pre-concentration HPLC-ICP-MS. Anal. Chim. Acta 622, 62–69. https://doi.org/10.1016/j.aca.2008.05.048.

Cicchella, D., Albanese, S., De Vivo, B., Dinelli, E., Giaccio, L., Lima, A., Valera, P., 2010. Trace elements and ions in Italian bottled mineral waters: Identification of anomalous values and human health related effects. J. Geochemical Explor. 107, 336–349. https://doi.org/10.1016/j.gexplo.2010.04.004.

Ciotoli, G., Guerra, M., 2016. Distribution and physico-chemical data of Italian bottled natural mineral waters. J. Maps 12, 917–935. https://doi.org/10.1080/17445647.2015.1096846.

Civita, M.V., 2008. L'assetto idrogeologico del territorio italiano: risorse e problematiche. Quad. della Soc. Geol. Ital. 3, 1–34.

Clifton, J.C., 2007. Mercury Exposure and Public Health. Pediatr. Clin. North Am. 54 (237) e1-237.e45. https://doi.org/10.1016/j.pcl.2007.02.005.

Cragin, J.H., 1979. Increased Mercury Contamination of Distilled and Natural Water Samples Caused by Oxidizing Preservatives. Anal. Chim. Acta 110, 313–319.

de Wuilloud, J.C.A., Wuilloud, R.G., Silva, M.F., Olsina, R.A., Martinez, L.D., 2002. Sensitive determination of mercury in tap water by cloud point extraction preconcentration and flow injection-cold vapor-inductively coupled plasma optical emission spectrometry. Spectrochim. Acta Part B-Atomic Spectrosc. 57, 365–374. https://doi.org/10.1016/s0584-8547(01)00393-7.

Dieguez-Acuña, F.J., Polk, W.W., Ellis, M.E., Simmonds, P.L., Kushleika, J.V., Woods, J.S., 2004. Nuclear factor κB activity determines the sensitivity of kidney epithelial cells to apoptosis: Implications for mercury-induced renal failure. Toxicol. Sci. 82, 114–123. https://doi.org/10.1093/toxsci/kfh236.

Dinelli, E., Lima, A., Albanese, S., Birke, M., Cicchella, D., Giaccio, L., Valera, P., De Vivo, B., 2012. Comparative study between bottled mineral and tap water in

Italy. J. Geochemical Explor. 112, 368–389. https://doi.org/10.1016/j.gexplo.2011.11.002.
D.Lgs 31/2001 (Legislative Decree), 2001. Decreto Legislativo 2 febbraio 2001 , n. 31 - Attuazione della direttiva 98/83/CE relativa alla qualità delle acque destinate al consumo umano. Gazz. Uff. della Repubb. Ital. 52, 1–23 del 3 marzo 2001 - Suppl. Ordin. n. 41.
98/83/EC, 1998. Council Directive 98/83/EC of 3 November 1998 on the quality of water intended for human consumption. Off. J. Eur. Communities L 330.
2003/40/EC, 2003. Commission Directive 2003/40/EC of 16 May 2003 establishing the list, concentration limits and labelling requirements for the constituents of natural mineral waters and the conditions for using ozone-enriched air for the treatment of natural mineral water. Off. J. Eur. Union L 126 (34).
2009/54/EC, 2009. Directive 2009/54/EC of the European Parliament and of the Council of 18 June 2009 on the exploitation and marketing of natural mineral waters. Off. J. Eur. Union L 164 (45).
Eisler, R., 2004. Mercury Hazards from Gold Mining to Humans, Plants, and Animals. Rev Env. Contam Toxicol. 181, 139–198. https://doi.org/10.1007/0-387-21733-9_4.
Ernst, E., Lauritsen, J.G., 1991. Effect of Organic and Inorganic Mercury on Human Sperm Motility. Pharmacol. Toxicol. 68, 440–444. https://doi.org/10.1111/j.1600-0773.1991.tb01267.x.
European Committee for Standardization, 2010. EN 15853:2010 Ambient air quality - Standard method for the determination of mercury deposition. Eur. Comm. Stand.
Falahee, M., MacRae, A.W., 1995. Consumer appraisal of drinking water: Multidimensional scaling analysis. Food Qual. Prefer. 6, 327–332. https://doi.org/10.1016/0950-3293(95)00035-6.
FAO, WHO, JEFCA, 2011. Safety Evaluation of Certain Contaminants in Food. WHO Food Addit. Ser. 63, FAO JECFA Monogr 8, 778.
Fitzgerald, W.F., Gill, G.A., 1979. Subnanogram Determination of Mercury by Two-Stage Gold Amalgamation and Gas Phase Detection Applied to Atmospheric Analysis. Anal. Chem. 51, 1714–1720. https://doi.org/10.1021/ac50047a030.
Geng, W., Nakajima, T., Takanashi, H., Ohki, A., 2008. Determination of mercury in ash and soil samples by oxygen flask combustion method-Cold vapor atomic fluorescence spectrometry (CVAFS). J. Hazard Mater. 154, 325–330. https://doi.org/10.1016/j.jhazmat.2007.10.029.
Gill, G.A., Fitzgerald, W.F., 1987. Picomolar mercury measurements in seawater and other materials using stannous chloride reduction and two-stage gold amalgamation with gas phase detection. Mar. Chem. 20, 227–243. https://doi.org/10.1016/0304-4203(87)90074-0.
Graham, N., 1999. Guidelines for Drinking-Water Quality, 1998, second ed. In: Addendum to Volume 1 – Recommendations. World Health Organisation, Geneva, p. 36. Urban Water. https://doi.org/10.1016/S1462-0758(00)00006-6.
Harada, M., 1968. Minamata Disease, Study Group of Minamata Disease.
Hussain, S., Rodgers, D.A., Duhart, H.M., Ali, S.F., 1997. Mercuric chloride-induced reactive oxygen species and its effect on antioxidant enzymes in different regions of rat brain. J. Environ. Sci. Heal. Part B 32, 395–409. https://doi.org/10.1080/03601239709373094.
ISO 17852, 2006. Water quality — Determination of mercury — Method using atomic fluorescence spectrometry. Int. Organ. Stand.
Ito, R., Kawaguchi, M., Sakui, N., Okanouchi, N., Saito, K., Seto, Y., Nakazawa, H., 2009. Stir bar sorptive extraction with in situ derivatization and thermal desorption-gas chromatography-mass spectrometry for trace analysis of methylmercury and mercury(II) in water sample. Talanta 77, 1295–1298. https://doi.org/10.1016/j.talanta.2008.09.001.
Jinadasa, B.K.K.K., Ahmad, S.B.N., Edirisinghe, E.M.R.K.B., Wicramasinghe, I., 2014. Mercury Content in Yellowfin Tuna (Thunnus albacares) and Swordfish (Xiphias gladius) and Estimation of Mercury Intake. J. Food Secur. 2, 23–26. https://doi.org/10.12691/jfs-2-1-3.
Knox, R., Kammin, W.R., Thomson, D., 1995. Atomic Fluorescence Determination of Mercury in Fresh Water Ecosystems. J. Automat. Chem. 17, 65–71. https://doi.org/10.1155/S1463924695000113.
Leopold, K., Foulkes, M., Worsfold, P.J., 2009. Gold-Coated Silica as a Preconcentration Phase for the Determination of Total Dissolved Mercury in Natural Waters Using Atomic Fluorescence Spectrometry. Solutions 34, 3421–3428. https://doi.org/10.1039/B820701A.
Leopold, K., Foulkes, M., Worsfold, P., 2010. Methods for the determination and speciation of mercury in natural waters-A review. Anal. Chim. Acta 663, 127–138. https://doi.org/10.1016/j.aca.2010.01.048.
Mann, J.L., Long, S.E., Kelly, W.R., 2003. Direct determination of mercury at picomole L-1 levels in bottled water by isotope dilution cold-vapor generation inductively coupled plasma mass spectrometry. J. Anal. At. Spectrom. 18, 1293–1296. https://doi.org/10.1039/b306640a.
Merkel, B.J., Planer-Friedrich, B., 2005. Groundwater Geochemistry A Practical Guide to Modeling of Natural and Contaminated Aquatic Systems. Springer, Springer-Verlag Berlin Heidelberg.
D.M. 29/12/2003 (Ministerial Decree), 2003. Decreto Ministeriale 29 dicembre 2003 - Attuazione della direttiva n. 2003/40/CE della Commissione nella parte relativa ai criteri di valutazione delle caratteristiche delle acque minerali naturali di cui al decreto ministeriale 12 novembre 1992, n. 542. Gazz. Uff. della Repubb. Ital. 302, 31-12-2003.
Minnich, M.G., Miller, D.C., Parsons, P.J., 2008. Determination of As, Cd, Pb, and Hg in urine using inductively coupled plasma mass spectrometry with the direct injection high efficiency nebulizer. Spectrochim. Acta Part B At. Spectrosc. 63, 389–395. https://doi.org/10.1016/j.sab.2007.11.033.
Morel, F.M.M., Kraepiel, A.M.L., Amyot, M., 1998. The Chemical Cycle and Bioaccumulation of Mercury. Annu. Rev. Ecol. Syst. 29, 543–566. https://doi.org/10.1146/annurev.ecolsys.29.1.543.
Naddeo, V., Zarra, T., Belgiorno, V., 2008. A comparative approach to the variation of natural elements in Italian bottled waters according to the national and international standard limits. J. Food Compos. Anal. 21, 505–514. https://doi.org/10.1016/j.jfca.2008.02.010.
Nordstrom, D.K., Plummer, L.N., Wigley, T.M.L., Wolery, T.J., Ball, J.W., Jenne, E.A., Bassett, R.L., Crerar, D.A., Florence, T.M., Fritz, B., Hoffman, M., Holdren, G.R., Lafon, G.M., Mattigod, S.V., Mcduff, R.E., Morel, F., Reddy, M.M., Sposito, G., Thrailkill, J., 1979. A Comparison of Computerized Chemical Models for Equilibrium Calculations in Aqueous Systems. Chem. Model. aqueous Syst. Speciation, sorption, solubility, Kinet. Am. Chem. Soc. Symp. 3, 857–892. https://doi.org/10.1021/bk-1979-0093.ch038.
OJEC, 1996. Registration of geographical indications and designations of origin. Reg. 1107/96/CE. Official Journal of the European Communities.
OJEC, 2010. List of Natural Mineral Waters Recognised by Member States. Off. J. Eur. Communities C 65/01, 45–58.
Parker, J.L., Bloom, N.S., 2005. Preservation and storage techniques for low-level aqueous mercury speciation. Sci. Total Environ. 337, 253–263. https://doi.org/10.1016/j.scitotenv.2004.07.006.
Passariello, B., Barbaro, M., Quaresima, S., Casciello, A., Marabini, A., 1996. Determination of mercury by Inductively Coupled Plasma - Mass Spectrometry. Microchem. J. 54, 348–354. https://doi.org/10.1006/mchj.1996.0110.
Peccerillo, A., 2005. Plio-Quaternary Volcanism in Italy, Plio-Quaternary Volcanism in Italy: Petrology, Geochemistry, Geodynamics. Springer-Verlag, Berlin/Heidelberg. https://doi.org/10.1007/3-540-29092-3.
Pokras, M., 2005. Essentials of medical geology: impacts of the natural environment on public health. In: Olle Selinus, Brian Alloway, José A. Centeno, Robert B. Finkleman, Ron Fuge, Ulf Lindh, and Pauline Smedley Burlington. Elsevier Academic Press, 2005.
Pourreza, N., Ghanemi, K., 2009. Determination of mercury in water and fish samples by cold vapor atomic absorption spectrometry after solid phase extraction on agar modified with 2-mercaptobenzimidazole. J. Hazard Mater. 161, 982–987. https://doi.org/10.1016/j.jhazmat.2008.04.043.
Rahmanian, N., Ali, S.H.B., Homayoonfard, M., Ali, N.J., Rehan, M., Sadef, Y., Nizami, A.S., 2015. Analysis of physiochemical parameters to evaluate the drinking water quality in the state of perak, Malaysia. J. Chem. 2015. https://doi.org/10.1155/2015/716125.
Ratcliffe, H.E., Swanson, G.M., Fischer, L.J., 1996. Human exposure to mercury: A critical assessment of the evidence of adverse health effects. J. Toxicol. Environ. Health 49, 221–270. https://doi.org/10.1080/00984108.1996.11667600.
Reimann, C., Siewers, U., Skarphagen, H., Banks, D., 1999. Does bottle type and acid-washing influence trace element analyses by ICP-MS on water samples? Sci. Total Environ. 239, 111–130. https://doi.org/10.1016/S0048-9697(99)00302-2.
Reimann, C., Birke, M., Filzmoser, P., 2012. Temperature-dependent leaching of chemical elements from mineral water bottle materials. Appl. Geochemistry 27, 1492–1498. https://doi.org/10.1016/j.apgeochem.2012.05.003.
Ricci, M., Kourtchev, I., Emons, H., 2012. Chemical water monitoring under the Water Framework Directive with Certified Reference Materials. TrAC Trends Anal. Chem. (Reference Ed.) 36, 47–57. https://doi.org/10.1016/j.trac.2012.03.006.
Ricci, M., Lava, R., Koleva, B., 2016. Matrix Certified Reference Materials for environmental monitoring under the EU Water Framework Directive: An update. TrAC Trends Anal. Chem. (Reference Ed.) 76, 194–202. https://doi.org/10.1016/j.trac.2015.11.002.
Rivaro, P., Ianni, C., Soggia, F., Frache, R., 2007. Mercury speciation in environmental samples by cold vapour atomic absorption spectrometry with in situ preconcentration on a gold trap. Microchim. Acta 158, 345–352. https://doi.org/10.1007/s00604-006-0712-9.
Różański, S.Ł., Castejón, J.M.P., Fernández, G.G., 2016. Bioavailability and mobility of mercury in selected soil profiles. Environ. Earth Sci. 75, 1065. https://doi.org/10.1007/s12665-016-5863-3.
Saad, B., Wei Pok, F., Sujari, A.N.A., Idiris Saleh, M., 1998. Analysis of anions and cations in drinking water samples by Capillary Ion Analysis. Food Chem. 61, 249–254. https://doi.org/10.1016/S0308-8146(97)00024-1.
Siegel, F.R., 2002. Sources and Origins of the Metals. Environ. Geochemistry Potential. Toxic Met. 1–218. https://doi.org/10.1007/978-3-662-04739-2.
Snyder, R.D., 1971. Congenital Mercury Poisoning. N. Engl. J. Med. 284, 1014–1016. https://doi.org/10.1056/NEJM197105062841806.
Soleo, L., Vacca, A., Vimercati, L., Bruno, S., Di Loreto, M., Zocchetti, C., Di Stefano, R., Candilio, G., Lasorsa, G., Franco, G., Foa, V., 1997. Minimal immunological effects on workers with prolonged low exposure to inorganic mercury. Occup. Environ. Med. 54, 437–442. https://doi.org/10.1136/oem.54.6.437.
Sørensen, N., Murata, K., Budtz-Jørgensen, E., Weihe, P., Grandjean, P., 1999. Prenatal Methylmercury Exposure as a Cardiovascular Risk Factor at Seven Years of Age. Epidemiology.
Spada, L., Annicchiarico, C., Cardellicchio, N., Giandomenico, S., Di Leo, A., 2012. Mercury and methylmercury concentrations in Mediterranean seafood and surface sediments, intake evaluation and risk for consumers. Int. J. Hyg Environ. Health 215, 418–426. https://doi.org/10.1016/j.ijheh.2011.09.003.
Sposito, G., 1989. The Chemistry of Soils. Oxford Univ. Press, pp. 1–277.
Sprovieri, F., Pirrone, N., Bencardino, M., D'Amore, F., Angot, H., Barbante, C., Brunke, E.G., Arcega-Cabrera, F., Cairns, W., Comero, S., Diéguez, M.C., Dommergue, A., Ebinghaus, R., Bin Feng, X., Fu, X., Elizabeth Garcia, P., Manfred

Gawlik, B., Hageström, U., Hansson, K., Horvat, M., Kotnik, J., Labuschagne, C., Magand, O., Martin, L., Mashyanov, N., Mkololo, T., Munthe, J., Obolkin, V., Ramirez Islas, M., Sena, F., Somerset, V., Spandow, P., Vardè, M., Walters, C., Wängberg, I., Weigelt, A., Yang, X., Zhang, H., 2017. Five-year records of mercury wet deposition flux at GMOS sites in the Northern and Southern hemispheres. Atmos. Chem. Phys. 17, 2689–2708. https://doi.org/10.5194/acp-17-2689-2017.

Tvermoes, B.E., Banducci, A.M., Devlin, K.D., Kerger, B.D., Abramson, M.M., Bebenek, I.G., Monnot, A.D., 2014. Screening level health risk assessment of selected metals in apple juice sold in the United States. Food Chem. Toxicol. 71, 42–50. https://doi.org/10.1016/j.fct.2014.05.015.

Ullrich, S.M., Tanton, T.W., Abdrashitova, S.A., 2001. Mercury in the Aquatic Environment: A Review of Factors Affecting Methylation. Crit. Rev. Environ. Sci. Technol. 31, 241–293. https://doi.org/10.1080/20016491089226.

US-EPA, 1995. Integrated Risk Information System (IRIS) Mercuric chloride (HgCl2) quickview. National Center for Environmental Assessment. Chem. Assess. Summ. 1–21.

US-EPA, 2002. Method 1631, revision E: mercury in water by oxidation, purge and trap, and cold vapor atomic fluorescence spectrometry. United States Environmental Protection Agency.

US-EPA, R., 2003. Definition and Procedure for the Determination of the Method Detection Limit, 40 CFR. Ch. I (7–1–03 Edition).

Valko, M., Morris, H., Cronin, M., 2005. Metals, Toxicity and Oxidative Stress. Curr. Med. Chem. 12, 1161–1208. https://doi.org/10.2174/0929867053764635.

Vardè, M., Cofone, F., Servidio, A., Rosselli, A., Hedgecock, I.M., Mannarino, V., Sprovieri, F., Gensini, M., Pirrone, N., 2014. Total Mercury in Surface and Deep Waters in the Western and Eastern Mediterranean Sea. In: 2014 AGU Fall Meeting American Geophysical Union. San Francisco, CA, USA p. OS53E–1091.

Vardè, M., Rosselli, A., Servidio, A., Cofone, F., Mannarino, V., Di Traglia, M., SCI, 2015. Mercury at picomole L^{-1} (pM) level in drinking water by cold vapor atomic fluorescence spectrometry (CV-AFS) along four provinces in Southern Italy (Calabria). In: XV Congresso Nazionale di Chimica dell'Ambiente e dei Beni Culturali, 14 – 18 Giugno 2015. Società Chimica Italiana, Bergamo, Italia, p. 178.

Vardè, M., Cofone, F., Rosselli, A., Servidio, A., Di Traglia, M., Dallo, F., Vespasiano, G., Apollaro, C., 2017. Quanto mercurio nelle acque minerali naturali della Campania?. In: XXVI Congresso Nazionale della Società Chimica Italiana. Paestum (SA), Italia, p. 36.

Vaselli, O., Nisi, B., Rappuoli, D., Bianchi, F., Cabassi, J., Venturi, S., Tassi, F., Raco, B., 2015. Geochemical characterization of the ground waters from the former Hg-mining area of Abbadia San Salvatore (Mt. Amiata, Central Italy): Criticalities and perspectives for the reclamation process. Ital. J. Geosci. 134, 304–322. https://doi.org/10.3301/IJG.2015.03.

Versari, A., Parpinello, G.P., Galassi, S., 2002. Chemometric Survey of Italian Bottled Mineral Waters by Means of their Labelled Physico-chemical and Chemical Composition. J. Food Compos. Anal. 15, 251–264. https://doi.org/10.1006/jfca.2002.1058.

Vespasiano, G., 2015. Hydrogeochemical, isotopic, and geological characterization of the thermal areas of Northern Calabria. PhD Thesis. Univ. Calabr. PhD Thesis, pp. 1–213.

Vespasiano, G., Apollaro, C., Muto, F., Dotsika, E., De Rosa, R., Marini, L., 2014. Chemical and isotopic characteristics of the warm and cold waters of the Luigiane Spa near Guardia Piemontese (Calabria, Italy) in a complex faulted geological framework. Appl. Geochemistry 41, 73–88. https://doi.org/10.1016/j.apgeochem.2013.11.014.

Vespasiano, G., Apollaro, C., De Rosa, R., Muto, F., Larosa, S., Fiebig, J., Mulch, A., Marini, L., 2015a. The Small Spring Method (SSM) for the definition of stable isotope-elevation relationships in Northern Calabria (Southern Italy). Appl. Geochemistry 63, 333–346. https://doi.org/10.1016/j.apgeochem.2015.10.001.

Vespasiano, G., Apollaro, C., Muto, F., De Rosa, R., Critelli, T., 2015b. Preliminary geochemical and geological characterization of the thermal site of Spezzano Albanese (Calabria, south Italy). Rend. Online Soc. Geol. Ital. 33, 108–110. https://doi.org/10.3301/ROL.2015.26.

Voigt, H.J., 1972. Genese und Hydrogeochemie mineralisierter Grundwässer. WTI Sonderh. 6-72, ZGI, Berlin, p. 150 in Ger. 150, 1972.

WHO - World Health Organization, 2005. Mercury in Drinking-water. World Heal. Organ, Geneva, pp. 1–8.

WHO - World Health Organization, 2008. Guidelines for drinking-water quality, , third ed.vol. 1. World Heal. Organ, Geneva, p. 516.

WHO - World Health Organization, 2011. Guidelines for Drinking-water Quality, fourth ed. World Heal. Organ, Geneva.

Wu, H., Jin, Y., Han, W., Miao, Q., Bi, S., 2006. Non-chromatographic speciation analysis of mercury by flow injection on-line preconcentration in combination with chemical vapor generation atomic fluorescence spectrometry. Spectrochim. Acta Part B At. Spectrosc. 61, 831–840. https://doi.org/10.1016/j.sab.2006.04.008.

Yu, L.-P., Yan, X.-P., 2004. Flow Injection On-Line Sorption Preconcentration Coupled with Cold Vapor Atomic Fluorescence Spectrometry and On-Line Oxidative Elution for the Determination of Trace Mercury in Water Samples. At. Spectrosc. 25, 145–153.

Zaporozec, A., 1972. Graphical Interpretation of Water-Quality Data. Groundwater 10, 32–43. https://doi.org/10.1111/j.1745-6584.1972.tb02912.x.

Zi, H.-J., Wu-Er, G., Su-Ping, H., Xian-Juan, J., Ling-Zhong, W., 2009. Determination of trace inorganic mercury in mineral water by flow injection on-line sorption preconcentration-cold vapor atomic fluorescence spectrometry. Fenxi Huaxue/Chinese J. Anal. Chem. 37, 1029–1032. https://doi.org/10.1016/S1872-2040(08)60116-4.

Supplementary Information

Ultra-trace determination of total mercury in Italian bottled waters

Massimiliano Vardè [a, b, *], Alessandro Servidio [c], Giovanni Vespasiano [d, g], Luisa Pasti [b], Alberto Cavazzini [b], Mario Di Traglia [e], Annalisa Rosselli [f], Franco Cofone [c], Carmine Apollaro [g], Elisa Scalabrin [h], Rosanna De Rosa [g] and Antonio Procopio [i]

[a] Istituto per la Dinamica dei Processi Ambientali – Consiglio Nazionale delle Ricerche (CNR-IDPA), Via Torino 155, I-30172, Venezia-Mestre, Italy

[b] Dipartimento di Scienze Chimiche e Farmaceutiche (DipSCF), Università degli Studi di Ferrara (Unife), Via Luigi Borsari 46, I-44121, Ferrara, Italy

[c] Istituto di Nanotecnologia – Consiglio Nazionale delle Ricerche (CNR-NANOTEC), Via P. Bucci 4, cubo 31C, I-87036, Arcavacata di Rende (CS), Italy

[d] EalCUBO (Environment, Earth, Engineering), Università della Calabria (Unical), Via P. Bucci 4, cubo 15B, I-87036, Arcavacata di Rende (CS), Italy

[e] Dipartimento di Sanità Pubblica e Malattie Infettive (DSPMI), Sapienza Università di Roma, Piazzale Aldo Moro 5, I-00185, Roma, Italy

[f] Dipartimento di Medicina Sperimentale, Università degli Studi della Campania "Luigi Vanvitelli", Via Santa Maria di Costantinopoli 16, I-80138, Napoli, Italy

[g] Dipartimento di Biologia, Ecologia e Scienze della Terra (DiBEST), Università della Calabria (Unical), Via P. Bucci 4, cubo 15B, I-87036, Arcavacata di Rende (CS), Italy

[h] Dipartimento di Scienze Ambientali, Informatica e Statistica (DAIS), Università Ca' Foscari Venezia, Via Torino 155, I-30172, Venezia-Mestre, Italy

[i] Dipartimento di Scienze della Salute, Università degli Studi "Magna Graecia" di Catanzaro (UMG), Viale Europa, Località Germaneto, I-88100, Catanzaro, Italy

Studies on bottled mineral waters in the literature

Over the past few decades several studies have focused their research on considering the chemical composition of bottled waters, by looking at the macro elements, the presence of potentially toxic trace elements, contamination from undesirable organic and inorganic substances, emerging contaminants and other unregulated substances (Al-Saleh and Al-Doush, 1998; Al Fraij et al., 1999; Ericson et al., 2008; Le Coadou et al., 2017; Leivadara et al., 2008; Liu and Mou, 2003; Mohebali and Jahromi, 2013; Nawrocki et al., 2002; Page et al., 1993; Rahmanian et al., 2015; Saleh et al., 2008, 2001; Serôdio and Nogueira, 2006; Signorile et al., 2007; Todorovic et al., 2013; Tombesi and Freije, 2002; Varrica et al., 2013; Wu et al., 2010). Some studies were carried out and suggest revision of safe bottled water guidelines (Cidu et al., 2011), other studies focus on the recognition of the role of water-rock interactions on mineral water composition (Al-Mudhaf and Abu-Shady, 2012; Dinelli et al., 2012). However, despite differences in various parameters, and looking at to guideline limits for both bottled and tap waters, researchers have provided their opinion on water quality, and generally conclude that there are many reasons to prefer the consumption of tap water over mineral water. In the absence of nutritional and health issues, tap water should be preferred, because could be a key factor in reducing the environmental impact of bottled water consumption (due to plastic production and transport of bottles). The Tracing Food commodities in Europe (TRACE) project funded by the European Commission focused on an overview of 39 compositional parameters for 571 mineral bottled waters marketed in 23 European countries. The main objective was to evaluate whether the constituent levels reported on the label corresponded with those found, and to check for parameters with no set limit values. A chemical data set for 23 elements, for some major cations and harmful trace metals have been reported for 132 bottled waters from 28 countries all over the world, to assess the concentrations of elements that are not yet regulated. In both of these two specific cases, mercury was not considered (Bertoldi et al., 2011; Krachler and Shotyk, 2009). During the European investigation EuroGeoSurvey Geochemical Expert Group Project (Reimann, 2010; Reimann and Birke, 2010), researchers carried out chemical analysis of macro and micro elements in a total of 1785 bottled mineral waters with the aim of assessing the amount and natural variations of these elements in groundwater on a national and European scale (38 countries). Physico-chemical and lithology data from the countries where the bottles were purchased, such as Germany (Birke et al., 2010a), Greece (Demetriades, 2010), Estonia (Bityukova and Petersell, 2010), Croatia (Peh et al., 2010), Hungary (Fugedi et al., 2010), Italy (Dinelli et al., 2010), allowed authors to evaluate, among many aspects, the influence of geology as a key factor in the variability of macro and micro elemental levels measured, and the impact of packaging on some parameters, considering that some of these elements were not yet regulated by legislation. Papers published by

this not-for-profit organization, representing 38 nations in Europe, means it is possible to compare the concentrations of elements and ions present in bottled and tap water and highlights that some parameters (such as nitrates, nitrites, fluoride, Na, As, Mn, Ni, Ba) in a small number of samples were present at levels at which health problems may arise (Dinelli et al., 2012). Many studies to assess concentration the levels of major and trace elements and organic compounds in bottled waters have been conducted in Europe, such as that by Misund (Misund et al., 1999) 66 elements in 56 brands from European countries, by Rosborg (Rosborg et al., 2005) 46 metals and ions in 33 brands found on the Swedish market, as well as by Barroso (Barroso et al., 2009) 11 trace elements in 10 brands of mineral and spring waters (with flavors and aromas) from supermarkets in Portugal. In the USA, Ikem (Ikem et al., 2002) performed analyses for 38 parameters in 25 brands purchased in three cities in Alabama, Saleh (Saleh et al., 2008) looked for 37 analytes between major cations and anions, trace elements, trihalomethanes, and physical and microbiological analysis in 35 brands collected in Texas. Sullivan (Sullivan and Leavey, 2011) studied 17 heavy metals from 6 sources of bottled waters sold in California (USA). In Italy, chemical and toxicological evaluations were performed for 37 parameters in 40 mineral water samples from different companies (Signorile et al., 2007), for 52 parameters in 371 brands (Naddeo et al., 2008) and, Cicchella (Cicchella et al., 2010) determined 71 chemical and chemical-physical parameters in 158 brands whilst Cidu (Cidu et al., 2011) studied 57 inorganic parameters in 37 brands of bottled water and 15 samples of tap water. Dinelli (Dinelli et al., 2010) determined 69 elements and ions in 178 brands and finally Varrica (Varrica et al., 2013) analysed 16 brands and 10 tap waters for 32 major and trace inorganic components. However, as can be seen in Table S4, few authors reported mercury concentrations in bottled waters. In Europe, throughout the EuroGeoSurvey Geochemical Expert Group Project, mercury was one of the trace elements evaluated. For this project Hg analyses were carried out in the linear range between 0.1 ng L^{-1} ÷ 100 µg L^{-1} by Atomic Fluorescence Spectroscopy (AFS) on more than 1700 bottled waters purchased from 38 European countries, but Hg was always below the lower reporting limit of 5 ng L^{-1} in all the samples (Birke et al., 2010b). Of these 1785 waters, 908 bottled waters were bought in Germany (Birke et al., 2010a), 186 in Italy (Cicchella et al., 2010), 61 in Greece (Demetriades, 2010), and for 5 brands from Estonia (Bityukova and Petersell, 2010) where Hg was determined by ICP-MS with reported concentrations of < 0.02 µg L^{-1} for all the samples tested. In a different study hydride generation atomic absorption spectrometry (HG-AAS) allowed the quantification of Hg in 39 water samples (10 brands) from Portugal in a range from 0.06 to 0.8 µg L^{-1} (Barroso et al., 2009). In 56 European samples mainly found on the Norwegian market, Hg was found in the range between LOQ < 0.005 to 0.26 µg L^{-1} (Misund et al., 1999), with a reported mean value 0.015 µg L^{-1}, whereas 33 brands found on the Swedish market showed

mercury ranging from the detection limit of 0.02 μg L^{-1} to 0.434 mg L^{-1}, with a median value of 2 μg L^{-1} (Rosborg et al., 2005) both using ICP-MS as the detection technique. On samples corresponding to 32 brands taken in the Houston area of Texas (USA), the mercury content in bottled water was found between 0.16 - 0.86 μg L^{-1} and was detected using Graphite Furnace Atomic Absorption Spectroscopy (GF – AAS), after oxidation with $KMnO_4$ and $SnCl_2$ as a reducing agent (Saleh et al., 2008). Using CV-AAS on 18 bottled mineral waters from six different sources in a study conducted in California (USA), Hg was found to be below the reported analytical method detection limit (RDL) of 0.025 μg L^{-1} (Sullivan and Leavey, 2011), while in 25 brands retrieved from three cities in Alabama, Hg analysed by ICP-OES were in the range < 0.01 - 79 μg L^{-1} (Ikem et al., 2002). Out of from 35 purchased in Illinois and Pennsylvania, Hg resulted higher than 0.1 μg L^{-1} (DL) in 11 samples with the range of 0.3 - 1.2 μg L^{-1} (Allen et al., 1989). For two foreign brands, Perrier and Radenska, that we have also considered in our study, Allen reported Hg concentrations exceeding the WHO, Canadian and European standards but not the 2.0 μg L^{-1} US regulation. The Italian brands Crodo Liesel, Ferrarelle, San Benedetto and San Pellegrino had mercury with concentrations < 0.1 μg L^{-1} (DL). Mann and coauthors employed ID CV-ICP-MS technique to determine mercury levels (range 0.11 - 2.32 ng L^{-1}) in 17 bottles from 7 different countries, demonstrating the capability of this system to detect trace mercury in mineral water and other environmental samples such as river water, seawater, and wet precipitation (e.g. ice and snow) (Mann et al., 2003). Two papers published by the same author investigated both physical and chemical parameters in 130 and 139 brands respectively of mineral waters in Turkey (Güler, 2007a, 2007b). Reporting mean mercury concentrations of 0.8 μg L^{-1} for spring waters, 0.5 μg L^{-1} for mineral and tap waters and a range between 0.05 to 1.0 μg L^{-1} for still waters (average value 0.85 μg L^{-1}). In the second paper a mean value of 1 μg L^{-1} is found for sparkling waters. Three different brands of commercial bottled waters sold in Egypt (Dakhlia governorate) were analysed by AAS for some heavy metals and Hg levels, they found a mean concentration of 0.16 μg L^{-1} (El-Harouny et al., 2009) whereas five brands retailed in the Egyptian market had mercury levels below 30 ng L^{-1} (Saleh et al., 2001). Trace element determinations were carried out on 93 brands of bottled waters from stores located within Kuwait, but many samples came from different countries. In this comparison study between tap and bottled waters, using ICP-MS instrumentation, Hg was found in bottled waters with a mean value of 0.47 μg L^{-1} similar to the 0.42 μg L^{-1} value registered as the mean value for all local tap waters (Al-Mudhaf and Abu-Shady, 2012). The presence of Hg was evaluated in tap (range 10 - 20 ng L^{-1}) and mineral waters (mean value 10 ng L^{-1}) in Malaysia (State of Perak) (Rahmanian et al., 2015). Measurements of macro and micro elements were conducted on 18 brands of bottled waters and for comparison, tap and well waters from different

139 places in Tehran, Iran. Mercury analyses were performed using HG-AAS and were found to be
140 always lower than 1 μg L^{-1} below the limits set by the WHO, US-EPA and Iranian (6 μg L^{-1})
141 standards (Mohebali and Jahromi, 2013). Five heavy metals were determined by the authors
142 (Hadiani et al., 2015) in 128 waters samples (42 different brands), Hg measured by HG-AAS was
143 found to have a mean of 0.5 μg L^{-1} in mineral and tap water and 0.6 μg L^{-1} in well waters. As
144 mentioned above only a few studies found bottled water mercury concentrations in excess of the
145 levels set by environmental regulation bodies (see Table 1 in the main text) (Allen et al., 1989;
146 Ikem et al., 2002), and therefore could potentially harm human health. However, numerous samples
147 had mercury concentrations in the range between the detection limit of the analytical technique
148 employed and 1 μg L^{-1}. Recent studies have demonstrated that specific Hg determination techniques
149 such as AFS and HG-AAS have greater sensitivity and hence are able to quantify this toxic metal
150 within a concentration range of a few part per trillion on a routine basis. Table S4 shows selected
151 publications where Hg measurements were reported.
152
153 **References**

154 Al-Mudhaf, H.F., Abu-Shady, A.S.I., 2012. Comparison of Trace Elements in Bottled and
155 Desalinated Household Drinking Water in Kuwait. Clean - Soil, Air, Water 40, 986–1000.
156 https://doi.org/10.1002/clen.201100618
157 Al-Saleh, I., Al-Doush, I., 1998. Survey of trace elements in household and bottled drinking water
158 samples collected in Riyadh, Saudi Arabia. Sci. Total Environ. 216, 181–92.
159 Al Fraij, K.M., Abd El Aleem, M.K., Al Ajmy, H., 1999. Comparative study of potable and mineral
160 waters available in the state of Kuwait. Desalination 123, 253–264.
161 https://doi.org/10.1016/S0011-9164(99)00081-8
162 Allen, H.E., Halley-Henderson, M.A., Hass, C.N., 1989. Chemical Composition of Bottled Mineral
163 Water. Arch. Environ. Heal. AEHLEV Vol.44 9896, 18 ref.
164 https://doi.org/10.1080/00039896.1989.9934383
165 Barroso, M.F., Ramos, S., Oliva-Teles, M.T., Delerue-Matos, C., Sales, M.G.F., Oliveira, M.B.P.P.,
166 2009. Survey of trace elements (Al, As, Cd, Cr, Co, Hg, Mn, Ni, Pb, Se, and Si) in retail
167 samples of flavoured and bottled waters. Food Addit. Contam. Part B Surveill. 2, 121–130.
168 https://doi.org/10.1080/02652030903081945
169 Bertoldi, D., Bontempo, L., Larcher, R., Nicolini, G., Voerkelius, S., Lorenz, G.D., Ueckermann,
170 H., Froeschl, H., Baxter, M.J., Hoogewerff, J., Brereton, P., 2011. Survey of the chemical
171 composition of 571 European bottled mineral waters. J. Food Compos. Anal. 24, 376–385.
172 https://doi.org/10.1016/j.jfca.2010.07.005

173 Birke, M., Rauch, U., Harazim, B., Lorenz, H., Glatte, W., 2010a. Major and trace elements in
174 German bottled water, their regional distribution, and accordance with national and
175 international standards. J. Geochemical Explor. 107, 245–271.
176 https://doi.org/10.1016/j.gexplo.2010.06.002
177 Birke, M., Reimann, C., Demetriades, A., Rauch, U., Lorenz, H., Harazim, B., Glatte, W., 2010b.
178 Determination of major and trace elements in European bottled mineral water — Analytical
179 methods. J. Geochemical Explor. 107, 217–226. https://doi.org/10.1016/j.gexplo.2010.05.005
180 Bityukova, L., Petersell, V., 2010. Chemical composition of bottled mineral waters in Estonia. J.
181 Geochemical Explor. 107, 238–244. https://doi.org/10.1016/j.gexplo.2010.07.006
182 Cicchella, D., Albanese, S., De Vivo, B., Dinelli, E., Giaccio, L., Lima, A., Valera, P., 2010. Trace
183 elements and ions in Italian bottled mineral waters: Identification of anomalous values and
184 human health related effects. J. Geochemical Explor. 107, 336–349.
185 https://doi.org/10.1016/j.gexplo.2010.04.004
186 Cidu, R., Frau, F., Tore, P., 2011. Drinking water quality: Comparing inorganic components in
187 bottled water and Italian tap water. J. Food Compos. Anal. 24, 184–193.
188 https://doi.org/10.1016/j.jfca.2010.08.005
189 Demetriades, A., 2010. General ground water geochemistry of Hellas using bottled water samples.
190 J. Geochemical Explor. 107, 283–298. https://doi.org/10.1016/j.gexplo.2010.10.012
191 Dinelli, E., Lima, A., Albanese, S., Birke, M., Cicchella, D., Giaccio, L., Valera, P., De Vivo, B.,
192 2012. Comparative study between bottled mineral and tap water in Italy. J. Geochemical
193 Explor. 112, 368–389. https://doi.org/10.1016/j.gexplo.2011.11.002
194 Dinelli, E., Lima, A., De Vivo, B., Albanese, S., Cicchella, D., Valera, P., 2010. Hydrogeochemical
195 analysis on Italian bottled mineral waters: Effects of geology. J. Geochemical Explor. 107,
196 317–335. https://doi.org/10.1016/j.gexplo.2010.06.004
197 El-Harouny, M.A., El-Dakroory, S.A., Attalla, S.M., Hasan, N.A., Hegazy, R., 2009. Chemical
198 quality of tap water versus bottled water: evaluation of some heavy metals and elements
199 content of drinking water in dakahlia governorate – Egypt. Internet J. Nutr. Wellness 9, 1–7.
200 Ericson, I., Nadal, M., Van Bavel, B., Lindström, G., Domingo, J.L., 2008. Levels of
201 perfluorochemicals in water samples from Catalonia, Spain: Is drinking water a significant
202 contribution to human exposure? Environ. Sci. Pollut. Res. 15, 614–619.
203 https://doi.org/10.1007/s11356-008-0040-1
204 Fugedi, U., Kuti, L., Jordan, G., Kerek, B., 2010. Investigation of the hydrogeochemistry of some
205 bottled mineral waters in Hungary. J. Geochemical Explor. 107, 305–316.
206 https://doi.org/10.1016/j.gexplo.2010.10.011

207 Güler, C., 2007a. Characterization of Turkish bottled waters using pattern recognition methods.
208 Chemom. Intell. Lab. Syst. 86, 86–94. https://doi.org/10.1016/j.chemolab.2006.08.009
209 Güler, C., 2007b. Evaluation of maximum contaminant levels in Turkish bottled drinking waters
210 utilizing parameters reported on manufacturer's labeling and government-issued production
211 licenses. J. Food Compos. Anal. 20, 262–272. https://doi.org/10.1016/j.jfca.2006.10.005
212 Hadiani, M.R., Dezfooli-Manesh, S., Shoeibi, S., Ziarati, P., Mousavi Khaneghah, A., 2015. Trace
213 elements and heavy metals in mineral and bottled drinking waters on the Iranian market. Food
214 Addit. Contam. Part B, Surveill. 8, 18–24. https://doi.org/10.1080/19393210.2014.947526
215 Ikem, A., Odueyungbo, S., Egiebor, N.O., Nyavor, K., 2002. Chemical quality of bottled waters
216 from three cities in eastern Alabama. Sci. Total Environ. 285, 165–175.
217 https://doi.org/10.1016/S0048-9697(01)00915-9
218 Krachler, M., Shotyk, W., 2009. Trace and ultratrace metals in bottled waters: Survey of sources
219 worldwide and comparison with refillable metal bottles. Sci. Total Environ. 407, 1089–1096.
220 https://doi.org/10.1016/j.scitotenv.2008.10.014
221 Le Coadou, L., Le Ménach, K., Labadie, P., Dévier, M.H., Pardon, P., Augagneur, S., Budzinski,
222 H., 2017. Quality survey of natural mineral water and spring water sold in France: Monitoring
223 of hormones, pharmaceuticals, pesticides, perfluoroalkyl substances, phthalates, and
224 alkylphenols at the ultra-trace level. Sci. Total Environ. 603–604, 651–662.
225 https://doi.org/10.1016/j.scitotenv.2016.11.174
226 Leivadara, S. V., Nikolaou, A.D., Lekkas, T.D., 2008. Determination of organic compounds in
227 bottled waters. Food Chem. 108, 277–286. https://doi.org/10.1016/j.foodchem.2007.10.031
228 Liu, Y., Mou, S., 2003. Simultaneous determination of trace level bromate and chlorinated
229 haloacetic acids in bottled drinking water by ion chromatography. Microchem. J. 75, 79–86.
230 https://doi.org/10.1016/S0026-265X(03)00055-9
231 Mann, J.L., Long, S.E., Kelly, W.R., 2003. Direct determination of mercury at picomole L-1 levels
232 in bottled water by isotope dilution cold-vapor generation inductively coupled plasma mass
233 spectrometry. J. Anal. At. Spectrom. 18, 1293–1296. https://doi.org/10.1039/b306640a
234 Misund, A., Frengstad, B., Siewers, U., Reimann, C., 1999. Variation of 66 elements in European
235 bottled mineral waters. Sci. Total Environ. 243–244, 21–41. https://doi.org/10.1016/S0048-
236 9697(99)00307-1
237 Mohebali, S., Jahromi, H.S., 2013. Evaluation of nitrate and trace elements concentration in
238 drinking water: Bottled, tap and well. Chinese J. Popul. Resour. Environ. 11, 142–148.
239 https://doi.org/10.1080/10042857.2013.800386
240 Naddeo, V., Zarra, T., Belgiorno, V., 2008. A comparative approach to the variation of natural

241 elements in Italian bottled waters according to the national and international standard limits. J.
242 Food Compos. Anal. 21, 505–514. https://doi.org/10.1016/j.jfca.2008.02.010
243 Nawrocki, J., Dąbrowska, A., Borcz, A., 2002. Investigation of carbonyl compounds in bottled
244 waters from Poland. Water Res. 36, 4893–4901. https://doi.org/10.1016/S0043-
245 1354(02)00201-4
246 Page, B.D., Conacher, H.B., Salminen, J., Nixon, G.R., Riedel, G., Mori, B., Gagnon, J., Brousseau,
247 Y., 1993. Survey of bottled drinking water sold in Canada. Part 2. Selected volatile organic
248 compounds. J. AOAC Int. 76, 26–31.
249 Peh, Z., Šorša, A., Halamić, J., 2010. Composition and variation of major and trace elements in
250 Croatian bottled waters. J. Geochemical Explor. 107, 227–237.
251 https://doi.org/10.1016/j.gexplo.2010.02.002
252 Rahmanian, N., Ali, S.H.B., Homayoonfard, M., Ali, N.J., Rehan, M., Sadef, Y., Nizami, A.S.,
253 2015. Analysis of physiochemical parameters to evaluate the drinking water quality in the state
254 of perak, Malaysia. J. Chem. 2015. https://doi.org/10.1155/2015/716125
255 Reimann, C., 2010. Foreword by the Chairman of the EuroGeoSurveys Geochemistry Expert
256 Group. J. Geochemical Explor. 107, v–vi. https://doi.org/10.1016/j.gexplo.2010.11.003
257 Reimann, C., Birke, M., 2010. Geochemistry of European Bottled Water © 2010, Borntraeger
258 Verlagsbuchhandlung, Stuttgart, Germany. Borntraeger Verlagsbuchhandlung, Stuttgart,
259 Germany.
260 Rosborg, I., Nihlgård, B., Gerhardsson, L., Gernersson, M.-L., Ohlin, R., Olsson, T., 2005.
261 Concentrations of inorganic elements in bottled waters on the Swedish market. Environ.
262 Geochem. Health 27, 217–227. https://doi.org/10.1007/s10653-004-1612-8
263 Saleh, M.A., Abdel-Rahman, F.H., Woodard, B.B., Clark, S., Wallace, C., Aboaba, A., Zhang, W.,
264 Nance, J.H., 2008. Chemical, microbial and physical evaluation of commercial bottled waters
265 in greater Houston area of Texas. J. Environ. Sci. Health. A. Tox. Hazard. Subst. Environ. Eng.
266 43, 335–347. https://doi.org/10.1080/10934520701795400
267 Saleh, M.A., Ewane, E., Jones, J., Wilson, B.L., 2001. Chemical Evaluation of Commercial Bottled
268 Drinking Water from Egypt. J. Food Compos. Anal. 14, 127–152.
269 https://doi.org/10.1006/jfca.2000.0858
270 Serôdio, P., Nogueira, J.M.F., 2006. Considerations on ultra-trace analysis of phthalates in drinking
271 water. Water Res. 40, 2572–2582. https://doi.org/10.1016/j.watres.2006.05.002
272 Signorile, G., Neve, A., Lugoli, F., Piccinni, M.C., Arena, R., Di Marino, R., 2007. Evaluation of
273 toxic chemical parameters and ecotoxicity levels in bottled mineral waters. J. Prev. Med. Hyg.
274 48, 10–16.

Sullivan, M.J., Leavey, S., 2011. Heavy metals in bottled natural spring water. J. Environ. Health 73, 8–13.

Todorovic, M., Papic, P., Cuk, M., Stojkovic, J., 2013. Rare earth elements in some bottled waters of Serbia. Geol. Anal. Balk. poluostrva 71–81. https://doi.org/10.2298/GABP1374071T

Tombesi, N.B., Freije, H., 2002. Application of solid-phase microextraction combined with gas chromatography-mass spectrometry to the determination of butylated hydroxytoluene in bottled drinking water. J. Chromatogr. A 963, 179–183. https://doi.org/10.1016/S0021-9673(02)00217-0

Varrica, D., Tamburo, E., Dongarrà, G., 2013. Sicilian bottled natural waters: Major and trace inorganic components. Appl. Geochemistry 34, 102–113. https://doi.org/10.1016/j.apgeochem.2013.02.017

Wu, Q., Zhang, T., Sun, H., Kannan, K., 2010. Perchlorate in tap water, groundwater, surface waters, and bottled water from China and its association with other inorganic anions and with disinfection byproducts. Arch. Environ. Contam. Toxicol. 58, 543–550. https://doi.org/10.1007/s00244-010-9485-6

List of Tables in supplementary information

Table S1. List of the bottled mineral waters from Italy (a) and other countries (b). In bold the region/country name and the corresponding abbreviations used in Fig. 1.

Table S2. Sample code, geographical coordinates (decimal degrees) and elevation spring (m a.s.l.).

Table S3. Physico-chemical parameters and major ions reported on the label in Italian bottled waters.

Table S4. Mercury concentrations (μg L^{-1}) found in bottled mineral waters in previous studies.

.

Table S1. List of the bottled mineral waters from Italy ([a]) and other countries ([b]). In bold the region/country name and the corresponding abbreviations used in Fig. 1.

Name	Tipologies
Abruzzo (ABR)[a]	
Fonte Valle Reale	Lightly Sparkling, Still, Sparkling
Ginevra-Fonte Primavera	Lightly Sparkling
Guizza	Lightly Sparkling, Still
Primavera	Lightly Sparkling, Still, Sparkling
Apulia (APU)[a]	
Amata	Still
Ginevra	Still
Vivissima	Still
Basilicata (BAS)[a]	
Alisea	Still
Fonte Itala	Naturally Sparkling, Still
Gaudianello	Naturally Sparkling, Sparkling
Leggera	Still
Lilia Calcica Felicia	Naturally Sparkling
Lilia Giovane	Still
Lilia Magnesiaca Toka	Naturally Sparkling
Monticchio B.	Still
Ninfa	Lightly Sparkling, Still
San Benedetto dal Parco Del Pollino	Still
Sveva	Naturally Sparkling
Toka	Naturally Sparkling
Calabria (CAL)[a]	
Calabria	Sparkling, Still
Fabrizia	Still
Flerì	Still
Fonte del Principe Mongiana	Still
Fontenoce	Sparkling, Still
Leo	Sparkling, Still
Limpida	Still
Mangiatorella	Sparkling, Still
Moschetta	Still
Olimpica	Sparkling, Still
Serricella	Still
Sorbello	Sparkling, Still
Vitasana	Sparkling, Still
Campania (CAL)[a]	
Don Carlo	Sparkling, Still
Don Carlo Cristalià	Lightly Sparkling, Still
Ferrarelle	Naturally Sparkling
Fiordacqua	Still
Emilia-Romagna (EMR)[a]	
Auchan	Lightly Sparkling, Sparkling, Still
Col-Fabrizia Varanina	Still
Galvanina	Sparkling, Still
Monte Cimone	Still
Friuli-Venezia Giulia (FVG)[a]	
Dolomia	Sparkling, Still
Goccia di Carnia	Still
Goccia di Carnia-Despar	Still
Pradis	Sparkling
Lazio (LAZ)[a]	
Acqua di Nepi	Naturally Sparkling
Blues-Fonte Vivia	Naturally Sparkling
Claudia	Naturally Sparkling, Sparkling
Cottorella	Lightly Sparkling, Still
Egeria	Naturally Sparkling, Sparkling, Still
Filette	Lightly Sparkling, Still
Fiuggi	Lightly Sparkling, Still
Fonte Vivia	Naturally Sparkling
Santa Maria alle Capannelle-Blu	Naturally Sparkling
Santa Maria alle Capannelle-Rossa	Naturally Sparkling
Lombardy (LOM)[a]	
Blues-Fonte Sant'Antonio	Still
Boario	Still
Bracca	Sparkling, Still
Chiarella	Sparkling, Still
Flavia	Sparkling
Fonte Essenziale	Still
Fonte Tavina	Still
Levissima	Lightly Sparkling, Sparkling, Still
Maniva	Lightly Sparkling, Sparkling, Still
Neha	Still
Neve	Sparkling, Still
Pineta	Still
San Carlo Spinone	Sparkling, Still
San Pellegrino	Sparkling
Sant'Antonio	Sparkling, Still
Vitasnella	Still
Marche (MAR)[a]	
Blues-Gaia-Genca	Lightly Sparkling, Still
Fonte Elisa	Still

Name	Tipologies	Name	Tipologies
Fonte Ofelia Classic	Lightly Sparkling	Frasassi	Lightly Sparkling, Still
Lete	Naturally Sparkling	Gaia	Still
Natia	Sparkling, Still	Nerea	Lightly Sparkling
Ofelia	Still	Santa Croce	Lightly Sparkling, Still
Prata	Still	Tinnea	Lightly Sparkling
Saguaro	Sparkling, Still		
Santagata	Naturally Sparkling	**Molise (MOL)[a]**	
Santo Stefano	Sparkling, Still	Molisia	Sparkling, Still
Sorgesana Pratella	Lightly Sparkling, Still	Sepinia	Still
Piedmont (PIE)[a]		**Tuscany (TUS)[a]**	
Blues-Rebruant	Still	Acqua Santa di Chianciano	Still
Bolle Stille	Sparkling, Still	Amorosa	Still
Cime Bianche-Carrefour	Sparkling, Still	Fonte de' Medici-Aretina	Sparkling, Still
Columbus Mugniva	Sparkling, Still	Fonte De' Medici-Despar	Lightly Sparkling, Sparkling, Still
Crodo Lisiel	Still	Ilaria	Sparkling, Still
Eva	Sparkling, Still	Maxim's	Lightly Sparkling
Fonte Delle Alpi-Crai	Still	Monteverde	Sparkling, Still
Lauretana	Still	Panna	Still
Mia-Valle Stura	Still	Perla	Sparkling, Still
Panorama Montoso-Pam	Sparkling, Still	San Carlo	Still
San Bernardo	Sparkling, Still	Silva	Still
Santa Barbara Bolle Stille di Lurisia	Still	Tesorino	Still
Sant'Anna di Vinadio	Lightly Sparkling, Still	Tesorino As Roma	Still
Sant'Anna Rebruant	Sparkling, Still	Tosca	Still
Sparea	Sparkling, Still	Uliveto	Naturally Sparkling
		Verna	Sparkling, Still
Sardinia (SAR)[a]			
Altura	Still	**Umbria (UMB)[a]**	
Altura-Sisa	Still	Amerino	Sparkling
Boschetta	Still	Blues-Amerino	Sparkling
Levia	Still	Clivia	Still
Pura	Still	Conad	Sparkling, Still
Quercetta	Still	Fabia	Still
San Giorgio	Still	Fabia Antiche Sorgenti Umbre-Coop	Sparkling, Still
San Martino	Still	Fonte Aura	Sparkling, Still
Santa Lucia	Sparkling	Fonte Santa Chiara	Sparkling, Still
Siete Fuentes	Still	Grazia	Naturally Sparkling
Smeraldina	Still	Lieve	Still
		Misia	Still
Sicily (SIC)[a]			
Cavagrande	Still	Rocchetta	Still
Fontalba	Still	Rocchetta Brio-Blu	Lightly Sparkling, Sparkling
Fonte Gerasia	Still	Rocchetta Brio-Rossa	Sparkling
Milicia	Lightly Sparkling	Rugiada	Lightly Sparkling, Still
Rocca Bianca	Still	Sangemini	Still
Roverella	Still	Sorgente Angelica Nocera Umbra	Lightly Sparkling, Still

Name	Tipologies	Name	Tipologies
Sabrinella	Sparkling, Still	Sorgente Angelica-Coop	Sparkling, Still
Santa Maria	Still	Viva Gubbio	Lightly Sparkling, Still
Serenella	Still		
Sorsy	Still	**Veneto (VEN)[a]**	
Vera S. Rosalia	Still	Alisea	Sparkling
Vitabella	Still	Dolomiti Valli del Pasubio	Sparkling
Vivizia	Still	Norda	Still
		Recoaro	Sparkling, Still
Trentino-South Tyrol (TST)[a]		San Benedetto	Lightly Sparkling, Sparkling, Still
Surgiva	Sparkling, Still	Vera in Bosco	Sparkling, Still

301

Name (Country)*	Tipologies	Name (Country)	Tipologies
Tiger / Denmark (DK)	Lightly Sparkling, Still	Evian (FR)	Still
Donat Mg (SI)	Sparkling	La Versoie-Carrefour (FR)	Still
Radenska (SI)	Still	Perrier (FR)	Naturally Sparkling
Font Vella (ES)	Still	Petillante (FR)	Sparkling
Veri (ES)	Still	Roche Des Ecrins (FR)	Still

302 N.B. *ISO 3166 code for the name of each foreign country.

303

304 **Table S2.** Sample code, geographical coordinates (decimal degrees) and elevation spring (m a.s.l.).

Sample ID	Lat	Lon	E	Sample ID	Lat	Lon	E	Sample ID	Lat	Lon	E
ITA001-1	42.1756	13.8214	300	ITA055-1	42.3895	12.8620	480	ITA109-2	40.4478	8.8572	350
ITA001-2	42.1756	13.8214	300	ITA055-3	42.3895	12.8620	480	ITA110-1	40.1782	8.6656	620
ITA001-3	42.1756	13.8214	300	ITA056-1	41.8538	12.5317	20	ITA111-1	40.8986	9.1511	650
ITA002-3	42.1756	13.8214	254	ITA056-2	41.8538	12.5317	20	ITA112-1	37.5745	14.9360	400
ITA003-1	42.1756	13.8214	300	ITA056-4	43.7277	4.2448	20	ITA113-1	37.9897	15.0133	1200
ITA003-3	42.1756	13.8214	300	ITA057-1	41.7921	13.3185	900	ITA114-1	38.0284	15.4108	450
ITA004-1	42.1697	13.8276	254	ITA057-3	41.7921	13.3185	900	ITA115-3	38.0196	13.5852	120
ITA004-2	42.1697	13.8276	254	ITA058-1	41.7912	13.2214	590	ITA116-1	38.1365	15.1683	450
ITA004-3	42.1697	13.8276	254	ITA058-3	41.7912	13.2214	590	ITA117-1	36.8036	14.8010	350
ITA005-1	40.9768	16.8879	300	ITA059-4	40.9508	15.5876	36	ITA118-1	38.0196	13.5852	120
ITA006-1	40.9768	16.8879	300	ITA060-4	41.8541	12.5431	45	ITA118-2	38.0196	13.5852	120
ITA007-1	40.9768	16.8879	390	ITA061-4	41.8538	12.5317	30	ITA119-1	36.8036	14.8010	350
ITA008-1	40.9508	15.5876	650	ITA062-1	45.7066	9.0381	313	ITA120-1	38.0196	13.5852	120
ITA009-1	40.8915	15.6605	450	ITA063-1	45.8937	10.1877	217	ITA121-1	38.0284	15.4108	450
ITA009-4	40.8939	15.6698	450	ITA064-1	45.8086	9.6838	440	ITA122-1	37.6139	13.5200	1000
ITA010-2	40.9508	15.5876	640	ITA064-2	45.1420	9.6838	440	ITA123-1	38.0196	13.5852	120
ITA010-4	40.9530	15.5607	640	ITA065-1	46.0478	9.2283	760	ITA124-1	38.0196	13.5852	120
ITA011-1	40.9508	15.5876	720	ITA065-2	46.0478	9.2283	760	ITA125-1	46.1615	10.7544	1134
ITA012-1	40.8939	15.6698	505	ITA066-2	45.8086	9.6838	400	ITA125-2	46.1615	10.7544	1134
ITA012-4	40.9530	15.5607	395	ITA067-1	45.8937	10.1877	225	ITA126-1	43.0423	11.8166	500
ITA012-4	42.0667	12.3015	450	ITA068-1	45.5978	10.5155	70	ITA127-1	44.0512	10.1640	600
ITA013-1	40.9508	15.5876	720	ITA069-1	46.4447	10.3596	1848	ITA128-1	43.3308	11.7346	450
ITA014-1	40.9508	15.5876	720	ITA069-2	46.4447	10.3596	1848	ITA128-2	43.3308	11.7346	450
ITA014-3	40.9508	15.5876	720	ITA069-3	46.4447	10.3596	1848	ITA129-1	43.3308	11.7346	450
ITA015-1	39.9732	16.0844	430	ITA070-1	45.8306	10.4514	800	ITA129-2	43.3308	11.7346	450
ITA016-4	42.2429	12.3469	491	ITA070-2	45.8306	10.4542	800	ITA129-3	43.3308	11.7346	450
ITA017-4	42.2429	12.3469	450	ITA070-3	45.8306	10.4542	800	ITA130-1	43.9071	10.4234	95
ITA018-1	38.8091	16.4003	750	ITA071-1	45.9790	9.4467	600	ITA130-2	43.9071	10.4234	95
ITA018-2	38.8091	16.4003	750	ITA072-1	45.7066	9.0381	313	ITA131-3	43.1502	11.0696	1200
ITA019-1	38.4892	16.2827	1000	ITA072-2	45.7066	9.0381	313	ITA132-1	44.0547	10.9080	900
ITA020-1	38.9297	16.3446	74	ITA073-1	45.8786	9.9281	700	ITA132-2	44.0547	10.9080	900
ITA021-1	38.5147	16.3044	1000	ITA074-1	45.7620	9.9167	400	ITA133-1	44.0652	11.2888	600
ITA022-1	39.1569	16.4806	1238	ITA074-2	45.7620	9.9167	400	ITA134-1	43.3308	11.7346	330
ITA022-2	39.1569	16.4806	1238	ITA075-2	45.8220	9.6746	358	ITA134-2	43.3308	11.7346	330
ITA023-1	39.0439	16.4526	1000	ITA076-1	45.7066	9.0381	313	ITA135-1	44.0410	10.1559	300
ITA023-2	39.0439	16.4526	1000	ITA076-2	45.7066	9.0381	313	ITA136-1	44.0547	10.9080	980
ITA024-1	38.9637	16.3873	74	ITA077-1	45.8937	10.1877	217	ITA137-1	43.6481	10.7625	98

Sample ID	Lat	Lon	E	Sample ID	Lat	Lon	E	Sample ID	Lat	Lon	E
ITA025-1	38.4852	16.3780	1200	ITA078-1	43.4184	12.9322	550	ITA138-1	43.6481	10.7625	98
ITA025-2	38.4852	16.3780	1200	ITA078-3	43.4184	12.9322	550	ITA139-1	43.6977	11.9348	960
ITA026-1	38.8091	16.4003	750	ITA079-1	43.4184	12.9322	240	ITA140-4	42.2429	12.3469	12
ITA027-1	38.9637	16.3873	300	ITA080-1	43.4184	12.9322	322	ITA141-1	43.6977	11.9348	960
ITA027-2	38.9637	16.3873	300	ITA080-3	43.4184	12.9322	322	ITA141-2	43.6977	11.9348	960
ITA028-1	38.4892	16.2827	1000	ITA081-1	43.4184	12.9322	322	ITA142-2	42.7006	12.5456	390
ITA029-1	39.0395	16.3467	1000	ITA082-3	42.9002	13.1440	780	ITA143-2	42.7006	12.5456	390
ITA029-2	39.0395	16.3467	1000	ITA083-1	41.9380	13.4155	800	ITA144-1	43.4027	12.6683	700
ITA030-1	38.9297	16.3446	74	ITA083-3	41.9380	13.4155	800	ITA145-1	43.1004	12.7665	500
ITA030-2	38.9297	16.3446	74	ITA084-3	42.9431	13.3340	700	ITA145-2	43.1004	12.7665	500
ITA031-1	40.6358	15.2325	250	ITA085-1	41.5855	14.4623	850	ITA146-1	42.6356	12.5476	330
ITA031-2	40.6358	15.2325	250	ITA085-2	41.5855	14.4623	850	ITA147-1	42.6356	12.5476	330
ITA032-1	40.6358	15.2325	250	ITA086-1	41.4167	14.6462	900	ITA147-2	42.6356	12.5476	330
ITA032-3	40.6358	15.2325	250	ITA087-1	44.2993	7.1485	1950	ITA148-1	42.6356	12.5476	350
ITA033-4	43.6890	10.5283	350	ITA088-1	44.2939	7.6965	1460	ITA148-2	42.6356	12.5476	350
ITA034-1	40.2809	15.6908	650	ITA088-2	44.2939	7.6965	1460	ITA149-1	43.0669	12.6683	700
ITA035-3	40.6358	15.2325	85	ITA089-1	44.2993	7.1485	1380	ITA149-2	43.4027	12.6683	700
ITA036-4	40.8939	15.6698	300	ITA089-2	44.2993	7.1485	1380	ITA150-4	40.8915	15.6605	525
ITA037-1	41.2552	14.1245	350	ITA090-1	44.8044	7.2417	505	ITA151-1	43.3522	12.5782	500
ITA037-2	41.2552	14.1245	350	ITA090-2	44.8044	7.2417	505	ITA152-1	42.8096	12.9142	351
ITA038-1	40.6358	15.2325	85	ITA091-1	46.2098	8.3192	510	ITA153-1	43.2131	12.7825	312
ITA039-1	41.4087	14.1877	300	ITA092-1	44.6823	7.2785	1820	ITA153-2	43.2131	12.7825	312
ITA040-1	40.6358	15.2325	85	ITA092-2	44.6823	7.2785	2042	ITA153-2	43.2131	12.7825	312
ITA040-2	40.6358	15.2325	250	ITA093-1	44.8044	7.2417	1100	ITA153-3	43.2131	12.7825	312
ITA041-4	42.6356	12.5476	98	ITA094-1	45.5627	7.9489	1050	ITA154-1	43.3522	12.5782	522
ITA042-1	40.2809	15.6908	650	ITA095-1	44.2993	7.1485	910	ITA154-3	43.3522	12.5782	522
ITA042-2	40.2809	15.6908	650	ITA096-1	44.8044	7.2417	1240	ITA155-1	42.6356	12.5476	380
ITA043-1	41.4087	14.1877	160	ITA096-2	44.8044	7.2417	1240	ITA156-1	43.1004	12.7665	605
ITA043-3	41.4087	14.1877	160	ITA097-1	44.2006	8.0179	1300	ITA156-3	43.1004	12.7665	605
ITA044-1	44.5668	9.6224	1495	ITA097-2	44.2006	8.0179	1300	ITA157-1	43.1004	12.7665	500
ITA044-2	44.5668	9.6224	1495	ITA098-1	44.2939	7.6965	1460	ITA157-2	43.1004	12.7665	500
ITA044-3	44.5668	9.6224	1495	ITA099-1	44.2993	7.1485	1950	ITA158-1	42.8096	12.9142	450
ITA045-1	44.7555	10.0386	225	ITA099-1	44.2993	7.1485	1503	ITA158-3	42.8096	12.9142	450
ITA046-1	44.0319	12.5353	380	ITA099-2	44.2993	7.1485	1950	ITA159-2	45.7437	11.2411	721
ITA046-2	44.0319	12.5353	380	ITA099-3	44.2993	7.1485	1503	ITA160-2	45.7437	11.2411	650
ITA047-1	44.1649	10.7931	935	ITA100-1	44.8044	7.2417	600	ITA161-1	45.7437	11.2411	1935
ITA048-1	46.2739	12.4569	833	ITA100-2	44.8044	7.2417	600	ITA162-1	45.7054	11.2318	880
ITA048-2	46.2739	12.4569	833	ITA101-1	40.8971	9.0627	536	ITA162-2	45.7054	11.2318	880

Sample ID	Lat	Lon	E	Sample ID	Lat	Lon	E	Sample ID	Lat	Lon	E
ITA049-1	46.5839	12.7792	1370	ITA102-1	40.8971	9.0627	536	ITA163-1	45.5802	12.1081	20
ITA050-1	46.5839	12.7792	1370	ITA103-1	39.2453	8.7662	154	ITA163-2	45.5802	12.1081	20
ITA051-2	46.2528	12.8826	650	ITA104-1	39.2453	8.7662	400	ITA163-3	45.5802	12.1081	20
ITA052-4	41.4087	14.1877	227	ITA105-1	39.2453	8.7662	400	ITA164-1	45.6057	11.8024	60
ITA053-4	41.2552	14.1245	36	ITA106-1	39.2453	8.7662	154	ITA164-2	45.6057	11.8024	60
ITA054-2	42.0667	12.3015	140	ITA107-1	39.2453	8.7662	400				
ITA054-4	41.2552	14.1245	140	ITA108-1	40.6866	8.6728	270				

Note: the last no. of the sample code indicates water typology: 1-still. 2-sparkling. 3-lightly sparkling. 4-naturally sparkling

307
308

Table S3. Physico-chemical parameters and major ions reported on the label in Italian bottled waters**.**

Sample ID	T (°C)	pH (20°C)	EC (20°C)	TDS (mg L^{-1})	CO_2 (mg L^{-1})	Na^+ (mg L^{-1})	K^+ (mg L^{-1})	Ca^{2+} (mg L^{-1})	Mg^{2+} (mg L^{-1})	HCO_3^- (mg L^{-1})	Cl^- (mg L^{-1})	SO_4^{2-} (mg L^{-1})	NO_3^- (mg L^{-1})	F^- (mg L^{-1})	SiO_2 (mg L^{-1})
ITA001-1	11.4	7.26	468	290	6	2.6	1.0	83.1	16.2	310.0	3.6	18.6	4.0	n.a.	3.6
ITA001-2	11.4	7.26	468	290	6	2.6	1.0	83.1	16.2	310.0	3.6	18.6	4.0	n.a.	3.6
ITA001-3	11.4	7.26	468	290	6	2.6	1.0	83.1	16.2	310.0	3.6	18.6	4.0	n.a.	2.6
ITA002-3	12.4	7.19	492	313	6	4.2	1.0	87.5	18.9	327.0	6.1	24.7	3.0	n.a.	4.1
ITA003-1	11.4	7.26	468	290	6	2.6	1.0	83.1	16.2	310.0	3.6	18.6	4.0	n.a.	3.6
ITA003-3	11.4	7.26	468	290	6	2.6	1.0	83.1	16.2	310.0	3.6	18.6	4.0	n.a.	3.6
ITA004-1	12.4	7.19	492	313	6	4.2	1.0	87.5	18.9	327.0	6.1	24.7	3.0	n.a.	4.1
ITA004-2	12.4	7.19	492	313	6	4.2	1.0	87.5	18.9	327.0	6.1	24.7	3.0	n.a.	4.1
ITA004-3	12.4	7.19	492	313	6	4.2	1.0	87.5	18.9	327.0	6.1	24.7	3.0	n.a.	4.1
ITA005-1	16.1	7.08	750	470	51	21.0	3.5	112.0	43.0	480.0	30.0	8.0	n.a.	0.2	18.0
ITA006-1	16.1	n.a.	730	465	52	18.9	3.5	112.0	44.0	480.0	23.2	8.2	n.a.	0.2	17.4
ITA007-1	16.1	7.08	750	470	51	21.0	3.5	112.0	43.0	480.0	30.0	8.0	n.a.	0.2	18.0
ITA008-1	14.7	8.1	426	274	5	1.0	1.2	55.8	29.2	253.0	1.1	n.a.	3.7	0.1	7.5
ITA009-1	16.0	6	630	478	1289	n.a.	n.a.	50.4	17.0	366.0	28.4	30.0	n.a.	n.a.	n.a.
ITA009-4	16.1	n.a.	625	394	n.a.	n.a.	n.a.	50.5	17.1	298.9	17.7	22.0	n.a.	n.a.	n.a.
ITA010-2	16.1	5.8	1520	1140	2890	133.0	52.0	158.0	59.0	989.0	39.0	122.0	3.0	n.a.	110.0
ITA010-4	16.1	5.8	1520	1140	2890	133.0	52.0	158.0	59.0	989.0	39.0	122.0	3.0	n.a.	110.0
ITA011-1	n.a.	n.a.	510	416	n.a.	n.a.	32.0	46.0	14.0	306.0	26.0	14.0	4.0	n.a.	105.0

Sample ID	T (°C)	pH (20°C)	EC (20°C)	TDS (mg L^{-1})	CO_2 (mg L^{-1})	Na^+ (mg L^{-1})	K^+ (mg L^{-1})	Ca^{2+} (mg L^{-1})	Mg^{2+} (mg L^{-1})	HCO_3^- (mg L^{-1})	Cl^- (mg L^{-1})	SO_4^{2-} (mg L^{-1})	NO_3^- (mg L^{-1})	F^- (mg L^{-1})	SiO_2 (mg L^{-1})
ITA012-1	15.8	6.65	420	341	125	n.a.	26.9	31.5	9.4	254.0	n.a.	n.a.	7.0	1.1	n.a.
ITA012-4	15.5	6.12	2680	2068	2185	n.a.	89.9	216.0	54.3	1585.0	n.a.	280.0	n.a.	0.8	n.a.
ITA012-4	19.1	5.9	1654	1288	2100	n.a.	47.8	167.0	n.a.	1061.0	n.a.	186.0	n.a.	0.5	n.a.
ITA013-1	n.a.	n.a.	510	416	n.a.	45.0	32.0	46.0	14.0	306.0	26.0	14.0	4.0	0.5	105.0
ITA014-1	n.a.	n.a.	510	416	n.a.	n.a.	32.0	46.0	14.0	306.0	26.0	14.0	4.0	n.a.	105.0
ITA014-3	n.a.	n.a.	510	416	n.a.	n.a.	32.0	46.0	14.0	306.0	26.0	14.0	4.0	n.a.	105.0
ITA015-1	9.5	7.72	335	230	n.a.	3.4	0.6	51.4	13.8	218.0	4.9	5.2	1.0	n.a.	2.4
ITA016-4	18.8	6.25	1854	1356	1900	n.a.	52.0	241.0	39.9	1280.0	n.a.	n.a.	3.0	1.0	n.a.
ITA017-4	15.5	6.12	2680	2068	2185	n.a.	89.9	n.a.	54.3	1585.0	n.a.	280.0	n.a.	0.8	n.a.
ITA018-1	12.0	7.7	138	122	2	9.8	1.7	12.4	6.0	79.3	12.5	11.0	1.0	0.1	27.2
ITA018-2	12.0	7.7	138	122	2	9.8	1.7	12.4	6.0	79.3	12.5	11.0	1.0	0.1	27.2
ITA019-1	11.7	6.7	125	78	18	13.0	0.7	5.2	2.9	36.6	8.2	9.6	8.0	n.a.	23.5
ITA020-1	17.4	7.84	352	266	4	12.3	2.7	52.0	14.3	201.0	20.1	33.0	7.5	0.1	12.0
ITA021-1	11.6	6.25	72	72	15	11.1	0.6	3.6	1.2	27.8	7.9	3.7	1.0	0.2	n.a.
ITA022-1	8.1	7.41	130	105	2	6.0	1.7	15.4	5.5	94.5	7.4	9.3	2.2	0.2	12.0
ITA022-2	8.1	7.41	130	105	2	6.0	1.7	15.4	5.5	94.5	7.4	9.3	2.2	0.2	12.0
ITA023-1	12.0	6.28	125	110	21	13.6	1.0	6.6	2.2	42.7	9.9	5.6	11.2	0.2	29.8
ITA023-2	12.0	6.28	125	110	21	13.6	1.0	6.6	2.2	42.7	9.9	5.6	11.2	0.2	29.8
ITA024-1	18.5	7.94	384	275	4	18.0	2.6	45.2	18.5	225.0	24.4	22.4	2.2	0.3	13.1

Sample ID	T (°C)	pH (20°C)	EC (20°C)	TDS (mg L^{-1})	CO_2 (mg L^{-1})	Na^+ (mg L^{-1})	K^+ (mg L^{-1})	Ca^{2+} (mg L^{-1})	Mg^{2+} (mg L^{-1})	HCO_3^- (mg L^{-1})	Cl^- (mg L^{-1})	SO_4^{2-} (mg L^{-1})	NO_3^- (mg L^{-1})	F^- (mg L^{-1})	SiO_2 (mg L^{-1})
ITA025-1	9.1	6.05	88	69	18	9.5	0.7	6.6	1.5	30.2	10.3	4.6	0.1	0.1	n.a.
ITA025-2	9.1	6.05	88	69	18	9.5	0.7	6.6	1.5	30.2	10.3	4.6	0.1	0.1	n.a.
ITA026-1	12.1	7.15	240	166	12	13.5	1.9	24.6	10.6	134.0	15.9	9.0	6.6	0.1	18.0
ITA027-1	18.5	7.94	384	275	4	18.0	2.6	45.2	18.5	225.0	24.4	22.4	2.2	0.3	13.1
ITA027-2	18.5	7.94	384	275	4	18.0	2.6	45.2	18.5	225.0	24.4	22.4	2.2	0.3	13.1
ITA028-1	11.6	6.6	100	70	16	13.0	0.2	3.6	4.6	42.7	3.9	4.9	2.7	n.a.	26.4
ITA029-1	9.5	5.28	52	40	9	6.4	n.a.	2.5	1.3	n.a.	n.a.	n.a.	0.9	n.a.	n.a.
ITA029-2	9.5	5.28	52	40	9	6.4	n.a.	2.5	1.3	n.a.	n.a.	n.a.	0.9	n.a.	n.a.
ITA030-1	n.a.	7.84	352	266	4	12.3	2.7	52.0	14.3	201.3	20.1	33.0	7.5	0.1	12.0
ITA030-2	17.4	7.84	352	266	4	12.3	2.7	52.0	14.3	201.3	20.1	33.0	7.5	0.1	12.0
ITA031-1	13.6	6.6	1084	757	164	23.0	2.7	187.1	17.0	708.0	29.0	14.0	3.8	n.a.	n.a.
ITA031-2	13.6	6.6	1084	757	164	23.0	2.7	187.1	17.0	708.0	29.0	14.0	3.8	n.a.	n.a.
ITA032-1	13.6	6.6	1084	757	164	23.0	2.7	187.1	17.0	708.0	29.0	14.0	3.8	n.a.	n.a.
ITA032-3	13.6	6.6	1084	757	164	23.0	2.7	187.1	17.0	708.0	29.0	14.0	3.8	n.a.	n.a.
ITA033-4	n.a.	6.1	1800	1290	2350	50.0	50.0	360.0	20.0	1342.0	20.0	4.0	5.0	1.1	85.0
ITA034-1	10.5	7.5	339	226	30	3.2	1.0	59.1	14.5	253.4	6.0	3.3	5.6	0.1	5.3
ITA035-3	14.7	n.a.	593	378	18	39.0	2.5	94.0	10.0	379.0	22.0	14.0	n.a.	n.a.	14.0
ITA036-4	n.a.	6.2	1260	850	1990	5.0	1.9	305.0	14.1	1005.2	9.8	n.a.	4.3	0.3	12.0
ITA037-1	n.a.	6.5	360	290	170	29.0	29.0	32.0	4.0	183.0	16.0	4.0	9.5	1.0	83.0

Sample ID	T (°C)	pH (20°C)	EC (20°C)	TDS (mg L^{-1})	CO_2 (mg L^{-1})	Na^+ (mg L^{-1})	K^+ (mg L^{-1})	Ca^{2+} (mg L^{-1})	Mg^{2+} (mg L^{-1})	HCO_3^- (mg L^{-1})	Cl^- (mg L^{-1})	SO_4^{2-} (mg L^{-1})	NO_3^- (mg L^{-1})	F^- (mg L^{-1})	SiO_2 (mg L^{-1})
ITA037-2	n.a.	6.5	360	290	170	29.0	29.0	32.0	4.0	183.0	16.0	4.0	9.5	1.0	83.0
ITA038-1	14.7	7.16	593	378	18	39.0	2.5	94.0	10.0	379.0	22.0	14.0	n.a.	n.a.	14.0
ITA039-1	n.a.	7.1	705	442	35	3.9	1.2	152.0	13.2	470.0	6.1	n.a.	3.5	0.2	7.0
ITA040-1	14.3	7.26	619	409	n.a.	35.0	1.7	77.0	11.4	342.0	27.0	13.8	0.5	n.a.	15.4
ITA040-2	13.7	7.9	986	638	n.a.	19.0	4.2	187.0	31.0	716.0	23.0	12.0	2.8	n.a.	9.4
ITA041-4	n.a.	6	1380	1035	2150	49.0	37.0	280.0	21.0	1128.0	18.0	5.0	4.0	1.0	84.0
ITA042-1	10.5	7.5	339	226	30	3.2	1.0	59.1	14.5	253.4	6.0	3.3	5.6	0.1	5.3
ITA042-2	10.5	7.5	339	226	30	3.2	1.0	59.1	14.5	253.4	6.0	3.3	5.6	0.1	5.3
ITA043-1	n.a.	7.1	465	270	14	3.5	0.9	92.0	11.5	320.0	5.7	n.a.	3.7	0.1	5.0
ITA043-3	n.a.	7.1	465	270	14	3.5	0.9	92.0	11.5	320.0	5.7	n.a.	3.7	0.1	5.0
ITA044-1	8.5	7.9	274	170	6	2.3	0.4	54.8	4.7	179.0	2.9	8.4	2.5	0.0	5.6
ITA044-2	8.5	7.9	274	170	6	2.3	0.4	54.8	4.7	179.0	2.9	8.4	2.5	0.0	5.6
ITA044-3	8.5	7.9	274	170	6	2.3	0.4	54.8	4.7	179.0	2.9	8.4	2.5	0.0	5.6
ITA045-1	n.a.	7.5	386	245	8	22.1	n.a.	n.a.	n.a.	n.a.	n.a.	n.a.	n.a.	n.a.	n.a.
ITA046-1	14.6	7.12	855	550	52	34.2	1.9	128.7	23.3	422.2	35.0	68.6	n.a.	n.a.	n.a.
ITA046-2	14.6	7.12	855	550	52	34.2	1.9	128.7	23.3	422.2	35.0	68.6	n.a.	n.a.	n.a.
ITA047-1	7.0	7.5	185	120	3	2.1	0.7	32.0	5.5	115.3	2.5	11.0	1.0	n.a.	n.a.
ITA048-1	7.7	8.1	200	108	2	0.2	n.a.	26.4	14.7	140.0	n.a.	2.1	1.8	0.0	0.9
ITA048-2	7.7	8.1	200	108	2	0.2	n.a.	26.4	14.7	140.0	n.a.	2.1	1.8	0.0	0.9

Sample ID	T (°C)	pH (20°C)	EC (20°C)	TDS (mg L^{-1})	CO_2 (mg L^{-1})	Na^+ (mg L^{-1})	K^+ (mg L^{-1})	Ca^{2+} (mg L^{-1})	Mg^{2+} (mg L^{-1})	HCO_3^- (mg L^{-1})	Cl^- (mg L^{-1})	SO_4^{2-} (mg L^{-1})	NO_3^- (mg L^{-1})	F^- (mg L^{-1})	SiO_2 (mg L^{-1})
ITA049-1	6.3	8.4	118	78	1	1.0	0.2	19.6	4.1	76.0	n.a.	3.0	2.0	n.a.	n.a.
ITA050-1	6.3	8.4	118	78	1	1.0	0.2	19.6	4.1	76.0	n.a.	3.0	2.0	n.a.	n.a.
ITA051-2	12.5	7.8	270	168	7	0.5	n.a.	35.3	19.4	n.a.	n.a.	n.a.	4.0	n.a.	n.a.
ITA052-4	n.a.	5.5	785	576	2380	29.9	42.5	77.5	28.4	415	18.8	37.2	12	1.4	78.0
ITA053-4	n.a.	5.5	767	592	2215	30.2	53.4	77.2	29.0	481.0	15.8	36.3	8.0	1.4	108.0
ITA054-2	21.9	6	939	536	1120	56.0	67.0	86.0	17.0	405.0	51.0	36.0	8.0	1.0	94.0
ITA054-4	21.9	6	939	536	1120	56.0	67.0	86.0	17.0	405.0	51.0	36.0	8.0	1.0	94.0
ITA055-1	15.3	7.43	466	291	34	5.4	0.5	101.5	3.9	318.0	9.8	5.8	0.3	0.1	6.7
ITA055-3	12.4	7.18	474	296	34	5.1	0.7	104.2	3.0	316.4	12.1	7.3	0.7	0.1	6.8
ITA056-1	19.0	5.8	940	650	740	41.5	63.0	86.5	24.0	n.a.	n.a.	n.a.	36.0	1.5	80.0
ITA056-2	19.0	5.8	940	650	740	41.5	63.0	86.5	24.0	n.a.	n.a.	n.a.	36.0	1.5	80.0
ITA056-4	19.0	5.8	940	650	740	41.5	63.0	86.5	24.0	n.a.	n.a.	n.a.	36.0	1.5	80.0
ITA057-1	n.a.	8.25	321	209	35	3.6	n.a.	78.0	1.2	241.0	n.a.	5.0	0.3	n.a.	n.a.
ITA057-3	n.a.	8.25	321	209	35	3.6	n.a.	78.0	1.2	241.0	n.a.	5.0	0.3	n.a.	n.a.
ITA058-1	n.a.	7.6	187	145	10	6.3	7.0	21.0	7.5	98.0	7.1	2.0	1.2	n.a.	48.0
ITA058-3	n.a.	7.6	187	145	n.a.	n.a.	n.a.	n.a.	n.a.	n.a.	n.a.	n.a.	n.a.	n.a.	n.a.
ITA059-4	n.a.	5.58	870	615	2274	30.3	48.0	81.0	29.8	468.0	24.5	38.6	8.0	1.4	79.0
ITA060-4	18.4	6.15	804	564	468	36.1	53.3	85.3	22.2	483.0	n.a.	n.a.	30.0	n.a.	n.a.
ITA061-4	18.4	6.15	804	564	468	36.1	53.3	85.3	22.2	483.0	n.a.	n.a.	30.0	n.a.	n.a.

Sample ID	T (°C)	pH (20°C)	EC (20°C)	TDS (mg L^{-1})	CO_2 (mg L^{-1})	Na^+ (mg L^{-1})	K^+ (mg L^{-1})	Ca^{2+} (mg L^{-1})	Mg^{2+} (mg L^{-1})	HCO_3^- (mg L^{-1})	Cl^- (mg L^{-1})	SO_4^{2-} (mg L^{-1})	NO_3^- (mg L^{-1})	F^- (mg L^{-1})	SiO_2 (mg L^{-1})
ITA062-1	15.7	7.9	202	131	3	4.4	0.6	33.1	5.3	133.0	1.2	1.5	3.7	n.a.	15.8
ITA063-1	n.a.	7.3	748	586	26	5.0	1.4	123.0	40.0	307.0	4.0	225.0	7.0	0.3	10.0
ITA064-1	12.3	7.8	480	294	12	1.0	n.a.	66.7	33.2	342.0	1.4	20.1	5.0	n.a.	n.a.
ITA064-2	12.3	7.8	480	294	12	1.0	n.a.	66.7	33.2	342.0	1.4	20.1	5.0	n.a.	n.a.
ITA065-1	10.7	7.6	310	205	9	0.9	0.2	41.6	23.0	234.0	0.7	6.4	6.1	n.a.	3.5
ITA065-2	10.7	7.6	310	205	9	0.9	0.2	41.6	23.0	234.0	0.7	6.4	6.1	n.a.	3.5
ITA066-2	n.a.	8	416	262	7	0.5	n.a.	61.6	25.8	287.0	0.7	24.9	1.7	n.a.	n.a.
ITA067-1	n.a.	7	2270	2500	44	8.0	n.a.	600.0	82.0	298.0	n.a.	1565.0	n.a.	n.a.	n.a.
ITA068-1	n.a.	7.8	541	348	12	18.1	1.9	74.0	26.7	367.0	n.a.	n.a.	2.6	0.1	n.a.
ITA069-1	4.8	7.9	118	80	3	1.9	1.7	19.9	1.9	57.0	n.a.	15.8	1.5	0.2	5.6
ITA069-2	4.8	7.9	118	80	3	1.9	1.7	19.9	1.9	57.0	n.a.	15.8	1.5	0.2	5.6
ITA069-3	5.0	n.a.	119	80	n.a.	1.9	1.6	20.4	1.8	57.4	n.a.	16.1	1.5	0.2	5.4
ITA070-1	8.9	8	138	98	2	2.5	0.8	23.2	3.5	83.0	2.8	8.0	3.9	0.1	n.a.
ITA070-2	8.9	8	138	98	2	2.5	0.8	23.2	3.5	83.0	2.8	8.0	3.9	0.1	n.a.
ITA070-3	8.9	8	138	98	2	2.5	0.8	23.2	3.5	83.0	2.8	8.0	3.9	0.1	n.a.
ITA071-1	8.0	8.1	63	46	1	2.2	0.6	7.9	1.5	33.0	0.6	6.0	3.2	n.a.	6.0
ITA072-1	14.8	7.9	201	130	3	4.3	0.5	32.6	5.2	132.0	1.3	1.8	3.7	n.a.	16.3
ITA072-2	14.8	7.9	201	130	3	4.3	0.5	32.6	5.2	132.0	1.3	1.8	3.7	n.a.	16.3
ITA073-1	n.a.	8.2	320	200	4	0.4	n.a.	52.3	16.3	235.0	0.5	3.5	5.3	n.a.	n.a.

Sample ID	T (°C)	pH (20°C)	EC (20°C)	TDS (mg L^{-1})	CO_2 (mg L^{-1})	Na^+ (mg L^{-1})	K^+ (mg L^{-1})	Ca^{2+} (mg L^{-1})	Mg^{2+} (mg L^{-1})	HCO_3^- (mg L^{-1})	Cl^- (mg L^{-1})	SO_4^{2-} (mg L^{-1})	NO_3^- (mg L^{-1})	F^- (mg L^{-1})	SiO_2 (mg L^{-1})
ITA074-1	14.1	7.5	605	405	20	7.6	0.6	100.1	28.8	375.0	7.0	n.a.	6.2	0.3	10.5
ITA074-2	14.1	7.5	605	405	20	7.6	0.6	100.1	28.8	375.0	7.0	n.a.	6.2	0.3	10.5
ITA075-2	22.2	n.a.	1125	915	n.a.	33.3	2.2	174.0	51.4	245.0	52.0	430.0	2.6	n.a.	7.1
ITA076-1	15.7	7.9	202	131	3	4.4	0.6	33.1	5.3	133.0	1.2	1.5	3.7	n.a.	15.8
ITA076-2	15.7	7.9	202	131	3	4.4	0.6	33.1	5.3	133.0	1.2	1.5	3.7	n.a.	15.8
ITA077-1	n.a.	7.5	584	400	26	3.3	1.4	86.0	32.0	314.0	3.6	93.0	4.6	0.3	9.2
ITA078-1	n.a.	7.53	472	307	13	16.8	1.7	92.3	3.0	279.0	19.5	n.a.	4.7	n.a.	10.0
ITA078-3	n.a.	7.53	472	307	13	16.8	1.7	92.3	3.0	279.0	19.5	n.a.	4.7	n.a.	10.0
ITA079-1	n.a.	7.39	469	300	19	10.0	1.7	96.0	3.0	280.0	18.5	n.a.	6.0	n.a.	10.0
ITA080-1	n.a.	7.39	518	332	20	18.4	2.2	98.2	3.8	309.0	20.0	n.a.	3.7	n.a.	11.3
ITA080-3	n.a.	7.39	518	332	20	18.4	2.2	98.2	3.8	309.0	20.0	n.a.	3.7	n.a.	11.3
ITA081-1	n.a.	7.53	472	307	13	16.8	1.7	92.3	3.0	279.0	19.5	n.a.	4.7	n.a.	10.0
ITA082-3	8.2	7.6	257	160	7	1.6	0.4	57.8	0.7	172.8	4.3	2.4	1.5	n.a.	6.4
ITA083-1	7.0	7.7	290	180	20	1.5	0.2	58.0	7.0	n.a.	n.a.	1.8	1.1	0.2	2.0
ITA083-3	7.0	7.7	290	180	20	1.5	0.2	58.0	7.0	n.a.	n.a.	1.8	1.1	0.2	2.0
ITA084-3	9.2	7.46	324	207	12	3.3	0.8	65.8	5.6	212.8	5.1	11.6	2.3	0.1	n.a.
ITA085-1	n.a.	7.3	368	234	n.a.	5.0	1.0	75.0	6.0	249.0	n.a.	6.0	2.0	n.a.	n.a.
ITA085-2	n.a.	7.4	367	229	n.a.	5.0	1.0	72.0	5.0	248.0	n.a.	6.0	2.0	n.a.	n.a.
ITA086-1	9.8	7.1	399	245	13	4.0	0.9	71.0	5.0	188.0	n.a.	n.a.	1.5	0.1	8.8

Sample ID	T (°C)	pH (20°C)	EC (20°C)	TDS (mg L^{-1})	CO_2 (mg L^{-1})	Na^+ (mg L^{-1})	K^+ (mg L^{-1})	Ca^{2+} (mg L^{-1})	Mg^{2+} (mg L^{-1})	HCO_3^- (mg L^{-1})	Cl^- (mg L^{-1})	SO_4^{2-} (mg L^{-1})	NO_3^- (mg L^{-1})	F^- (mg L^{-1})	SiO_2 (mg L^{-1})
ITA087-1	6.4	6.9	25	22	2	1.8	0.2	2.8	0.5	9.5	0.2	3.6	1.0	n.a.	7.3
ITA088-1	15.0	6.6	32	35	10	2.6	0.9	n.a.	0.4	18.0	n.a.	n.a.	n.a.	n.a.	14.4
ITA088-2	15.0	6.6	32	35	10	2.6	0.9	n.a.	0.4	18.0	n.a.	n.a.	n.a.	n.a.	14.4
ITA089-1	6.4	7.3	81	50	3	1.8	0.5	12.9	1.2	38.0	n.a.	8.8	0.8	n.a.	5.1
ITA089-2	6.8	7.3	73	48	3	1.4	0.5	12.8	1.2	38.0	n.a.	7.5	0.4	n.a.	5.1
ITA090-1	7.9	7	21	24	1	1.3	0.5	2.4	0.5	6.2	0.6	n.a.	2.5	0.2	9.3
ITA090-2	7.9	7	21	24	1	1.3	0.5	2.4	0.5	6.2	0.6	n.a.	2.5	0.2	9.3
ITA091-1	10.1	7.7	328	228	3	5.4	2.8	57.2	7.2	110.0	3.0	86.5	3.4	0.1	7.7
ITA092-1	5.4	6.9	71	47	3	0.3	0.3	10.2	4.0	48.8	0.2	1.7	2.5	n.a.	2.8
ITA092-2	3.2	7.6	76	48	4	0.3	0.3	10.2	4.4	52.0	0.2	1.8	2.3	n.a.	2.5
ITA093-1	7.4	6.7	21	17	2	1.3	0.6	n.a.	0.3	n.a.	n.a.	2.1	1.9	n.a.	n.a.
ITA094-1	9.1	6.3	15	14	4	1.0	0.2	1.5	0.4	5.0	0.4	1.2	2.3	n.a.	4.5
ITA095-1	n.a.	n.a.	n.a.	47	n.a.	1.4	n.a.	n.a.	n.a.	n.a.	n.a.	n.a.	n.a.	n.a.	n.a.
ITA096-1	7.0	7.1	25	23	1	1.3	0.6	2.9	0.5	n.a.	0.2	3.8	2.1	0.2	7.0
ITA096-2	7.0	7.1	25	23	1	1.3	0.6	2.9	0.5	n.a.	0.2	3.8	2.1	0.2	7.0
ITA097-1	n.a.	7	48	35	6	0.8	0.4	9.1	0.6	27.9	0.8	2.6	1.4	n.a.	4.2
ITA097-2	n.a.	7	48	35	6	0.8	0.4	9.1	0.6	27.9	0.8	2.6	1.4	n.a.	4.2
ITA098-1	n.a.	6.6	32	35	10	2.6	n.a.	n.a.	n.a.	n.a.	n.a.	n.a.	n.a.	n.a.	n.a.
ITA099-1	5.7	7.4	69	43	2	1.2	n.a.	12.0	n.a.	29.0	n.a.	n.a.	0.8	n.a.	3.7

Sample ID	T (°C)	pH (20°C)	EC (20°C)	TDS (mg L^{-1})	CO_2 (mg L^{-1})	Na^+ (mg L^{-1})	K^+ (mg L^{-1})	Ca^{2+} (mg L^{-1})	Mg^{2+} (mg L^{-1})	HCO_3^- (mg L^{-1})	Cl^- (mg L^{-1})	SO_4^{2-} (mg L^{-1})	NO_3^- (mg L^{-1})	F^- (mg L^{-1})	SiO_2 (mg L^{-1})
ITA099-1	6.4	6.9	25.4	22.0	2	1.5	n.a.	2.9	n.a.	10	n.a.	n.a.	0.81	n.a.	n.a.
ITA099-2	6.4	6.9	24.5	23.8	2.5	1.7	n.a.	2.4	n.a.	7.5	n.a.	3.8	1.1	n.a.	9
ITA099-3	5.7	7.4	69	43	2	1.2	n.a.	12.0	n.a.	29.0	n.a.	n.a.	0.8	n.a.	3.7
ITA100-1	9.4	6.8	27	20	1	1.8	0.5	n.a.	0.5	n.a.	0.6	4.0	n.a.	n.a.	n.a.
ITA100-2	9.4	6.8	27	20	1	1.8	0.5	n.a.	0.5	n.a.	0.6	4.0	n.a.	n.a.	n.a.
ITA101-1	20.5	6.9	361	231	11	35.0	2.1	19.4	5.0	58.0	63.5	4.2	0.8	0.3	6.3
ITA102-1	20.5	6.9	361	231	11	35.0	2.1	19.4	5.0	58.0	63.5	4.2	0.8	0.3	6.3
ITA103-1	23.0	7.4	674	332	21	53.1	2.0	43.4	17.6	223.2	63.4	n.a.	0.7	0.2	20.6
ITA104-1	21.5	7.3	479	282	20	44.2	1.8	28.8	17.1	163.1	62.4	n.a.	0.3	0.4	28.1
ITA105-1	22.0	7.2	494	296	24	51.1	2.0	26.3	15.2	160.5	61.0	n.a.	0.6	0.5	33.3
ITA106-1	28.0	7.4	674	332	21	53.1	2.0	43.4	17.6	223.2	63.4	n.a.	0.7	0.2	20.6
ITA107-1	24.0	6.9	497	278	50	43.5	1.8	28.2	17.4	166.1	58.1	n.a.	0.5	0.1	26.5
ITA108-1	22.0	6.6	3630	3082	1118	780.0	91.0	180.0	54.0	2092.9	285.0	237.5	0.8	0.9	13.9
ITA109-2	18.0	6.45	1842	1380	1434	295.0	n.a.	n.a.	70.0	1354.5	n.a.	n.a.	0.2	1.9	18.4
ITA110-1	13.0	7.6	167	130	2	28.5	1.2	6.0	4.0	33.9	28.3	20.7	6.2	0.2	21.7
ITA111-1	15.0	6.14	205	133	21	22.5	1.1	7.7	3.0	22.9	n.a.	5.8	n.a.	0.2	10.9
ITA112-1	13.0	7.01	283	215	3	35.0	7.1	8.3	7.2	n.a.	26.8	34.0	n.a.	0.3	n.a.
ITA113-1	12.3	6.83	212	152	15	11.4	n.a.	25.6	7.7	89.1	14.9	n.a.	0.6	0.2	n.a.
ITA114-1	13.1	7.56	242	168	7	14.5	2.0	29.5	5.2	78.6	17.4	36.7	1.0	0.4	n.a.

Sample ID	T (°C)	pH (20°C)	EC (20°C)	TDS (mg L^{-1})	CO_2 (mg L^{-1})	Na^+ (mg L^{-1})	K^+ (mg L^{-1})	Ca^{2+} (mg L^{-1})	Mg^{2+} (mg L^{-1})	HCO_3^- (mg L^{-1})	Cl^- (mg L^{-1})	SO_4^{2-} (mg L^{-1})	NO_3^- (mg L^{-1})	F^- (mg L^{-1})	SiO_2 (mg L^{-1})
ITA115-3	16.5	7.61	937	611	21	84.5	2.8	76.1	n.a.	213.0	n.a.	36.1	n.a.	0.2	n.a.
ITA116-1	14.1	7.34	246	163	9	13.1	1.9	26.5	9.8	103.1	n.a.	18.9	5.0	0.7	n.a.
ITA117-1	19.7	7.06	513	383	n.a.	16.8	2.3	88.8	6.1	274.6	32.7	8.1	n.a.	0.2	n.a.
ITA118-1	18.9	7.31	553	362	29	29.1	1.9	64.6	27.6	302.0	41.8	n.a.	n.a.	n.a.	n.a.
ITA118-2	18.9	7.31	553	362	29	29.1	1.9	64.6	27.6	302.0	41.8	n.a.	n.a.	n.a.	n.a.
ITA119-1	19.7	7.06	513	383	n.a.	16.8	2.3	88.8	6.1	274.6	32.7	8.1	n.a.	0.2	n.a.
ITA120-1	n.a.	6.7	251	146	n.a.	n.a.	n.a.	n.a.	n.a.	47.0	n.a.	n.a.	n.a.	n.a.	n.a.
ITA121-1	13.9	7.48	251	173	8	16.1	1.7	30.2	5.6	82.4	18.2	38.8	0.9	0.5	n.a.
ITA122-1	15.2	7.64	424	265	8	7.2	0.9	60.8	20.0	256.0	14.2	14.9	2.0	0.6	8.1
ITA123-1	n.a.	6.7	251	146	n.a.	n.a.	n.a.	n.a.	n.a.	47.0	n.a.	n.a.	n.a.	n.a.	n.a.
ITA124-1	n.a.	6.7	251	146	n.a.	n.a.	n.a.	n.a.	n.a.	47	n.a.	n.a.	n.a.	n.a.	n.a.
ITA125-1	6.8	6.7	44	36	4	1.7	n.a.	6.7	n.a.	24.0	n.a.	n.a.	4.7	n.a.	n.a.
ITA125-2	6.8	6.7	44	36	4	1.7	n.a.	6.7	n.a.	24.0	n.a.	n.a.	4.7	n.a.	n.a.
ITA126-1	33.3	6.1	3430	3465	689	27.0	6.2	702.0	185.0	860.0	24.0	1889.0	1.2	2.8	34.0
ITA127-1	9.8	5.6	43	28	14	4.7	0.1	0.7	0.9	7.3	6.9	0.5	4.2	n.a.	3.8
ITA128-1	19.0	7.4	509	311	16	28.0	1.2	40.0	17.0	175.0	43.0	26.0	0.2	0.1	9.9
ITA128-2	19.0	7.4	509	311	16	28.0	1.2	40.0	17.0	175.0	43.0	26.0	0.2	0.1	9.9
ITA129-1	19.0	7.4	509	311	16	28.0	1.2	40.0	17.0	175.0	43.0	26.0	0.2	0.1	9.9
ITA129-2	19.0	7.4	509	311	16	28.0	1.2	40.0	17.0	175.0	43.0	26.0	0.2	0.1	9.9

Sample ID	T (°C)	pH (20°C)	EC (20°C)	TDS (mg L^{-1})	CO_2 (mg L^{-1})	Na^+ (mg L^{-1})	K^+ (mg L^{-1})	Ca^{2+} (mg L^{-1})	Mg^{2+} (mg L^{-1})	HCO_3^- (mg L^{-1})	Cl^- (mg L^{-1})	SO_4^{2-} (mg L^{-1})	NO_3^- (mg L^{-1})	F^- (mg L^{-1})	SiO_2 (mg L^{-1})
ITA129-3	19.0	7.4	509	311	16	28.0	1.2	40.0	17.0	175.0	43.0	26.0	0.2	0.1	9.9
ITA130-1	16.3	7.4	399	248	8	11.2	1.0	68.5	5.3	211.0	17.3	11.4	11.5	n.a.	10.5
ITA130-2	16.3	7.4	399	248	8	11.2	1.0	68.5	5.3	211.0	17.3	11.4	11.5	n.a.	10.5
ITA131-3	5.9	7	115	79	6	3.1	0.5	19.0	1.6	58.6	5.3	5.9	4.1	n.a.	2.2
ITA132-1	11.6	8	282	190	4	8.9	1.0	39.7	12.0	160.0	4.8	29.5	1.6	n.a.	10.1
ITA132-2	11.6	8	282	190	4	8.9	1.0	39.7	12.0	160.0	4.8	29.5	1.6	n.a.	10.1
ITA133-1	10.3	8	222	141	4	6.7	0.9	32.0	6.4	103.0	9.0	22.7	2.9	n.a.	7.1
ITA134-1	18.5	7.5	1079	620	32	118.0	3.0	68.0	35.0	388.0	115.0	64.0	13.0	0.2	11.0
ITA134-2	18.5	7.5	1079	620	32	118.0	3.0	68.0	35.0	388.0	115.0	64.0	13.0	0.2	11.0
ITA135-1	13.4	5.7	76	58	29	9.0	0.4	2.4	2.8	12.2	13.5	2.5	9.6	n.a.	9.2
ITA136-1	11.3	8	2	156	3	4.8	0.6	31.1	11.7	112.0	5.0	36.7	0.6	n.a.	9.2
ITA137-1	14.0	7.3	940	635	34	43.0	1.9	131.0	28.0	351.0	39.0	181.0	n.a.	0.1	16.0
ITA138-1	14.0	7.3	940	635	34	43.0	1.9	131.0	28.0	351.0	39.0	181.0	n.a.	0.1	16.0
ITA139-1	11.0	7.3	240	157	8	6.2	0.9	39.0	5.8	135.0	7.1	18.9	0.7	0.1	8.4
ITA140-4	n.a.	5.8	1122	180	1404	73.1	7.3	172.0	26.2	574.0	81.1	102.0	7.2	1.0	8.3
ITA141-1	11.0	7.3	240	157	8	6.2	0.9	39.0	5.8	135.0	7.1	18.9	0.7	0.1	8.4
ITA141-2	11.0	7.3	240	157	8	6.2	0.9	39.0	5.8	135.0	7.1	18.9	0.7	0.1	8.4
ITA142-2	9.8	7.27	721	498	70	13.8	1.7	162.0	8.6	444.0	17.2	n.a.	4.3	n.a.	16.6
ITA143-2	14.9	7.27	721	498	70	13.8	1.7	162.0	8.6	444.0	17.2	n.a.	4.3	n.a.	16.6

Sample ID	T (°C)	pH (20°C)	EC (20°C)	TDS (mg L^{-1})	CO_2 (mg L^{-1})	Na^+ (mg L^{-1})	K^+ (mg L^{-1})	Ca^{2+} (mg L^{-1})	Mg^{2+} (mg L^{-1})	HCO_3^- (mg L^{-1})	Cl^- (mg L^{-1})	SO_4^{2-} (mg L^{-1})	NO_3^- (mg L^{-1})	F^- (mg L^{-1})	SiO_2 (mg L^{-1})
ITA144-1	n.a.	7.54	546	388	13	22.4	1.9	90.0	15.9	235.0	26.8	87.6	2.2	0.2	6.7
ITA145-1	11.9	7.38	335	222	36	3.2	0.5	75.2	1.2	231.0	6.8	2.6	2.6	n.a.	10.1
ITA145-2	11.2	7.29	352	231	38	3.3	0.6	75.4	1.9	226.0	7.1	2.8	2.5	n.a.	n.a.
ITA146-1	12.1	7.05	714	460	81	17.4	1.6	146.0	6.8	427.0	n.a.	46.4	7.2	n.a.	n.a.
ITA147-1	12.1	7.05	714	460	81	17.4	1.6	146.0	6.8	427.0	n.a.	46.4	7.2	n.a.	n.a.
ITA147-2	12.1	7.05	714	460	81	17.4	1.6	146.0	6.8	427.0	n.a.	46.4	7.2	n.a.	12.4
ITA148-1	14.4	7.17	627	465	83	10.8	1.7	138.0	6.0	379.0	15.8	36.1	14.4	n.a.	11.8
ITA148-2	n.a.	7.17	627	465	83	10.8	1.7	138.0	6.0	379.0	15.8	36.1	14.4	n.a.	11.8
ITA149-1	n.a.	7.54	546	388	13	22.4	1.9	90.0	15.9	235.0	26.8	87.6	2.2	0.2	6.7
ITA149-2	n.a.	7.54	546	388	13	22.4	1.9	90.0	15.9	235.0	26.8	87.6	2.2	0.2	6.7
ITA150-4	16.5	6.2	1661	1195	1749	13.3	2.4	461.0	5.5	1245.0	n.a.	n.a.	8.1	n.a.	n.a.
ITA151-1	n.a.	7.57	454	291	12	18.9	2.5	60.9	17.1	245.0	9.9	54.3	n.a.	1.2	9.8
ITA152-1	n.a.	7.67	331	226	8	3.4	0.9	76.6	4.1	201.0	6.1	22.8	1.8	n.a.	7.3
ITA153-1	n.a.	7.55	282	178	8	4.5	0.5	57.7	3.3	181.6	7.5	7.7	1.4	0.1	5.1
ITA153-2	n.a.	7.56	276	174	8	4.1	0.4	57.4	3.2	182.1	6.8	6.8	1.1	0.1	4.2
ITA153-2	n.a.	7.55	282	178	8	4.5	0.5	57.7	3.3	181.6	7.5	7.7	1.4	0.1	5.1
ITA153-3	n.a.	7.55	282	178	8	4.5	0.5	57.7	3.3	181.6	7.5	7.7	1.4	0.1	5.1
ITA154-1	n.a.	7.5	462	284	14	16.8	1.7	63.3	20.9	254.0	11.1	50.1	0.7	0.9	11.2
ITA154-3	n.a.	7.5	462	284	14	16.8	1.7	63.3	20.9	254.0	11.1	50.1	0.7	0.9	11.2

Sample ID	T (°C)	pH (20°C)	EC (20°C)	TDS (mg L^{-1})	CO_2 (mg L^{-1})	Na^+ (mg L^{-1})	K^+ (mg L^{-1})	Ca^{2+} (mg L^{-1})	Mg^{2+} (mg L^{-1})	HCO_3^- (mg L^{-1})	Cl^- (mg L^{-1})	SO_4^{2-} (mg L^{-1})	NO_3^- (mg L^{-1})	F^- (mg L^{-1})	SiO_2 (mg L^{-1})
ITA155-1	11.0	6.19	1365	932	870	19.5	3.4	326.0	15.4	1155.0	17.3	69.3	0.8	0.3	33.5
ITA156-1	10.3	7.42	415	265	34	3.0	n.a.	93.6	1.8	261.0	6.4	2.2	8.8	n.a.	10.5
ITA156-3	10.3	7.42	415	265	34	3.0	n.a.	93.6	1.8	261.0	6.4	2.2	8.8	n.a.	10.5
ITA157-1	10.3	7.42	415	265	34	3.0	n.a.	93.6	1.8	261.0	6.4	2.2	8.8	n.a.	10.5
ITA157-2	10.3	7.42	415	265	34	3.0	n.a.	93.6	1.8	261.0	6.4	2.2	8.8	n.a.	10.5
ITA158-1	n.a.	7.58	417	288	12	2.9	1.0	89.4	10.5	231.0	4.2	53.2	2.4	0.2	7.7
ITA158-3	n.a.	7.58	417	288	12	2.9	1.0	89.4	10.5	231.0	4.2	53.2	2.4	0.2	7.7
ITA159-2	n.a.	n.a.	510	416	n.a.	n.a.	32.0	46.0	n.a.	306.0	26.0	14.0	4.0	n.a.	105.0
ITA160-2	9.6	8.1	166	105	2	1.1	0.9	22.2	8.2	88.0	0.5	19.3	1.8	0.1	7.0
ITA161-1	8.5	8.1	233	141	3	1.3	0.6	30.2	15.7	158.0	1.3	8.7	3.3	0.1	6.8
ITA162-1	11.1	7.9	238	154	4	1.0	0.2	34.4	15.5	160.0	0.7	16.1	3.8	n.a.	1.7
ITA162-2	11.1	7.9	238	154	4	1.0	0.2	34.4	15.5	160.0	0.7	16.1	3.8	n.a.	1.7
ITA163-1	15.1	7.52	420	265	8	6.0	0.9	50.3	30.8	313.0	2.2	3.7	9.0	n.a.	12.0
ITA163-2	15.1	7.52	420	265	8	6.0	0.9	50.3	30.8	313.0	2.2	3.7	9.0	n.a.	12.0
ITA163-3	15.1	7.52	420	265	8	6.0	0.9	50.3	30.8	313.0	2.2	3.7	9.0	n.a.	12.0
ITA164-1	n.a.	7.9	251	162	4	2.1	0.5	36.3	12.7	150.0	2.3	18.9	4.4	n.a.	n.a.
ITA164-2	n.a.	n.a.	251	162	n.a.	2.1	0.5	36.3	12.7	150.0	2.3	18.9	4.4	n.a.	n.a.

Note: n.a. = not available

Table S4. Mercury concentrations (μg L^{-1}) found in bottled mineral waters in previous studies

No. Brands	LOD μg L^{-1}	Min	Max	Analytical Technique	Country	References
37	0.1	0.1	1.2	AAS	[a] World	Allen et al. (1989)
56	0.005	< 0.005	0.26	ICP-MS	[b] EU	Misund et al. (1999)
5	0.02	0.01	0.03	HG-ICP-MS	Egypt	Saleh et al. (2001)
25	0.50	0.50	79	ICP-OES	USA	Ikem et al. (2002)
7	0.00001	0.0001	0.00232	ID-CV-ICP-MS	[c] World	Mann et al. (2003)
33	0.02	0.02	0.43	ICP-MS	Sweden	Rosborg et al. (2005)
35	0.02	0.16	0.86	ICP-MS	USA	Saleh et al. (2008)
39	0.02	0.06	0.8	AAS	Portugal	Barroso et al. (2009)
158	< 0.005	< 0.005	< 0.005	AFS	Italy	Cicchella et al. (2010)
5	0.001	< 0.02	< 0.02	ICP-MS	Estonia	Bityukova et al. (2010)
93	0.02	0.47	0.47	ICP-MS	Kuwait	Al-Mudhaf et al. (2010)
18	< 1.0	< 1.0	< 1.0	AAS	Iran	Mohebali et al. (2010)
42	0.1	0.47	0.5	HG-AAS	Iran	Hadiani et al. (2010)
502	0.0001	< 0.005	< 0.005	AFS	Germany	Birke. Rauch et al. (2010)
1247	0.0001	< 0.005	< 0.005	AFS	[d] EU	Birke. Reimann et al. (2010)
174	< 0.00009	< 0.00009	0.00539	CV-AFS	[e] Italy	Present study

[a] 10 countries, [b] 15 countries, [c] 7 countries, [d] 40 countries, [e] 5 countries

Chemosphere 197 (2018) 306–317

Contents lists available at ScienceDirect

Chemosphere

journal homepage: www.elsevier.com/locate/chemosphere

Feedback mechanisms between snow and atmospheric mercury: Results and observations from field campaigns on the Antarctic plateau

Andrea Spolaor [a, *], Hélène Angot [b, 1], Marco Roman [a], Aurélien Dommergue [b], Claudio Scarchilli [c], Massimiliano Vardè [a], Massimo Del Guasta [d], Xanthi Pedeli [e], Cristiano Varin [e], Francesca Sprovieri [f], Olivier Magand [b], Michel Legrand [b], Carlo Barbante [a, e], Warren R.L. Cairns [a]

[a] CNR-Institute for the Dynamics of Environmental Processes (IDPA), 30172, Venice-Mestre, Italy
[b] Univ. Grenoble Alpes, CNRS, IRD, Grenoble INP, Institut des Géosciences de l'Environnement (IGE), 38000, Grenoble, France
[c] ENEA, C.R. Casaccia, 00123, Roma, Italy
[d] CNR-National Institute of Optics (INO), 50019, Sesto Fiorentino, Italy
[e] Department of Environmental Sciences, Informatics and Statistics, University Ca' Foscari of Venice, 30172, Venice -Mestre, Italy
[f] CNR-Institute of Atmospheric Pollution Research (IIA), Division of Rende, 87036, Rende, Italy

HIGHLIGHTS

- Three sampling summer campaigns from 2013 to 2015.
- Daily and hourly mercury and halogens concentration in surface snow.
- Inverse relationship between mercury in snow and atmosphere.
- Fast decreasing rate after snow fall events.

GRAPHICAL ABSTRACT

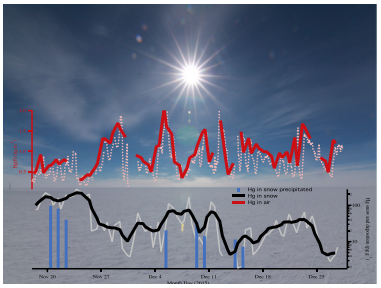

ARTICLE INFO

Article history:
Received 12 September 2017
Received in revised form
21 December 2017
Accepted 28 December 2017
Available online 5 January 2018

Handling Editor: R Ebinghaus

Keywords:
Mercury
Antarctica
Dome C

ABSTRACT

The Antarctic Plateau snowpack is an important environment for the mercury geochemical cycle. We have extensively characterized and compared the changes in surface snow and atmospheric mercury concentrations that occur at Dome C. Three summer sampling campaigns were conducted between 2013 and 2016.

The three campaigns had different meteorological conditions that significantly affected mercury deposition processes and its abundance in surface snow. In the absence of snow deposition events, the surface mercury concentration remained stable with narrow oscillations, while an increase in precipitation results in a higher mercury variability. The Hg concentrations detected confirm that snowfall can act as a mercury atmospheric scavenger. A high temporal resolution sampling experiment showed that surface concentration changes are connected with the diurnal solar radiation cycle. Mercury in surface snow is highly dynamic and it could decrease by up to 90% within 4/6 h. A negative relationship between

* Corresponding author.
E-mail address: andrea.spolaor@unive.it (A. Spolaor).
[1] Now at Institute for Data, Systems and Society. Massachusetts Institute of Technology, Cambridge, USA.

https://doi.org/10.1016/j.chemosphere.2017.12.180

Halogens
Precipitation
Snow

surface snow mercury and atmospheric concentrations has been detected suggesting a mutual dynamic exchange between these two environments.

Mercury concentrations were also compared with the Br concentrations in surface and deeper snow, results suggest that Br could have an active role in Hg deposition, particularly when air masses are from coastal areas.

This research presents new information on the presence of Hg in surface and deeper snow layers, improving our understanding of atmospheric Hg deposition to the snow surface and the possible role of re-emission on the atmospheric Hg concentration.

1. Introduction

The Antarctic Plateau snowpack has been identified as a sink and source of atmospheric mercury.

A pioneering study, conducted at Dome C in 2013, highlighted the roles of photochemical reactions, the oxidative capacity of the boundary layer, and the dynamics of chemical exchanges of Hg at the air–snow interface (Angot et al., 2016c).

The Antarctic continent is considered a natural laboratory for environmental studies. Its distance from the main anthropogenic sources makes Antarctica one of the best locations for experiments to understand chemical and physical processes, especially those that define features of the biogeochemical cycles of anthropogenically and naturally emitted elements. Antarctica is isolated by the circumpolar vortex from the rest of the troposphere meaning that only long lived contaminants such as Hg(0) can reach the plateau (Dommergue et al., 2010). Understanding the role of Antarctica and the Antarctic Plateau (AP) (altitude > 2500 m a.s.l.) in the global mercury cycle is crucial since the Antarctic Plateau and its snowpack are considered both a sink and a source of atmospheric mercury (Angot et al., 2016b).

Mercury (Hg) is an element with a known toxicity and it is present in the environment in several different chemical forms. Mercury is reactive in the environment and undergoes photochemical reactions that change its speciation and chemical behaviour.

Continuous measurements of atmospheric Hg in Antarctica are scarce (Angot et al., 2016a). A few years ago, long-term atmospheric Hg measurements started at the near-coastal Norwegian Station Troll (TRS) (Pfaffhuber et al., 2012). In the framework of the Global Mercury Observation System (GMOS) project (Sprovieri et al., 2016, 2017), Hg measurements in air and wet deposition were initiated in 2012, including in the 40 ground-based monitoring sites of this network, the French coastal station Dumont D'Urville (DDU) (Angot et al., 2016b) and at the Italo-French station Concordia at Dome C (DC) on the Antarctic Plateau (Angot et al., 2016c).

On the Plateau, where the snowpack is perennial and very distant from coastal influences; the local atmospheric conditions are very different from those observed at coastal sites where most of the measurements have been made up to now. Observations already made on the Antarctic Plateau suggest that deposition of mercury in the snowpack occurs in summer, resulting in levels of total Hg in the surface snow of up to 200 of pg g^{-1} (Han et al., 2014; Angot et al., 2016c). After the dark and more stable winter conditions, Hg(0) concentrations on the Antarctic Plateau become highly variable during the sunlit period due to photochemical processes. Occasionally, and less intensively than at coastal sites, Atmospheric Mercury Depletion Events (AMDEs) associated with coastal air masses enriched in halogen radicals can be observed in the spring (Angot et al., 2016c). Spring increases in gas phase Br have been detected at DC (Legrand et al., 2016b) suggesting that during this period, emissions from sea ice might reach the Antarctic plateau and interact with Hg. Mercury in the atmosphere is present in its gaseous elemental form (Hg(0), GEM) or as particulate (Hg(p))/gaseous (reactive gaseous mercury (RGM) or gaseous oxidized mercury (GOM)) divalent mercury (Hg(II)) that can undergo wet and dry deposition (Schroeder et al., 1998).

Mercury in its oxidized form can be deposited onto the snowpack, altering Hg concentrations in the upper snow strata. Once present in the snowpack, Hg is very labile, it can be reduced back to Hg(0) and can undergo dynamic exchange with the atmosphere above (Steffen et al., 2002). Photochemical reactions are important in altering the speciation of Hg in the snowpack and depend on environmental properties and snowpack chemistry. The role of the snowpack is crucial in the mercury cycle in Polar Regions since it acts as both a sink (deposition, accumulation) and a source (re-emission).

Several studies have already been carried out on the Antarctic continent with the aim of determining the extent of mercury recycling between the surface snow and the lower atmosphere over the plateau (Brooks et al., 2008; Dommergue et al., 2012; Han et al., 2014; Angot et al., 2016c; Wang et al., 2016).

Differences in concentration between the surface snow and deeper snow pit samples suggests a significant re-emission of Hg from surface snow to the atmosphere (Han et al., 2014). Combining the results from Han et al. (2014), with atmospheric measurements from the South Pole (Brooks et al., 2008) and Dome C, and total Hg measurements in the Dome Fuji snowpack, it can be inferred that the Antarctic Plateau snowpack might act as a temporary reservoir for Hg from mid-winter to mid-summer, but changes to a source of atmospheric Hg(0) during mid to late-summer. However, the overall understanding of the mechanism is still not fully clear.

Estimates by Brooks et al. (2008) suggest that the Hg(II) deposited to the snowpack is subsequently photo-reduced and re-emitted as Hg(0) from the surface, and that only 10% of the deposited Hg is sequestered and deeply buried. In the Arctic snow it is estimated that 24 h after deposition, a fraction of Hg is already re-emitted as Hg(0) to the atmosphere (Lalonde et al., 2002; Dommergue et al., 2003). It has been shown that surface Arctic snow could lose up to 90% of its total Hg content within 48 h (Poulain et al., 2004). Similar re-emission/loss rates of Hg from surface (35–50%) and drifting snow (65–75%) over 10.5 h have been suggested by Sherman et al., (2010) (Sherman et al., 2010) in chamber experiments. Several studies have evaluated the loss rate of mercury in the Arctic and the general behaviour of this element, however there is still lack of knowledge regarding the Antarctic continent. Some studies evaluate the role of snow precipitation on the Antarctic coast (Douglas et al., 2005, 2008; Domine et al., 2011) and only recently experiments trying to evaluate the mercury cycle in the Antarctic Plateau have been carried out (Dommergue et al., 2012; Angot et al., 2016c). No studies deeply investigate the processes at the snow atmosphere interface as well as the role of snow precipitation on the mercury cycle on the inner Antarctic plateau. To understand this it is crucial to understand the mechanisms and

parameters governing/controlling mercury at the snow surface on the Plateau, and the roles of snowfall and diamond dust (DD), the main forms of precipitation, in non-coastal areas has yet to be determined. It has been shown that a significant part of the precipitation that falls on the Antarctic Plateau (Bromwich, 1988; Fujita and Abe, 2006; Stenni et al., 2016) is in the form of DD under clear-sky conditions. Additionally, bromine radicals are also thought to play a major part in Hg oxidation and therefore deposition (Goodsite et al., 2004; Holmes et al., 2010).

The results presented in this paper build on the work reported by Angot et al. (2016c), on weekly surface snow samples collected at DC in 2013. The snow sampling has been intensified and we focused on the summertime when Hg reactivity was at its highest. The results reported here cover three campaigns: 1st) November-December 2013, 2nd) December 2014-January 2015 and the 3rd) November-December 2015. The objective was to investigate the daily and hourly Hg variations in surface snow. Mercury concentrations in surface snow were combined with atmospheric Hg(0) measurements to evaluate the interchange of Hg at the air-snow interface. Additionally, halogens (I, Br) and Na were analysed in surface snow samples to investigate their potential interactions with Hg and their use as markers of marine air masses. Bromine (Br) concentrations in the snow could give indications on the presence/abundance of bromine radicals present at Dome C.

2. Experimental section

2.1. Dome C research station

Concordia station, located at Dome C (DC), is approximately 1200 km away from the coastline at an elevation of 3220 m above sea level. Temperature, relative humidity, wind speed and direction, and incoming solar radiation are routinely monitored (www.climantartide.it). DC is characterized by a high-pressure system favouring, for most of the year, clear sky conditions. However, cyclonic systems forming in coastal areas can occasionally reach the Antarctic Plateau causing snow deposition and intromission of relatively humid air masses (Scarchilli et al., 2011; Stenni et al., 2016). The annual precipitation is in the range of 30 mm of water equivalent (around 10 cm of snow) per year (Genthon et al., 2013, 2016; Schlosser et al., 2016).

2.2. Atmospheric mercury measurements

Concomitant continuous measurements of gaseous elemental mercury (Hg(0)) concentrations in ambient air have been routinely performed at Dome C since 2012 (Angot et al., 2016c). During the three campaigns discussed in this paper (see section 2.3.1), atmospheric Hg(0) measurements were performed using a Tekran 2537A analyser (Tekran Inc., Toronto, Canada) located in a above-surface shelter in the “clean area”, approximately 800 m away and upwind of the main camp with respect to the dominant wind direction (south to north). As described in details by (Angot et al., 2016c), bi-monthly to monthly routine maintenance operations were performed – following strict quality assurance and quality control procedures as detailed in the GMOS standard operating procedures – to provide a high-quality dataset. Concentrations are expressed in nanograms per cubic meter (ng m^{-3}) at standard temperature and pressure (273.15 K, 1013.25 hPa).

Until December 2014, a 0.45 μm PTFE filter was used at the entrance inlet of the unheated PTFE sample line and it was assumed that only Hg(0) (vs. total gaseous mercury (TGM), defined as the sum of gaseous mercury species, GEM + GOM) was efficiently collected and analysed (Angot et al., 2016c). From 12 December 2014 to 11 January 2015, and from 7 to 30 December 2015, a Polyethersulfone (PES) cation-exchange membrane (0.45 μm, 47 mm) was used at the entrance inlet of the sample line to collect Hg(II) species (resulting in time-integrated samples). The Tekran instrument was further protected by a 0.2 μm PTFE filter. Although chemical analysis of the membranes has yet to be performed, the use of PES cation-exchange membranes is relatively common practise for the collection of airborne Hg(II) species (Ebinghaus et al., 1999; Caldwell et al., 2006; Lyman et al., 2009, 2010; Castro et al., 2012; Huang et al., 2012). This gives us a greater confidence that only Hg(0) was collected and analysed by the Tekran instrument during the above-mentioned time periods.

2.3. Surface snow sampling and analysis

2.3.1. Three campaigns

Three sampling campaigns were conducted at DC and are designated with their Italian expedition number in Roman numerals here onwards. The first (XXIX campaign) from the 22nd of November 2013 to the 5th December 2013 (12 days), the second (XXX campaign) from the 15th of December 2014 to the 17th of January 2015 (33 days), and the third (XXXI campaign) from the 17th of November 2015 to the 27th of December 2015 (40 days). It should be noted that the three campaigns were performed at increasing sampling intervals and different periods of summer (Nov to mid-Feb, as defined by Angot et al., 2016c) and that the intensity of the various physical-chemical processes involved at the air-snow interface might differ between them. Previous studies show that the oxidation of atmospheric Hg(0) on the Antarctic Plateau is more active in mid and late summer (Dec-Jan) than early summer (Nov) and spring (Sep-Oct) (Brooks et al., 2008; Angot et al., 2016a). Fig. 1 shows that the daily cycle of Hg(0) concentrations at DC intensifies throughout summer and peaks in January when incoming solar radiation is maximum. This is due to a dynamic daily cycle of Hg(0) oxidation, Hg(II) deposition to the snowpack, and Hg(0) re-emissions from the snowpack when light is present (Angot et al., 2016c).

The main objectives of the XXIX campaign were to investigate the potential influence of the station activities on the surface snow samples and to collect snow pit samples. Daily surface snow samples were then collected during the XXX campaign. The sampling frequency increased further in the XXXI campaign with surface snow samples being collected twice a day for the entire campaign and hourly during an intensive 72 h sampling period.

Once the snow was collected and safely stored in Venice, the samples were melted and analysed for Hg. To extract more

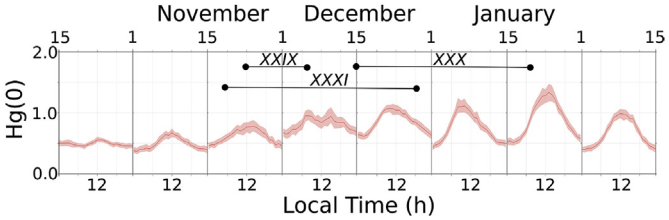

Fig. 1. Hourly (local time) mean variation, along with the 95% confidence interval for the mean, of Hg(0) concentrations in ambient air (in ng m^{-3}) measured at Dome C from the second half of October to the first half of February. The diurnal cycle intensifies throughout summer and peaks during the second-half of January, suggesting a more dynamic cycle of Hg(0) oxidation, deposition, and re-emission at the air-snow interface. Note that the hourly mean variation was calculated based on Hg(0) concentrations measured at Dome C from January 2012 to December 2015. The dates of the three campaigns are also reported. The first one (XXIX) occurred from the 22nd of November 2013 to the 5th of December 2013, the second one (XXX) from the 15th of December 2014 to the 17th of January 2015, and the third one (XXXI) from the 17th of November 2015 to the 27th of December 2015.

information and to help interpret the behaviour of Hg, total bromine (Br), iodine (I) and sodium (Na) in the snow samples were also analysed. Bromine radicals, are involved in the oxidation of Hg(0) (Goodsite et al., 2004; Wang et al., 2014) favouring Hg deposition to the snowpack so the determination of total Br concentration (mainly in the forms of Br^-) in the snow could give some indication of the amount of the bromine and its radical present in the Dome C atmosphere. Sodium is generally indicative of the presence of marine aerosol in the atmosphere, whilst iodine, that can be photochemically activated, could be used as an indicator of activation by incoming solar radiation (Spolaor et al., 2014). Another parameter we include in the evaluation is the Bromine enrichment. The Br enrichment factor is calculated as $Br_{enr} = Br/Na^*0.006$, and indicates eventual excesses of bromine in the air or snow compared to its seawater abundance. Total Br in the snow can be enriched due to the presence of additional sources other than marine aerosol, such as sea ice gas phase bromine production (Spolaor et al., 2013).

2.3.2. Sampling procedure

As for the atmospheric Hg measurements, the snow samples for the determination of total Hg, Na, I, Br and its enrichment factor, were collected in the "clean area" to minimize the influence of contamination from the station activities.

To verify the actual cleanliness of the clean area, surface snow samples were collected at different distances from the station. To evaluate the spatial variability each year in the designated area for daily sampling, a surface snow area of 2 × 2 m was marked out at the beginning of the campaign and 10 surface snow samples were collected. The upper 3 cm of the snowpack was collected using a glass container pre-cleaned with 1% *v/v* ultra pure hydrochloric acid (Romil, Cambridge, UK) in ultra pure water, then rinsed 3 times with ultra pure water (UPW) to reduce the Br, I and Na blank. Snow pit samples were collected using polypropylene vials (pre-cleaned in the same way) by pushing them directly into the snow wall with a 5 cm resolution. The snow wall was cleaned with a Teflon scraper before sampling to remove possible contamination from the digging process. In accordance with the best sampling procedures for ultra-trace elements in remote areas, gloves and full clean room clothing were worn over the cold weather gear. All the surface snow and snow pit samples were immediately stored in the dark and kept frozen until chemical analysis was performed at the IDPA-CNR in Venice.

2.3.3. Snowfall samples and precipitation measurements

Precipitation (snowfall and diamond dust) samples were collected from a small (50 cm × 50 cm) bench set 1 m above the surface close to the Atmospheric science shelter, a structure located approximatively 800 m south from Dome C main station and close to the clean area. It was at a height of 1 m above the surface to reduce sampling of wind blown snow, as the sampling frequency depended on the amount of snow deposited over the bench. The bench surface was made of teflon and was carefully cleaned before and after so that all the snow particles were recovered after sampling. The snow present on the bench was collected in acid cleaned polypropylene tubes and were kept in the dark and frozen until analysis at the IDPA-CNR laboratories in Venice. Total precipitation is studied at DC in terms of crystal morphology as well in terms of amount of precipitation. An ice camera records the amount of precipitation in terms of mm^2 of area covered by snow crystals over a standardized surface of one square metre (expressed as mm^2 m^{-2}). A specific description of the *ICE-CAMERA* is present in the supplementary online materials.

2.3.4. Analytical procedure

The total Hg concentration was determined using a Thermo Element Inductively Coupled Plasma Sector Field Mass Spectrometry (ICP-SFMS Element2, Thermo-Fischer, Bremen, Germany) in low resolution scanning mode using ^{202}Hg as the analytical mercury mass with 5 replicates per sample measurement. The instrument was calibrated using standards prepared from a mono-elemental Hg solution (*TraceCert®*, purity grade, Sigma-Aldrich, MO, USA). Indium was added at a concentration of 1 ng g^{-1} concentration as an internal standard to correct for eventual drift in the instrument response and matrix effects during the analysis sequence. Hg calibration standards were re-analysed every 20 samples as an additional quality control check. The percent relative standard deviation (n = 5) ranged from 0.5% at 500 pg g^{-1} to 10% at 1 pg g^{-1}, and amounted to 2.6% on average.

Considering the high volatility and instability of Hg in solution, the samples were acidified at 2% *v/v* with ultrapure hydrochloric acid before they were melted and analysed. Each sample was weighed and the exact amount of HCl was added to reach a final concentration of 2% (Planchon et al., 2004).

Halogens and sodium analysis was conducted on non-acidified samples. Total sodium (Na), bromine (Br) and iodine (I) concentrations were determined by ICP-SFMS (Spolaor et al., 2016). Each analytical run started and ended with an ultra pure water (UPW) cleaning session of 3 min to ensure a stable background level throughout the analysis. The external standards that were used to calibrate the analytes were prepared by diluting a 1000 ppm stock IC solution (TraceCERT® purity grade, Sigma-Aldrich, MO, USA). The standard concentrations ranged between 1 and 100 ng g^{-1} for sodium, 1 and 400 pg g^{-1} for iodine and between 0.05 and 2 ng g^{-1} for bromine. The residual standard deviation (RSD) was low for both halogens and ranged between 1–2% and 2–10% for Br and I, respectively.

3. Results

3.1. Spatial variability and influence of the station activities

The first objective of the XXIX campaign was to investigate whether station activities could influence concentrations in the surface snow samples. Five samples were collected consecutively on the same day at 150, 300, 450, 600 m from the station and within the clean area (approximately at 800 m from the station). The results show a possible contamination for Hg in the two surface snow samples collected closest to the station (Table 1). The mean (±standard deviation) Hg concentrations were 23 ± 2 pg g^{-1} and 21 ± 1 pg g^{-1} in samples collected at 150 and 300 m from the station, respectively. The concentrations dropped to 6 ± 1 pg g^{-1} and 5 ± 1 pg g^{-1} in samples collected at 450 and 600 m from the station, these concentrations are in the same range as those within the clean area (6 ± 1 pg g^{-1}). We detected a similar contamination effect for Br, the two samples collected closest to the station had twice as much Br (1.2 ± 0.1 ng g^{-1}) compared to the clean area (0.7 ± 0.1 ng g^{-1}). Na and I concentrations were not significantly different in samples collected at different distances from the station. Several sources might interfere with the natural abundance of the elements investigated, such as the exhaust from the power

Table 1
Results obtained evaluating the possible influence of the station activities on the elements investigate. The distance is considered from the Dome C station.

Distance	Hg (pg g^{-1})	Br (ng g^{-1})	Na (ng g^{-1})	I (pg g^{-1})
150 m	23 ± 2	1.2 ± 0.1	43 ± 2	17 ± 2
300 m	21 ± 1	1.3 ± 0.1	42 ± 2	16 ± 2
450 m	5 ± 1	0.6 ± 0.1	42 ± 2	17 ± 2
600 m	6 ± 1	0.7 ± 0.1	42 ± 3	16 ± 2
Clean area (800 m)	6 ± 1	0.67 ± 0.04	43 ± 2	17 ± 2

plant units, the vehicles used around the DC station and in general all the activities for running and maintaining the station. It is not the aim of this paper to discuss the possible causes of modifications in the natural concentration of Hg, Br, Na and I. Traversi et al., 2014 (Traversi et al., 2014) suggested that contamination due to station activities could affect the clean area when the wind direction is between 0 and 90°. During the XXX and XXXI campaigns the wind direction blew from this sector only on the 12th of December 2015th (Figs. S1 and S2). Considering the results obtained, all the surface snow samples, collected within the "clean area" during the 3 campaigns have been considered as not affected by station activities.

The spatial variability of the analytes was also tested, i.e., the difference in total Hg concentrations in surface snow samples collected at the same time within a 4 m^2 sampling area. The area selected for test the spatial variability, as well as for further sampling in both XXX and XXXI campaigns, had an homogeneous snow surface in terms of density and roughness minimizing possible sampling artefacts due to different snow conditions (for example wind crust formation). Ten surface snow samples were collected to check the spatial variability. The mean total Hg concentration was of 11 ± 1 pg g^{-1}, suggesting a 10% uncertainty driven by spatial variability. Using this value, from here onwards we assume that a variation in total Hg concentration between two samples below 10% cannot be ascribed to a specific natural process but is a result of sampling variation.

3.2. XXIX campaign

During this 12-day campaign, the meteorological conditions were stable without any snow-fall for the entire period. Given the short time available, we collected samples to characterize the spatial variability of the surface snow composition. We also collected daily samples. These data are reported without reference to specific meteorological data. Fig. 2 (in blue) shows the total Hg, Br and Br_{enr}, Na and I concentrations found in the surface snow samples. The mean total Hg concentration was 12 ± 10 pg g^{-1}, with a peak of 37 ± 4 pg g^{-1}. The mean concentrations for Br, I, and Na were 1.0 ± 0.2 ng g^{-1}, 21 ± 13 pgg^{-1}and 46 ± 9 ng g^{-1} respectively.

A snow pit was also dug and the total Hg, Br and Na concentrations are reported in Fig. 3. Total Hg ranged from 4 pg g^{-1} in the upper layers to ~2 pg g^{-1} in the bottom layers (at 120 cm of depth). This decreasing trend with depth is opposite to the results obtained by others (Han et al., 2014). Likewise, Br showed the highest concentrations in the upper 20 cm (~0.5 ng g^{-1}) and decreased with depth to ~ 0.2 ng g^{-1} at the bottom. We did not detect any appreciable decreasing trend with depth for Na, with average concentrations of 40 ± 11 ng g^{-1}. Iodine had stable concentrations in the first 50 cm (11 ± 3 pg g^{-1}) while in the lower samples the concentration and variability increased to 34 ± 2 pg g^{-1}.

3.3. XXX campaign

Meteorological data were collected daily during the entire campaign (Fig. S1). This campaign was characterized by stable weather conditions and no appreciable precipitation. The daily air and surface snow (3 cm depth) temperature ranged from −36 to −25 °C. Wind speed was on average 3 m s^{-1} with only sporadic events above 4 m s^{-1}. The wind direction, as reported by previous authors (e.g., Genthon et al., 2013), was predominantly from south to north. On the 15th and the 28th of December 2014 the direction changed to from the north-west.

Total Hg results in daily surface snow samples do not show any particular trends (Fig. 2, red line, and Fig. 4 black line, log scale). The mean total Hg concentration was 9 ± 3 pg g^{-1} with a maximum of

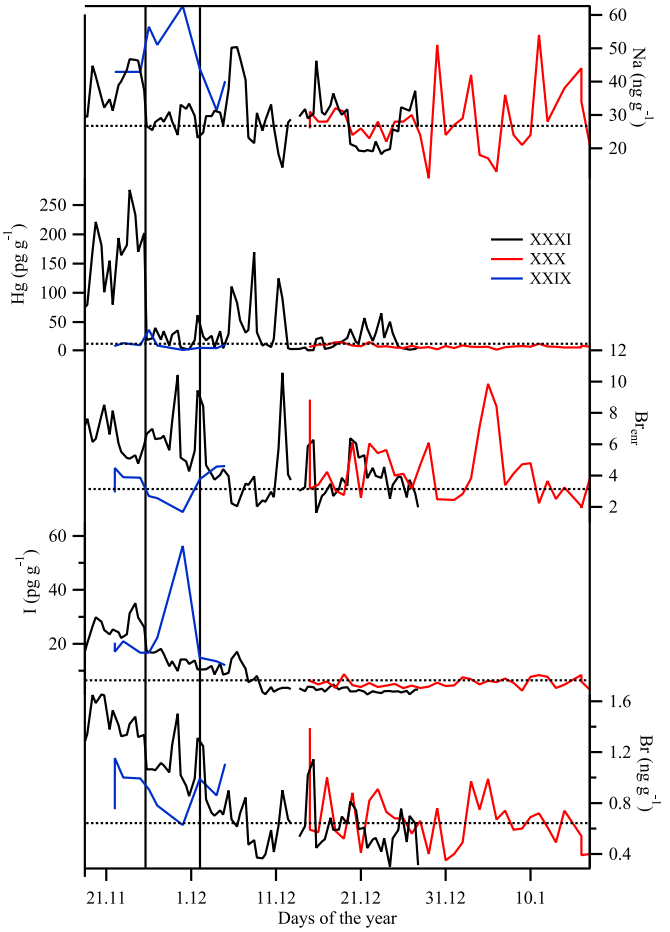

Fig. 2. Concentration of Hg (pg.g^{-1}), Br (ng g^{-1}, and its enrichment compared to the sea water abundance) and I (pg g^{-1}) in the surface snow samples collected at Dome C. The results obtained during the XXIX, XXX, and XXXI campaigns correspond to the blue, red, and black lines, respectively. During the XXXI campaign, the concentrations detected between the 20th and the 27th of November are above the average (dashed horizontal line) calculated from the three campaigns. (For interpretation of the references to colour in this figure legend, the reader is referred to the Web version of this article.)

16 pg g^{-1} and a minimum of 3 pg g^{-1}. The highest concentrations were observed between the 16th and 19th of December 2014 with a mean concentration of 13 ± 2 pg g^{-1}. The period afterwards was characterized by lower concentrations (8 ± 2 pg g^{-1}) with only two days where surface concentrations rose up to 12 pg g^{-1} (22nd of December 2014 and the 11th of January 2015).

Br concentrations ranged from 0.4 to 1.4 ng g^{-1} with an average of 0.7 ± 0.2 ng g^{-1}. Na ranged from 11 ng g^{-1} to 54 ng g^{-1} with an average concentration of 29 ± 9 ng g^{-1}. Iodine had concentrations in the range of 3–9 pg g^{-1} with an average of 6 ± 2 pg g^{-1}. Na and I showed similar trends – suggesting similar sources – with constant snow surface concentrations between the 14th December to the 28th, with a high variability towards the end of the experiment.

Hourly averaged Hg(0) concentrations in air showed two distinct periods (Fig. 4): the first (14th of December 2014 to the 5th of January 2015) had an average concentration of 1.0 ± 0.4 ng m^{-3}; the second (5th to the 17th of January) had an average concentration of 0.6 ± 0.3 ng m^{-3}. In agreement with 2012–2015 data in Fig. 1, Hg(0) concentrations exhibited a diurnal cycle ranging from ~0.5 ng m^{-3} in the evening to ~ 1.2 ng m^{-3} around noon (data not shown).

Atmospheric ozone (O_3) concentrations, sampled with an hourly resolution, were variable and ranged from 18 to 38 ppbv

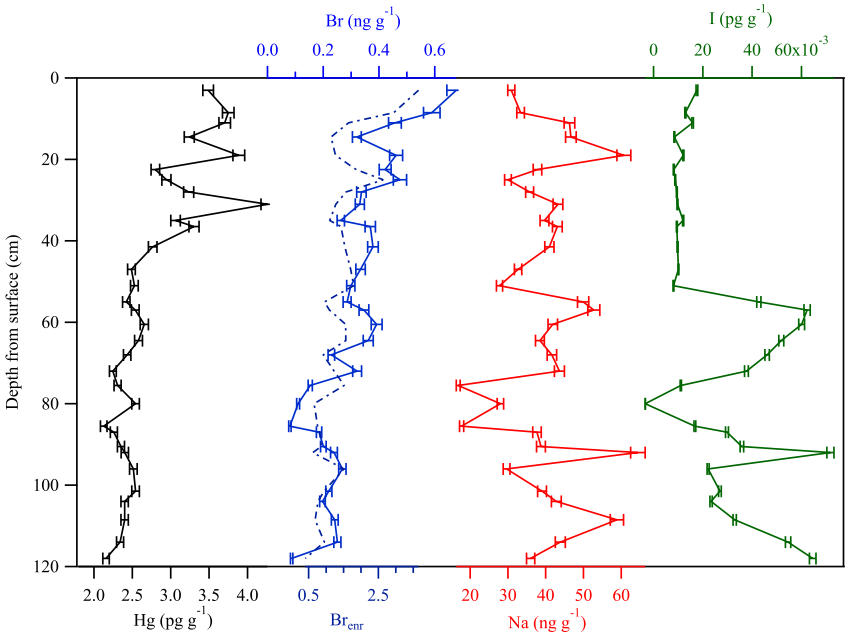

Fig. 3. Hg (pg g^{-1}, black line), Br (ng g^{-1}, blue line) and Br_{enr} (blue dashed lines) profiles obtained from the 120 cm snow pit dung during the XXIX campaign. The results are compared with iodine (pg g^{-1} green line) and sodium results (ng g^{-1} red line). The error bars are the relative standard deviation of the analytical measurements. (For interpretation of the references to colour in this figure legend, the reader is referred to the Web version of this article.)

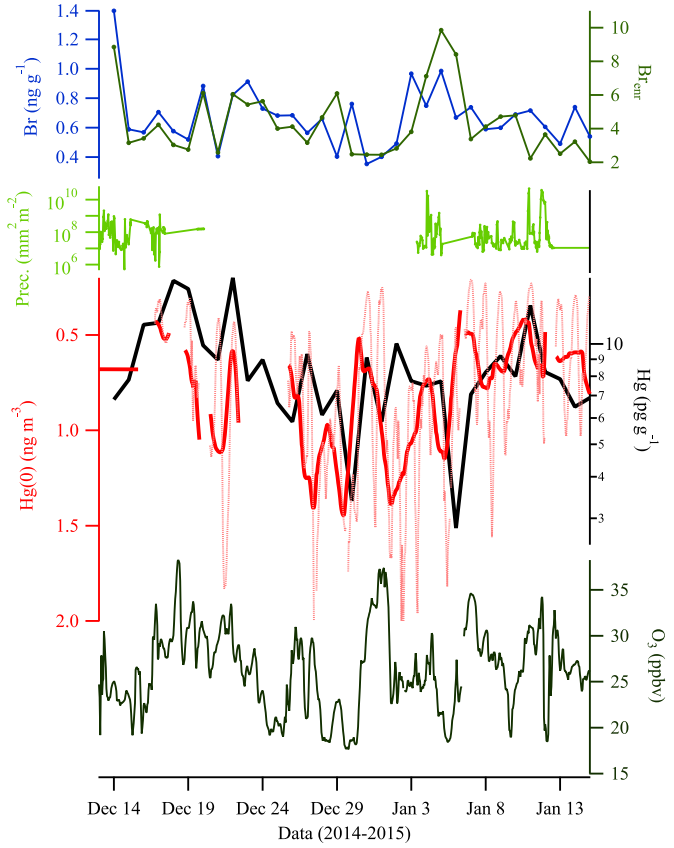

Fig. 4. Summary of the results obtained during the XXX campaign. Blue lines indicate the Br concentration in surface snow, green lines the Br_{enr} in surface snow, black lines the Hg concentration into the surface snow, the red dashed lines are the raw Hg(0) data and the solid red lines the smoothed atmospheric Hg(0) concentrations (reverse scale), the dark green the O_3 atmospheric concentrations and the light green the amount of precipitation with hourly resolution expressed in terms of surface area cover by the snow particles on the ice camera surface (expressed in $mm^2\ m^{-2}$). (For interpretation of the references to colour in this figure legend, the reader is referred to the Web version of this article.)

(26 ± 5 ppbv). This result is in agreement with the large daily variability reported from mid-November to mid-January over the 2007–2014 period (Legrand et al., 2016a).

3.4. XXXI campaign

This campaign started at the beginning of November, when radiation differences between day and night were more pronounced. Meteorological parameters and snow surface temperatures were recorded, and two surface snow samples per day were collected. One in the morning (at 10.00 a.m., local time) and another in the evening (at 18.00 p.m.).

Wind speed and direction were more variable during this campaign. Wind speeds were higher during the period of the 18th to the 28th of November ($7 \pm 2\ m\ s^{-1}$) than afterwards ($4 \pm 2\ m\ s^{-1}$). Even though the average wind direction was from the south during the experiment, many oscillations were measured, as shown in Fig. S2.

In this campaign, the surface snow total Hg concentrations were more variable (Fig. 2 in black and Fig. 5) and ranged between 2 pg g^{-1} (14th of December at 18.00 p.m.) to 276 pg g^{-1} (23rd of November at 18.00 p.m.). Two periods can be identified: the first (18th to the 25th of November), and the second (25th of November until the end of the experiment). The first period was characterized by: i) an average total Hg concentration in surface snow samples of 166 ± 60 pg g^{-1}, ii) an average atmospheric Hg(0) concentration of 0.5 ± 0.2 ng m^{-3}, and iii) total Hg concentrations in snowfall samples (bullet shaped ice crystals, Supplementary material) of 97, 81 and 40 pg g^{-1} on the 21st, 22nd and 23rd of November, respectively. The second period was characterized by: i) an average total Hg concentration in surface snow samples of 28 ± 31 pg g^{-1}, ii) an average atmospheric Hg(0) concentration of 0.8 ± 0.3 ng m^{-3}, and iii) total Hg concentrations in snowfall samples (mainly diamond dust) of 21, 36, 14, 11 and 7 pg g^{-1} on the 5th, the 9th, the 10th, the 14th and the 15th of December 2015, respectively. Although Hg(0) concentrations were significantly lower during the first period, they exhibited a distinct diurnal cycle throughout the entire campaign, ranging from ~0.6 ng m^{-3} in the evening to ~ 0.9 ng m^{-3} around noon.

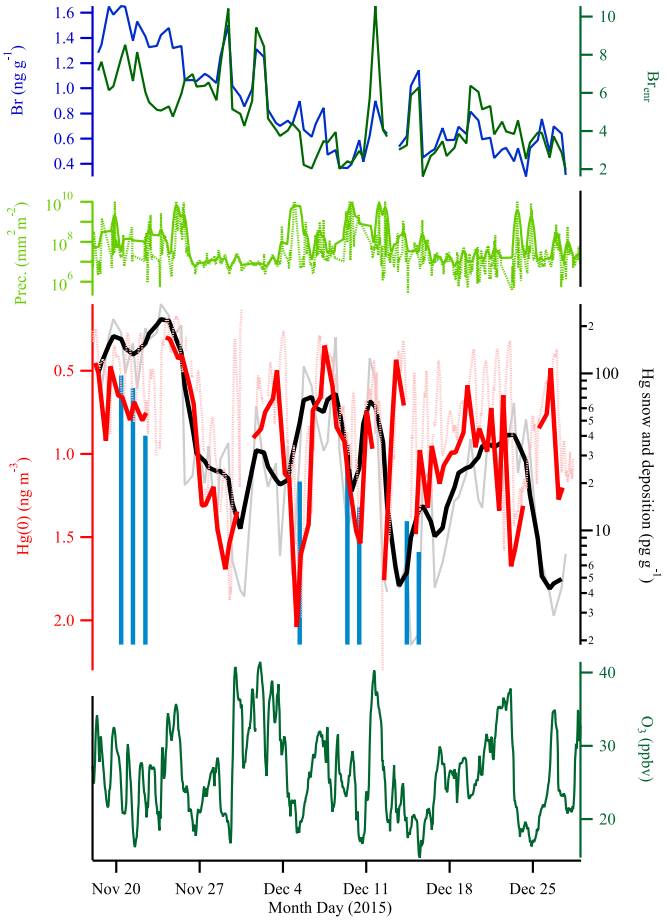

Fig. 5. Summary of the results obtained during the XXXI campaign. Upper panel: blue and green lines indicate the Br concentration and Br_{enr} in surface snow samples, respectively. Central panel: black and red lines indicate the total Hg concentration (pg g^{-1}) in the surface snow samples and the smoothed atmospheric Hg(0) concentration (reverse scale), light green the amount of precipitation with hour resolution express in terms of surface are covered by the snow particles on the ice camera surface (express in mm^2 m^{-2}). The blue bars show the Hg concentration in snowfall samples. Lower panel: O_3 atmospheric concentration. (For interpretation of the references to colour in this figure legend, the reader is referred to the Web version of this article.)

Similarly, to the XXX campaign, ozone concentrations showed a pronounced variability, they ranged from 15 ppbv to 42 ppbv. However, no significant difference between the two periods mentioned above (26 ± 4 ppbv during the first vs. 27 ± 6 ppbv during the second) was observed.

Surface snow samples were analysed for Na, Br, and I, their concentrations are more variable compared to previous campaigns. The behaviour of Br and I was similar to that of Hg. The highest concentrations for Br were detected between the 18th to 25th of November (1.5 ± 0.1 ng g^{-1}) compared to (0.7 ± 0.3 ng g^{-1}) afterwards. Likewise, Br_{enr} varied between 6 ± 1 and 4. $\pm$ 2 during the two periods. Mean iodine concentrations peaked between the 18th to 25th of November, averaging 26 ± 5 pg g^{-1} over that period, and decreased rapidly afterwards to 7 ± 5 pg g^{-1}. Na also peaked in the same period with a mean of 39 ± 6 ng g^{-1} that decreased afterwards to 29 ± 8 ng g^{-1} but with occasional increases of up to ~40 ng g^{-1} (Fig. 5).

To interpret the elevated concentrations of total Hg, I and Br at the beginning of the experiment, back trajectories were computed using the HYSPLIT model (Fig. S3) (see description in the online supplementary material). We found that between the 18th and the 20th November, air masses were continental in origin whilst between the 21st to the 23rd they originated from the Ross Sea. On the 24th and the 25th of November 2015 they once again originated from the Antarctic Plateau. These variations, determined by BT calculations as well as by MODIS satellite images probably caused the increased precipitation and the rapid temperature increases (see Fig. 5) that were observed.

3.5. High-resolution surface snow experiment

In addition to the daily surface snow samples, a high temporal resolution experiment over a 72-h period (called from here onwards "*72-h*") was conducted from the 8th to the 11th of December. Surface snow samples were collected hourly to investigate a possible diurnal cycle of total Hg in surface snow samples, in line with the atmospheric Hg(0) daily cycle. During the 72 h of the experiment, total Hg concentrations in surface snow samples ranged from 2 pg g^{-1} (10th of December at 1 p.m.) to 180 pg g^{-1} (8th of December at 11.00 a.m.) (Fig. 6). Total Hg concentrations in the snow do not exhibit a clear diurnal cycle as has been determined for TGM, but show the highest values during the insolation minima suggesting that the mercury in the snow might be influenced by the daily differences in solar incoming radiation.

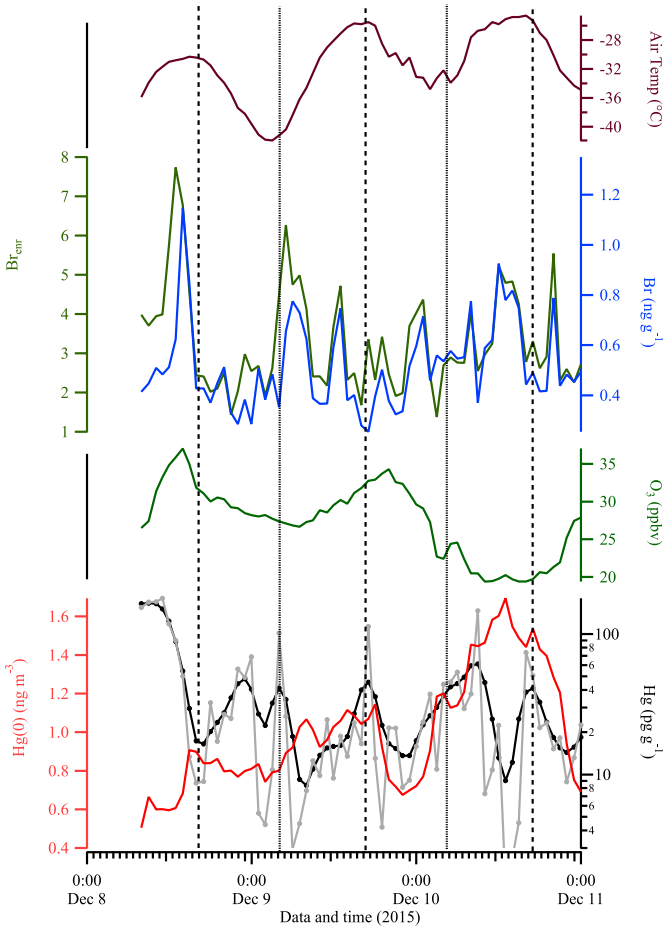

Fig. 6. High-resolution surface snow experiment. Blue lines indicate the Br concentration in the surface snow, green line the Br_{enr} in surface snow, black (3 h average smoothing) and grey (raw data) line of the Hg concentration in the surface snow, red lines the hourly atmospheric Hg(0) concentrations and the dark green the O_3 atmospheric concentrations. Purple lines indicate the air temperature. (For interpretation of the references to colour in this figure legend, the reader is referred to the Web version of this article.)

3.6. Statistical analysis

Potential associations between Hg concentrations in the surface snow and other snow and atmospheric chemistry inputs were analysed using classical and slot correlations (Rehfeld et al., 2011). Data analysis revealed that the Hg concentrations in the surface snow and the atmospheric Hg(0) concentrations were highly skewed in all the campaigns. So they were both log-transformed before analysis to reduce skewness and linearize the relationship.

The high temporal resolution "72-h" experiment includes consecutive (hourly) measurements with all data being sampled on identical time points. Therefore, no specific treatment was required for handling irregular sampling and the final correlation estimates were obtained based on the standard Pearson correlation coefficient.

For the analysis of the XXX and XXXI campaigns a more sophisticated approach was adopted since the time series recorded during these two campaigns were unevenly spaced and were also sampled at different time points. In particular, we considered a correlation slotting approach with a Gaussian kernel (Rehfeld et al., 2011). To investigate the statistical significance of the resulting correlation estimates, 95% pivotal confidence intervals were constructed based on 5000 bootstrap samples. The bootstrap replicates of the series were obtained by resampling the de-trended series and then adding the trend. For an estimation of the trend we used smoothing splines as implemented in the R (R Core Team, 2017) mgcv package (Wood, 2006).

Table 1 summarizes the correlations between the total Hg concentrations in the surface snow (log scale) and atmospheric Hg(0) concentrations (log scale), Br in surface snow and O_3 atmospheric concentrations. For all the campaigns, we ran statistical analyses using a same day synchronization and one considering the mercury air concentration over the 24-h before sampling (Table 2). The 24 h of atmospheric mercury concentrations before snow sampling was chosen to identify if there is a time lag between mercury present in the snow and that in the atmosphere. This was done to understand if the atmospheric mercury concentration before snow sampling could influence the mercury concentration into the snow. The table displays 95% confidence intervals and point estimates of the correlations. Significant correlations are marked in bold. Results indicate a significant negative association between total snow Hg and Hg(0) in all the campaigns. A negative correlation, without any time delay, has been determined for the twice daily samples taken during the XXXI campaign and the hourly data for the 72-h experiment from the same expedition (72-h $r = -0.36$, XXXI campaign $r = -0.23$). No significant correlation was found if Hg(0) air concentrations from the previous 24 h were taken into consideration for these two experiments. For the XXX campaign we detected a significant correlation considering the measurements over the previous 24-h (XXX campaign, $r = -0.32$), but, no significant correlation was obtained using the values from the same solar day. A positive significant association without any time adjustment has been found between total Hg and Br concentrations in surface snow and total Hg in the snow and O_3 during the XXXI campaign (with Br $r = 0.49$ and with $O_3 = 0.19$). Looking at the XXX campaign we do not detect any correlation between total Hg and Br (with and without any time adjustment) likely due to the absence of meteorological events able to bring air masses from the coast. A positive correlation has been detected between total Hg and O_3 and the correlation increases from 0.31 to 0.68 when applying a 24 h time adjustment.

Table 2
Estimates of (slotting) correlation coefficients and 95% confidence intervals (in parenthesis) between Hg concentration into the surface snow (log scale) and atmospheric Hg(0) concentrations (log scale), Br in surface snow and O_3 atmospheric concentrations at the same day and with 24-h delay. Bold numbers indicate statistically significant associations at 95% level.

	Same day effect	24-h lagged effect
72-h campaign		
Hg(0)	**−0.36 (-0.55, -0.13)**	0.22 (−0.07, 0.48)
Br	−0.19 (−0.41, 0.05)	0.03 (−0.26, 0.31)
O_3	0.15 (−0.09, 0.37)	−0.21 (−0.47, 0.08)
XXX campaign		
Hg(0)	0.02 (−0.14, 0.16)	**−0.32 (-0.49, -0.18)**
Br	−0.19 (−0.49, 0.11)	−0.18 (−0.46, 0.11)
O_3	**0.31 (0.16, 0.46)**	**0.68 (0.55, 0.84)**
XXXI campaign		
Hg(0)	**−0.23 (-0.30, -0.15)**	0.05 (−0.03, 0.12)
Br	**0.49 (0.38, 0.63)**	**0.48 (0.36, 0.61)**
O_3	**0.19 (0.11, 0.27)**	0.003 (−0.08, 0.09)

4. Discussion

4.1. Snow and atmospheric mercury connection

The 3 campaigns had markedly different meteorological conditions and numbers of snowfall events (Figs. 4 and 5 light green panels), which could explain the different patterns in total Hg surface snow concentrations. The total Hg concentration in the snow was stable during the XXIX and the XXX campaigns (Figs. 2 and 4), which could be explained by a lack of meteorological events such as cyclonic intrusions from the coast and important oxidation events.

Total Hg concentrations slightly above the average were found between the 15th to 22nd of December 2014 (12 ± 3 pg g^{-1} compared to 8 ± 2 pg g^{-1}) and may be associated with above average ozone concentrations (28 ± 4 ppbv compared to 25 ± 4 ppbv in the following period, Fig. 4). Considering the whole dataset, and not only specific periods, for the XXX campaign we found a positive correlation between Hg in the snow and O_3 (Table 1). These results could suggest a gas-phase oxidation of Hg(0) by ozone leading to Hg(II) deposition to the snowpack, however this reaction is unlikely to proceed as a homogeneous reaction (Pal and Ariya, 2004; Ariya et al., 2009; Hynes et al., 2009). The dominant oxidation pathway is currently thought to involve an initial recombination of Hg(0) and Br followed by the addition of a second radical (e.g., NO_2, HO_2) (Goodsite et al., 2004; Dibble et al., 2012; Wang et al., 2014; Horowitz et al., 2017). Legrand et al. (2016a) recently showed that the surface ozone mixing ratio at DC in summer is strongly influenced by the synoptic origin of the air masses, with the highest ozone values being observed when transport during the 5 days prior to its arrival at DC was over the highest part of the Antarctic Plateau. These transport conditions favour photochemical production and/or accumulation of ozone related to snowpack emissions of NO_x to the air masses arriving at the site. These results support the use of ozone as an indicator of the oxidative capacity of the atmosphere. High concentrations of O_3 could reflect air masses from the interior of the plateau where the oxidative capacity of the atmosphere (e.g., NOx, HO_2 concentrations) is the highest. The positive correlation between total Hg in surface snow samples and ambient O_3 (maximized using the 24-h lag time) suggests that under high O_3 conditions (i.e., likely under high NOx/HO_2 conditions), Hg(0) was oxidized leading to Hg(II) deposition onto the surface snow. The XXX campaign was mainly characterized by air masses originating from the Antarctic plateau with a quasi absence of snow and diamond dust deposition. The results show a negative correlation (using a 24-h delay approach; see section 3.5) between atmospheric Hg(0) and total Hg concentrations in surface snow samples during the campaign, suggesting a mutual and rapid exchange between atmospheric and surface snow Hg.

As already suggested, after deposition to the snowpack, Hg concentrations show a marked decrease, suggesting re-emission processes that can influence Hg(0) concentrations in the atmospheric boundary layer.

Photochemical studies of Hg within the snowpack have shown that redox reactions occur within the first few centimetres. This re-emission process most obvious during the XXXI campaign based on the results of the daily/hourly surface snow samplings (Fig. 5). The meteorological conditions during the XXXI campaign (Fig. S2) were significantly different to those of the previous two (Fig. S1). The daily surface samplings captured several snow deposition events (light blue bars in Fig. 5, showing the total Hg concentration in each snow fall) and covered a period of intrusion of cyclonic air masses from the coast (Fig. S3). During the first week of sampling (18th to 25th of November), the high concentration of total Hg in the surface snow was concomitant with the arrival at Dome C of cyclonic air masses originating from the Ross Sea (Fig. S3). These snow deposition events were captured by an *ICE CAMERA* installed at the edge of the "clean area" (Video S4). The video compilation shows that the most intense precipitation, characterized by smaller snow/ice grain (<1 mm), occurred between the 20th and the 25th of November, and between the 4th and the 12th of December 2015 and coincided with the highest total Hg concentrations in surface snow. We focus here on the precipitation events that occurred between the 20th and the 21st of November and between the 24th and the 25th of November because the high mercury levels of Hg detected in surface snow (Fig. 5). These specific precipitation events were characterized mainly by smaller ice grains, however some snow/ice crystals of larger size (bullet, combination of bullets, columns shapes) have been identified suggesting the occurrence of diamond dust deposition and also snow deposition (Video S4). The precipitation event that occurred between the 24th and the 25th of November was not sampled from the suspended bench (daily snow surface were samples as described before) since there was not enough snow (likely associated with the small grain size and the wind velocity) to be collected for the instrumental analysis.

Supplementary data related to this article can be found online at https://doi.org/10.1016/j.chemosphere.2017.12.180.

Angot et al. (2016c) have suggested that the presence of ice crystals could enhance the dry deposition of Hg(II). Indeed, due to an elevated specific surface area, the mercury-capture efficiency of ice crystals is high (Douglas et al., 2008). Additionally, the air masses coming from the coast could have brought onto the Antarctic plateau halogen radicals produced from the sea ice, through the bromine explosion (Spolaor et al., 2016) explaining the correlation between total Hg and Br in surface snow samples. The approaching of coastal air masses is also suggested by an increasing in sodium concentration. It has been suggested that the sodium in central Antarctica is driven by sea spray and sea ice production linked with the atmospheric condition able to bring it to the Antarctic interior (Levine et al., 2014). The increasing sodium and bromine levels, together with the BT calculations, strong suggests coastal origins for these air masses. The air masses rich in bromine radicals, together with snow precipitation could have favoured mercury deposition (as highlighted by the apparent correlation shown in Table 1 between Br and total Hg). It has been found that deposition of Hg during AMDEs (Atmospheric Mercury Depletion Events) that occurs at the coast or not far inland, are usually associated with a decrease in ozone concentrations or Ozone Depletion Events (ODEs). Our results seem to be an AMDE from the extremely high concentration of Hg in the surface snow (up to ~ 270 pg g^{-1}) and the high value of Br and its enrichment factor. However, the absence of a decrease in ozone and the high surface area covered by the snowflakes as determined by the ice camera support the idea that the increase of mercury in the snow is more likely due to enhanced snow/ice crystal deposition, particularly due to the high abundance of smaller high surface area snowflakes. During cloudy periods (18th to the 25th of November), incoming solar radiation was limited and probably limited Hg(II) reduction within the upper layers of the snowpack and decreased the formation of Hg(0) and its emission to the atmosphere. After the 25th of November, the meteorological conditions changed with air masses coming from the interior. A large fraction of the Hg that accumulated in the surface snow during the bad-weather period was most likely reduced to Hg(0) and was emitted into the atmosphere following photo-reduction processes in the upper layers of the snowpack. This suggests that in the absence of additional snow precipitation events, the surface snow started acting as a source. The same behaviour has been observed for Iodine, in that, similarly to mercury, it can undergo photochemical processes to produce gaseous iodine species as already suggested (Spolaor et al., 2013). A marked change in the total Hg surface snow concentration was observed on the 25th of November. This day was characterized by air masses from the higher part of the plateau but with a marked reduction in ozone. Between 11.00 a.m. and 6.00 p.m. on the 25th, i.e., within 6 h, the total Hg concentration in surface snow dropped from 200 pg g^{-1} to 20 pg g^{-1}, a much faster decrease (and likely emission) rate than that reported by Lalonde, 2002 and Dommergue, 2003 (Lalonde et al., 2002; Dommergue et al., 2003). A similar change is also reflected in the atmospheric Hg(0) with concentrations increasing from 0.5 ng m^{-3} to 1.5 ng m^{-3}. However, the increase of atmospheric mercury is not as sharp as the emission from the snow as it reaches a maximum during the 27th of November. This delay could be explained by a combination of different processes. We have detected fast recycling of mercury from the first 3 cm of surface snow but the release of mercury from the lower strata probably requires more time. Secondly between the 25th to the 27th (until the morning) the wind speed was relatively high for Dome C (9 m s^{-1}, Fig. S2) so the mercury released form the snow could have been dispersed. The decrease in wind speed during the 27th of November probably produced a more stable vertical structure of the atmosphere where the gaseous Hg(0) could accumulate. In any case the sharp increase in atmospheric Hg(0), following the fast decrease in total Hg in the surface snow supports the idea that the snowpack can act as a significant source of Hg. The periods when coastal cyclonic air masses approached Dome C, had total average Hg concentrations in the surface snow of 180 pg g^{-1} for almost 7 days, higher than the concentrations found by other studies (Han et al., 2014; Angot et al., 2016c).

Between the 4th to the 12th of December during the XXXI campaign, there were diamond dust deposition events. Although less intense, these snow deposition events were able to decrease the atmospheric Hg(0) concentration from 1.5 to 0.5 ng m^3 and increase the total Hg concentration in surface snow (from 20 to 80 pg g^{-1}) (Fig. 5) - highlighting the extremely efficient Hg scavenging potential of diamond dust. It should be noted that these events were not associated with intense cyclonic air mass intrusions but were caused by local meteorological conditions, as suggested by the poor correlation between mercury and bromine during this period. In this lapse, pronounced mercury oscillations in the surface snow and in the atmosphere were detected (concentrations ranging from 10 to 90 pg g^{-1} in surface snow samples and between 1.5 and 0.5 ng m^{-3} in ambient air). The data obtained during the XXXI campaign clearly suggest that snow deposition events can play a central role in mercury deposition and scavenging from the lower atmosphere. However, the release of Hg from the snow can be rapid in the presence of sunlight, as already suggested by other authors, reducing the Hg concentration in surface snow by an order of magnitude in several hours. This fast decrease in Hg in the surface snow and the opposing increase in atmospheric

mercury concentration supports the idea that mercury is continuously recycled between the snow pack and the lower atmosphere for the entire light period.

In contrast to the Hg(0) concentrations in ambient air, total Hg concentrations in surface snow exhibited a less pronounced diurnal cycle during the 72-h experiment (Fig. 6). However, the negative correlation obtained between the two parameters ($r = -0.36$) still suggests a direct interconnection between snow and atmospheric mercury. Sharp increases and higher variability was found (unsmoothed grey line Fig. 6) suggesting a rapid chemistry cycle able to recycle mercury from the snow to the atmosphere and vice-versa. The concentrations detected for Br do not seem linked or influencing mercury deposition apart from the notable Br peak at the beginning of the experiment. The simultaneous increase in Br (and its enrichment factor) and Hg could suggest a role for Br radicals in mercury deposition, but this is not always the case on the Antarctic Plateau. The highest total Hg concentrations detected in surface snow at the beginning of the experiment were associated with a snow/ice deposition event that occurred just before the high-resolution sampling began. The simultaneous increase in Br and its enrichment factor suggests that air masses may have originated at the coast. Total Hg concentrations in surface snow subsequently dropped from 170 pg g^{-1} to 20 pg g^{-1} in 4 h. This fast decrease is similar in intensity to the one observed on the 25th of November. These results from the 72-h experiment also corroborate the idea that Hg deposited onto the surface snow could be quickly re-emitted to the atmosphere. The comparison between atmospheric mercury measurements and mercury in the surface snow shows a negative correlation in both campaigns demonstrating intense chemical exchanges at the air-snow interface.

So, the differences between the 72-h experiment and the XXXI campaign compared to the XXX campaign data are essentially for two main reasons i) the sampling frequency ii) and the absence of meteorological events (such as snowfall events) during the XXX campaign. The surface samples collected daily during the XXX campaign are probably influenced by the atmospheric concentrations over the 24 h period before sampling, but obviously are not affected by the air concentrations after sampling, which is probably why the solar day air concentrations do not correlate. The double daily sampling strategy adopted for the XXXI campaign reduced the time between each sample making the comparison with the atmospheric concentrations more comparable for the same solar day.

To avoid evaluation errors and false results, during each campaign, the snow sampling strategy was extremely systematic. It is important to underline that this study reports mercury behaviour in snow surface samples and the relationship with atmospheric mercury concentration and other snow and atmospheric chemistry inputs. Further field campaigns are already planned to continue this work and provide new records for Hg in snow surface samples, and data to calculate Hg evasion fluxes from the snowpack to the atmosphere (Hg evasion fluxes not available with the current Hg dataset).

4.2. Mercury and bromine in surface and buried snow

Results on snow pit samples show an intriguing correlation between Br (mean $r = 0.68$, range 0.45–0.84) and its enrichment (mean $r = 0.52$, range 0.20–0.73) factor with total mercury concentration (Fig. 3). It is well known that bromine radicals are involved in mercury oxidation and deposition, particularly during AMDEs. An increase of Br in snow and its enrichment factor, suggest an increase of reactive bromine species generated mainly in coastal areas over sea ice during springtime that could drive an increase in mercury deposition and might preserve mercury deposited in the snow pack. The fast mercury reactivity and re emission/re-cycling from the snow pack, as shown in our results, make the interpretation of the Hg signal in the snow much more complicated. In particular, the highest concentrations of mercury are detected in the upper 20 cm where a gaseous diffusion of mercury could still be present altering the pristine signal present in the snow. However, from the snow pit samples that should cover a roughly 40-year interval (considering the average accumulation rate at Dome C of 30 mm water equivalent – w.e.- per year) we determined a decrease in bromine and its enrichment factor similar to the profile of mercury concentrations. It has already been suggested that the Hg concentration in buried snow could be influenced by increasing sea salt (Yeongcheol et al., 2017) however from our results there is a negative correlation between Hg and iodine (mean $r = -0.47$, range −0.71 -0.15) and no correlation between Hg and Na (mean $r = 0.18$, range −0.18 - 0.50). Sea salt elements and ionic compounds are transported from the coast to the interior, bringing not only the elements but also the halogen radicals produced in the coastal areas. These results could be explained in two ways, i) more intromission of air masses during the spring time with the result of more Br and Cl radicals reaching the Antarctic plateau or ii) an increase of first year sea ice, as detected by the satellite measurements from 1978, that could have increased the production of Br radicals and hence their presence in the Antarctic lower troposphere with the consequent favouring of mercury deposition. Some authors have been suggest that Br is not entirely preserved in the surface snow (Legrand et al., 2016b) of the Antarctic plateau, however Br concentration might continue to preserve the information regarding the two hypothesis proposed. These hypothesis are only based on a single 1.3 m snow pit but if the same correlation (mean $r = 0.68$, range 0.45–0.84) is found elsewhere in Antarctica (or in the Arctic) a more robust discussion can be made evaluating the role of sea ice in regulating the oxidizing capacity of the polar atmosphere (Barbante et al., 2017).

5. Conclusions

The data extracted from the three campaigns provide a large dataset that produce a picture of the main environmental parameters involved in the mercury cycle in the surface snow on the Antarctic Plateau. The sampling strategy was modified year by year by to obtain the best operational condition for producing reliable results, and improving our understanding of the factors that control the presence of mercury in surface snow and their contribution to the total atmospheric Hg abundance. We have also demonstrated that the designated clean sampling area at Dome C is not influenced by station activities or exhaust from the generators.

The decrease in snow mercury and its likely release into the atmosphere have a direct effect on atmospheric mercury concentrations. The increase in atmospheric mercury detected is delayed by 24/36 h and may depend on the vertical structure and mixing rate of the atmosphere (as well by the meteorological conditions), These results confirm the idea of a mutual influence between the mercury present into the snow and in the atmosphere.

Mercury deposition at Dome C and in general on the Antarctic Plateau is enhanced by the approach of cyclonic air masses from coastal areas and subsequent snowfall events. Snowfall, especially that characterized by small snow/ice crystals act as a sink for mercury present in the atmosphere, concentrating it at the surface snow. Additionally, the data suggest a fast recycling, as within less than 6 h, up to 90% of mercury deposited onto the surface snow is lost.

Frequent snowfall and the intrusion of cyclonic air masses favoured the role of radicals (in this case Br as identified from its enrichment factor) produced at the coastal areas (or in their proximity), and snow depositions that acted a scavenger for mercury present in the atmosphere.

Although some evidence has emerged from our results, discerning the predominant processes is not easy, and additional studies over longer temporal scale are necessary to identify the role of cyclonic air mass intrusion and medium to long-range transport processes on mercury atmospheric levels on the Antarctic Plateau.

The impact of halogen radicals produced at coastal area and their transport in the inner plateau is also poorly understood. Understanding the role of the processes listed above will improve our knowledge of interactions and exchange of mercury between the snow and the atmosphere.

Acknowledgements

This work was supported by the Programma Nazionale per la Ricerca in Antartide (PNRA, project number 2013/AC3.03 PEA 2013–2015). Analytical instrument resources for the elements determination in the snow were provided by the Institute for the Dynamic of Environmental Process (IDPA-CNR) of the National Research Council. Atmospheric Hg measurements were also supported by the FP7 (2010–2015) Global Mercury Observation System (GMOS) project. This work contributed to the EU-FP7 project Global Mercury Observation System (GMOS, www.gmos.eu) and has been supported by a grant from Labex OSUG@2020 (Investissements d'avenir – ANR10 LABX56). Logistical and financial support was provided by the French Polar Institute IPEV (Program 1028, GMOstral). Hélène Angot, Olivier Magand, and Aurélien Dommergue thank the overwintering crew: S. Aubin, A. Barbero, N. Hueber, C. Lenormant, R. Jacob, and P. Serre at DC. Calculations, model comparison and analysis have been conducted in the framework of the PRE-REC projects, funded by PNRA-MIUR. Data and meteorological information were obtained from IPEV/PNRA Project 'Routine Meteorological Observation at Station Concordia' - http://www.climantartide.it/. The authors gratefully acknowledge Elga Lab water for the supply of the ultrapure water systems used during this study.

Appendix A. Supplementary data

Supplementary data related to this article can be found at https://doi.org/10.1016/j.chemosphere.2017.12.180.

References

Angot, H., Dastoor, A., De Simone, F., Gårdfeldt, K., Gencarelli, C.N., Hedgecock, I.M., Langer, S., Magand, O., Mastromonaco, M.N., Nordstrøm, C., Pfaffhuber, K.A., Pirrone, N., Ryjkov, A., Selin, N.E., Skov, H., Song, S., Sprovieri, F., Steffen, A., Toyota, K., Travnikov, O., Yang, X., Dommergue, A., 2016a. Chemical cycling and deposition of atmospheric mercury in polar regions: review of recent measurements and comparison with models. Atmos. Chem. Phys. 16, 10735–10763.

Angot, H., Dion, I., Vogel, N., Legrand, M., Magand, O., Dommergue, A., 2016b. Multi-year record of atmospheric mercury at Dumont d'Urville, East Antarctic coast: continental outflow and oceanic influences. Atmos. Chem. Phys. 16, 8265–8279.

Angot, H., Magand, O., Helmig, D., Ricaud, P., Quennehen, B., Gallée, H., Del Guasta, M., Sprovieri, F., Pirrone, N., Savarino, J., Dommergue, A., 2016c. New insights into the atmospheric mercury cycling in central Antarctica and implications on a continental scale. Atmos. Chem. Phys. 16, 8249–8264.

Ariya, P.A., Peterson, K., Snider, G., Amyot, M., 2009. Mercury chemical transformations in the gas, aqueous and heterogeneous phases: state-of-the-art science and uncertainties. In: Mason, R., Pirrone, N. (Eds.), Mercury Fate and Transport in the Global Atmosphere: Emissions, Measurements and Models. Springer US, Boston, MA, pp. 459–501.

Barbante, C., Spolaor, A., Cairns, W.R.L., Boutron, C., 2017. Man's Footprint on the Arctic Environment as Revealed by Analysis of Ice and Snow. Earth-Science Reviews.

Bromwich, D.H., 1988. Snowfall in high southern latitudes. Rev. Geophys. 26, 149–168.

Brooks, S., Arimoto, R., Lindberg, S., Southworth, G., 2008. Antarctic polar plateau snow surface conversion of deposited oxidized mercury to gaseous elemental mercury with fractional long-term burial. Atmos. Environ. 42, 2877–2884.

Caldwell, C.A., Swartzendruber, P., Prestbo, E., 2006. Concentration and dry deposition of mercury species in Arid South Central New Mexico (2001–2002). Environ. Sci. Technol. 40, 7535–7540.

Castro, M.S., Moore, C., Sherwell, J., Brooks, S.B., 2012. Dry deposition of gaseous oxidized mercury in Western Maryland. Sci. Total Environ. 417–418, 232–240.

Dibble, T.S., Zelie, M.J., Mao, H., 2012. Thermodynamics of reactions of ClHg and BrHg radicals with atmospherically abundant free radicals. Atmos. Chem. Phys. 12, 10271–10279.

Domine, F., Gallet, J.-C., Barret, M., Houdier, S., Voisin, D., Douglas, T.A., Blum, J.D., Beine, H.J., Anastasio, C., Bréon, F.-M., 2011. The specific surface area and chemical composition of diamond dust near Barrow, Alaska. J. Geophys. Res. Atmos. 116 (n/a-n/a).

Dommergue, A., Barret, M., Courteaud, J., Cristofanelli, P., Ferrari, C.P., Gallée, H., 2012. Dynamic recycling of gaseous elemental mercury in the boundary layer of the Antarctic Plateau. Atmos. Chem. Phys. 12, 11027–11036.

Dommergue, A., Ferrari, C.P., Gauchard, P.-A., Boutron, C.F., Poissant, L., Pilote, M., Jitaru, P., Adams, F.C., 2003. The fate of mercury species in a sub-arctic snowpack during snowmelt. Geophys. Res. Lett. 30 (n/a-n/a).

Dommergue, A., Sprovieri, F., Pirrone, N., Ebinghaus, R., Brooks, S., Courteaud, J., Ferrari, C.P., 2010. Overview of mercury measurements in the Antarctic troposphere. Atmos. Chem. Phys. 10, 3309–3319.

Douglas, T.A., Sturm, M., Simpson, W.R., Blum, J.D., Alvarez-Aviles, L., Keeler, G.J., Perovich, D.K., Biswas, A., Johnson, K., 2008. Influence of snow and ice crystal formation and accumulation on mercury deposition to the arctic. Environ. Sci. Technol. 42, 1542–1551.

Douglas, T.A., Sturm, M., Simpson, W.R., Brooks, S., Lindberg, S.E., Perovich, D.K., 2005. Elevated mercury measured in snow and frost flowers near Arctic sea ice leads. Geophys. Res. Lett. 32 (n/a-n/a).

Ebinghaus, R., Jennings, S.G., Schroeder, W.H., Berg, T., Donaghy, T., Guentzel, J., Kenny, C., Kock, H.H., Kvietkus, K., Landing, W., Mühleck, T., Munthe, J., Prestbo, E.M., Schneeberger, D., Slemr, F., Sommar, J., Urba, A., Wallschläger, D., Xiao, Z., 1999. International field intercomparison measurements of atmospheric mercury species at Mace Head, Ireland. Atmos. Environ. 33, 3063–3073.

Fujita, K., Abe, O., 2006. Stable isotopes in daily precipitation at Dome Fuji, East Antarctica. Geophys. Res. Lett. 33 (n/a-n/a).

Genthon, C., Six, D., Gallée, H., Grigioni, P., Pellegrini, A., 2013. Two years of atmospheric boundary layer observations on a 45-m tower at Dome C on the Antarctic plateau. J. Geophys. Res. Atmos. 118, 3218–3232.

Genthon, C., Six, D., Scarchilli, C., Ciardini, V., Frezzotti, M., 2016. Meteorological and snow accumulation gradients across Dome C, East Antarctic plateau. Int. J. Climatol. 36, 455–466.

Goodsite, M.E., Plane, J.M.C., Skov, H., 2004. A theoretical study of the oxidation of Hg0 to HgBr2 in the troposphere. Environ. Sci. Technol. 38, 1772–1776.

Han, Y., Huh, Y., Hong, S., Hur, S.D., Motoyama, H., 2014. Evidence of air-snow mercury exchange recorded in the snowpack at Dome Fuji, Antarctica. Geosci. J. 18, 105–113.

Holmes, C.D., Jacob, D.J., Corbitt, E.S., Mao, J., Yang, X., Talbot, R., Slemr, F., 2010. Global atmospheric model for mercury including oxidation by bromine atoms. Atmos. Chem. Phys. 10, 12037–12057.

Horowitz, H.M., Jacob, D.J., Zhang, Y., Dibble, T.S., Slemr, F., Amos, H.M., Schmidt, J.A., Corbitt, E.S., Marais, E.A., Sunderland, E.M., 2017. A new mechanism for atmospheric mercury redox chemistry: implications for the global mercury budget. Atmos. Chem. Phys. 17, 6353–6371.

Huang, J., Choi, H.-D., Landis, M.S., Holsen, T.M., 2012. An application of passive samplers to understand atmospheric mercury concentration and dry deposition spatial distributions. J. Environ. Monit. 14, 2976–2982.

Hynes, A.J., Donohoue, D.L., Goodsite, M.E., Hedgecock, I.M., 2009. Our current understanding of major chemical and physical processes affecting mercury dynamics in the atmosphere and at the air-water/terrestrial interfaces. In: Mason, R., Pirrone, N. (Eds.), Mercury Fate and Transport in the Global Atmosphere: Emissions, Measurements and Models. Springer US, Boston, MA, pp. 427–457.

Lalonde, J.D., Poulain, A.J., Amyot, M., 2002. The role of mercury redox reactions in snow on snow-to-air mercury transfer. Environ. Sci. Technol. 36, 174–178.

Legrand, M., Preunkert, S., Savarino, J., Frey, M.M., Kukui, A., Helmig, D., Jourdain, B., Jones, A.E., Weller, R., Brough, N., Gallée, H., 2016a. Inter-annual variability of surface ozone at coastal (Dumont d'Urville, 2004–2014) and inland (Concordia, 2007–2014) sites in East Antarctica. Atmos. Chem. Phys. 16, 8053–8069.

Legrand, M., Yang, X., Preunkert, S., Theys, N., 2016b. Year-round records of sea salt, gaseous, and particulate inorganic bromine in the atmospheric boundary layer at coastal (Dumont d'Urville) and central (Concordia) East Antarctic sites. J. Geophys. Res. Atmos. 121, 997–1023.

Levine, J.G., Yang, X., Jones, A.E., Wolff, E.W., 2014. Sea salt as an ice core proxy for past sea ice extent: a process-based model study. J. Geophys. Res. Atmos. 119, 5737–5756.

Lyman, S.N., Gustin, M.S., Prestbo, E.M., 2010. A passive sampler for ambient gaseous oxidized mercury concentrations. Atmos. Environ. 44, 246–252.

Lyman, S.N., Gustin, M.S., Prestbo, E.M., Kilner, P.I., Edgerton, E., Hartsell, B., 2009. Testing and application of surrogate surfaces for understanding potential gaseous oxidized mercury dry deposition. Environ. Sci. Technol. 43, 6235–6241.

Pal, B., Ariya, P.A., 2004. Studies of ozone initiated reactions of gaseous mercury: kinetics, product studies, and atmospheric implications. Phys. Chem. Chem. Phys. 6, 572–579.

Pfaffhuber, K.A., Berg, T., Hirdman, D., Stohl, A., 2012. Atmospheric mercury observations from Antarctica: seasonal variation and source and sink region calculations. Atmos. Chem. Phys. 12, 3241–3251.

Planchon, F.A.M., Gabrielli, P., Gauchard, P.A., Dommergue, A., Barbante, C., Cairns, W.R.L., Cozzi, G., Nagorski, S.A., Ferrari, C.P., Boutron, C.F., Capodaglio, G., Cescon, P., Varga, A., Wolff, E.W., 2004. Direct determination of mercury at the sub-picogram per gram level in polar snow and ice by ICP-SFMS. J. Anal. Atomic Spectrom. 19, 823–830.

Poulain, A.J., Amyot, M., Findlay, D., Telor, S., Barkay, T., Hintelmann, H., 2004. Biological and photochemical production of dissolved gaseous mercury in a boreal lake. Limnol. Oceanogr. 49, 2265–2275.

R Core Team, 2017. R: a Language and Environment for Statistical Computing. R Foundation for Statistical Computing, Vienna. https://www.R-project.org/.

Rehfeld, K., Marwan, N., Heitzig, J., Kurths, J., 2011. Comparison of correlation analysis techniques for irregularly sampled time series. Nonlinear Process Geophys. 18, 389–404.

Scarchilli, C., Frezzotti, M., Ruti, P.M., 2011. Snow precipitation at four ice core sites in East Antarctica: provenance, seasonality and blocking factors. Clim. Dynam. 37, 2107–2125.

Schlosser, E., Stenni, B., Valt, M., Cagnati, A., Powers, J.G., Manning, K.W., Raphael, M., Duda, M.G., 2016. Precipitation and synoptic regime in two extreme years 2009 and 2010 at Dome C, Antarctica – implications for ice core interpretation. Atmos. Chem. Phys. 16, 4757–4770.

Schroeder, W.H., Anlauf, K.G., Barrie, L.A., Lu, J.Y., Steffen, A., Schneeberger, D.R., Berg, T., 1998. Arctic springtime depletion of mercury. Nature 394, 331–332.

Sherman, L.S., Blum, J.D., Johnson, K.P., Keeler, G.J., Barres, J.A., Douglas, T.A., 2010. Mass-independent fractionation of mercury isotopes in Arctic snow driven by sunlight. Nat. Geosci. 3, 173–177.

Spolaor, A., Vallelonga, P., Gabrieli, J., Martma, T., Björkman, M.P., Isaksson, E., Cozzi, G., Turetta, C., Kjær, H.A., Curran, M.A.J., Moy, A.D., Schönhardt, A., Blechschmidt, A.M., Burrows, J.P., Plane, J.M.C., Barbante, C., 2014. Seasonality of halogen deposition in polar snow and ice. Atmos. Chem. Phys. 14, 9613–9622.

Spolaor, A., Vallelonga, P., Plane, J.M.C., Kehrwald, N., Gabrieli, J., Varin, C., Turetta, C., Cozzi, G., Kumar, R., Boutron, C., Barbante, C., 2013. Halogen species record Antarctic sea ice extent over glacial–interglacial periods. Atmos. Chem. Phys. 13, 6623–6635.

Spolaor, A., Vallelonga, P., Turetta, C., Maffezzoli, N., Cozzi, G., Gabrieli, J., Barbante, C., Goto-Azuma, K., Saiz-Lopez, A., Cuevas, C.A., Dahl-Jensen, D., 2016. Canadian Arctic sea ice reconstructed from bromine in the Greenland NEEM ice core. Sci. Rep. 6, 33925.

Sprovieri, F., Pirrone, N., Bencardino, M., D'Amore, F., Angot, H., Barbante, C., Brunke, E.G., Arcega-Cabrera, F., Cairns, W., Comero, S., Diéguez, M.D.C., Dommergue, A., Ebinghaus, R., Feng, X.B., Fu, X., Garcia, P.E., Gawlik, B.M., Hageström, U., Hansson, K., Horvat, M., Kotnik, J., Labuschagne, C., Magand, O., Martin, L., Mashyanov, N., Mkololo, T., Munthe, J., Obolkin, V., Ramirez Islas, M., Sena, F., Somerset, V., Spandow, P., Vardè, M., Walters, C., Wängberg, I., Weigelt, A., Yang, X., Zhang, H., 2017. Five-year records of mercury wet deposition flux at GMOS sites in the Northern and Southern hemispheres. Atmos. Chem. Phys. 17, 2689–2708.

Sprovieri, F., Pirrone, N., Bencardino, M., D'Amore, F., Carbone, F., Cinnirella, S., Mannarino, V., Landis, M., Ebinghaus, R., Weigelt, A., Brunke, E.G., Labuschagne, C., Martin, L., Munthe, J., Wängberg, I., Artaxo, P., Morais, F., Barbosa, H.D.M.J., Brito, J., Cairns, W., Barbante, C., Diéguez, M.D.C., Garcia, P.E., Dommergue, A., Angot, H., Magand, O., Skov, H., Horvat, M., Kotnik, J., Read, K.A., Neves, L.M., Gawlik, B.M., Sena, F., Mashyanov, N., Obolkin, V., Wip, D., Feng, X.B., Zhang, H., Fu, X., Ramachandran, R., Cossa, D., Knoery, J., Marusczak, N., Nerentorp, M., Norstrom, C., 2016. Atmospheric mercury concentrations observed at ground-based monitoring sites globally distributed in the framework of the GMOS network. Atmos. Chem. Phys. 16, 11915–11935.

Steffen, A., Schroeder, W., Bottenheim, J., Narayan, J., Fuentes, J.D., 2002. Atmospheric mercury concentrations: measurements and profiles near snow and ice surfaces in the Canadian Arctic during Alert 2000. Atmos. Environ. 36, 2653–2661.

Stenni, B., Scarchilli, C., Masson-Delmotte, V., Schlosser, E., Ciardini, V., Dreossi, G., Grigioni, P., Bonazza, M., Cagnati, A., Karlicek, D., Risi, C., Udisti, R., Valt, M., 2016. Three-year monitoring of stable isotopes of precipitation at Concordia Station, East Antarctica. Cryosphere 10, 2415–2428.

Traversi, R., Udisti, R., Frosini, D., Becagli, S., Ciardini, V., Funke, B., Lanconelli, C., Petkov, B., Scarchilli, C., Severi, M., Vitale, V., 2014. Insights on nitrate sources at Dome C (East Antarctic Plateau) from multi-year aerosol and snow records. Tellus B 66 (2014).

Wang, F., Saiz-Lopez, A., Mahajan, A.S., Gómez Martín, J.C., Armstrong, D., Lemes, M., Hay, T., Prados-Roman, C., 2014. Enhanced production of oxidised mercury over the tropical Pacific Ocean: a key missing oxidation pathway. Atmos. Chem. Phys. 14, 1323–1335.

Wang, J., Zhang, L., Xie, Z., 2016. Total gaseous mercury along a transect from coastal to central Antarctic: spatial and diurnal variations. J. Hazard Mater. 317, 362–372.

Wood, S.N., 2006. Generalized Additive Models: an Introduction with R. Chapman and Hall/CRC.

Yeongcheol, H., Youngsook, H., Soon, D.H., Sungmin, H., JiWoong, C., Hideaki, M., 2017. Net deposition of mercury to the Antarctic Plateau enhanced by sea salt. Sci. Total Environ. 583, 81–87.

ELECTRONIC SUPPLEMENTARY MATERIALS

Feedback mechanisms between snow and atmospheric mercury: Results and observations from field campaigns on the Antarctic plateau

Andrea Spolaor[1], Hélène Angot[2,*], Marco Roman, Aurélien Dommergue[2], Claudio Scarchilli[3], Massimiliano Vardè[1], Massimo Del Guasta[4], Cristiano Varin[5], Xanthi Xanthipi Penteli[5], Francesca Sprovieri[6], Olivier Magand[2], Michel Legrand[2], Carlo Barbante[1,5] and Warren R.L. Cairns[1]

[1]CNR-Institute for the Dynamics of Environmental Processes (IDPA), 30172, Venice-Mestre, Italy.

[2]Univ. Grenoble Alpes, CNRS, IRD, Grenoble INP, Institut des Géosciences de l'Environnement (IGE), 38000 Grenoble, France.

[3]ENEA, C.R. Casaccia, 00123, Roma, Italy.

4CNR-National Institute of Optics (INO), 50019, Sesto Fiorentino, Italy.

[5]Department of Environmental Sciences, Informatics and Statistics, University Ca' Foscari of Venice, 30172, Venice -Mestre , Italy.

[6]CNR-Institute of Atmospheric Pollution Research (IIA), Division of Rende, 87036, Rende, Italy.

[*]now at Institute for Data, Systems and Society. Massachusetts Institute of Technology, Cambridge, USA.

Figure S1. Metereological condition during the XXX campaign. Red lines show the surface snow temperature while the black line the Air temperature (both express as °C). Wind speed (ms^{-1}) and wind direction (°) are show in green and blue respectively. Pressure (hPa) are shown in grey while the relative humidity (%) in purple.

Figure S2. Metereological condition during the XXXI campaign. Red lines show the surface snow temperature while the black line the Air temperature (both express as °C). Wind speed (ms^{-1}) and wind direction (°) are show in green and blue respectively. Pressure (hPa) are shown in grey while the relative humidity (%) in purple.

Figure S3. Panel A) Five days backtrajectories from 18-11-2015 to 25-11-2015 starting at 12 UTC at 500 m (yellow lines), 1000 m (orange lines), 2000 m (red lines) and 3000 m (dark red lines) above Dome C (DC). Panel B-F) Daily images of MODIS-Terra corrected Reflectance (Bands 3-6-7) from 19-11-2015 to 23-11-2015, respectively. The synoptic analysis of the 18-26 November 2015 event is based on five days backtrajectories (TJ) calculation. TJ are calculated with the HYSPLIT Lagrangian model(Draxler and and Rolph, 2012) initialised with the European Centre Medium Range Weather Forecast (ECMWF) ERA INTERIM atmospheric model data Re-analysis with a 1°x1° regular grid(Dee et al., 2011). TJ are starting at the synoptical hours (00/06/12/18) and from different heights above the selected site. The error in TJ calculation after 5 days is estimated in the 10-30% range of the travel distance(Schlosser et al., 2008; Scarchilli et al., 2011). From 18 to 21 November the sampling site is experienced by a southward flow representing the predominant wind pattern over DC area (Traversi et al., 2014) with air masses TJ coming, at all levels, from the East plateau and Dronning Maud land (Fig XXa). Between 21-23 November a large low pressure system positioned over Amundsen Sea (not shown) conveyed air masses from ocean toward West Antarctica. Daily composite of Modis-Terra images highlight the structured cloud system related to strong cyclonic activity moving over Ross Ice shelf and intruding over the continent toward DC (Fig XX b-f) and producing cloudy condition over the site between 23 and 24 November. As a

consequences, from 21 to 24 November, calculated TJs at higher levels (2000-3000m) show a drastic change in their provenance area from East Antarctica to Bellingshausen and Amundsen sea.

Video S4. Collection of the most representative snow precipitation imagines obtained from the ice camera install at Dome C. Ice Camera is an instrument built to collect high resolution imagine (5 micron) of ice crystal in polar environment. The instrument collects the snow\ice precipitation on a doubles glass and every hour make a picture of the crystal deposit. The acquired imagines is processed using a MAtlab software developed by the CNR-INO (National research council – national optical institute). The developed software recognise the single crystals, measuring the shape and the size. The final imagine contain only the crystal recognise, order by the size determined. Every hour the external glass is warmed with the aim to sublimate the crystal present and initiate a new measurements cycle. ICE-CAMERA is the only instrument able to measure completely automatizes the type and the dimension of the ice crystal deposit from the precipitation in polar environment. For further and deeply detail visit: http://lidarmax.altervista.org/lidar/Precipitazioni%20in%20Antartide.php.

The ice camera imagines clearly show that the snow precipitation at Dome C between the 24th and the 25th of November 2015, are higher compare the other days considered. The higher concentration of Mercury determine in the surface snow (up to 270 pgg^{-1}) occurred during this periods. The precipitation was mainly characterize by small snow\ice crystal suggesting that this kind of precipitation could have a higher scavenging effect of the atmospheric mercury

References

Dee, D.P., Uppala, S.M., Simmons, A.J., Berrisford, P., Poli, P., Kobayashi, S., Andrae, U., Balmaseda, M.A., Balsamo, G., Bauer, P., Bechtold, P., Beljaars, A.C.M., van de Berg, L., Bidlot, J., Bormann, N., Delsol, C., Dragani, R., Fuentes, M., Geer, A.J., Haimberger, L., Healy, S.B., Hersbach, H., Hólm, E.V., Isaksen, L., Kållberg, P., Köhler, M., Matricardi, M., McNally, A.P., Monge-Sanz, B.M., Morcrette, J.J., Park, B.K.,

Peubey, C., de Rosnay, P., Tavolato, C., Thépaut, J.N., Vitart, F., 2011. The ERA-Interim reanalysis: configuration and performance of the data assimilation system. Quarterly Journal of the Royal Meteorological Society 137, 553-597.

Draxler, R.R., and Rolph, G.D., 2012. HYSPLIT (HYbrid Single- 1150 Particle Lagrangian Integrated Trajectory). NOAA Air Resources Laboratory, Silver Spring, MD. Model access via NOAA ARL READY Website. Online at: http://ready.arl.noaa.gov/ HYSPLIT.php.

Scarchilli, C., Frezzotti, M., Ruti, P.M., 2011. Snow precipitation at four ice core sites in East Antarctica: provenance, seasonality and blocking factors. Climate Dynamics 37, 2107-2125.

Schlosser, E., Oerter, H., Masson-Delmotte, V., and Reijmer, C., 2008. Atmospheric influence on the deuterium excess signal in polar firn: implications for ice-core interpretation. J. Glaciol. 54, 117-124.

Traversi, R., Udisti, R., Frosini, D., Becagli, S., Ciardini, V., Funke, B., Lanconelli, C., Petkov, B., Scarchilli, C., Severi, M., Vitale, V., 2014. Insights on nitrate sources at Dome C (East Antarctic Plateau) from multi-year aerosol and snow records. Tellus B; Vol 66 (2014).

Figure S1

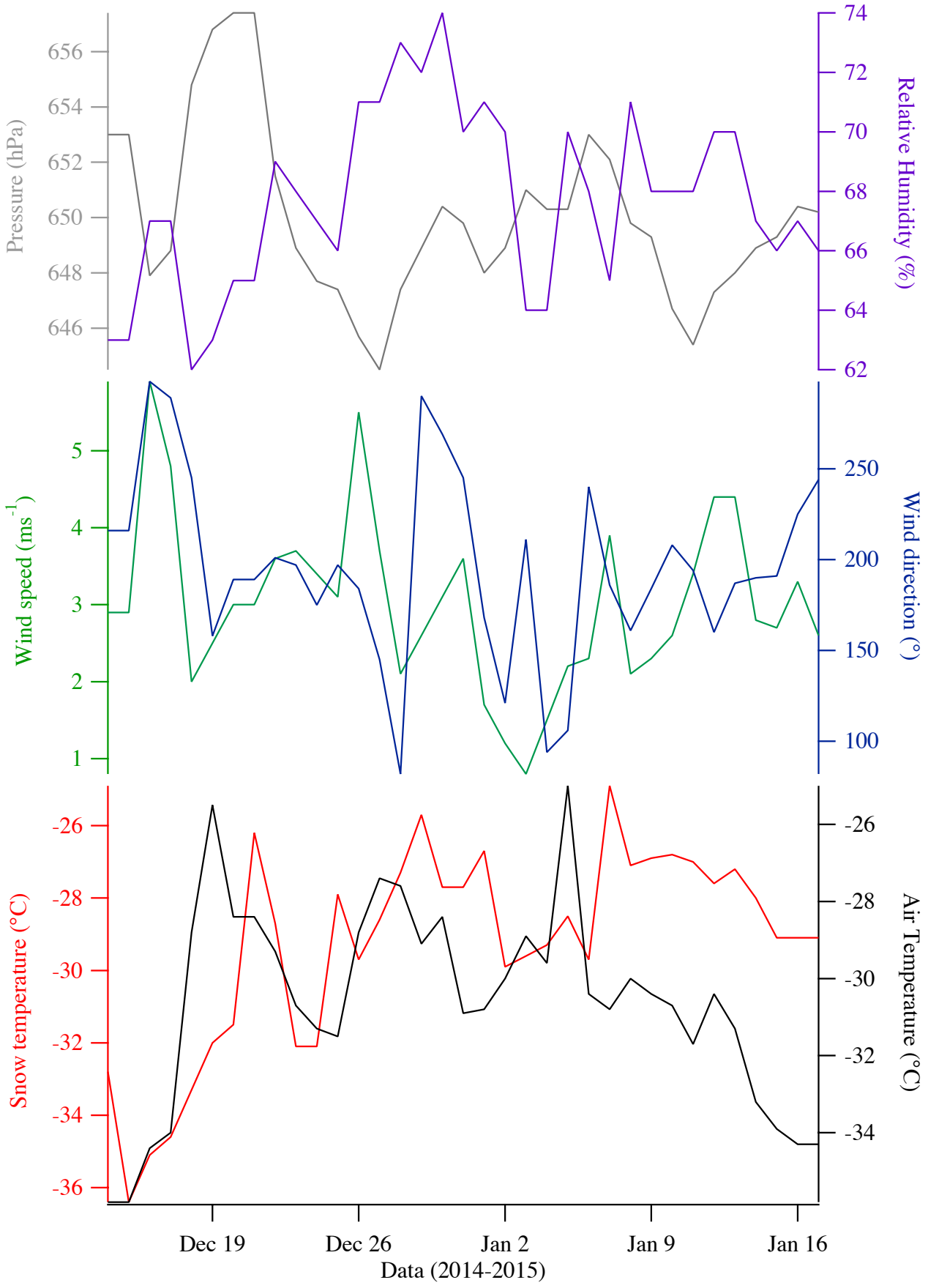
Pressure (hPa)
656
654
652
650
648
646
Relative Humidity (%)
74
72
70
68
66
64
62
Wind speed (ms-1)
5
4
3
2
1
Wind direction (°)
250
200
150
100
Snow temperature (°C)
-26
-28
-30
-32
-34
-36
Air Temperature (°C)
-26
-28
-30
-32
-34
Dec 19
Dec 26
Jan 2
Jan 9
Jan 16
Data (2014-2015)

Figure S2

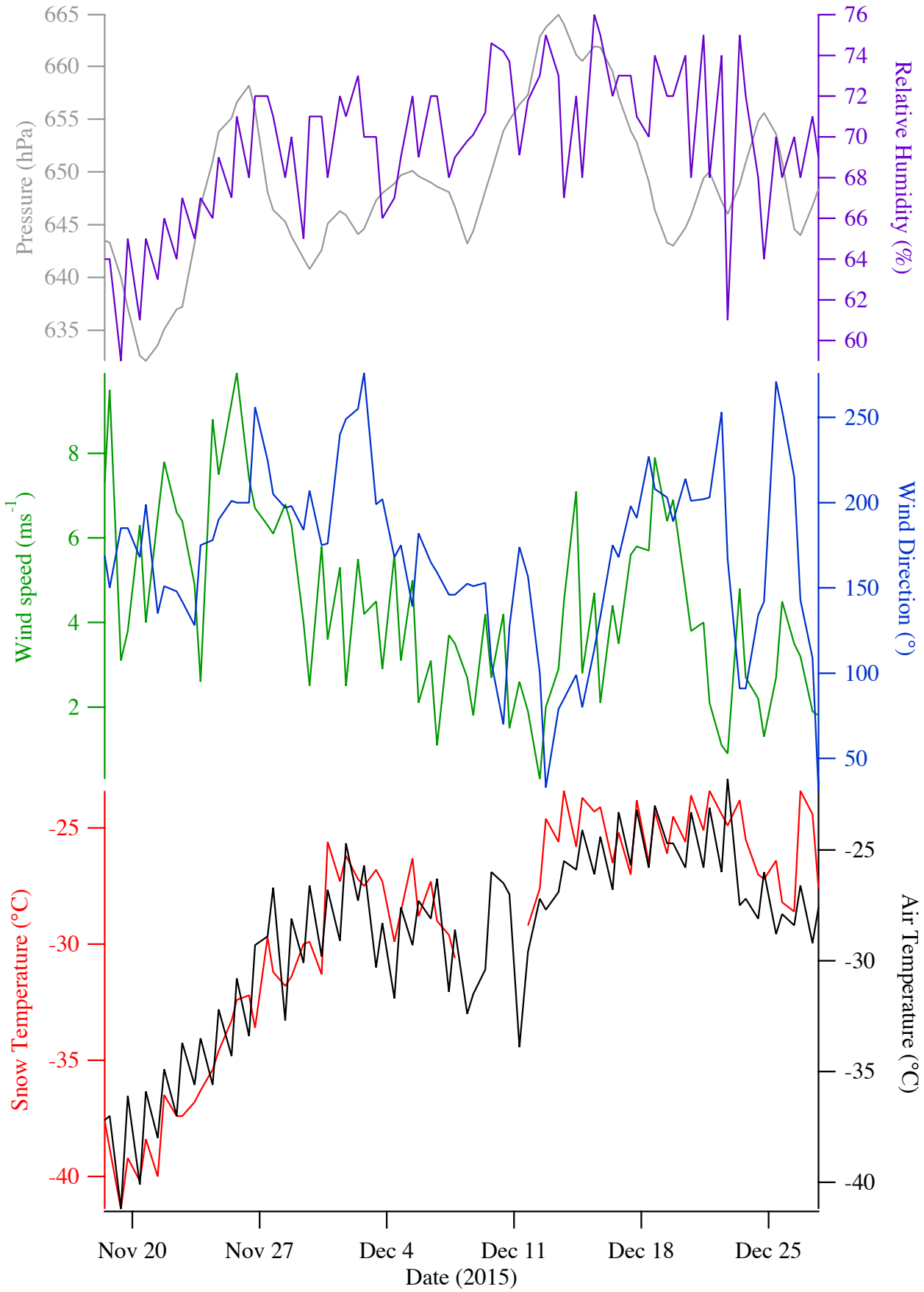
Pressure (hPa)
665
660
655
650
645
640
635
Relative Humidity (%)
76
74
72
70
68
66
64
62
60
Wind speed (ms-1)
8
6
4
2
Wind Direction (°)
250
200
150
100
50
Snow Temperature (°C)
-25
-30
-35
-40
Air Temperature (°C)
-25
-30
-35
-40
Nov 20
Nov 27
Dec 4
Dec 11
Dec 18
Dec 25
Date (2015)

Figure S3

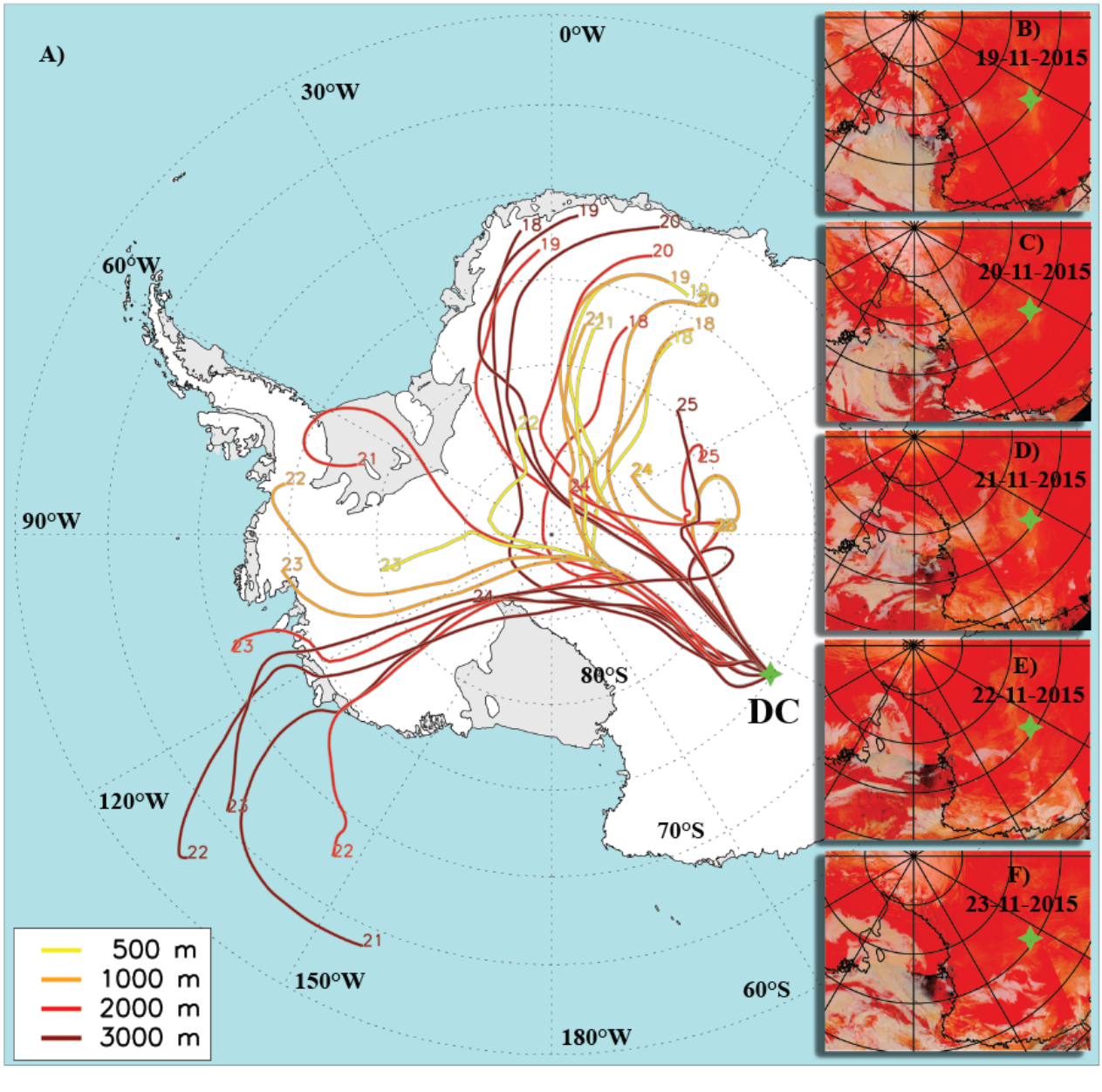
A)
0°W
30°W
60°W
90°W
120°W
150°W
180°W
80°S
70°S
60°S
DC
500 m
1000 m
2000 m
3000 m
B)
19-11-2015
C)
20-11-2015
D)
21-11-2015
E)
22-11-2015
F)
23-11-2015

...Where did all the blue skies go?
Poison is the wind that blows from the North and South and East…
Oh, things ain't what they used to be, no no
Oil wasted on the oceans and upon our seas, fish full of mercury…
(Marvin Gaye, What's Going On, Mercy Mercy Me-The Ecology)

...Aria sporca, aria riciclata, Compra l'aria già confezionata,
Tu compra l'aria per tutta la tua giornata… (Litfiba, Spirito, Ora d'aria)

...Stanno uccidendo il mare e noi li lasciamo fare,
L'indifferenza è comoda, L'ipocrisia... (Litfiba, 3, Peste)

Ricevuta di compilazione del questionario fine corso

dal 1994 Consorzio Interuniversitario
ALMALAUREA
Soluzioni con lode per l'Università e il mondo del lavoro

Università degli Studi di Ferrara

VARDE' MASSIMILIANO
Data di nascita 8/6/1972
Luogo di nascita VIBO VALENTIA
Codice fiscale VRDMSM72H08F537H

UNIVERSITÀ DEGLI STUDI DI FERRARA
SCIENZE CHIMICHE (D.M. 45/2013)
Tipo corso: Dottorato
Username AlmaLaurea: MASSIMILIANO.VARDE

Consenso al trattamento dei dati personali per le finalità e nelle modalità indicate nell'informativa: **ACCONSENTO**

Consensi relativi ad altre finalità specificate nell'informativa e al trasferimenti dei dati del CV extra-UE:
- Utilizzo recapiti per Indagini statistiche: acconsento
- Utilizzo dati CV per Analisi statistiche: acconsento
- Trasferimento CV in paesi extra-UE: acconsento

Informativa completa su https://www.almalaurea.it/info/condizioni/privacy/informativa-d2

Il tuo indirizzo e-mail

massimiliano.varde@edu.unife.it

Oggetto:

Dichiarazione di conformità della tesi di Dottorato

Io sottoscritto Dott. (Cognome e Nome)

Vardè Massimiliano

Nato a:

Vibo Valentia

Provincia:

Vibo Valentia

Il giorno:

08/06/1972

Avendo frequentato il Dottorato di Ricerca in:

Scienze Chimiche

Ciclo di Dottorato

33

Titolo della tesi:

Studio della distribuzione di mercurio in matrici ambientali

Titolo della tesi (traduzione):

Tutore: Prof. (Cognome e Nome)

Pasti Luisa; Cavazzini Alberto

Settore Scientifico Disciplinare (S.S.D.)

CHIM/01; CHIM/12

Parole chiave della tesi (max 10):

Mercurio; Atmosfera; Acque potabili; Acque minerali; Neve superficiale; Mercury; Atmosphere; Drinking waters; Natural mineral waters; Surface snow

Consapevole, dichiara

CONSAPEVOLE: (1) del fatto che in caso di dichiarazioni mendaci, oltre alle sanzioni previste dal codice penale e dalle Leggi speciali per l'ipotesi di falsità in atti ed uso di atti falsi, decade fin dall'inizio e senza necessità di alcuna formalità dai benefici conseguenti al provvedimento emanato sulla base di tali dichiarazioni; (2) dell'obbligo per l'Università di provvedere al deposito di legge delle tesi di dottorato al fine di assicurarne la conservazione e la consultabilità da parte di terzi; (3) della procedura adottata dall'Università di Ferrara ove si richiede che la tesi sia consegnata dal dottorando in 2 copie, di cui una in formato cartaceo e una in formato pdf non modificabile su idonei supporti (CD-ROM, DVD) secondo le istruzioni pubblicate sul sito : http://www.unife.it/studenti/dottorato alla voce ESAME FINALE – disposizioni e

modulistica; (4) del fatto che l'Università, sulla base dei dati forniti, archivierà e renderà consultabile in rete il testo completo della tesi di dottorato di cui alla presente dichiarazione attraverso l'Archivio istituzionale ad accesso aperto "EPRINTS.unife.it" oltre che attraverso i Cataloghi delle Biblioteche Nazionali Centrali di Roma e Firenze. DICHIARO SOTTO LA MIA RESPONSABILITA': (1) che la copia della tesi depositata presso l'Università di Ferrara in formato cartaceo è del tutto identica a quella presentata in formato elettronico (CD-ROM, DVD), a quelle da inviare ai Commissari di esame finale e alla copia che produrrà in seduta d'esame finale. Di conseguenza va esclusa qualsiasi responsabilità dell'Ateneo stesso per quanto riguarda eventuali errori, imprecisioni o omissioni nei contenuti della tesi; (2) di prendere atto che la tesi in formato cartaceo è l'unica alla quale farà riferimento l'Università per rilasciare, a mia richiesta, la dichiarazione di conformità di eventuali copie. PER ACCETTAZIONE DI QUANTO SOPRA RIPORTATO

Dichiarazione per embargo

12 mesi

Richiesta motivata embargo

5. Tutela della proprietà intellettuale

Liberatoria consultazione dati Eprints

Consapevole del fatto che attraverso l'Archivio istituzionale ad accesso aperto "EPRINTS.unife.it" saranno comunque accessibili i metadati relativi alla tesi (titolo, autore, abstract, ecc.)

Firma del dottorando

Ferrara, li 27/01/2021 (data) Firma del Dottorando Massimiliano Conti

Firma del Tutore

Visto: Il Tutore Si approva Firma del Tutore Luisa Pasti

Alberto Cavazzini